CHARACTERIZATION OF HETEROGENEITIES CONTROLLING TRANSPORT AND FATE OF POLLUTANTS IN UNCONSOLIDATED SAND AND GRAVEL AQUIFERS: SECOND YEAR REPORT

A research project of the
University Research Initiative
Research Initiation Program
U.S. Department of Defense

Carl D. McElwee and James J. Butler, Jr.
Kansas Geological Survey
The University of Kansas

with

Gwendolyn L. Macpherson
Department of Geology
The University of Kansas

Geoffrey C. Bohling, Richard D. Miller
Christine M. Mennicke, Terrance Huettl
Matthias Zenner, Zafar Hyder, Wenzhi Liu, and Micheal Orcutt
Kansas Geological Survey
The University of Kansas

June, 1993

Kansas Geological Survey
Open-file Report 93-21

REPORT DOCUMENTATION PAGE

Form Approved
OMB No. 0704-0188

1. AGENCY USE ONLY (Leave blank)	2. REPORT DATE	3. REPORT TYPE AND DATES COVERED
	30 June 93	Annual Technical, 1 June 92- 31 May 93

4. TITLE AND SUBTITLE
Characterization of heterogeneities controlling transport and fate of pollutants in unconsolidated sand and gravel aquifers: Second year report

5. FUNDING NUMBERS
G
AFOSR-91-0298

6. AUTHOR(S)
C. D. McElwee and J. J. Butler, Jr.

7. PERFORMING ORGANIZATION NAME(S) AND ADDRESS(ES)
Kansas Geological Survey
The University of Kansas
1930 Constant Avenue
Lawrence, KS

8. PERFORMING ORGANIZATION REPORT NUMBER
KGS
OFR 93-21

9. SPONSORING/MONITORING AGENCY NAME(S) AND ADDRESS(ES)
AFOSR/NL
Building 410
Bolling AFB DC 20332-6448

10. SPONSORING/MONITORING AGENCY REPORT NUMBER

11. SUPPLEMENTARY NOTES

12a. DISTRIBUTION/AVAILABILITY STATEMENT
Available from Publication Office of Kansas Geological Survey

12b. DISTRIBUTION CODE
OFR 93-21

13. ABSTRACT (Maximum 200 words)

The purpose of this project is to evaluate promising methodologies for characterization of heterogeneities in hydraulic conductivity. A major thrust of the second year of this project was an assessment of well tests in heterogeneous formations. The theoretical components of this effort included the development of a general slug-test model, a study of the use of slug tests to describe vertical variations in conductivity, an application of the principles of tomography to site characterization, an investigation of sinusoidal pulse tests in simple heterogeneous aquifers, and an examination of the effective parameters obtained from slug tests in wells with skins. The field component of this work emphasized slug tests. A program of multiwell slug tests was initiated at GEMS, which led to the development of a new model for the analysis of multiwell slug-test data. Additional field testing led to the development of new nonlinear slug-test models based on frictional losses, non-Darcian flow, and inertial effects. Additional field work included an aqueous geochemistry study; drilling and sampling activities; modification of the bladder sampler; laboratory analyses of cores; a wireline log survey; and a seismic survey. Overall, the research of year two produced results of considerable practical significance.

14. SUBJECT TERMS
Heterogeneities, alluvial aquifers, slug tests, site characterization, pollutant transport, pulse testing

15. NUMBER OF PAGES
221

16. PRICE CODE

17. SECURITY CLASSIFICATION OF REPORT	18. SECURITY CLASSIFICATION OF THIS PAGE	19. SECURITY CLASSIFICATION OF ABSTRACT	20. LIMITATION OF ABSTRACT

CHARACTERIZATION OF HETEROGENEITIES CONTROLLING TRANSPORT AND FATE OF POLLUTANTS IN UNCONSOLIDATED SAND AND GRAVEL AQUIFERS: SECOND YEAR REPORT

A research project of the
University Research Initiative
Research Initiation Program
U.S. Department of Defense

Carl D. McElwee and James J. Butler, Jr.
Kansas Geological Survey
The University of Kansas

with

Gwendolyn L. Macpherson
Department of Geology
The University of Kansas

Geoffrey C. Bohling, Richard D. Miller
Christine M. Mennicke, Terrance Huettl
Matthias Zenner, Zafar Hyder, Wenzhi Liu, and Micheal Orcutt
Kansas Geological Survey
The University of Kansas

June, 1993

ABSTRACT

A considerable body of research has shown that large-scale spatial variations (heterogeneities) in hydraulic conductivity play an important role in controlling the movement of a contaminant plume in the subsurface. Quantifying these heterogeneities, however, can be a very difficult task. If we are to improve our predictive capabilities of the fate and transport of pollutants in the subsurface, it is critical to develop methodology that enables a more accurate characterization of hydraulic conductivity variations to be obtained. The purpose of the research of this project is to evaluate, through both theoretical and field experiments, promising methodologies for the characterization of heterogeneities in hydraulic conductivity.

A major thrust of the second year of this research was an assessment of the type of information that can be obtained from well tests in heterogeneous formations. This effort had both theoretical and field components. The theoretical components included the development of a semianalytical solution to a general mathematical model describing the flow of groundwater in response to a slug test, a detailed study of the use of slug tests to describe vertical variations in hydraulic conductivity, an application of the principles of tomography to the characterization of spatial variations in flow properties, an investigation of the viability of sinusoidal pulse tests in simple heterogeneous aquifers, and a further examination of the effective transmissivity obtained from slug tests performed in wells surrounded by a finite-radius skin. Results of considerable practical significance were obtained from these theoretical analyses.

The field components of this study of well tests in heterogeneous formations concentrated on slug tests. A program of multiwell slug tests (slug tests with observation wells) was initiated at GEMS. The results of this field testing and a complementary theoretical analysis led to the development of a new analytical model for the analysis of multiwell slug tests at GEMS. Results of tests at most of the wells in the alluvial aquifer at GEMS indicate that slug tests in the sand and gravel section at GEMS are being affected by mechanisms not accounted for in the conventional theory on which the standard methods for slug-test data analysis are based. New nonlinear models based on frictional losses, non-Darcian flow, and inertial effects have been developed in an attempt to explain the gross features of the observed field behavior. Although further refinement of these non-linear models is clearly needed, careful application of these models to the field data does produce results superior to conventional approaches.

In addition to the research on well tests in heterogeneous formations, a significant amount of the work in year two was directed at increasing our knowledge of the

subsurface at GEMS. This work included a detailed study of the aqueous geochemistry of the alluvium and underlying bedrock at GEMS; continued drilling and sampling activities; continued laboratory analysis of the cores obtained with the bladder sampler; the beginning of a detailed wireline log survey; and a second seismic survey. These characterization efforts, which will continue throughout this project, are directed towards the development of a detailed picture of the subsurface at GEMS, so that we can better assess the results of the hydraulic and tracer tests that are being performed as part of this research.

A considerable amount of acquisition, construction, and modification of equipment took place during the second year of this project in support of the research effort. The equipment included new pressure transducers for field and laboratory use, an expanded laboratory permeameter for moderate to high permeability samples, a permeameter for the measurement of the hydraulic conductivity of low permeability samples, a portable water quality monitoring system for use in the field and laboratory, new large diameter auger flights for drilling large diameter monitoring wells, a grout machine for use in monitoring well completion, new surveying equipment, a portable digital borehole logging system for small-diameter boreholes, and additional computer equipment.

The research team for this project is composed of professional staff from the Kansas Geological Survey and the Department of Geology of the University of Kansas. Four graduate students (two funded by this project) are using aspects of the work of this project for their thesis research. Additional graduate students are benefitting from this project as a result of the establishment of a computer laboratory for graduate students in hydrogeology and the incorporation of material from this work into courses at the University of Kansas taught by members of the research team.

Acknowledgment

This research was sponsored in part by the Air Force Office of Scientific Research, Air Force Systems Command, USAF, under grant number AFOSR 91-0298. The views and conclusions contained in this document are those of the authors and should not be interpreted as necessarily representing the official policies, either expressed or implied, of the Air Force Office of Scientific Research or of the U.S. Government. The U.S. Government is authorized to reproduce and distribute reprints for Governmental purposes notwithstanding any copyright notation thereon.

TABLE OF CONTENTS*

* - Note that pages are numbered according to section and subsection.

I. INTRODUCTION

A. RESEARCH OBJECTIVES

The accurate prediction of pollutant transport and fate in aquifers is one of the most difficult and pressing problems in hydrogeology today. Physical, chemical, and microbial processes all play major roles in controlling contaminant movement in the subsurface. Before we can begin to understand the influence of the chemical and biological side of this problem, however, we must fully understand the role of physical processes and, specifically, the influence of the physical hydrogeological properties. Many researchers now recognize (e.g., Molz et al., 1989) that if we are to improve our predictive capabilities for subsurface transport, we must first improve our capabilities for measuring and describing conditions in the subsurface. That is the focus of the research described in this report. The specific objective of this research is to assess the potential of advanced well-testing technology for providing more accurate estimates of spatial variations in the physical properties that control contaminant plume movement in saturated porous media. Although effective porosity is clearly an important consideration, the major emphasis of this work is on characterizing spatial variations (heterogeneities) in hydraulic conductivity.

Ideally, heterogeneities in hydraulic conductivity must be studied and characterized at several different scales in order to understand their influence on the movement of a contaminant plume. Although theoretical modeling work is an important element of any study of the influence of spatial variations in hydraulic conductivity, a rigorous study of this subject must have a major field component. A field site at which researchers at the University of Kansas can pursue work on the effect of heterogeneities in aquifer properties on subsurface transport has been set up as part of this research. The specific site of the field effort is the Geohydrologic Experimental and Monitoring Site (GEMS), which is located just north of Lawrence, Kansas on land owned by the University of Kansas Endowment Association. Figure 1 is a map showing the location of GEMS and some of the major features at the site. GEMS overlies approximately 70 feet (21.3 m) of Kansas River valley alluvium. These recent unconsolidated sediments overlie and are adjacent to materials of Pleistocene and Pennsylvanian age. A cross-sectional view of the subsurface at one of the well nests at GEMS is shown in Figure 2. The alluvial facies assemblage at this site consists of approximately 35 feet (10.7 m) of clay and silt overlying 35 feet (10.7 m) of sand and gravel. The stratigraphy is a complex system of stream-channel sand and overbank deposits. The general nature of the stratigraphy would lead one to expect that a considerable degree of lateral and vertical

heterogeneity in hydraulic conductivity would be found in the subsurface at GEMS. Although analyses of sampled cores do indicate considerable variability in hydraulic conductivity within the sand and gravel interval at GEMS, it is not yet clear how the variability at the small scale of a core translates into variability at larger scales.

In the second year of this research, the focus of the work was again on the use of slug tests to describe spatial variations in hydraulic conductivity. The analysis of response data from slug tests at GEMS has turned out to be considerably more challenging than expected. It is clear from our work that conventional methodology for the analysis of slug-test data is not adequate when dealing with very high conductivity media, wells that are only partially screened across a formation, wells with disturbed zones created by drilling activities, and layered media. Since the slug test has become the most common technique for estimation of hydraulic conductivity at sites of groundwater contamination, we have expended much more effort on this phase of the project than was originally anticipated. However, this research has produced a number of very interesting results of practical significance, so we feel that it has been a profitable redirection of effort. As a result of this redirection of our efforts, the work on pulse testing, which we had planned to be the main component of work during the second year of this project, has not progressed as far as originally expected. Some work on pulse testing, however, has begun. The natural first step in an investigation of pulse testing is a study of the use of observation wells with slug tests (multiwell slug tests), where the excitation consists of a single pulse (slug). This year we carried out both a theoretical and field examination of multiwell slug tests. A logical extension of this work is to use several pulses (slugs) separated in time or to use a continuous time varying signal (e.g., a sine wave) as the excitation source. This year we began a theoretical investigation of the use of a multiple-pulse excitation for the characterization of aquifer heterogeneities. Tomography has proven to be a valuable imaging tool, capable of exposing heterogeneities in media properties, when propagating wave phenomena are used to probe the media. We have initiated a theoretical examination of hydraulic tomography (another form of pulse testing) as a means of imaging the flow properties in aquifers. Since a pulsing signal in systems where the governing physical processes have a diffusive character (such as the flow of groundwater in aquifers) is a strongly attenuated wave, its range of investigation will be much shorter than for a propagating wave system. Although at this point the capabilities of hydraulic tomography are unknown, our initial results indicate that it clearly deserves further investigation.

This year, a considerable amount of additional work has again been directed at increasing our knowledge of the subsurface at GEMS. This effort has involved further

analysis of the aqueous geochemistry at GEMS, continued drilling and sampling of the alluvium, continued laboratory analysis of sampled cores, wireline logging surveys, and a second seismic survey. These characterization efforts are directed at providing the detailed information that will allow us to better assess the quality of the information provided by the various well-testing approaches evaluated in this work. In addition, this information will help us design the tracer tests to be performed in the third year of the project. The ultimate goal of these characterization efforts is to describe the site in enough detail that it effectively becomes an underground laboratory at which new technology can be evaluated.

B. BRIEF OUTLINE OF REPORT

The remainder of this report is divided into six major sections, each of which is essentially a self-contained unit. Pages, figures, and equations are labelled by section and, when warranted, subsection.

The first section describes theoretical work directed at developing a better understanding of the information that can be obtained from well tests in heterogeneous media. The first subsection deals with slug tests in partially penetrating wells. The second subsection looks in detail at the use of slug tests to delineate horizontal layering in aquifers. Some improvements that were made to SUPRPUMP, a well-test analysis package developed at the Kansas Geological Survey, are then described. Note that SUPRPUMP is used throughout this work to carry out analyses of hydraulic tests. A theoretical examination of hydraulic tomography is then considered in the next subsection. This is followed by an examination of the use of a sinusoidally varying signal to investigate a simple two-zone aquifer. The final subsection presents some new material on the effective transmissivity determined from a slug test in the presence of a well skin. Note that the first two subsections are essentially the text of articles on these topics that were submitted for publication during the second year of this project.

The second section primarily describes further field investigations using slug tests. The first subsection deals with the use of observation wells with slug tests (multiwell slug tests). The results of a program of field testing at GEMS and a subsequent theoretical analysis motivated by those results are described. The second subsection presents an update of the new nonlinear model for slug tests introduced in the report on year one activities. This model, which accounts for some of the mechanisms affecting the GEMS slug-test data, has now been derived using three different physical mechanisms to represent the nonlinear behavior. This section concludes with the application of the nonlinear model to data from slug tests at GEMS.

The third section primarily describes activities directed at increasing our knowledge of the subsurface at GEMS. A continuation of the aqueous geochemistry study at GEMS begun in year one is given in the first subsection. After a description of the drilling and sampling activities that occurred over the last year at GEMS, work in the KGS core measurement laboratory is discussed. The section concludes with a report on the status of wireline logging activities and a detailed description of the shallow seismic survey that was undertaken at GEMS in the second year of this project.

The fourth section describes new equipment that was built or purchased during the second year of this project.

The fifth section describes the personnel of the research team that has been organized to pursue this work, and lists relevant publications of the team over the last year. The section concludes with a discussion of the interactions with other research groups that have occurred during the last year.

The sixth section summarizes the report and briefly outlines the work planned for the third year of this project.

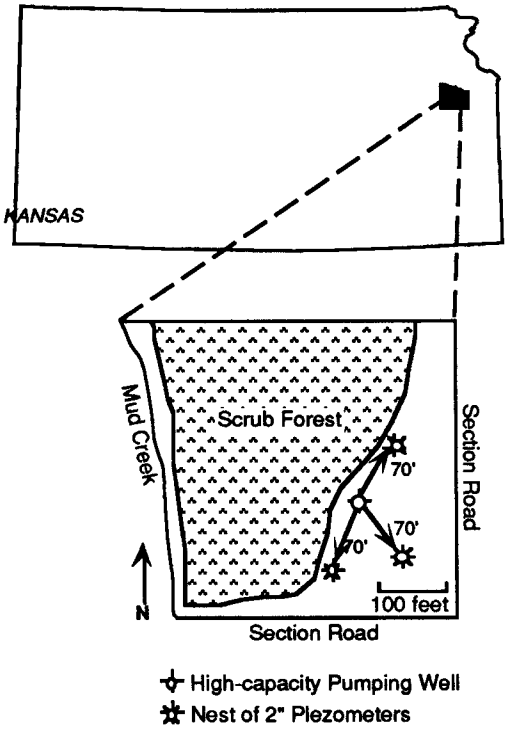

Figure 1 - Location map for the Geohydrologic Experimental and Monitoring Site (GEMS).

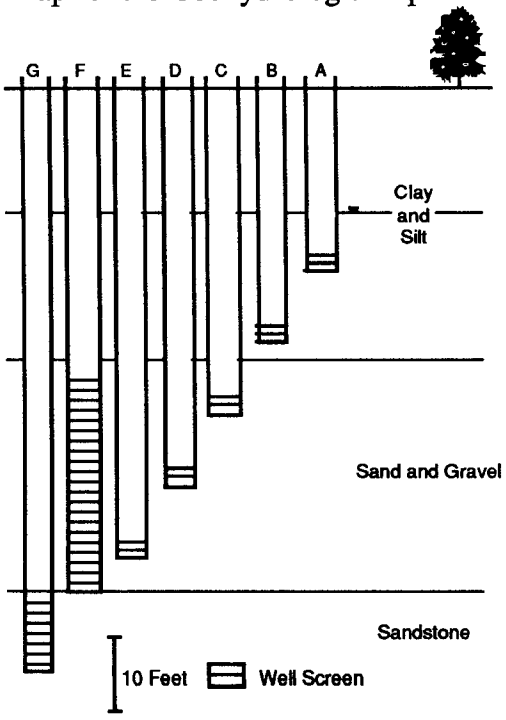

Figure 2. A typical well nest cross-section

II. THEORETICAL INVESTIGATIONS OF WELL TESTS IN HETEROGENEOUS MEDIA

A. SLUG TESTS IN PARTIALLY PENETRATING WELLS

Abstract

In this section, a semianalytical solution to a general mathematical model describing the flow of groundwater in response to a slug test in an unfractured formation is presented. The model incorporates the effects of partial penetration, anisotropy, finite-radius well skins of either higher or lower permeability than the formation as a whole, and upper and lower boundaries of either a constant-head or an impermeable form. This model is used to assess the error that is introduced into parameter estimates by employing conventional methods for the analysis of data from slug tests in configurations not strictly addressed in the derivation of those methods. The parameter error is largest for tests performed in the presence of low-permeability well skins and in wells with small aspect ratios (well radius/screen length) located in anisotropic formations. The magnitude of the error arising in different configurations is used as the basis for recommendations for approaches to the analysis of slug-test data that can be utilized by field practitioners.

Introduction

The slug test is probably the most commonly used technique by hydrogeologists for estimating hydraulic conductivity in the field (Kruseman and de Ridder, 1989). This technique, which is quite simple in practice, consists of measuring the recovery of head in a well after a near instantaneous change in water level at that well. The slug test has become a preferred field method because of its several logistical and economic advantages. These include the small amount of equipment and manpower required to perform a test, the relatively short duration of the test, the perceived ease of the analysis of the recovery data, and the need for only a small amount of water (if any) to be added/removed from the well during the course of the test. A slug test can be initiated by introducing/removing an object of known volume to/from the water column or by pneumatic means (Orient et al., 1987; McLane et al., 1990), thus avoiding problems arising due to introduction of waters of different composition or disposal of potentially contaminated waters.

Approaches for the analysis of the recovery data collected during a slug test are based on analytical solutions to mathematical models describing the flow of groundwater to/from the test well. Over the last thirty years, solutions have been developed for a number of test configurations commonly found in the field (see Chirlin (1990) for a summary of much of the past work). In terms of slug tests in confined aquifers, the earliest proposed method is that of Hvorslev (1951), which is based on a series of simplifying assumptions concerning the slug-induced flow system (e.g., specific storage can be ignored, finite effective radius, etc.). Much of the work following Hvorslev has been directed at removing one or more of these simplifying assumptions. Cooper et al. (1967) developed a fully transient solution to the case of a slug test in a well fully screened across a confined aquifer. Moench and Hsieh (1985) extended the solution of Cooper et al. to the case of a fully penetrating well with a finite radius well skin. A number of workers (e.g., Dougherty and Babu, 1984; Hayashi et al., 1987) have developed solutions for slug tests in wells partially penetrating isotropic, confined aquifers. Butler and McElwee (1990) presented a general solution for slug tests in wells partially penetrating confined aquifers that incorporates the effects of anisotropy and a finite-radius skin at the test well. In most field applications, the methods of Hvorslev (1951) or Cooper et al. (1967) are employed. The error that is introduced into hydraulic conductivity estimates by employing these models in cases where their assumptions are inappropriate has not yet been fully evaluated.

In terms of slug tests in unconfined aquifers, solutions for the mathematical model describing flow in response to the induced disturbance are difficult to obtain because of the nonlinear nature of the model in its most general form. Currently, most field practitioners use the technique of Bouwer and Rice (Bouwer and Rice, 1976; Bouwer, 1989), which is based on steady-state simulations using an electrical analog model, for the analysis of slug tests in unconfined flow systems. Dagan (1978) presents an analytical solution based on assumptions similar to those of Bouwer and Rice (1976). Amoozegar and Warrick (1986) summarize related methods employed by agricultural engineers. All of these techniques result from the application of several simplifying assumptions to the mathematical description of flow to a well in an unconfined aquifer. The most important of these assumptions are: 1) the specific storage of the aquifer is negligible, 2) changes in the position of the water table due to a slug test are so small that the water table can be represented as a constant-head boundary, 3) flow above the water table can be ignored, 4) there is no zone of disturbance created by drilling or development, and 5) the formation is isotropic with respect to hydraulic conductivity. As with the confined case, the ramifications of these assumptions have not yet been fully

evaluated.

In this section, a semianalytical solution to a general mathematical model describing the flow of groundwater in response to an instantaneous change in water level at a central well is presented. The model incorporates the effects of partial penetration, anisotropy, finite-radius well skins of either higher or lower permeability than the formation as a whole, and upper and lower boundaries of either a constant-head or an impermeable form. This model can be employed for the analysis of data from slug tests in a wide variety of commonly met field configurations. Although packers are not explicitly included in the formulation, earlier numerical work has shown that this model can also be used for the analysis of multilevel slug-test data when packers of moderate length (.75 meters or longer) are employed (e.g., Bliss and Rushton, 1984; Butler et al., in review).

The major purpose of this section is to delineate the conditions when the slug-test model developed here is needed. This will be done by quantifying the error that is introduced into parameter estimates as a result of using currently accepted practices for the analysis of data from slug tests in configurations not strictly addressed in the derivation of those methods. The magnitude of the error arising in different configurations will then serve as the basis for recommendations for approaches to the analysis of slug-test data that can be utilized by field practitioners.

Statement of Problem

The problem of interest here is that of the head response, as a function of r, z, and t, produced by the instantaneous introduction of a pressure disturbance into the screened or open section of a well. For the purposes of this initial development, the well will be assumed to be located in the confined aquifer shown in Figure II.A.1. Note that, as shown on Figure II.A.1, there is a well skin of radius r_{sk} that extends through the full width of the aquifer. The skin has transmissive and storage properties that may differ from the formation as a whole. Flow properties are assumed uniform within both the skin and formation, although the vertical (K_z) and radial (K_r) components of hydraulic conductivity may differ.

The partial differential equation representing the flow of groundwater in response to an instantaneous change in water level at a central well is the same for both the skin and the aquifer and can be written as

$$\frac{\partial^2 h_i}{\partial r^2}+\frac{1}{r}\frac{\partial h_i}{\partial r}+\left(\frac{K_{z_i}}{K_{r_i}}\right)\frac{\partial^2 h_i}{\partial z^2}=\left(\frac{S_{s_i}}{K_{r_i}}\right)\frac{\partial h_i}{\partial t} \qquad \text{(II.A.1)}$$

where

h_i = head in zone i, [L];

S_{s_i} = specific storage of zone i, [1/L];

K_{z_i}, K_{r_i} = vertical and radial components, respectively, of the hydraulic conductivity of zone i, [L/T];

t = time, [T];

r = radial direction, [L];

z = vertical direction, z=0 at the top of the aquifer and increases downward, [L];

i = zone designator, for $r_w < r \leq r_{sk}$, i = 1, and for $r_{sk} \leq r$, i = 2;

r_w = screen radius, [L];

r_{sk} = outer radius of skin, [L].

The initial conditions can be written as

$$h_1(r,z,0) = h_2(r,z,0) = 0,\ r_w < r < \infty,\ 0 < z < B \qquad \text{(II.A.2)}$$

$$H(0) = H_0 \qquad \text{(II.A.3)}$$

where

B = aquifer thickness, [L];

H(t) = level of water in well, [L];

H_0 = height of initial slug, [L].

The boundary conditions are the following:

$$h_2(\infty,z,t) = 0,\ t > 0,\ 0 < z < B \qquad \text{(II.A.4)}$$

$$\frac{\partial h_i(r,0,t)}{\partial z} = \frac{\partial h_i(r,B,t)}{\partial z} = 0,\ r_w < r < \infty,\ t > 0 \qquad \text{(II.A.5)}$$

$$h_1(r_w,z,t) = H(t),\ t > 0,\ d \le z \le d + b \qquad \text{(II.A.6)}$$

$$2\pi r_w K_{r_1} \frac{\partial h_1(r_w,z,t)}{\partial r} = \frac{\pi r_c^2}{b} \frac{dH(t)}{dt} \square(z),\ t>0 \qquad \text{(II.A.7)}$$

where

r_c = radius of well casing, casing and screen do not have to be of equal radius, [L];

$\square(z)$ = boxcar function = 0, $z < d$, $z > b+d$,
= 1, elsewhere;

d = distance from the top of the aquifer to the top of the screen, [L];

b = screen length, [L].

Note that (II.A.7) indicates that the horizontal hydraulic gradient is assumed uniform along the well screen.

In order to ensure continuity of flow between the skin and the formation, auxiliary conditions at the skin-formation boundary ($r=r_{sk}$) must also be met:

$$h_1(r_{sk},z,t) = h_2(r_{sk},z,t),\ 0<z<B,\ t>0 \qquad \text{(II.A.8)}$$

$$K_{r_1} \frac{\partial h_1(r_{sk},z,t)}{\partial r} = K_{r_2} \frac{\partial h_2(r_{sk},z,t)}{\partial r},\ 0<z<B,\ t>0 \qquad \text{(II.A.9)}$$

Equations (II.A.1)-(II.A.9) describe the flow conditions of interest here. Appendix A in Section IX provides the details of the solution derivation. In summary,

the approach employs a series of integral transforms (Laplace transform in time and a finite Fourier cosine transform in the z direction) to obtain functions in transform space that satisfy the transform-space analogues of (II.A.1)-(II.A.9). The transform-space function that is obtained for the head in a partially penetrating well with a finite-radius well skin in an anisotropic confined aquifer can be written in a non-dimensional form as

$$\Phi(p)=\frac{\frac{\gamma}{\alpha}F_c^{-1}(F_c(\omega)f_1)}{[1+\frac{\gamma}{\alpha}pF_c^{-1}(F_c(\omega)f_1)]} \qquad \text{(II.A.10)}$$

where

$\Phi(p)$ = the nondimensional Laplace transform of H(t);

p = Laplace-transform variable;

ω = Fourier-transform variable;

$\alpha = (2r_w^2S_{s2}b)/r_c^2$;

$\gamma = K_{r2}/K_{r1}$;

$F_c(\omega)$ = finite Fourier cosine transform of $\square(z)$;

F_c^{-1} = inverse finite Fourier cosine transform;

$$f_1 = \frac{[\Delta_2K_0(\nu_1)-\Delta_1I_0(\nu_1)]}{\nu_1[\Delta_2K_1(\nu_1)+\Delta_1I_1(\nu_1)]};$$

$$\nu_i = (\frac{A_i}{a^2}\omega^2 + \frac{K_{r2}/S_{s2}}{K_{ri}/S_{si}}p)^{.5};$$

$A_i = K_{zi}/K_{ri}$;

$a = b/r_w$;

$$\Delta_1=K_0(\nu_1\xi_{sk})K_1(\nu_2\xi_{sk})-[\frac{N}{\gamma}]K_0(\nu_2\xi_{sk})K_1(\nu_1\xi_{sk});$$

$$\Delta_2=I_0(\nu_1\xi_{sk})K_1(\nu_2\xi_{sk})+[\frac{N}{\gamma}]K_0(\nu_2\xi_{sk})I_1(\nu_1\xi_{sk});$$

$N = \nu_1/\nu_2$;

$\xi_{sk} = r_{sk}/r_w$.

For the unconfined case, the upper no-flow boundary condition in eqn. (II.A.5) is changed into a constant-head boundary condition, so the upper and lower boundary conditions are rewritten as:

$$h_i(r,0,t) = 0,\ r_w < r < \infty,\ t > 0 \qquad \text{(II.A.11)}$$

$$\frac{\partial h_i(r,B,t)}{\partial z} = 0,\ r_w < r < \infty,\ t > 0 \qquad \text{(II.A.12)}$$

Appendix A in Section IX also provides the details of the solution derivation for the unconfined case. The transform-space function that is obtained for the head in a partially penetrating well with a finite-radius well skin in an anisotropic unconfined aquifer can be written in a non-dimensional form as

$$\Phi_{uc}(p) = \frac{\frac{\gamma}{\alpha} F_s^{-1}(F_s(\omega^*) f_1)}{[1 + \frac{\gamma}{\alpha} p F_s^{-1}(F_s(\omega^*) f_1)]} \qquad \text{(II.A.13)}$$

where

$\Phi_{uc}(p)$ = the Laplace transform of the nondimensional form of H(t) for the unconfined case;

$F_s(\omega^*)$ = modified finite Fourier sine transform of $\square(z)$;

ω^* = Fourier transform variable for the modified sine transform.

For expressions of the complexity of (II.A.10) and (II.A.13), the analytical back transformation from transform space to real space is only readily performed under quite limited conditions. In the general case, the transformation is best performed numerically. Initially, the Fourier inversion was performed using an infinite series summation in a manner similar to that employed by Butler and McElwee (1990). This approach,

however, proved to be computationally inefficient, requiring such a large amount of time on a microcomputer as to limit the practical use of the solution. As an alternative, numerical evaluation of the Fourier transforms and their inversions were done here using Discrete Fourier Transforms (Brigham, 1974), thereby allowing computationally efficient Fast Fourier Transform techniques (Cooley and Tukey, 1965) to be utilized. This approach, which is briefly outlined in Appendix B of Section IX, did not introduce significant error into the inversion procedure. An algorithm developed by Stehfest (1970), which has been found to be of great use in hydrologic applications (Moench and Ogata, 1984), was employed to perform the numerical Laplace inversion.

Several checks were performed in order to verify that (II.A.10) and (II.A.13) were solutions to the mathematical model outlined here. Substitution of (II.A.10) and (II.A.13) into the respective transform-space analogues of (II.A.1)-(II.A.9) and (II.A.11)-(II.A.12) demonstrated that the proposed solutions honor the governing equation and auxiliary conditions in all cases. In addition, if the test well is assumed to be fully screened across an isotropic, confined aquifer, (10) reduces to the Laplace-space form of the solution of Moench and Hsieh (1985). Likewise, in the no-skin case, (II.A.10) reduces to the Laplace-space form of the solution of Cooper et al. (1967). Butler et al. (1993) describe additional checks performed to verify the solution proposed here.

Ramifications for Data Analysis

As discussed in the Introduction, the primary purpose of this paper is to evaluate the error that is introduced into parameter estimates when employing currently accepted practices to analyze the response data from slug tests performed in well configurations similar to those described in the previous section. This evaluation is carried out by using (II.A.10) and (II.A.13) to simulate slug tests in a variety of configurations. The simulated response data are analyzed using conventional approaches. The parameter estimates are then compared to the parameters employed in the original simulations to assess the magnitude of the error introduced into the parameter estimates through use of a particular approach for the data analysis. The simulation and analysis of slug tests were performed in this work using SUPRPUMP, an automated well-test analysis package developed at the Kansas Geological Survey (Bohling and McElwee, 1992). In all of the simulations, the set of parameters given in Table II.A.1 for a slug test in a homogeneous, isotropic aquifer were used as the base case.

Partial Penetration Effects

The first factor examined here was the effect of partial penetration on parameter

estimates in a homogeneous aquifer (no skin case). Figure II.A.2 displays a plot of the hydraulic conductivity ratio (K_{est}/K_r) versus aspect ratio (b/r_w) for a configuration in which the upper and lower boundaries are at such a large distance from the screened interval that they have no effect. In this case, the hydraulic conductivity estimates are obtained using the solution of Cooper et al. (1967), which assumes that the well is fully screened across the aquifer (i.e. flow is purely radial). Figure II.A.2 shows that the error arising from the radial flow assumption decreases greatly with increases in aspect ratio, as would be expected since the proportion of vertical flow decreases as the aspect ratio increases. Note that decreases in the anisotropy ratio further reduce this error as a result of the flow becoming increasingly constrained to the horizontal plane as K_r increases relative to K_z. Also note that the error in the conductivity estimates increases greatly with decreases in specific storage. This is in keeping with the results of Hayashi et al. (1987) who noted that for a constant aspect ratio vertical flow increases with decreases in the storage parameter. Based on Figure II.A.2, it is clear that, in many field situations, application of the Cooper et al. solution for slug tests performed in wells with aspect ratios greater than 200 should introduce little if any error into the parameter estimates. Only in the case of a very low specific storage will significant error ($> 25\%$) be introduced into the estimates. Even in that case, however, if there is any degree of anisotropy in hydraulic conductivity, the parameter estimates should still be reasonable. Note that Figure II.A.2 is an extension of the findings of Hayashi et al. (1987) to the case of slug tests in open wells, a more common configuration for groundwater applications than the pressurized slug test configuration that they examined.

Currently, the most common method for analysis of slug tests in partially penetrating wells is that proposed by Hvorslev (1951). Hvorslev developed a model for the analysis of slug tests performed in a screened interval of finite length in a uniform, anisotropic, vertically unbounded medium. Figure II.A.3a displays a plot analogous to Figure II.A.2 for the case of the Hvorslev model being used to obtain the conductivity estimates. Note that the Hvorslev model requires the use of a "shape factor", which is related to the geometry of the well intake region. The shape factor used in Figure II.A.3a is that for Case 8 described in Hvorslev (1951) and results in the following expression for the radial component of hydraulic conductivity:

$$K_{HV} = \frac{r_c^2 \ln[b/(A^{.5}2r_w) + \sqrt{1+(b/(A^{.5}2r_w))^2}]}{2bT_0} \qquad \text{(II.A.14)}$$

where

T_0 = basic time lag, time at which a normalized head of .37 is reached.

As the aspect ratio gets large, (II.A.14) will reduce to Hvorslev's expression for a fully penetrating well (Case 9) if the effective radius is set equal to the screen length in Case 9. Note that the anisotropy ratio (A) and K_{HV} are perfectly correlated in (II.A.14), so these parameters cannot be estimated independently. In Figure II.A.3a, all analyses using (II.A.14) were performed assuming that the formation was isotropic. Given the difficulty in knowing the appropriate degree of anisotropy in natural systems, this assumption was considered a reasonable representation of conditions found in the field. Figure II.A.3b displays the estimates obtained using Hvorslev's expression for a fully penetrating well in which an effective radius of 200 times the well radius was employed as recommended by the U.S. Dept. of Navy (1961).

Figure II.A.3a indicates that the estimates provided by (II.A.14) will be quite good in the isotropic case (within 15%) for aspect ratios up to about 200. As the screen length continues to increase, however, the error introduced into the parameter estimates increases. This increased error arises due to the implicit assumption in (II.A.14) of the effective radius being equal to the screen length when the aspect ratio gets large. Note that although several standard references (e.g., Freeze and Cherry, 1979) recommend use of (II.A.14), these results indicate that it is only appropriate for wells with aspect ratios less than about 200. Note also that in anisotropic situations, (II.A.14) must be used with caution at small aspect ratios.

Figure II.A.3b indicates that the fully penetrating well model of Hvorslev (using an effective radius of 200 times the well radius) is appropriate for aspect ratios greater than 200 in the isotropic case. If K_r is much greater than K_z, the aspect ratios at which the fully penetrating model is appropriate are much smaller. It is important to emphasize that the results presented on Figures II.A.3a and II.A.3b are for particular values of S_s and K. The error introduced into the parameter estimates is directly proportional to S_s and inversely proportional to K. Figure II.A.4 displays the dependence of these results on S_s and K for aspect ratios commonly found in the field. Chirlin (1989) provides a detailed discussion of the dependence of Hvorslev estimates on the storage parameter.

The uncertainty concerning anisotropy and specific storage in natural systems makes it difficult to propose guidelines for the analysis of response data from slug tests in partially penetrating wells with small to moderate aspect ratios. Clearly, at large aspect ratios (a > 200), the Cooper et al. (1967) model is most appropriate. At aspect ratios between 100 and 200, the fully penetrating model of Hvorslev (1951) using an

effective radius of $200r_w$ would be the best for the most general case. At aspect ratios smaller than 100, the partially penetrating model of Hvorslev is best in the most general case. However, if there is some prior information about specific storage and the anisotropy ratio, Figures II.A.2-4 can be used to assess which method is most appropriate for the analysis of the response data.

Boundary Effects

The previous discussion has focussed on the effects of partial penetration in a vertically infinite system. Although many natural systems can be considered as vertically infinite for the purposes of the analysis of response data from slug tests, there will be situations in which the upper and/or lower boundaries of the system influence the response data. Thus, the next factor examined here was the effect of impermeable and constant-head boundaries in the vertical plane on the parameter estimates. Figure II.A.5 displays a plot of the hydraulic conductivity ratio versus the distance to the closest boundary. Results are shown for both impermeable and constant-head boundaries. In all cases, the Hvorslev model (eqn. (II.A.14)) is used to obtain the conductivity estimates. It is clear from Figure II.A.5 that only when the screen is very close to the boundary (i.e. within several meters) will the boundary have a sizable effect on the parameter estimates. If there is any degree of anisotropy in hydraulic conductivity, the influence of the boundary will be considerably lessened. Note that Hvorslev (1951) also proposed a semi-infinite, partially penetrating model (single impermeable boundary with screen extending to boundary) for slug tests. The equation for estimation of hydraulic conductivity in this case is the same as (II.A.14) except r_w is used instead of $2r_w$ in the logarithmic term. The circles and triangles on Figure II.A.5 show the estimates that would be obtained using this model for the confined case. Although all of the parameter estimates in Figure II.A.5 were obtained using the Hvorslev model, the method of Bouwer and Rice (1976) would normally be employed if an unconfined boundary is suspected. Hyder and Butler (in review) provide a detailed discussion of the error introduced into parameter estimates using the Bouwer and Rice model.

The above discussion focusses on results when only a single boundary is influencing parameter estimates. In thin aquifers, one may face conditions when both the upper and lower boundaries are close enough to the screen to be affecting the slug test responses. Figure II.A.6 displays a plot of the hydraulic conductivity ratio versus aquifer thickness for the case of a screen 2.5 m in length located at the center of the unit. Clearly, in thin confined systems, the Hvorslev model provides estimates considerably less than the actual hydraulic conductivity of the aquifer. In thin unconfined systems,

the lower impermeable boundary acts in an opposite manner to the upper constant-head boundary so that the estimates are more reasonable than in the single boundary case. The results of this section indicate that, except in cases of very thin aquifers or screens located very close to a boundary, the assumption of a vertically infinite system does not introduce a large amount of error into the parameter estimates obtained using the Hvorslev model. Note that no analyses were performed in this section using the Cooper et al. (1967) model. In the previous section, a range of aspect ratios were defined for which the Cooper et al. model would provide reasonable estimates. Since boundaries in the vertical plane will only introduce sizable errors into parameter estimates when there is a considerable component of vertical flow, the effects of boundaries will be very small if the Cooper et al. model is only applied over the previously defined range.

Well Skin Effects

Figures II.A.2-6 display results for the case of slug tests performed in ideal, homogeneous aquifers. Often, however, as illustrated in Figure II.A.1, well drilling and development creates a disturbed, near-well zone (well skin) of properties differing from those of the formation as a whole. Depending on the drilling method, the method of well emplacement, the type of development activities, and the nature of the formation, this well skin can be either of lower or higher permeability than the formation in which the well is screened. Clearly, the effect of well skins on parameter estimates obtained from slug tests must be understood in order to avoid using parameter estimates representative of skin properties to characterize the formation as a whole.

Figure II.A.7 shows a plot of hydraulic conductivity ratio versus aspect ratio for a broad range of contrasts between the conductivity of the skin and that of the formation. As in the previous sections, the parameter estimates were obtained using the variant of the Hvorslev model given in (II.A.14). Note that the existence of a well skin can have a dramatic effect on the Hvorslev estimates. In the case of a skin of lower permeability than the formation, a conductivity estimate differing from the actual formation value by over an order of magnitude can easily be obtained. The difference is greatest at low aspect ratios because the low conductivity skin is suppressing vertical flow, which, as has been shown earlier, is most important under those conditions.

Figure II.A.8 displays a plot of a simulated slug test and the best-fit Hvorslev model, which is representative of all the low-conductivity skin cases shown in Figure II.A.7. As can be seen from Figure II.A.8, the Hvorslev model provides an excellent fit to the simulated data. In fact, a large number of additional simulations have shown that the Hvorslev fit for the low-conductivity skin case is almost always better than that

for the homogeneous-aquifer case. This is especially true at moderate to large aspect ratios where the response data for the homogeneous case generally will display a distinct concave upward curvature (e.g., Chirlin, 1989). When the vast majority of the flow is in the radial direction, an underlying assumption of the Hvorslev model is that there is an effective radius beyond which the slug-induced disturbance has no effect on aquifer heads. Clearly, in the low-conductivity skin case, this assumption is a very close approximation of reality. As shown in Figure II.A.9, almost all of the head drop occurs across the skin; heads in the formation are essentially unaffected by the slug test. Another major assumption of Hvorslev is that the specific storage of the formation can be neglected. In the case depicted in Figure II.A.9, the thickness of the skin is so small that one can essentially ignore the influence of skin storage properties on slug-test responses. Thus, the assumptions of the Hvorslev model actually appear to be more reasonable in the low-conductivity skin case than in the homogeneous-aquifer case. In fact, if one assumes an effective radius equal to the skin radius, the estimated conductivities will approximately equal the conductivity of the skin in the case of a skin two orders of magnitude less conductive than the formation (bottom dashed line in Figure II.A.7). Hyder and Butler (in review) show that a low-conductivity skin has a similar effect on parameter estimates obtained using the Bouwer and Rice (1976) method.

In the low-conductivity skin case, the Cooper et al. model will provide an estimate that is heavily weighted towards the conductivity of the skin (McElwee and Butler, 1992). Table II.A.2 summarizes the results of a series of analyses in which the Cooper et al. model is applied to the low-conductivity skin, large aspect ratio cases given in Figure II.A.7. Note that although certain authors (e.g., Faust and Mercer, 1984; Moench and Hsieh, 1985) state that the application of the Cooper et al. model to data from a well with a low-conductivity skin will enable a very good estimate of the conductivity of the formation to be obtained, such a result was not found in this work. As shown in Table II.A.2, the storage estimate will absorb a considerable amount of the skin effect if the storage estimate is assumed unknown and allowed to change to physically unrealistic values. Although the best-fit Cooper et al. model will closely match the simulated responses in this case, the conductivity estimate will still not be an accurate reflection of the formation conductivity. If the storage estimate is assumed known or constrained to physically realistic values, there will always be a considerable deviation between the best-fit Cooper et al. model and the response data in a manner similar to that shown in Figure II.A.10. At large aspect ratios, the combination of a very good Hvorslev fit and a systematic deviation between the Cooper et al. model and the test data appears to be a very good indication of a low-conductivity skin.

In the high-conductivity skin case, as shown in Figure II.A.7, parameter estimates will be greater than the formation conductivity as a result of a considerable amount of vertical flow along the more conductive skin. The difference will be greatest at low aspect ratios because of the greater importance of vertical flow under those conditions. Note that the difference between the parameter estimates obtained in the one-order and two-order more conductive skin cases becomes small at high aspect ratios because of the lessening importance of vertical flow. Figure II.A.11 displays a plot of the simulated response data and the best-fit Hvorslev model for the case of a high-conductivity skin. Clearly, the fit is much poorer than that shown in Figure II.A.8. The concave-upward curvature and the quality of the fit is more in keeping with what one would expect to see in the homogeneous case.

Since there is a very small head drop in the radial direction across a high-conductivity skin, the Hvorslev predictions for the high-conductivity skin case can be considerably improved by assuming the radius of the well screen equals the radius of the high-conductivity skin. As shown in Table II.A.3, very reasonable estimates can be obtained in the case of a skin one order of magnitude more conductive than the formation for moderate aspect ratios. As also shown in Table II.A.3, the Cooper et al. model using a well screen radius equal to the radius of the high-conductivity skin will provide excellent estimates of the formation conductivity at large aspect ratios. Unfortunately, as with the low conductivity skin case, there may be considerable uncertainty about the appropriate value for the skin radius. Clearly, bounding estimates can be obtained by using the radius of the sand pack as the minimum radius and a short distance into the formation as the maximum. Note that the high-conductivity skin cases considered here were based on the assumption that no seal or an inadequate one had been placed in the annular space above the screened interval. If there is an adequate seal in the annulus, little to no vertical flow will occur and the effect of the skin can be accounted for by simply adjusting the radius of the screen as described above.

SUMMARY AND CONCLUSIONS

A semianalytical solution to a general model describing the flow of groundwater in response to a slug test in a unfractured formation has been presented. The major motivation for the development of this model was the delineation of conditions in which the conventional methods for analysis of response data from slug tests were inappropriate. The results of the investigation described in this article can be summarized as follows:

1) In a homogeneous, isotropic aquifer, the Hvorslev model should provide acceptable estimates (within 25%) of the hydraulic conductivity of the formation for tests performed in wells with aspect ratios less than about 200. For tests performed in wells with higher aspect ratios, the Cooper et al. model will provide excellent conductivity estimates. Note that in formations with a large specific storage, the aspect ratio at which the Cooper et al. model provides better estimates than that of Hvorslev is much smaller;

2) In a homogeneous, anisotropic (degree of anisotropy unknown) aquifer, the Hvorslev model will provide acceptable estimates of the radial component of conductivity for aspect ratios between 50 and 200 if the effective radius of the test is assumed to be 200 times the well radius and the formation is assumed to be isotropic. The Cooper et al. model will provide very good estimates for aspect ratios greater than 100 (greater than 50 for strongly anisotropic systems);

3) In most cases, boundaries in the vertical plane will have little influence on parameter estimates obtained using conventional approaches. Only for tests performed in wells with small aspect ratios (i.e. $<$ 10-20) and screened intervals very close (i.e. within one or two meters) to one or both boundaries will the influence of the boundaries produce unacceptable parameter estimates. If the formation has any degree of anisotropy in hydraulic conductivity, the effect of the boundaries will be further limited;

4) In the case of a low conductivity skin, neither the Hvorslev nor the Cooper et al. model provide acceptable estimates of hydraulic conductivity of the formation. The Hvorslev model will produce an estimate very close to the conductivity of the skin if the effective radius is assumed equal to an approximate skin radius. If the storage parameter is constrained to physically reasonable values, the Cooper et al. model will provide estimates that are heavily weighted towards the conductivity of the skin. If the storage parameter is not constrained to the range of physical plausibility, conductivity estimates either higher or lower than the formation conductivity can be obtained using the Cooper et al. model;

5) In the case of a high conductivity skin, conventional models can provide acceptable estimates in many cases if the radius of the screen is set equal to an approximate skin radius. In the general case, the Hvorslev model should provide acceptable estimates for aspect ratios between 100 and 200. In skins only moderately more conductive than the formation (i.e. conductivities within an order of magnitude of each other) and/or when an adequate seal has been placed in the annulus above the screened interval, the Hvorslev model will provide acceptable estimates for aspect ratios as small as 20. The Cooper et al. model will provide excellent estimates of formation conductivity for aspect ratios greater than 200.

As described above, there are many conditions under which the conventional models can provide acceptable parameter estimates. If it does appear that the conventional models will provide acceptable results for a given configuration, they should always be used. Only in cases where it does not appear that conventional approaches can provide acceptable results should the model developed here be employed. This recommendation is based on the principle of parsimony. The model developed here has more parameters than the conventional approaches and thus may be somewhat more difficult to use for parameter estimation. If it is unclear if conventional approaches can be employed in a certain configuration, the model developed here can be used to quickly assess the error that is introduced by employing a particular model to analyze a hypothetical test in a configuration similar to the conditions expected in the field.

Clearly, this investigation has shown that the most worrisome condition for slug tests in unfractured media is that of a low conductivity skin. None of the conventional models provide reasonable estimates in the presence of a low conductivity skin. However, rather than immediate application of the model developed here, which requires five parameters in the skin case, we recommend that the data be first analyzed with the Hvorslev model using an effective radius equal to the best estimate of the skin radius. Then, assuming the skin conductivity is known, one can employ the model of Ramey et al. (1975), which assumes the skin is of an infinitely small radius. In this case, the number of estimated parameters has been reduced from five to two (conductivity and specific storage of formation). Moench and Hsieh (1985) have shown that the infinitely thin skin model is appropriate for most open-hole slug tests. Unfortunately, this approach would not be appropriate for pressurized slug tests, so the model developed here would be required.

The second most worrisome case is that of slug tests in wells with small aspect ratios in homogeneous, anisotropic systems. Unless there is some additional information on the degree of anisotropy, one may have considerable difficulty in obtaining reliable estimates of the radial component of hydraulic conductivity. This is primarily due to the correlation between the effects of the radial and vertical components of conductivity on the response data. McElwee and Butler (1993) propose multiwell slug-test approaches based on the model developed here that can be employed to separate the radial and vertical components of hydraulic conductivity.

Note that the results of this study must be considered in the light of the three major assumptions used in the mathematical definition of the slug-test model employed in this work. First, in equation (II.A.7), we assumed a uniform hydraulic gradient along the well screen as a mathematical convenience. In actuality, one would suspect that the

gradient would be larger at either end of the screen producing a U-shaped profile in the vertical plane. However, Butler et al. (1993) have performed detailed simulations with a numerical model to show that the hydraulic gradient along the well screen can be closely approximated by a boxcar function for aspect ratios greater than one. Thus, the use of this mathematical convenience introduces a negligible degree of error to the results reported here and virtually all practical applications.

Second, in equations (II.A.8) and (II.A.9), we assumed that the skin fully penetrates the formation being tested. Although this assumption is appropriate for the case of multilevel slug tests performed in a well fully screened across the formation, it is clearly not representative of reality in the general case. In the case of a low-conductivity skin, this assumption is of little significance since a low-conductivity skin will constrain flow to the horizontal plane. In the case of a high-conductivity skin, however, this assumption will produce considerably more vertical flow in the skin than would actually occur. Butler et al. (1993) have shown through numerical simulation that a slug test performed in a partially penetrating well with a high conductivity skin that extends to the bottom of the screen is indistinguishable from a slug test performed in a configuration similar except that the well screen terminates against a lower impermeable layer. Thus, for the high conductivity skin cases examined here, the slug tests were simulated assuming that the screen abutted against a lower impermeable layer. Note that this approach is only appropriate for a skin an order of magnitude or more conductive than the formation as a whole. This approach would not be appropriate for the case of a skin of only slightly higher conductivity than the formation.

Third, in equation (II.A.11), we assumed that the water table could be represented as a constant-head boundary. Given the small amount of water that is introduced to/removed from a well during a slug test, this assumption is considered reasonable under most conditions. The cases in which this assumption may be suspect are that of a well that is screened across the water table or a well screened over a deeper interval with a gravel pack that extends above the water table. Ongoing numerical and field investigations are currently being undertaken to assess the error that is introduced through this assumption and to suggest approaches for data analysis when that error is unacceptably large.

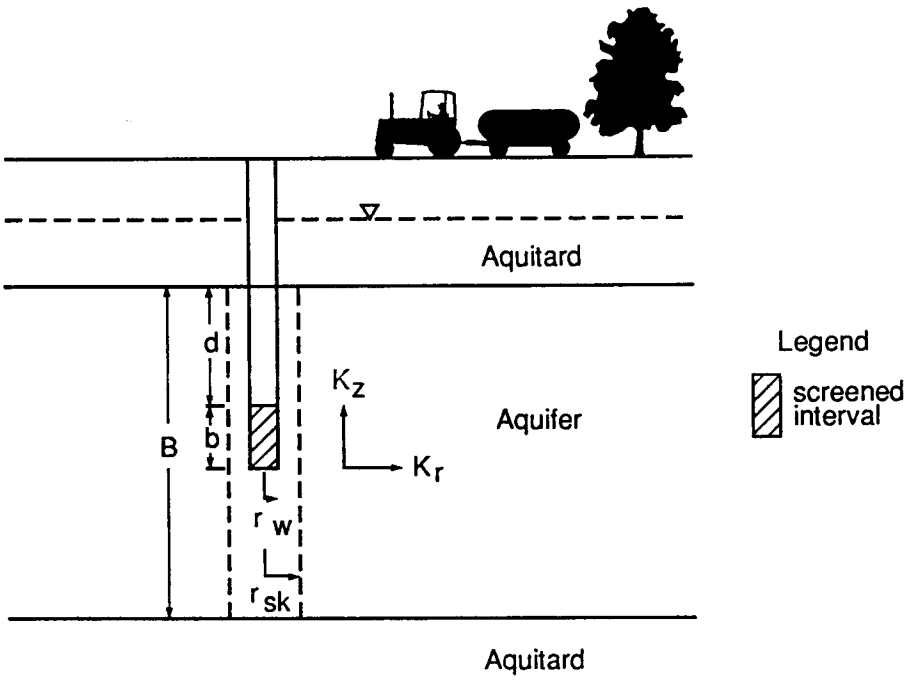

FIGURE II.A.1 - Cross-sectional view of a hypothetical confined aquifer (notation explained in text).

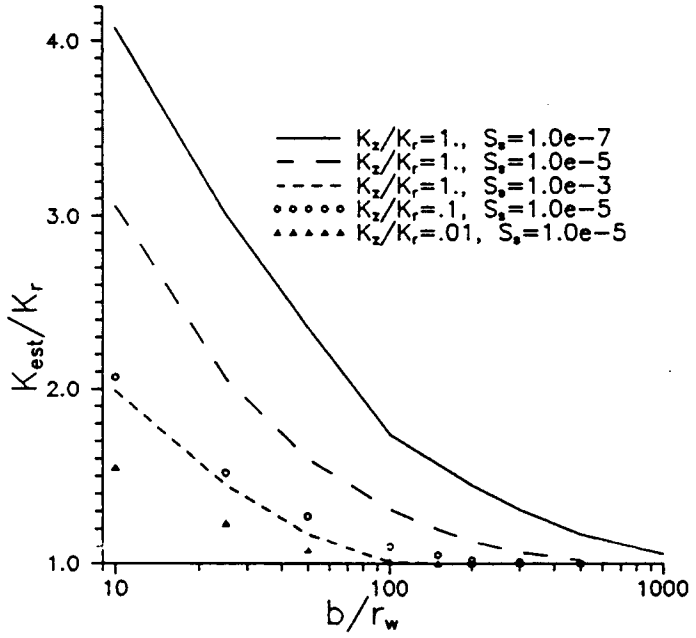

FIGURE II.A.2 - Plot of conductivity ratio (Cooper et al. estimate (K_{est}) over actual conductivity (K_r)) versus aspect ratio (b/r_w) for the case of a well screened at the center of a very thick aquifer.

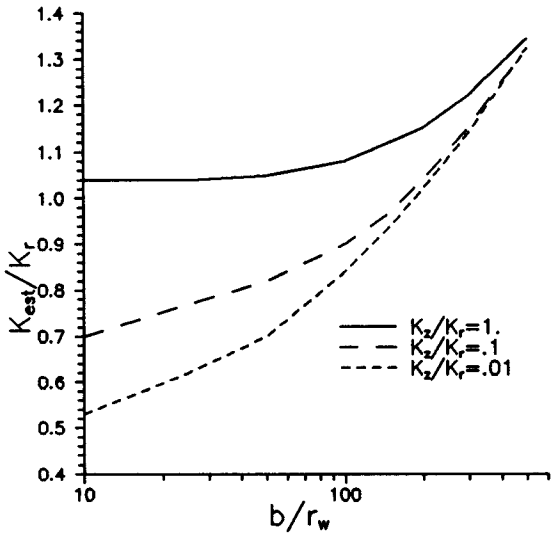

FIGURE II.A.3a - Plot of conductivity ratio (Hvorslev estimate (K_{est}) over actual conductivity (K_r)) versus aspect ratio (b/r_w) for the case of a well screened at the center of a very thick aquifer using Hvorslev estimates obtained with equation (14).

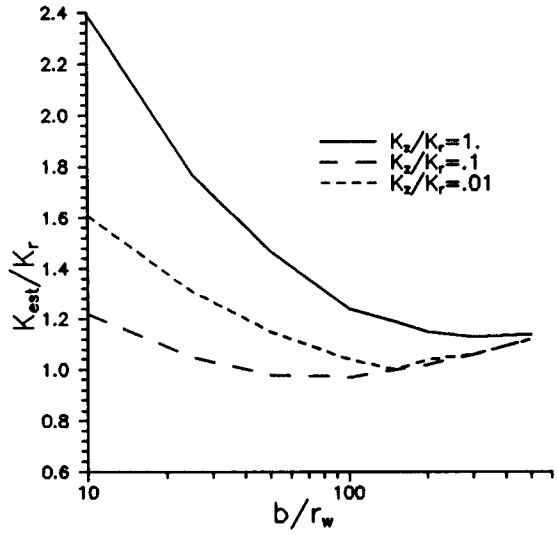

FIGURE II.A.3b - Plot of conductivity ratio (Hvorslev estimate (K_{est}) over actual conductivity (K_r)) versus aspect ratio (b/r_w) for the case of a well screened at the center of a very thick aquifer using Hvorslev estimates obtained assuming an effective radius equal to $200r_w$.

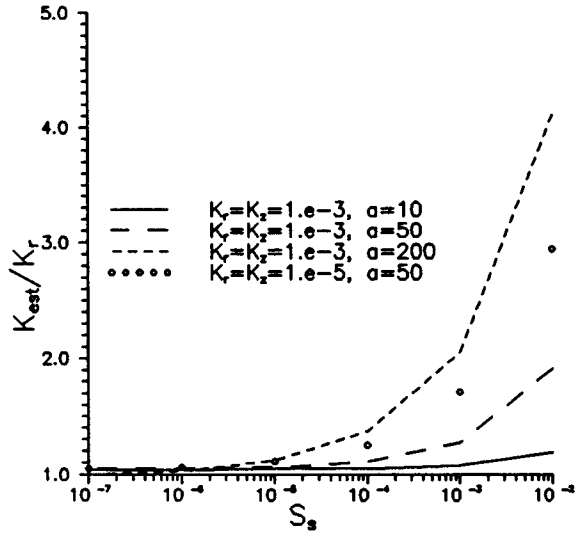

FIGURE II.A.4 - Plot of conductivity ratio (Hvorslev estimate (K_{est}) over actual conductivity (K_r)) versus specific storage for the case of a well screened at the center of a very thick aquifer.

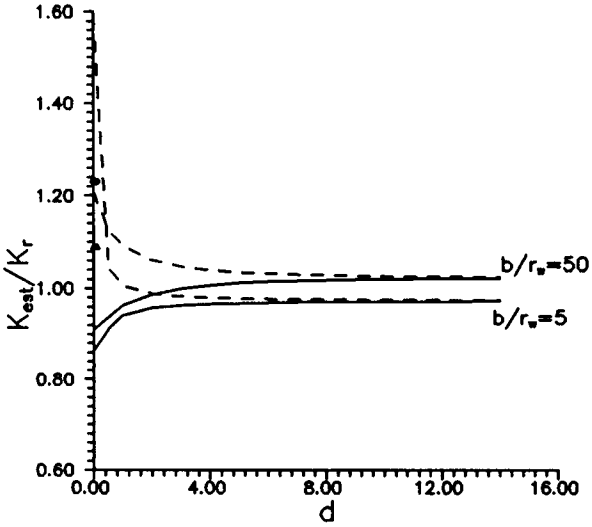

FIGURE II.A.5 - Plot of conductivity ratio (Hvorslev estimate (K_{est}) over actual conductivity (K_r)) versus depth below upper boundary (solid lines designate confined case, dashed lines designate unconfined case; circles and triangles designate estimates obtained using the semi-infinite variant of the Hvorslev model for aspect ratios of 5 and 50, respectively).

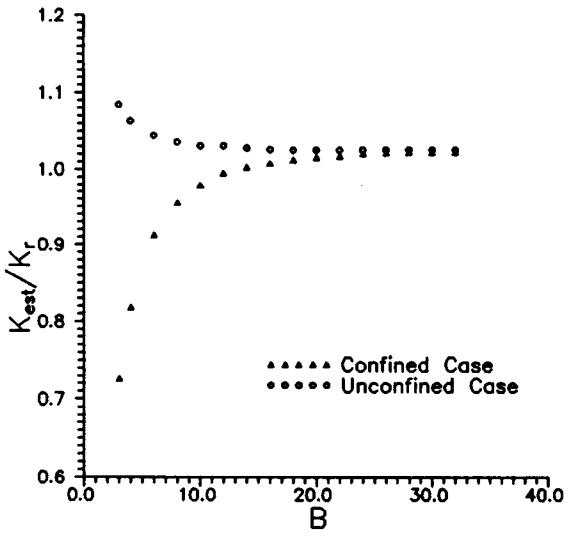

FIGURE II.A.6 - Plot of conductivity ratio (Hvorslev estimate (K_{est}) over actual conductivity (K_r)) versus aquifer thickness (b/r_w=50).

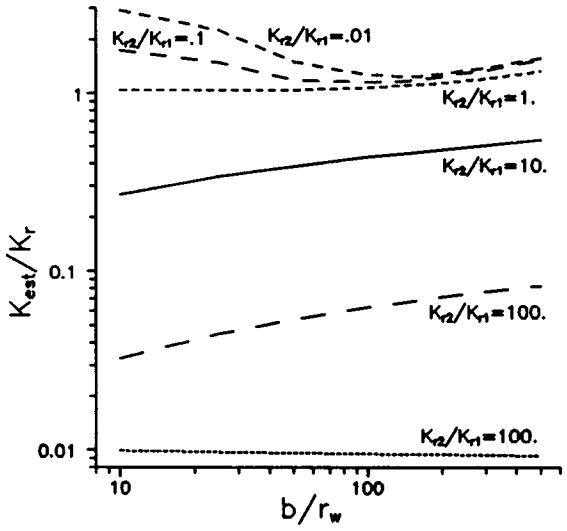

FIGURE II.A.7 - Plot of conductivity ratio (Hvorslev estimate (K_{est}) over actual formation conductivity (K_r)) versus aspect ratio for the case of high and low conductivity well skins (r_{sk}=.10 m; bottom dashed line designates Hvorslev estimates obtained assuming an effective radius equal to r_{sk}).

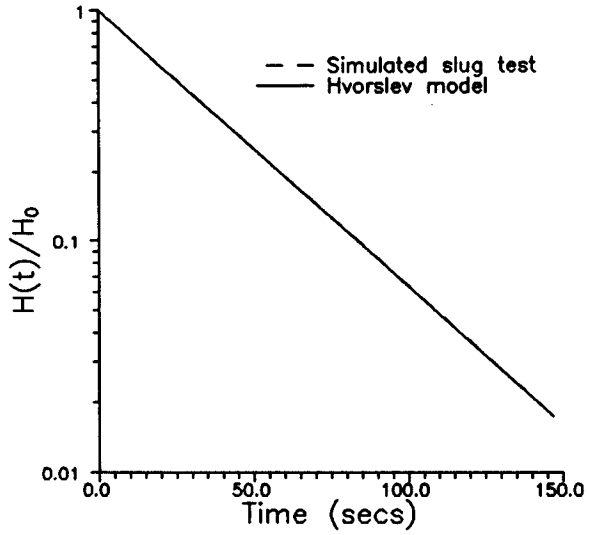

FIGURE II.A.8 - Normalized head versus time plot of simulated slug-test data and the best-fit Hvorslev model for the case of a skin two orders in magnitude less conductive than the formation (b/r_w = 50, r_{sk}=.10 m).

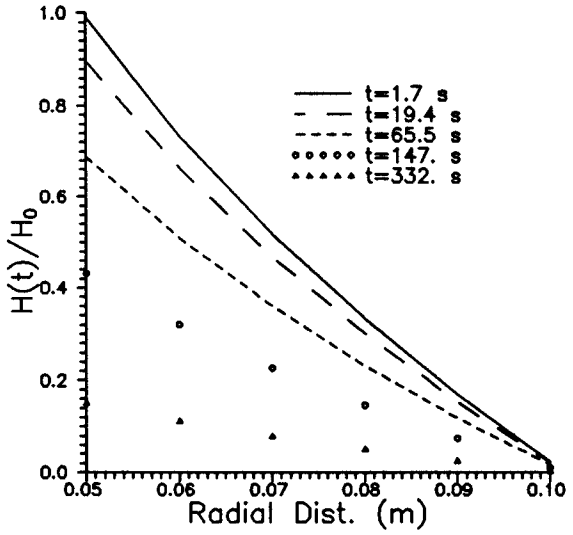

FIGURE II.A.9 - Plot of normalized head versus radial distance from the stressed well for the case of a skin two orders in magnitude less conductive than the formation (b/r_w = 50, r_{sk}=.10 m).

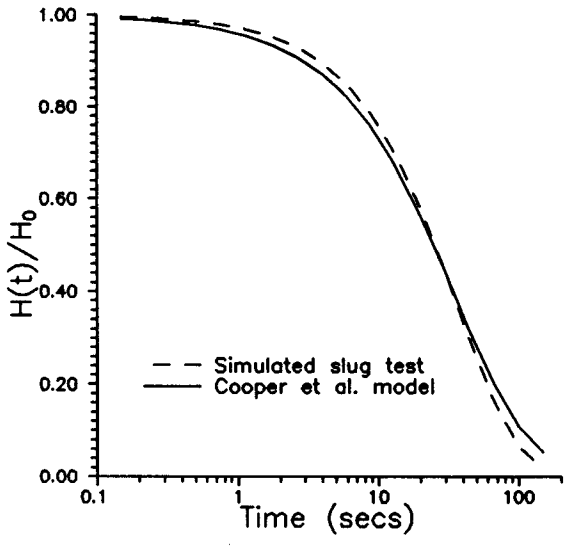

FIGURE II.A.10 - Normalized head versus time plot of simulated slug-test data and the best-fit Cooper et al. model for the case of a skin two orders in magnitude less conductive than the formation (b/r_w = 50, r_{sk}=.10 m).

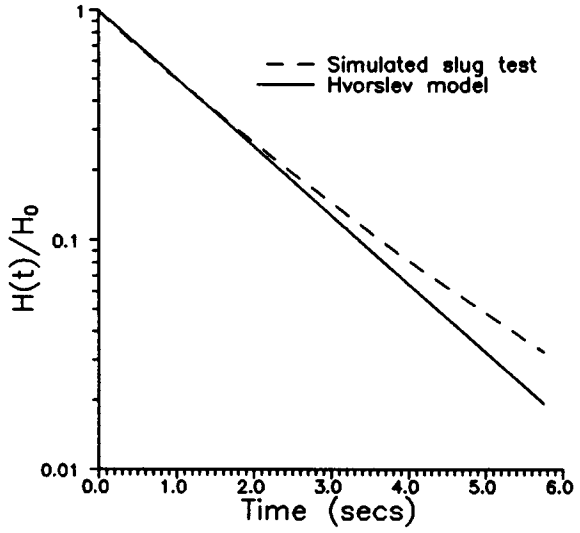

FIGURE II.A.11 - Normalized head versus time plot of simulated slug-test data and the best-fit Hvorslev model for the case of a skin two orders in magnitude more conductive than the formation (b/r_w = 50, r_{sk}=.10 m).

$K_r = K_z = .001$ m/s;

$S_s = .00001$ /m;

$r_w = r_c = .05$ m.

TABLE II.A.1 - Parameter set used as base case for all simulations.

b/r_w	K_{cst}/K_r	S_s
	$K_{r1} = .0001$ m/s, S_s unknown	
200	2.35	2.73e-23
300	1.75	6.26e-18
500	1.21	5.24e-13
	$K_{r1} = .00001$ m/s, S_s unknown	
200	.473	1.00e-30
300	.469	1.00e-30
500	.466	1.00e-30
	$K_{r1} = .0001$ m/s, S_s known	
200	.466	1.00e-05
300	.442	1.00e-05
500	.417	1.00e-05
	$K_{r1} = .00001$ m/s, S_s known	
200	.070	1.00e-05
300	.067	1.00e-05
500	.063	1.00e-05

TABLE II.A.2 - Results of a series of analyses in which the Cooper et al. model is applied to the low-conductivity skin, large aspect ratio cases of Figure II.A.7.

b/r_w	K_{HV}/K_{r2}	K_{CBP}/K_{r2}
	K_{r1} = .01 m/s	
10	1.25	4.63
50	0.99	1.59
100	0.99	1.22
200	1.09	1.05
500	1.38	0.99
	K_{r1} = .1 m/s	
10	2.09	7.73
50	1.25	2.02
100	1.09	1.35
200	1.13	1.09
500	1.41	1.01

TABLE II.A.3 - Results of a series of analyses in which the Hvorslev and Cooper et al. models (assuming $r_w=r_{sk}$) are applied to the high-conductivity skin cases of Figure II.A.7.

B. THE USE OF SLUG TESTS TO DESCRIBE VERTICAL VARIATIONS IN HYDRAULIC CONDUCTIVITY

Abstract

Multilevel slug tests provide one means of obtaining estimates of hydraulic conductivity on a scale of relevance for contaminant transport investigations. In this section, a numerical model is employed to assess the potential of multilevel slug tests to provide information about vertical variations in hydraulic conductivity under conditions commonly faced in field settings. The results of the numerical simulations raise several important issues concerning the effectiveness of this technique. If the length of the test interval is on the order of the layer thickness, considerable error may be introduced into the conductivity estimates due to the effects of adjoining layers. The influence of adjoining layers is dependent on the aspect ratio (length of test interval/well radius) of the test interval and the flow properties of the individual layers. If a low permeability skin is present at the well, the measured vertical variations will be much less than the actual due to the influence of the skin conductivity on the parameter estimates. A high permeability skin can also produce apparent vertical variations that are much less than the actual due to water flowing vertically along the conductive skin. In cases where the test interval spans a number of layers, a slug test will yield an approximate thickness-weighted average of the hydraulic conductivities of the intersected layers. In most cases, packer circumvention should not be a major concern when packers of .75 m or longer are employed. Several of the results of this study are substantiated by recently reported field tests that demonstrate the importance of well emplacement and development activities for obtaining meaningful estimates from a program of multilevel slug tests.

Introduction

Over the last decade, a considerable amount of theoretical, laboratory, and field research on the mechanisms of large-scale solute transport has identified the spatial distribution of hydraulic conductivity as a significant factor in determining how a plume of a conservative tracer will move in the subsurface (e.g., Freyberg, 1986; Gelhar, 1986; Dagan, 1986; Moltyaner and Killey, 1988; Hess et al., 1992). The measurement of hydraulic conductivity in the subsurface on a scale of relevance for contaminant transport investigations, however, has proven to be a rather difficult task. Conventional pumping tests will provide large-scale volumetric averages of hydraulic conductivity, which may be of rather limited use in transport investigations (e.g., Butler and Liu, 1993). Multiwell tracer tests, which can provide information on the average interwell

conductivity, are rather expensive in terms of time, money, and effort. Other techniques are needed if information on conductivity variations is to be used by practicing hydrogeologists outside of the research community.

Techniques that have been reported on in the literature include multilevel (straddle-packer) slug tests, borehole flowmeter surveys, laboratory core analyses, correlation with geophysical logs, and a variety of single-well tracer tests. Melville et al. (1991) describe a program of multilevel slug tests at a research site and show that the results compare favorably with the information obtained from a large-scale multiwell tracer test. A number of workers in both the petroleum and groundwater fields (e.g., Hufschmied, 1986; Ehlig-Economides and Joseph, 1987; Morin et al., 1988; Rehfeldt et al., 1989; Molz et al., 1989; Hess et al., 1992) have shown that borehole flowmeters have the potential to provide detailed information about the vertical variations in hydraulic conductivity at a well. Laboratory analysis of sampled cores is undoubtedly the most common method of assessing vertical variations in hydraulic conductivity. However, the collection of reasonably intact cores in permeable unconsolidated materials, the geologic media in many contaminant transport investigations, can be a rather difficult task (e.g., Zapico et al., 1987; McElwee et al., 1991). In addition, the time and expense of performing permeameter analyses on a complete set of cores can be considerable. Taylor et al. (1990) describe several recently developed techniques for characterizing vertical variations in hydraulic conductivity. One particularly interesting approach is the single-well electrical tracer test (Taylor and Molz, 1990), which involves using a focussed induction downhole probe to measure changes in electrical conductivity as an electrically conductive tracer moves away from the borehole.

The focus of this article is on an evaluation of multilevel slug tests to provide information about vertical variations in hydraulic conductivity. Slug tests have both economic and logistical advantages over the other techniques described in the previous paragraph. A logistical advantage that cannot be overemphasized for waste-site investigations is that a slug test can be configured so that water is neither added nor removed from the test well. Such a slug test can be initiated by introducing/removing an object of known volume to/from the water column or by pneumatic means (e.g., Orient et al., 1987; McLane et al., 1990). Problems arising due to the injection of waters of different compositions or the disposal of potentially contaminated waters can thus be avoided. In addition, the analysis of data from a series of multilevel slug tests may be more straightforward than data from a flowmeter survey since the head measurements are not taken in a well being actively pumped.

A number of authors have examined multilevel slug tests or the related multilevel

constant-head injection tests using both analytical and numerical approaches. In terms of analytical approaches, Dagan (1978) employed Green's functions and a steady-state approximation to simulate tests in partially penetrating wells in unconfined flow systems. Dougherty and Babu (1984) present a fully transient analytical solution for slug tests performed in partially penetrating wells in isotropic confined systems. Hayashi et al. (1987) develop an analytical solution for multilevel slug tests in vertically unbounded, isotropic confined systems that explicitly includes the effects of packers above and below the test zone. Butler et al. (1990) present a solution for slug tests in partially penetrating wells in vertically bounded, anisotropic confined units that includes the effect of a finite-radius well skin (a revised form of this solution is discussed in Section II.A of this report). None of the above contributions, however, consider the effects of formation layering due to the difficulty of incorporating a general representation of formation layering into an analytical solution. Karasaki (1986) looked at the effect of layering on a slug test performed in a well that is fully screened across a layered aquifer in which flow is only in the radial direction. An extension to the general case of unrestricted flow in the vertical direction has apparently not been attempted.

In terms of numerical approaches, Braester and Thunvik (1984) present results of a series of transient numerical simulations of multilevel constant-head injection tests. In a somewhat similar study, Bliss and Rushton (1984) used a steady-state model to simulate constant-head injection tests in a fractured aquifer. More recently, Widdowson et al. (1990) used a steady-state numerical model to develop an approach for analyzing multilevel slug tests based on a method similar to that of Dagan (1978). Melville et al. (1991) employ this approach to analyze multilevel slug tests from an experimental field site.

Although several of the articles cited in the previous paragraphs have touched upon important aspects of the issue of the viability of multilevel slug tests, there are still many unanswered questions about the usefulness of the information provided from such tests under conditions commonly faced in the field, where anisotropy, layering, and well skins of either higher or lower permeability than the undamaged formation may be influencing the measured response data. The purpose of this article is to address many of these questions in the context of a theoretical assessment of the potential of multilevel slug tests to provide information about vertical variations in hydraulic conductivity in the vicinity of the well bore. Since no general analytical solution has been developed for the case of slug tests in layered aquifers, this assessment will be performed through numerical simulation. The major objectives of this work are 1) to assess possible techniques for the analysis of slug tests in layered systems; 2) to evaluate the effects of

various geologic features (e.g., density of layering, anisotropy within layers, distance from boundaries, etc.) and well-construction features (e.g., well skins, length of the test interval, etc.) on the parameters estimated from slug-test data; 3) to explore the nature of vertical averaging in slug tests in layered aquifers; 4) to assess the effects of packer length and determine under what conditions packer circumvention may be an important mechanism; and 5) to make recommendations for the performance of multilevel slug tests in layered systems that can be utilized by the field practitioner.

Problem Statement

The problem of interest here is that of the head response, as a function of r, z, and t, produced by the introduction of an instantaneous slug of water in a portion of the screened interval of a well. As shown in Figure II.B.1, the portion of the screened interval through which the slug is introduced is isolated from adjacent screened sections of the well by a pair of inflatable packers (straddle packer). Different intervals of the screen can be tested by moving the string of packers and pipes up and down in the well. A third packer is set above the top of the screen, isolating the well casing from the screened sections of the well outside of the test interval. Note that this configuration is in keeping with that commonly used in the field for multilevel slug tests (e.g., Melville et al., 1991; Butler and McElwee, 1992). In this analysis, flow properties are assumed to be invariant in the angular direction and radial variations are limited to changes between a well skin created during drilling and development and the adjacent formation. Variations in flow properties of any magnitude are allowed between layers in the vertical direction.

The partial differential equation representing the flow of groundwater in response to an instantaneous slug of water introduced at a central well is

$$\frac{\partial}{\partial r}\left(K_r \frac{\partial h}{\partial r}\right) + \frac{K_r}{r}\frac{\partial h}{\partial r} + \frac{\partial}{\partial z}\left(K_z \frac{\partial h}{\partial z}\right) = S_s \frac{\partial h}{\partial t} \qquad \text{(II.B.1)}$$

where h is the hydraulic head, [L]; K_r is the component of hydraulic conductivity in the radial direction, [L/T]; K_z is the component of hydraulic conductivity in the vertical direction, [L/T]; S_s is the specific storage, [1/L]; t is the time, [T]; r is the radial direction, [L]; and z is the vertical direction, [L].

The initial conditions can be written as

$$h(r,z,0)=0,\ r_w<r<\infty,\ 0<z<B \tag{II.B.2}$$

$$h(r_w,z,0) = \begin{cases} H_0,\ a \le z \le a+b \\ 0,\ \text{elsewhere} \end{cases} \tag{II.B.3}$$

where r_w is the radius of the screen in the test interval, [L]; B is the thickness of the aquifer, [L]; H_0 is the height of the initial slug, [L]; a is the distance of the bottom of the test interval above the base of the aquifer, [L]; and b is the width of the test interval, [L].

The boundary conditions are the following:

$$h(\infty,z,t) = 0,\ t > 0,\ 0 < z < B \tag{II.B.4}$$

$$\frac{\partial h(r,0,t)}{\partial z} = \frac{\partial h(r,B,t)}{\partial z} = 0,\ r_w < r < \infty,\ t > 0 \tag{II.B.5}$$

$$h(r_w,z,t) = H(t),\ t > 0,\ a \le z \le a+b \tag{II.B.6}$$

$$2\pi r_w \int_a^{a+b} K_r \frac{\partial h(r_w,z,t)}{\partial r} dz = \pi r_c^2 \frac{dH(t)}{dt} \tag{II.B.7}$$

$$\frac{\partial h(r_w,z,t)}{\partial r} = 0, t>0, a-p \le z < a,\ a+b < z \le a+b+p \tag{II.B.8}$$

$$\frac{\partial h(0,z,t)}{\partial r} = 0,\ t>0,\ 0 < z < a-p \qquad \text{(II.B.9)}$$

$$\frac{\partial h(r_p,z,t)}{\partial r} = 0,\ t>0,\ a + b + p < z < B \qquad \text{(II.B.10)}$$

where H(t) is the head within the well in the test interval, [L]; r_c is the radius of the cased portion of the well above the upper packer, [L]; r_p is the radius of the pipe through which the slug has been introduced to the test interval, [L]; and p is the length of the straddle packer, [L]. Note that conditions (II.B.8)-(II.B.10) are a no-flow condition for the portion of the screen sealed by the packers, a symmetry boundary below the packers, and a no-flow condition along the pipe connecting the straddle packers to the upper packer, respectively.

Equations (II.B.1)-(II.B.10) describe the flow conditions of interest here. Given the generality of the property variations allowed in the vertical direction, analytical approaches are not feasible. Thus, for this work, a numerical model was employed in order to obtain approximate solutions to the mathematical model represented by the above equations.

Numerical Model

In this work, a cylindrical-coordinate, three-dimensional, finite-difference model (3DFDTC), developed at the Kansas Geological Survey (Butler and McElwee, 1992), was employed to simulate multilevel slug tests. The model was centered on the well in which the slug tests were being performed. The influence of well bore storage is taken into consideration using an approach based on earlier work of Settari and Aziz (1974), Rushton and Chan (1977), and Butler (1986). As described by Butler (1986), the approach is based on rewriting the classical pipe flow equation (Vennard and Street, 1975) in a Darcy Law like formulation and defining a term (involving the friction factor, the cross-sectional area of the well bore, and distance along the well bore) analogous to hydraulic conductivity. This approach allows flow inside the well bore to be governed by the porous media flow equation (equation (II.B.1)). Note that the implementation of this approach for this study produces an approximation of well-bore behavior that is equivalent to the hydrostatic head assumption employed in most analytical representations of the well bore (e.g., Papadopulos and Cooper, 1967; Cooper et al., 1967).

In order to demonstrate the validity of the well-bore approximation, the model has been checked against many analytical solutions for both pumping and slug tests. Figure

II.B.2 displays the results of two such comparisons. The first example illustrates model performance when the hydraulic conductivity of adjacent grid cells differs by several orders of magnitude. A slug test in a well surrounded by a low permeability well skin of finite radius was simulated. The well was assumed to be screened throughout the aquifer. Figure II.B.2a illustrates a comparison of the heads simulated by 3DFDTC with the results from the analytical solution of Moench and Hsieh (1985) for a slug test in a well with a skin of finite radius. The plots of the results essentially fall on top of one another. The small differences that do exist are attributed mainly to the error caused by the spatial discretization scheme employed in 3DFDTC. Further simulations have shown that by increasing the number of nodes in the radial direction, the difference between the analytical solution and 3DFDTC results will gradually disappear.

The second example is selected to illustrate model performance when there is a strong component of vertical flow, such as might occur in multilevel slug tests. A slug test is simulated in a well that is screened for only a portion of the aquifer thickness. The aquifer is assumed to be homogeneous and isotropic with respect to flow properties. Figure II.B.2b displays a comparison of the heads simulated by 3DFDTC with the results of the analytical solution of Butler et al. (1990) for a slug test in a well partially penetrating a confined aquifer. As with the previous example, 3DFDTC yields results that are essentially indistinguishable from those of the analytical solution. Note that the error introduced by the radial discretization scheme employed in these examples was considered acceptable for the purposes of this work. Further issues concerning the vertical discretization scheme are discussed in a later section.

Techniques for Analysis of Slug Tests in Layered Systems

The approach employed in this research was to simulate a series of multilevel slug tests using the 3DFDTC model and then estimate the hydraulic conductivity of the portion of the formation opposite the screened interval from the simulated results. Several methods were considered for the analysis of the simulated slug-test results. The analytical solution of Cooper, Bredehoeft, and Papadopulos (CBP) (Cooper et al., 1967) for the case of a slug test in a well fully screened across a perfectly confined uniform aquifer was initially employed. Figure II.B.3a shows the results of a series of trial simulations to evaluate the CBP approach for this application. In this case, a series of multilevel slug test simulations was run in a layered aquifer using a test interval that is 2.5 times the well radius (aspect ratio = test interval length/well radius = 2.5). As a result of the small aspect ratio, there was a considerable amount of vertical flow at either end of the test interval. Figure II.B.3a clearly demonstrates that the analysis of

multilevel slug tests under the assumption of negligible vertical flow can result in a significant overestimation of the horizontal hydraulic conductivity. Note that the overestimation of K_r is worse under isotropic conditions than under anisotropic conditions as a result of the flow being increasingly constrained to the horizontal plane as the ratio of vertical to hydraulic conductivity decreases. Figure II.B.3b presents the simulated and CBP best-fit head values for two of the simulations included in Figure II.B.3a. The CBP model heads consistently fall below the simulated heads early in the test and above the simulated heads later in the test. This systematic lack of fit, which was seen in all of the analyses, is the result of neglecting the vertical component of flow.

Although the CBP model is clearly an overly simplified representation of the flow system, analyses of slug-test responses using this model do provide at least a gross picture of vertical variations in conductivity. Given this situation, it is reasonable to assume that analyzing the slug-test data with a more appropriate model, i.e. one that accounts for the vertical component of flow, would reduce the overestimation of K_r. Several additional models, which incorporate partial penetration effects, were considered here for use in the analysis of multilevel slug-test data.

Hvorslev (1951) developed a model for the analysis of slug tests performed in a screened interval of finite length in a uniform, vertically unbounded, medium with a vertical to horizontal anisotropy in hydraulic conductivity. A major assumption of the Hvorslev approach is that the specific storage of the aquifer can be neglected. Since the head response at the stressed well is relatively insensitive to specific storage, this assumption may be acceptable in many cases. Figure II.B.4a shows the results of Hvorslev analyses of the same simulated tests as employed in Figure II.B.3a. Note that the Hvorslev model requires the use of a "shape factor", which is related to the geometry of the well intake region. The shape factor used here is that for Case 8 described in Hvorslev (1951). The Hvorslev function for this case is in the form of a two-parameter (K_r and anisotropy ratio) model. Unfortunately, the two parameters are perfectly correlated, so they cannot be estimated independently. For the analyses presented in Figure II.B.4a, three different values of the anisotropy ratio are employed. The true value of the ratio of horizontal to vertical conductivity is 10. As shown in Figure II.B.4a, the resulting overestimation or underestimation of K_r is not strongly influenced by the improper specification of the anisotropy ratio. The correlation between the two parameters is also apparent, since the estimated hydraulic conductivity changes by a multiplicative constant for all analyses as a result of using a different value for the anisotropy ratio. Even when using only a rough approximation of the actual anisotropy ratio, it is clear that the solution of Hvorslev provides estimates considerably better than

those of the CBP model. Figure II.B.4b shows the Hvorslev model fits for the same intervals as given in Figure II.B.3b for the CBP analyses. The plots, displayed in the format used with the CBP model, are for the case in which the true anisotropy ratio is known. The fitted results, however, would be essentially identical for all values of the anisotropy ratio, due to the perfect correlation between the model parameters. A comparison of Figures II.B.3 and II.B.4 indicates that use of the Hvorslev model improves the estimates of K_r and provides a better fit to the observed data.

As discussed in the introduction, Butler et al. (1990) have developed an analytical solution for slug tests in partially penetrating wells with skins, which can be readily configured to analyze data from multilevel slug tests in homogeneous, anisotropic aquifers (an revised version of this model is presented in Section II.A of this report). Although this solution avoids the simplifying approximations of the Hvorslev approach, the calculated parameters are not significantly different from those estimated using the model of Hvorslev. One major drawback of this model is that it is computationally intensive as a result of the use of both Fourier and Laplace integral transforms to obtain the solution. Given the computationally intensive nature of the solution and the fact that the estimated parameters are not significantly different from those of Hvorslev, the model of Hvorslev was considered more appropriate for the purposes of this work.

Dagan (1978) and Widdowson et al. (1990) have developed techniques for the analysis of multilevel slug tests that are based on a series of graphs/charts developed from simulation of slug tests under conditions similar to those considered by Hvorslev (1951). Given the similarity to the approach of Hvorslev and since additional simulations are required for each new configuration, the model of Hvorslev was considered more appropriate for the purposes of this work.

Given its advantages of computational efficiency and acceptable accuracy, the Hvorslev model was considered the most appropriate model for use here. Thus, in the remainder of this paper, the Hvorslev model is employed for the analysis of simulated slug-test responses. The analyses were performed using the implementation of the Hvorslev model found in the SUPRPUMP automated well-test analysis package of the Kansas Geological Survey (Bohling and McElwee, 1992). This use of the Hvorslev model, however, should not be considered a blanket endorsement of the approach as the model must be used with caution when analyzing actual field data due to its neglect of storage effects on slug-test responses (Chirlin, 1989), its poor performance in the presence of a well skin (Butler et al., 1990), and its increasing error in wells with small aspect ratios (Hvorslev, 1951).

Dependence of Multilevel Slug Test Results on Aspect Ratio and Formation Boundaries

An initial series of simulations was performed in order to assess the dependence of conductivity estimates on the aspect ratio (b/r_w) and on proximity to a horizontal impermeable boundary. Figure II.B.5 presents the results of a set of simulations in which the effects of the magnitude of the aspect ratio on slug tests in a uniform aquifer are investigated. This figure indicates that the largest difference between the estimated K_r and the true K_r is at small aspect ratios (short test intervals). As mentioned by Hvorslev (1951), the error introduced by the approximations incorporated in the shape function used here is largest at small aspect ratios. It is apparent from Figure II.B.5 that the approximations are certainly acceptable for aspect ratios greater than four or five.

Figure II.B.6 presents the results of simulations designed to examine the effects of impermeable boundaries on slug-test estimates. A number of simulations were performed in the uniform aquifer configuration employed in Figure II.B.5 using a test interval one meter in length, with the test interval being progressively moved from the center of the aquifer to the upper impermeable boundary. A test interval with a small aspect ratio (=2.5) was employed in order to emphasize the effects of vertical flow. The boundary effects are straightforward. As the test interval approaches the boundary, the vertical flow out of the interval is constrained, resulting in a decrease in the K_r estimate. Note that these results were obtained assuming a test interval with a small aspect ratio and an isotropic aquifer. The effect of impermeable horizontal boundaries is less dramatic with larger aspect ratios and/or the presence of a pronounced anisotropy ($K_r > K_v$). In most cases, slug tests performed in an interval several meters below an impermeable boundary should not be significantly affected by the boundary.

Dependence on Density of Layering

The simulations discussed above illustrate the performance of multilevel slug tests in ideal homogeneous systems. Many aquifers in nature, however, consist of layers of differing flow properties. In this section, a set of simulations designed to investigate the effect of layering density on multilevel slug tests is described. For these simulations, the test interval length is constrained to be less than or equal to the layer thickness, which is assumed to be constant for any particular simulation. In a later section, simulations using test intervals of lengths greater than the layer thickness are described. In all cases, the results of these simulations are displayed as the range of conductivities estimated from a series of slug tests performed as the packer string was moved in small increments up the well bore. Figure II.B.7 displays a plot of hydraulic conductivity values estimated

from such a series of multilevel slug-test simulations. The results are shown for just one pair of a series of alternating high and low conductivity layers in order to clarify the definition of the range as the distance between the peak and trough of the conductivity versus depth plot. Note that all simulations discussed in the remainder of this paper were performed with test intervals at a large enough distance from an impermeable boundary that boundary effects were negligible.

The modelled configuration consisted of an aquifer made up of alternating layers of constant thickness consisting of two distinct materials (denoted here as A and B). The model parameters are listed in Table II.B.1. A grid of 20 nodes in the radial (same discretization scheme as used in simulations of Figure II.B.2) and 48-96 nodes in the vertical directions was employed. The number of nodes in the vertical varied depending on the layering and test interval length used in a particular scenario. In order to assess the error introduced by the various vertical discretization schemes, a number of additional simulations were performed using increasingly finer vertical discretization. In all cases, the discretization schemes used here were found to introduce an error of less than 2% to the calculated parameters. These errors were considered acceptable for the purposes of this work.

Figure II.B.8 displays the results of a series of simulations in which the test interval length was assumed to equal layer thickness. In these simulations, the test interval length (and thus the layer thickness) was gradually decreased from 5 meters (aspect ratio = 100) to .15 meters (aspect ratio = 3). The results are displayed in the form of a plot of the range of the estimated conductivities versus aspect ratio. Clearly, the computed range decreases significantly with decreases in aspect ratio. Note that the majority of this decrease is a result of the conductivity estimated for layer B becoming increasingly smaller than the actual conductivity due to suppression of vertical flow by the adjoining layers of material A. Hayashi et al. (1987) describe how a decrease in aspect ratio promotes partial penetration effects, i.e. vertical flow out either end of the test interval. Thus, adjoining lower conductivity layers will have a greater impact on slug-test responses as the aspect ratio decreases and the importance of vertical flow increases. Hayashi et al. (1987) show that partial penetration effects should be rather small for wells with aspect ratios greater than about 100, a result that is in agreement with Figure II.B.8.

The general result of these simulations is that the effect of adjoining layers on multilevel slug tests becomes increasingly important as the layers decrease in thickness. Figure II.B.8, however, should only be considered as an example of these effects. The exact nature of the influence of adjoining layers will depend on a number of additional

factors including the specific storage of the layers and the nature of anisotropy in layer conductivity. The above simulations were performed assuming a specific storage of $1x10^{-5}$ m^{-1}. Additional simulations have shown that use of a smaller specific storage results in the pressure disturbance induced by the slug test spreading out more rapidly in all directions, causing the effect of adjoining lower conductivity layers to be accentuated. The increased influence of adjoining lower conductivity layers produces considerably lower values for the estimated layer B conductivities. Likewise, a specific storage larger than that used in Figure II.B.8 lessens the influence of adjoining layers on conductivity estimates. Thus, the specific storage can have a considerable influence on the estimated conductivity in layered systems. This is in contrast to slug tests in homogeneous systems where specific storage has relatively little influence on conductivity estimates obtained from heads at the stressed well (Cooper et al., 1967).

The addition of anisotropy ($K_r > K_v$) into the configuration does not produce results significantly different from those displayed in Figure II.B.8. The influence of adjoining layers is clearly diminished by the addition of anisotropy as a result of the suppression of vertical flow. The suppression of vertical flow itself, however, causes a decrease in the estimated conductivities. The net result is a decrease in the conductivities estimated for both layers and calculated ranges slightly narrower than those displayed in Figure II.B.8. Note that the analyses described in this paragraph were performed assuming isotropic layers. This is a reasonable assumption since, in most situations, one will not know what degree of anisotropy is appropriate. As discussed earlier, the anisotropy ratio and the horizontal conductivity are perfectly correlated in the Hvorslev model. Thus, some uncertainty will always be introduced into the parameter estimates as a results of the uncertainty concerning anisotropy.

The results displayed in Figure II.B.8 were obtained assuming that the test interval length was equal to layer thickness. If the test interval length is less than the layer thickness, adjoining layers will have less of an impact on the estimated conductivity. Figure II.B.9 displays the results of a series of simulations in which the layer thickness was progressively increased, while the test interval was not changed (aspect ratio constant=25.). As expected, increases in the ratio of layer thickness to test interval length decrease the impact of adjoining layers. In Figure II.B.9, the effects of adjoining layers are essentially negligible for ratios of four or greater. Note that the exact nature of the decrease in the effects of adjacent layers will depend on the aspect ratio (the larger the aspect ratio, the more rapid the decrease).

Dependence on Well Skins

The results depicted in Figures II.B.8 and II.B.9 were determined for the ideal case in which formation layering extends to the well screen. Often, however, as illustrated in Figure II.B.1, well drilling and development creates a near-well zone (well skin) of properties differing from those of the formation in which the well is screened. An additional series of simulations was performed here to assess the effects of well skins on multilevel slug test results.

Figure II.B.10 depicts the results from a set of simulations in which a low-permeability well skin was employed. The results are displayed in the form of a plot of the range of estimated conductivities versus simulation case. These results show that the addition of a low permeability skin produces a near complete suppression of the vertical variations in conductivity (calculated conductivity ranges are 2.9% and 1.7% of actual for cases A and B, respectively). In addition to the suppression of the conductivity variations, the estimated conductivities are much lower than in the no-skin case as a result of the heavy weighting of the low permeability skin in the parameter estimates. Butler et al. (1990) discuss the nature of the weighting of a low permeability well skin in conductivity estimates obtained using the Hvorslev model (see also Section II.A of this report). Note that the estimated conductivities are lower in case B as a result of the greater importance of vertical flow with smaller aspect ratios. In this case, the vertical flow is being suppressed by the low permeability well skin, resulting in lower calculated conductivities.

Figure II.B.11 displays a typical plot of the simulated responses and the best-fit Hvorslev model from the simulations of case B of Figure II.B.10. Note the very close fit of the Hvorslev model to the simulated responses, demonstrating that there will be little indication of well skins on Hvorslev plots. As pointed out by Butler et al. (1990) and in section II.A of this report, the assumptions of the Hvorslev model are actually more reasonable in a slug test in a well with a low permeability skin than under the no-skin case, so close fits between the model and slug-test responses are to be expected under such conditions. Unfortunately, as described by Butler and McElwee (1992), it is very difficult using conventional approaches to estimate the properties of the undamaged formation when a low permeability well skin is present. One approach that does appear to hold some promise is the prematurely terminated slug-test method recently proposed by Karasaki (1990).

A well skin may be of higher permeability than the formation as a result of voids forming along the well screen during well emplacement activities or a high permeability sand pack. A high conductivity skin can serve as a conduit for additional vertical flow. Figure II.B.12 displays the results of a series of simulations in which a high permeability

skin of .11 meters in radius was employed for most cases. Once again, the results are given in the form of a plot of the range of estimated conductivities versus simulation case. Note that, in relatively thick layers, the width of the calculated conductivity range does not change greatly from the no-skin case (see Figure II.B.8), although the estimated conductivities themselves increase significantly. As the thickness of the layers decreases, the layers become thin enough such that when the test interval is opposite a layer of material A, substantial amounts of water flow vertically along the well skin and into the layers of material B. This results in a great increase in the conductivity estimated for layers of material A and a dramatic decrease in the calculated conductivity range. As shown by case G, this effect increases with the thickness of the skin. Clearly, a highly conductive skin in an aquifer consisting of thin layers can cause multilevel slug tests to be of rather limited effectiveness for describing vertical variations in hydraulic conductivity.

Given that a highly conductive skin can greatly limit the effectiveness of multilevel slug tests, a series of additional simulations was performed in order to assess if well-construction measures could be taken to reduce the effect of a conductive skin. One possibility suitable for wells where the sand pack is the high conductivity skin would be to place very thin layers (1-2 cm) of low conductivity material (e.g., bentonite pellets) in the sand pack at relatively frequent intervals. These layers would serve to decrease the vertical movement of water in the sand pack but would have very little impact on horizontal flow. This scheme was evaluated here by simulating slug tests in wells with high conductivity skins in which an anisotropy in conductivity was assumed for the skin. Figure II.B.13 presents the results of a series of simulations in which anisotropy ratios (K_r/K_v) of 1, 2, and 10 were employed (K_r remaining constant, K_v decreasing). As shown in the figure, increases in the anisotropy ratio cause the calculated conductivity range to increase and the estimated conductivities to decrease towards the no skin case. These results indicate that if a well is to be used for multilevel slug tests, periodic thin layers of low conductivity material in the sand pack would be useful in partially mitigating the effect of a high conductivity skin. Unfortunately, in cases where the high conductivity skin is not the sand pack (e.g., uncased wells in consolidated rock), such an approach would not be possible, thereby making it difficult to remove the effect of a high conductivity skin in those situations.

Vertical Averaging in Slug Tests in Layered Aquifers

One issue of considerable interest to hydrogeologists is the way in which flow properties are averaged in various types of hydraulic tests in heterogeneous systems (e.g.,

Desbarats, 1992; Harvey, 1992). Since a number of layers may be spanned by the test interval in a multilevel slug test, the issue of the manner in which the properties of those layers are averaged to form the effective parameter estimated from the response data is of some importance. In this work, the nature of this vertical averaging was explored empirically through numerical simulation.

The initial step of this investigation was to assess the manner in which hydraulic conductivity values that vary in the vertical direction are averaged in a slug test performed over the entire screened interval of a well fully penetrating the aquifer (fully penetrating slug test). Figure II.B.14a displays the results of numerical simulations of slug tests in aquifers with the same thickness-weighted average of layer conductivities, but with different patterns of conductivity variations. The simulations include a uniform, anisotropic aquifer case, and three layered-aquifer cases with alternating layers of high and low conductivity (see Table II.B.2 for the parameters used in each case). The layering schemes are shown in Figure II.B.14b. Note that all three layering schemes have a thickness weighted average K_r of 4.6 m/d, which is the same value for K_r as used in the uniform aquifer case.

As shown in Figure II.B.14a, the simulated heads at the stressed well are essentially identical in the uniform and all three layered cases. Clearly, slug tests over the entire screened interval in fully penetrating wells can provide little information about vertical variations in conductivity when the stressed well is the measurement location. In all cases, the estimated conductivity will be a thickness-weighted arithmetic average of the horizontal conductivities of the individual layers. Note that this result is an extension of the work of Karasaki (1986), who found the same result using an analytical solution for slug tests in layered aquifers in which there is no vertical flow between layers. Thus, the vertical averaging in fully penetrating slug tests appears to be independent of the degree of vertical flow between layers.

Figure II.B.14a shows that no indication of layering will be evident from the head response at the stressed well in a fully penetrating slug test. An obvious question of importance for multilevel slug tests is how much will layering be suppressed as the test interval gets larger than the average layer thickness. Additional simulations have shown that the degree of suppression will depend on vertical variations in the arithmetic average of the conductivities of the test interval and the aspect ratio. In all cases, when the aspect ratio is much greater than 100, the estimated conductivity can be assumed to be a thickness-weighted average of the conductivities of the layers intersected by the test interval.

Effect of Packer Length

All of the multilevel slug test simulations described above were performed assuming that the well was cased everywhere in the aquifer except at the test interval (infinite packer). This was done in order to remove any effects due to the circumvention of the packers from the results. In field applications, however, packer circumvention is a very real concern. Increased vertical flow due to packer circumvention can result in an overestimation of layer conductivities and an underestimation of the degree of vertical variations.

A series of additional simulations was performed in order to assess the effect of packer length on parameters estimated from multilevel slug tests. In the 3DFDTC model packers are simulated as no-flow boundaries in the well bore, so there is no restriction on the length of the modelled packers. Four configurations were employed in this analysis (Cases 1-4 of Table II.B.3) in order to allow the effects of packer length to be evaluated in homogeneous and layered situations, both with and without a high conductivity skin. Figure II.B.15 presents the results of these simulations in the form of a plot of packer length versus the difference between the estimated conductivity using a packer of that length (K_{packer}) and the estimated conductivity using an infinite packer ($K_{\infty packer}$) normalized by the infinite packer estimate. Note that a dramatic decrease in this difference is seen in all cases with an increase in packer length. This plot clearly indicates that a highly conductive skin will exacerbate packer circumvention problems. In all cases, however, these results demonstrate that the relationships derived in this work are essentially the same as would be obtained using packers of .75-1.5 meters in length, which is the length range of many commercially available packers. Given the very conductive skin that was used in the simulations, these results indicate that packers greater than .75 meters in length should be adequate for most field applications. Bliss and Rushton (1984) found similar results for the effect of packer length on constant-head injection tests. Note that the results reported here are dependent on the thickness of the high conductivity skin. In cases where very thick skins are suspected, longer packers or a number of packers in series should be employed. However, as demonstrated in an earlier section, a thick high conductivity skin will hinder the effectiveness of multilevel slug tests even without packer circumvention.

Recent Field Experiences

Recently reported field experiences with multilevel slug tests in unconsolidated aquifers support some of the findings of this study. Melville et al. (1991) report on a program of multilevel slug tests whose results compared favorably with information

obtained from tracer tests. Butler and McElwee (1992), on the other hand, describe a program of multilevel slug tests whose results indicated essentially no vertical variations in flow properties, a finding that was not in agreement with existing core data. Although the test procedures followed in both studies were quite similar, the well drilling and emplacement procedures were not. Melville et al. (1991) describe a procedure of well emplacement using mud rotary drilling followed by forcing a slotted pipe of slightly smaller diameter into the drilled hole. The small annular space between the slotted pipe and the drilled hole was filled by collapsing material from the borehole wall. The wells were then extensively developed in order to remove as much of the drilling mud as possible from the formation. Butler and McElwee (1992) describe a procedure of well emplacement using hollow-stem auger drilling followed by placing a slotted pipe down the center of the augers and withdrawing the auger flights from about the pipe. In this case, a much larger annular space was formed, which was then filled by a natural sand pack consisting of material collapsing inward from the borehole wall. Permeameter analyses of cores from this same formation (Jiang, 1991; Butler and McElwee, 1992) have shown that repacked cores have considerably higher conductivities than the original sampled cores, indicating that the collapsed zone would probably form a skin of higher conductivity than the formation as a whole. The poor results of the tests reported by Butler and McElwee (1992) may well be due to preferential water movement along this thick high conductivity skin. The success of the Melville et al. (1991) program appears to be largely due to the thin well skin coupled with unremoved drilling muds that are apparently preferentially impeding vertical flow. Although their approach seems to have met with success, Melville and coworkers would have suffered from the same effects as illustrated in Figure II.B.10 without a very extensive program of well development. Thus, it is clear that well drilling and development procedures cannot be overemphasized in the planning of multilevel slug tests.

An approach for multilevel slug testing in unconsolidated formations that appears to minimize many of the problems arising due to well emplacement is described by Hinsby et al. (1992). This approach is based on progressively driving a well point and short screen into the formation. At any level desired, well driving can be stopped and a slug test performed. Although the results of the slug tests will still be a function of layering density, etc., as outlined here, this approach appears to have less potential for producing a thick high conductivity skin along the driven pipe. Ongoing work at the Kansas Geological Survey and elsewhere is presently evaluating this approach in more detail.

Summary and Conclusions

The results of this modeling investigation of the viability of slug tests for the purpose of describing vertical variations in hydraulic conductivity can be summarized as follows:

1) When the length of the test interval is on the order of the layer thickness, considerable error can be introduced into the description of vertical variations in hydraulic conductivity as a result of the influence of layers adjoining the test interval. The magnitude of the influence of the adjoining layers will strongly depend on the aspect ratio (test interval length/r_w). The specific storage of the tested layer will also be an important factor;

2) Regardless of layering density, a low conductivity skin will make it difficult to describe vertical variations in hydraulic conductivity because the estimated conductivity will be strongly influenced by the conductivity of the skin;

3) A high conductivity skin will make it difficult to describe vertical variations in hydraulic conductivity when the test interval and the layer thickness are both small. In this case, a large amount of vertical flow can occur along the skin, making it difficult to detect the existence of layers of low conductivity. Emplacing thin, low conductivity layers in the sand pack can help decrease vertical flow and allow a more accurate description of the conductivity variations to be obtained;

4) When the aspect ratio is large, a slug test will yield an approximate thickness-weighted average of the hydraulic conductivities of the layers intersecting the test interval (exact average in the case of a fully penetrating slug test). As the aspect ratio decreases, the properties of layers outside of the test interval will influence the calculated conductivity due to the increased vertical flow;

5) Packer circumvention should not be a major problem in most cases when packers of .75 meters or longer are employed. Packer circumvention is of greatest concern in the case of a thick, high permeability skin.

In summary, multilevel slug tests can provide considerable information about vertical variations in hydraulic conductivity under the right conditions. The best conditions would be thick layers using test intervals considerably smaller than the average layer thickness. Even under these conditions, however, well skins can dramatically decrease the effectiveness of the approach. Considerable attention must therefore be given to well construction and development in order to minimize the impact of a well skin on test results. Results from recently reported field tests demonstrate the importance of well construction and development procedures.

Note that the findings of this study must be considered in the light of two major assumptions employed in this work. First, the simulated responses from each slug test were analyzed using a homogeneous-aquifer model, an approach in keeping with standard field practices. Analysis of each test in isolation from the others in the same series of multilevel tests, however, led to the strong dependence of test results on layering density and, in many cases, to a significant underestimation of the actual conductivity variations. A more rigorous approach would be to analyze all the test results together using a numerical model coupled to an optimization routine. An initial attempt at such an approach for a series of drill-stem tests is given by Yu and Lloyd (1992). Even if such a technique was used, however, it would not remove the effects of well skins or vertical averaging from test results. Given the nature of current field practices, the approach employed here was considered appropriate.

Second, the findings discussed in this article were based on a series of simulations performed in perfectly stratified aquifers, i.e. layering is continuous throughout the entire model domain. Many aquifers in nature consist of a series of discontinuous layers. In most natural systems, the rate of variation in flow properties in the direction perpendicular to the plane of layering would be expected to be considerably larger than that parallel to layering (Butler, 1986; Hess et al., 1992). The results presented here should thus be applicable to many field situations. Further work, however, is required to fully assess the effect of layer discontinuity on slug tests.

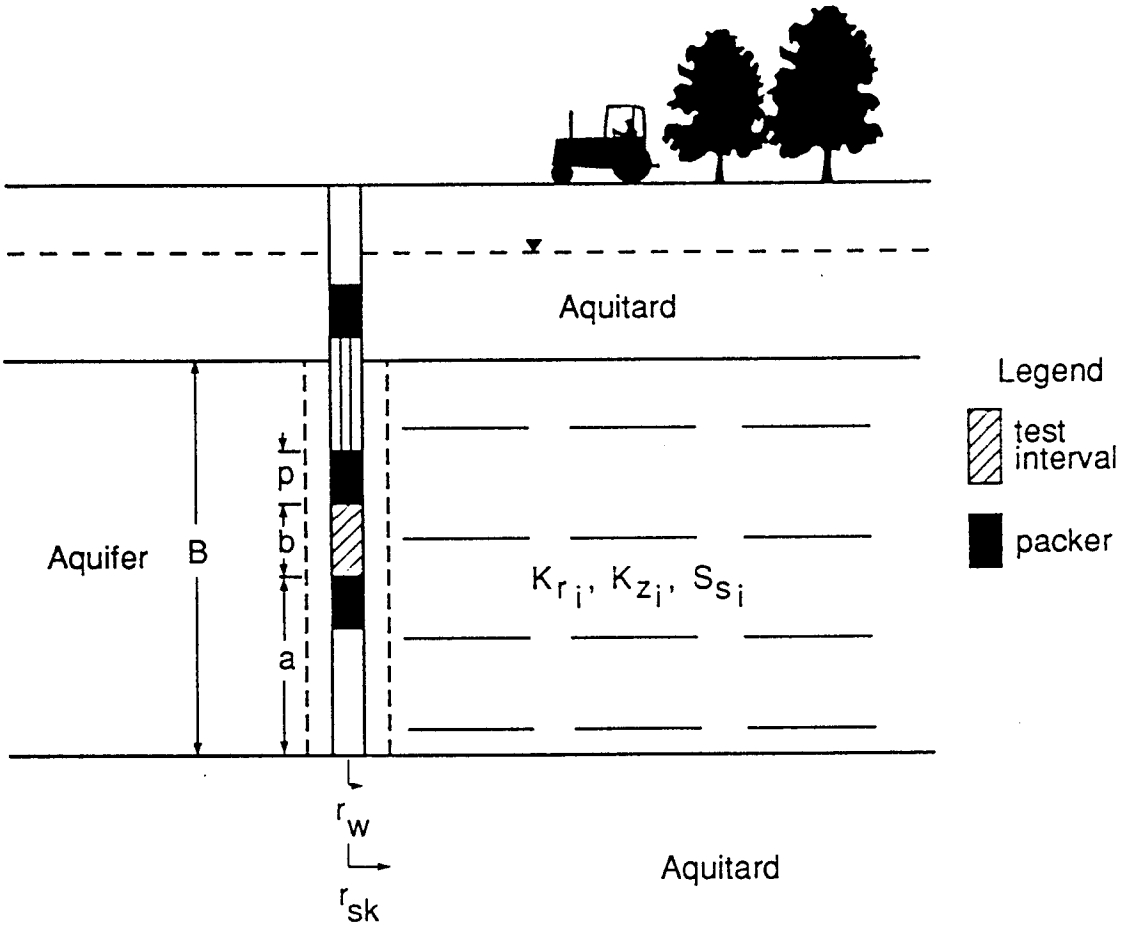

FIGURE II.B.1 - Cross-sectional view of multilevel slug test configuration (r_w=radius of test interval, r_{sk}=radius of skin, B= thickness of aquifer, a=distance of the bottom of the test interval above the base of the aquifer, b=width of the test interval, p=packer length, K_r, K_z, S_s =radial component of conductivity, vertical component of conductivity, and specific storage, respectively, of layer i). Note that layering is assumed to extend throughout the cross section.

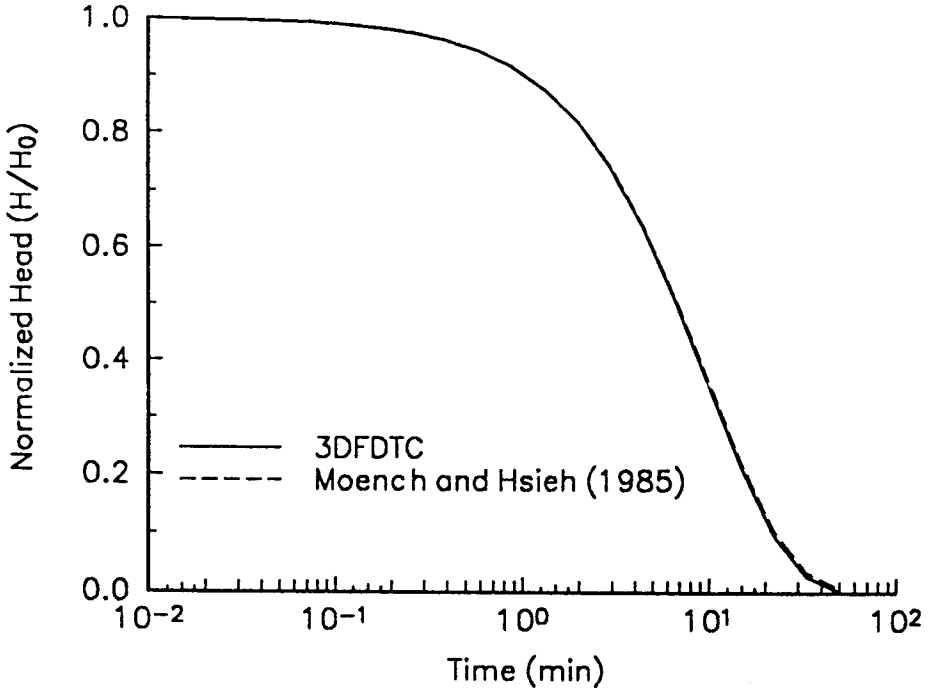

FIGURE II.B.2a - Normalized head ($H(t)/H_0$) versus time plot comparing analytical solution of Moench and Hsieh (1985) to 3DFDTC results (r_w=.167 m, r_{sk}=.33 m, T_{sk}=.001 m^2/min, S_{sk}=.001, T_{aq}=1 m^2/min, S_{aq}=.00001).

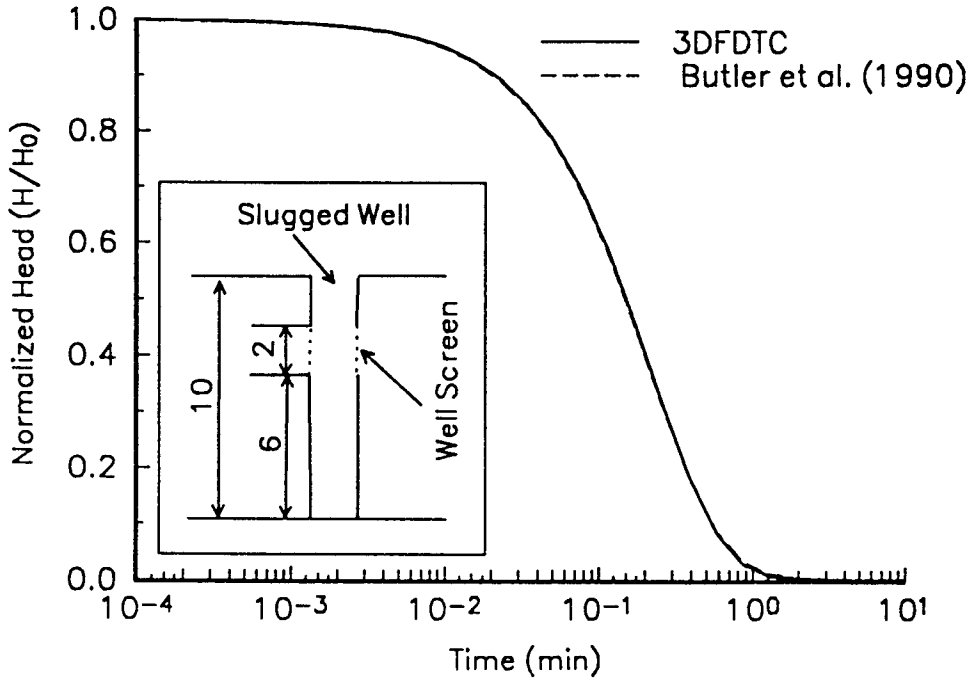

FIGURE II.B.2b - Normalized head ($H(t)/H_0$) versus time plot comparing analytical solution of Butler et al. (1990) to 3DFDTC results (r_w=.167 m, K=.1 m/min, S_s=.000001 /m).

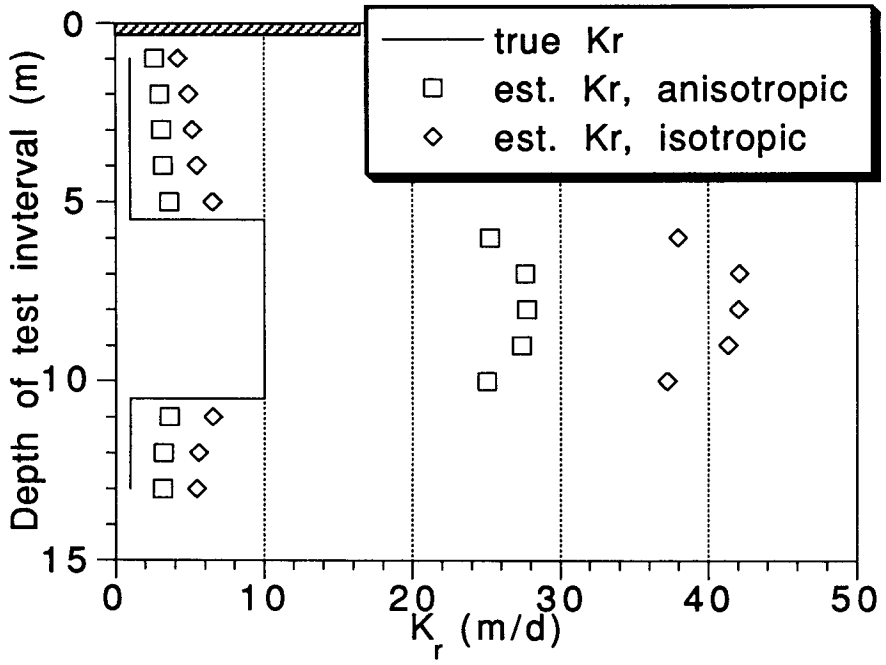

FIGURE II.B.3a - Plot of results of estimated K_r using the CBP model versus vertical position of test interval (K_{high} = 10 m/d, K_{low} = 1 m/d, aspect ratio (b/r_w) = 2.5, layer thickness (L)=5 m, K_v=.1K_r in anisotropic case).

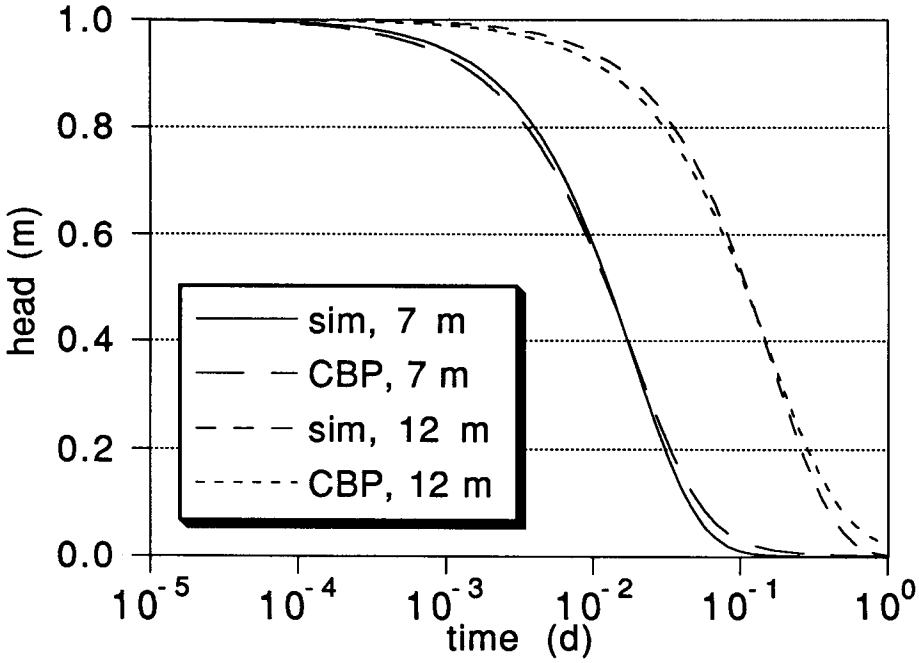

FIGURE II.B.3b - Simulated heads and best-fit CBP model when slug-test interval is 7 and 12 meters below the top of the aquifer.

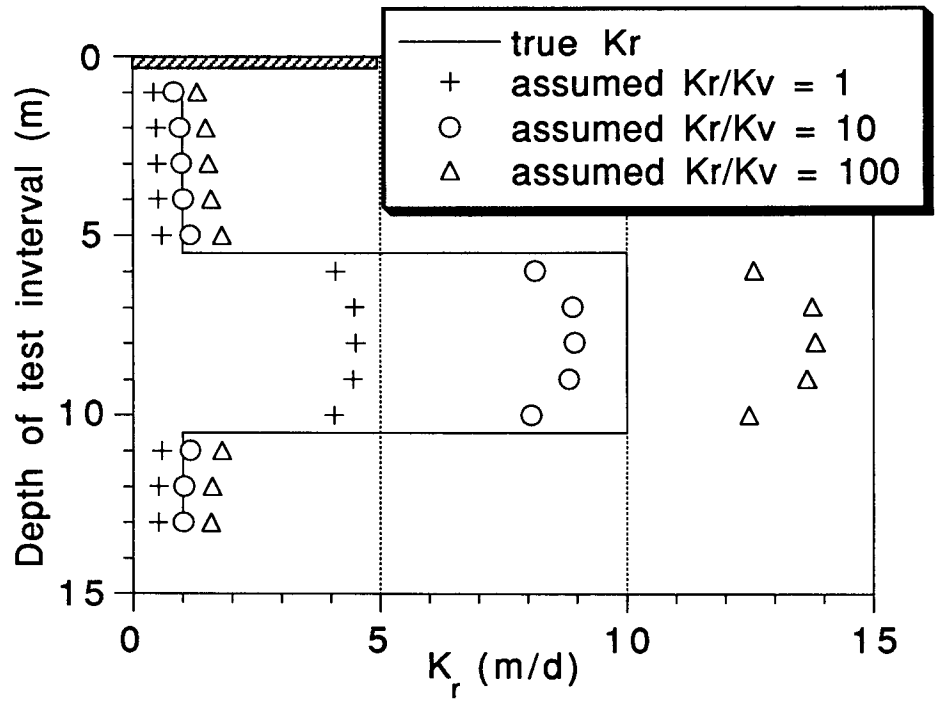

FIGURE II.B.4a - Plot of estimated K_r using the Hvorslev model versus vertical position of test interval (same configuration as in Figure II.B.3a).

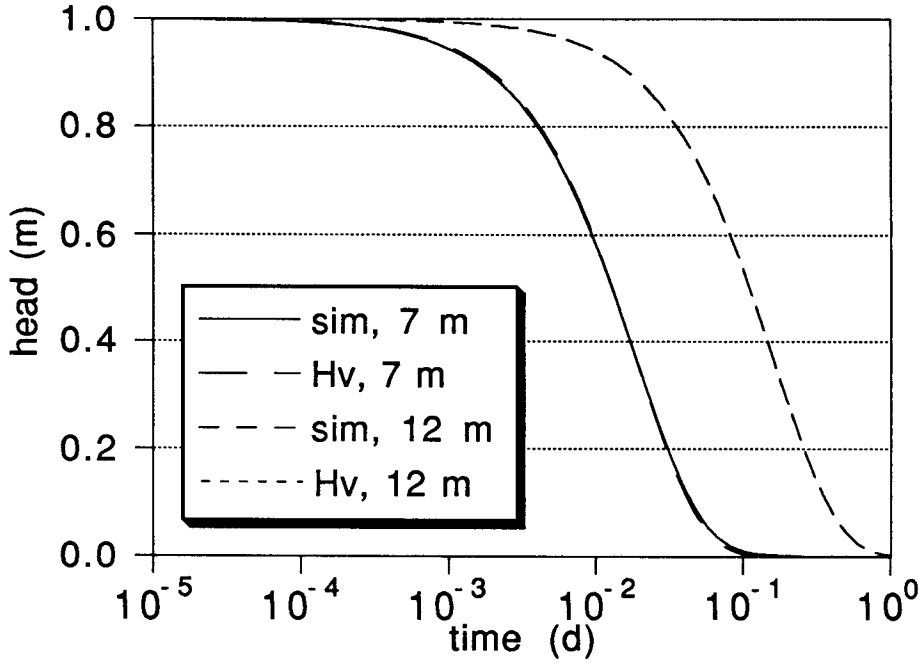

FIGURE II.B.4b - Simulated heads and best-fit Hvorslev model when slug-test interval is 7 and 12 meters below the top of the aquifer.

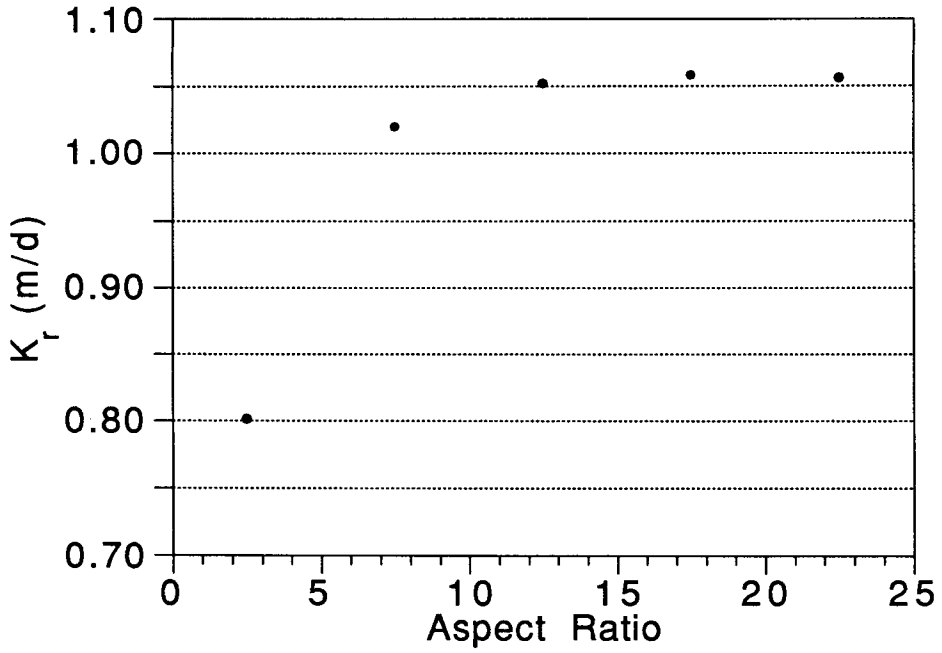

FIGURE II.B.5 - Aspect ratio (b/r_w) versus estimated conductivity (K_r) plot (true K_r value = 1 m/d).

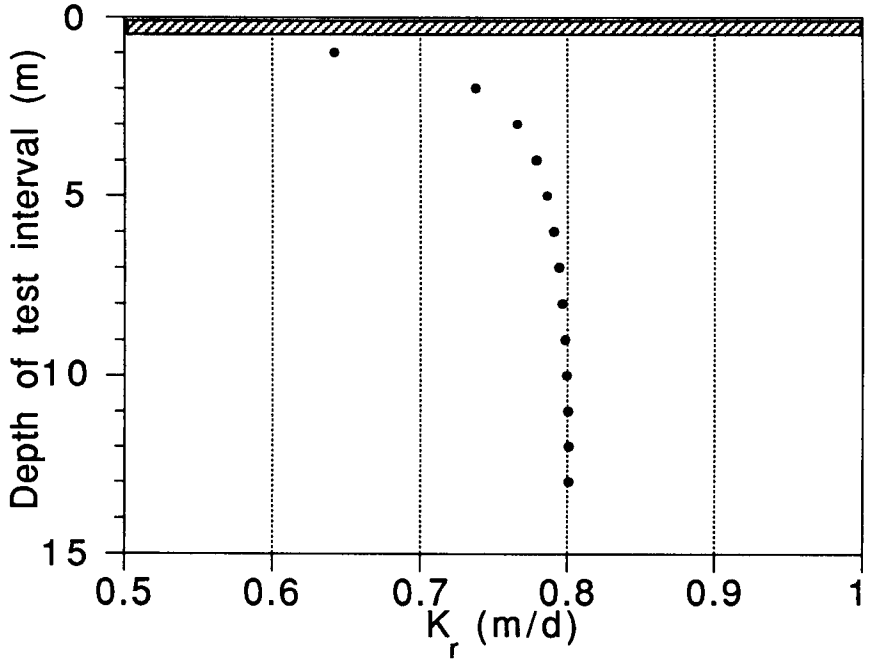

FIGURE II.B.6 - Plot of estimated conductivity (K_r) versus vertical position of test interval (true K_r value = 1 m/d, aspect ratio (b/r_w) = 2.5).

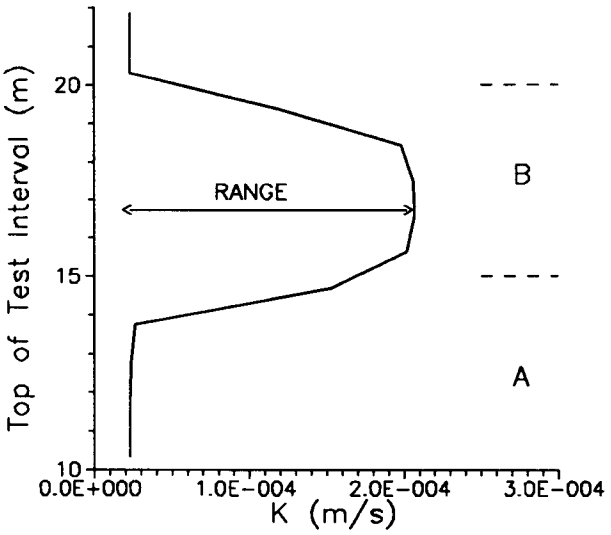

FIGURE II.B.7 - Estimated conductivity versus depth to top of test interval plot for multilevel slug tests simulated in a layered aquifer consisting of alternating layers of material A and B (see Table II.B.1 - L (layer thickness) = 5 m, b (length of test interval) = 1.25 m). Range is defined as distance between the maximum and minimum estimated conductivity.

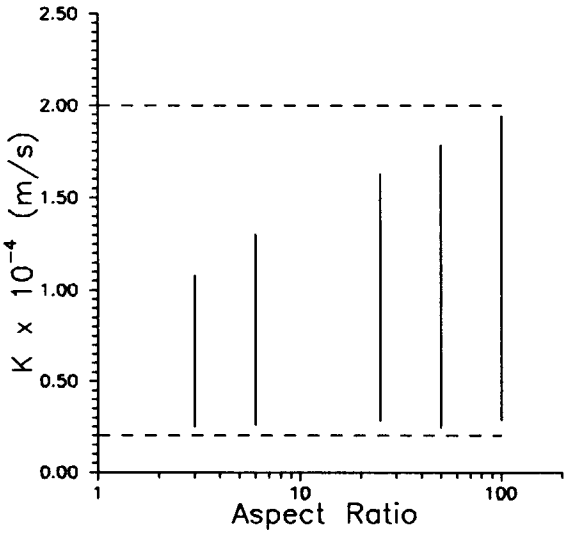

FIGURE II.B.8 - Range of estimated conductivities versus aspect ratio (b/r_w) plot. Note that layer thickness changes in the same manner as b. Lower and upper dashed lines indicate the conductivities of layers A and B, respectively.

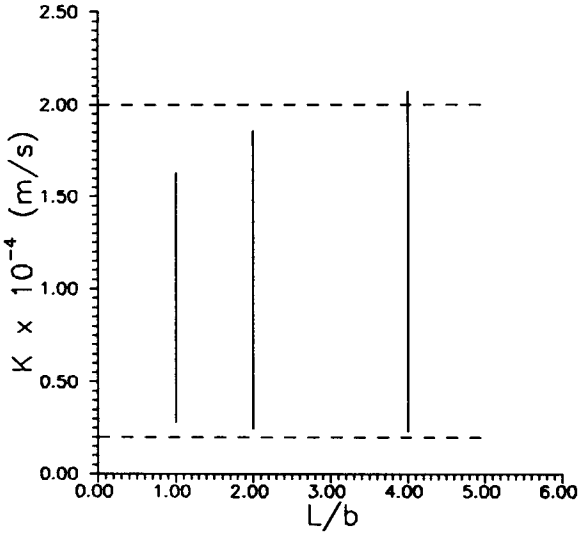

FIGURE II.B.9 - Range of estimated conductivities versus L (layer thickness) over b (length of test interval) plot. Note that b remains constant (=1.25 m) for the cases displayed on this plot. Lower and upper dashed lines indicate the conductivities of layers A and B, respectively.

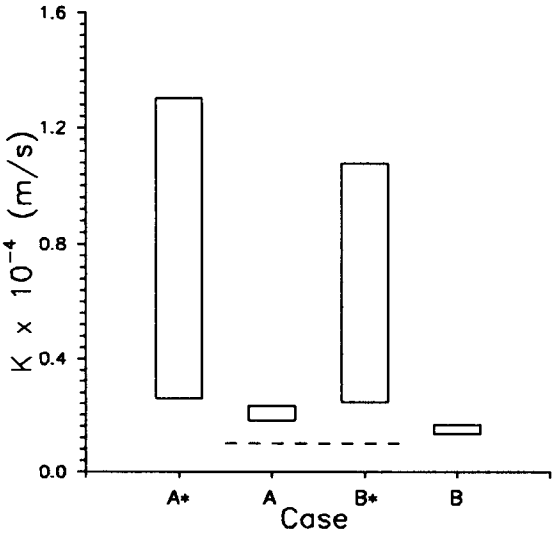

FIGURE II.B.10 - Range of estimated conductivities versus simulation case plot for the low permeability (K_{sk}=.00001 m/s) skin scenario (Case A* - no skin case, L=b=.312 m; Case A - L=b=.312 m, r_{sk}=.11 m; Case B* - no skin case, L=b=.156 m; Case B - L=b=.156 m, r_{sk}=.11 m). Dashed line indicates the skin conductivity.

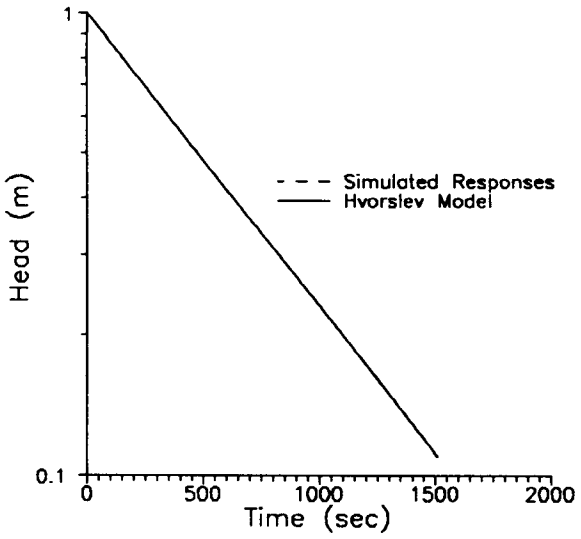

FIGURE II.B.11 - Simulated heads and best-fit Hvorslev model for the low permeability skin case (Case B of Figure II.B.10).

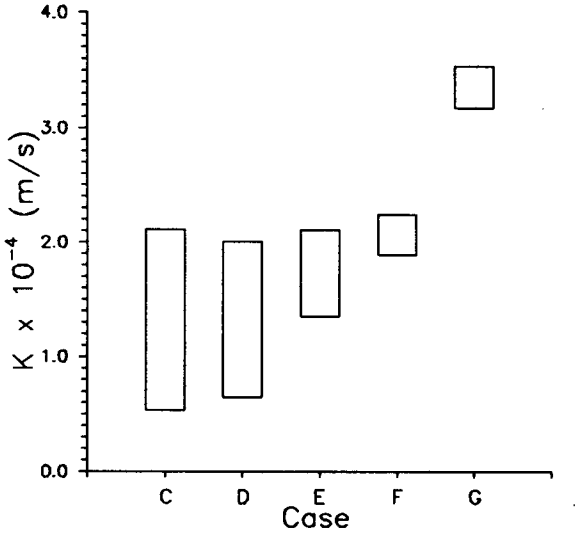

FIGURE II.B.12 - Range of estimated conductivities versus simulation case plot for the high permeability (K_{sk}=.001 m/s) skin scenario (Case C - L=b=2.5 m, r_{sk}=.11 m; Case D - L=b=1.25 m, r_{sk}=.11 m; Case E - L=b=.312 m, r_{sk}=.11 m; Case F - L=b=.156 m, r_{sk}=.11 m; Case G - L=b=.312 m, r_{sk}=.22 m).

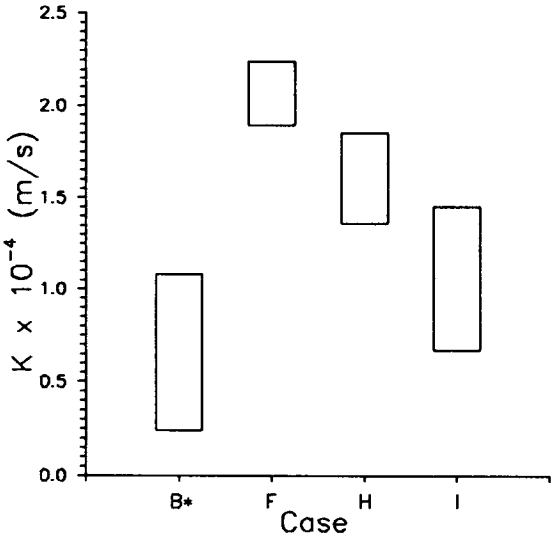

FIGURE II.B.13 - Range of estimated conductivities versus simulation case plot for the high permeability skin with anisotropy scenario (Case B* - no skin case, L=b=.156 m; Case F - same as in Figure II.B.12; Case H - Case F except $K_{r(skin)}/K_{v(skin)}$ = 2.; Case I - Case F except $K_{r(skin)}/K_{v(skin)}$ = 10.).

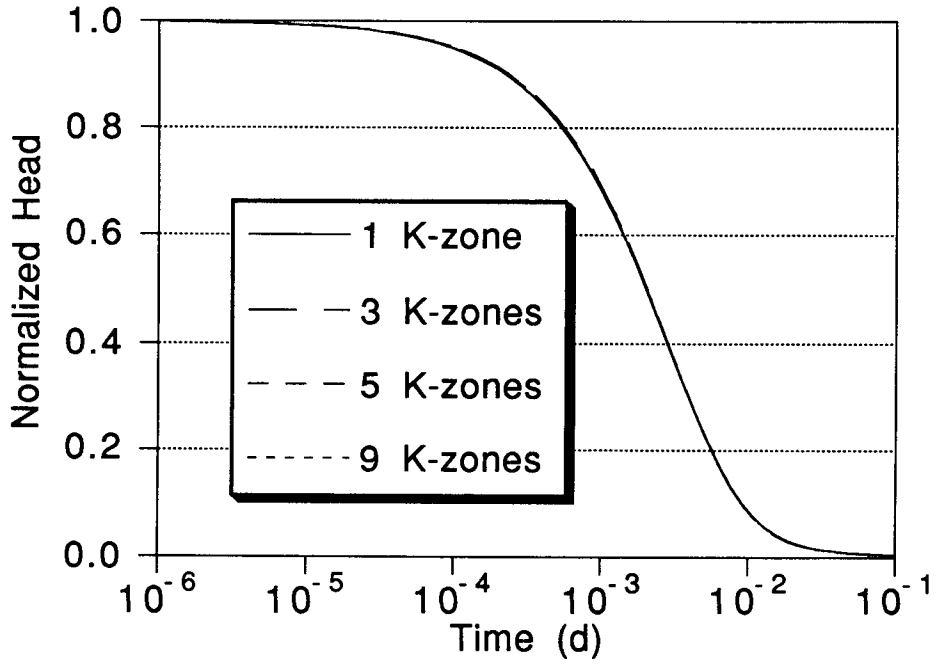

FIGURE II.B.14a - Plot of normalized head ($H(t)/H_0$) at the stressed well versus time for the case of a fully-penetrating slug test in a layered aquifer.

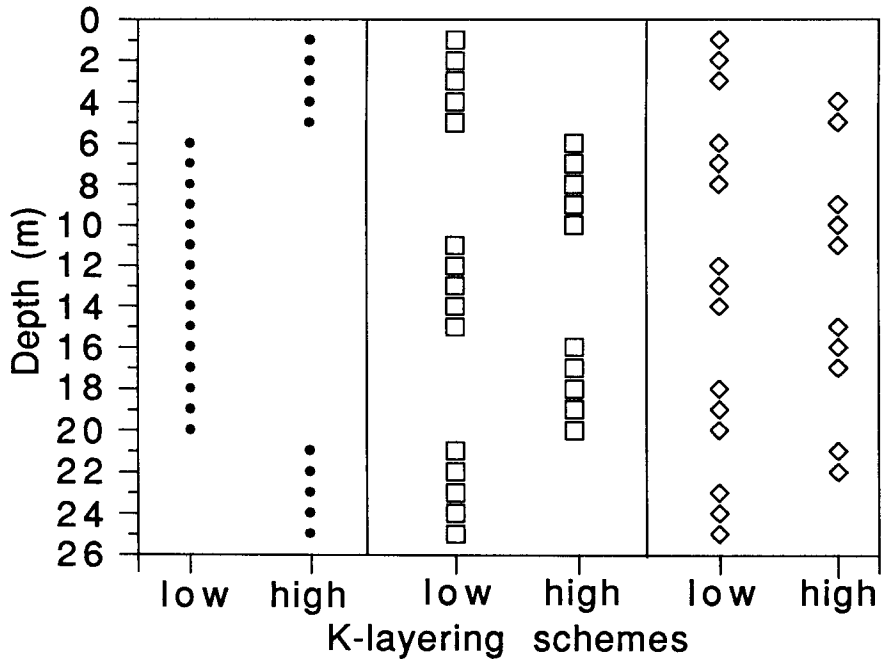

FIGURE II.B.14b - Layering schemes employed in the simulations shown in Figure II.B.14a (K_{low} and K_{high} defined in Table II.B.2).

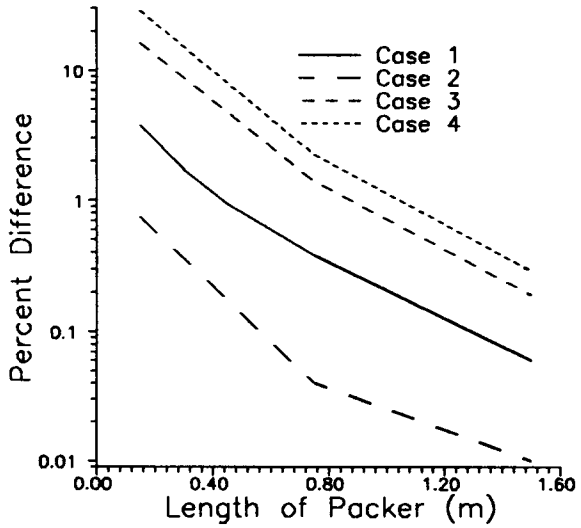

FIGURE II.B.15 - Packer length versus normalized difference ((K_{packer} - $K_{\infty\ packer}$)/$K_{\infty packer}$ x 100.) plot for Cases 1-4 of Table II.B.3. Plotted results are for case of test interval opposite layer A.

H_0 = 1.0 m;
r_w = 0.05 m;
K_A = $2x10^{-5}$ m/s;
K_B = $2x10^{-4}$ m/s;
S_{SA} = S_{SB} = $1x10^{-5}$ m^{-1};
B = aquifer thickness = 25 m;
r_{bnd} = radial distance to outer boundary = 37,364. m.

TABLE II.B.1 - Model parameters employed in the analysis of the effects of layering density on slug test results.

uniform, anisotropic case

K_r=4.6 m/d, K_z=0.46 m/d;

layered cases

low conductivity layer K_r=1. m/d, K_z=0.1 m/d;

high conductivity layer K_r=10. m/d, K_z=1. m/d.

TABLE II.B.2 - Model parameters employed in the analysis of the effects of variable layering on the parameters estimated from fully penetrating slug tests.

Case 1

$K_A = K_B = 2x10^{-5}$ m/s;
$S_{SA} = S_{SB} = 1x10^{-5}$ m^{-1};
b = .15 m;

Case 2

$K_A = 2x10^{-5}$ m/s;
$K_B = 2x10^{-4}$ m/s;
$S_{SA} = S_{SB} = 1x10^{-5}$ m^{-1};
b = .15 m;
L = .15 m;

Case 3

$K_A = K_B = 2x10^{-5}$ m/s;
$S_{SA} = S_{SB} = 1x10^{-5}$ m^{-1};
$K_{sk} = .001$ m/s;
b = .15 m;
$r_{sk} = .11$ m;

Case 4

$K_A = 2x10^{-5}$ m/s;
$K_B = 2x10^{-4}$ m/s;
$S_{SA} = S_{SB} = 1x10^{-5}$ m^{-1};
$K_{sk} = .001$ m/s;
b = .15 m;
L = .15 m;
$r_{sk} = .11$ m.

TABLE II.B.3 - Scenarios employed in the analysis of the effects of packer length on parameters estimated from multilevel slug tests.

C. IMPROVEMENTS TO SUPRPUMP

Work on the general purpose well test analysis program SUPRPUMP continued throughout this grant period. This analysis program has been a very important part of the research effort since much of the field data taken for this project are analyzed by SUPRPUMP. The two most significant accomplishments were the development of a more efficient implementation of an analytical solution describing slug tests in partially penetrating wells affected by well skin (Zafar et al. 1993) and the development of a batch mode version. The previous implementation of the partially penetrating slug test with skin solution ran too slowly to be of practical use for well test analysis. The new version will allow the rapid analysis of slug tests under a wider range of practical field conditions.

The batch mode version of SUPRPUMP was developed for the sake of greater portability, improved computational reliability, and greater ease in analyzing large data sets or large numbers of closely related well tests. The interactive interface to SUPRPUMP can become tedious to work with when one is analyzing a large number of similar tests, with only slight variations in input specifications. The batch mode program, which reads data and input parameters from ASCII input files, allows the same data set to be analyzed in a number of different ways in one program run. In addition, simple editing changes allow different data sets to be analyzed using the same input parameters, without having to retype repeated information every time the program is run. The batch mode program also uses a more reliable parameter estimation algorithm (Levenberg-Marquardt) than the interactive version. Several new features that have been included in the batch mode program are the ability to 'fit' an unkown boundary (estimate its location), the ability to perform weighted regression (with more reliable data sources being weighted more heavily than less reliable sources), and the performance of a test for systematic lack of model fit (aiding in the selection of the best of a number of candidate models).

Future work will involve developing a Microsoft Windows interface to the batch mode version of SUPRPUMP. This interactive interface will help the user manage data, set up the input files for and spawn the batch mode program, and provide a 'back-end' interpreter for the output files, including graphical display of results.

D. HYDRAULIC TOMOGRAPHY

Introduction

Some of the important early papers on the groundwater inverse problem, such as those by Nelson [1960, 1961, 1968] and Neuman [1973], pointed out the relationship between this problem and the one-dimensional Cauchy problem. If heads and source and sink values are known at every point in a one-dimensional problem, then the conductivity at every point in the domain can be determined uniquely as long as either conductivity or flux is known at one point in the domain. This same result can be applied along streamtubes or streamlines in a two-dimensional flow problem. This leads to a direct inverse solution for conductivities based on flow net analysis, as in Nelson [1968], and more recently in Scott [1992]. In both of these works the flow net is created by interpolating from observed head values, in one way or another.

The hydraulic tomography method presented here is essentially an iterative least squares solution of the Cauchy problem, with streamlines being iteratively identified based on a computed head field, rather than from observed data. The head drop between any two points on a streamline is given by a line integral of the flux along the streamline multiplied by the hydraulic resistivity, which is the inverse of hydraulic conductivity. Streamline trajectories and flux integrals are computed from a finite difference solution for head based on an estimate of the resistivity distribution. Computing flux integrals along a number of streamlines with known heads at each end results in a system of linear equations which can be solved for an updated set of resistivities. Heads and flux integrals are recomputed and the process repeats until the resistivity estimates converge.

Flow Path Within a Finite Difference Cell

Figure 1 is a sketch of a finite difference cell with one possible flow path passing through it. This diagram and the development of the equations describing the flow path trajectory are taken from Pollock [1988], with minor modifications. Using a block-centered formulation, with computational nodes at the center of the cell and flux values computed at the cell faces, the flux field within the cell can be approximated using bilinear interpolation. The x-component of the specific flux, for example, is given by linear interpolation between q_{x1} on the left face and q_{x2} on the right face, and similarly for the y-component. Given this description of the flux field it is straightforward to work out the trajectory of a particle traveling through the cell, from its entry point (x_p,y_p), to its exit point, (x_e,y_e). The flux field is in steady state here, not varying with time. However, any given particle will encounter varying fluxes as it travels along its flow path. Also note that this development uses Darcy velocity or specific flux in place of actual flow

velocity. The time variable employed is not real-world travel time, but is travel time scaled by the value of porosity. Time is used only as a convenient variable of integration, however, and the scaling by porosity does not have any effect on the final results.

Flux Field Within Cell

Using a local coordinate system ranging from -Δx/2 to +Δx/2 and from -Δy/2 to +Δy/2 within each cell, where Δx and Δy are the cell dimensions, the equations describing the flux field within the finite difference cell are:

$$q_x(x) = q_{x0} + A_x x \qquad q_y(y) = q_{y0} + A_y y \tag{II.D.1}$$

with

$$q_{x0} = \frac{(q_{x2} + q_{x1})}{2} \qquad q_{y0} = \frac{(q_{y2} + q_{y1})}{2} \tag{II.D.2}$$

and

$$A_x = \frac{(q_{x2} - q_{x1})}{\Delta x} \qquad A_y = \frac{(q_{y2} - q_{y1})}{\Delta y} \tag{II.D.3}$$

The locations of the cell-face fluxes, q_{x1}, q_{x2}, q_{y1} and q_{y2}, are shown on Figure 1. In the current implementation of the method, the fluxes at the cell faces are calculated from differences of computed head values in adjacent finite difference cells. Thus the flux gradient terms, A_x and A_y, are computed from differences of differences of computed head values. This is a potential source of problems, since differences of computed values can be in error by arbitrarily large amounts regardless of the accuracy of the original computed values. However, every inverse algorithm depends in some way on computation of head gradients, if not higher-order differences, so this problem is not unique to this particular method.

Particle Trajectory Within Cell

As a particle travels through a cell, it follows a flow path determined by the following two ordinary differential equations:

$$\frac{dq_x(t)}{dt} = A_x q_x(t) \qquad \frac{dq_y(t)}{dt} = A_y q_y(t) \tag{II.D.4}$$

Again, t is the real-world travel time scaled by porosity. The equation on the left states that the time rate of change in x-component flux experienced by a particle is given by the flux gradient, A_x, multiplied by the current flux value, q_x. This is an application of the chain rule -- A_x is dq/dx and q_x is dx/dt. The first integral gives the two flux components as exponential functions of travel time through the cell:

$$q_x(t) = q_{xp}\exp(A_x t) \qquad q_y(t) = q_{yp}\exp(A_y t) \qquad \text{(II.D.5)}$$

where q_{xp} and q_{yp} are the flux components at the point where the particle enters the cell. The second integral gives the particle trajectory, x and y coordinates as functions of travel time:

$$x(t) = \frac{1}{A_x}\left(q_{xp}\exp\left(A_x t\right) - q_{x0}\right) \qquad y(t) = \frac{1}{A_y}\left(q_{yp}\exp\left(A_y t\right) - q_{y0}\right) \qquad \text{(II.D.6)}$$

The actual travel time through the cell is determined by testing the potential travel time to each cell face. The minimum positive value gives the travel time through the cell, t_c. The coordinates of the particle's exit point, x_e and y_e, are then obtained by plugging the travel time into the trajectory equations. The particle moves into an adjacent cell and the algorithm continues to trace this path through successive cells until it reaches a boundary and exits the model domain.

Constant Hydraulic Resistivity Solution

Figure 2 shows the head contours and pathlines traced by the algorithm for flow through a square domain with a constant hydraulic resistivity of 1.0. The model domain, nine units on a side, was discretized into a 45X45 grid of finite difference cells for this and following examples. For this particular run the five cells between y=4 and y=5 on the left and right sides were given specified heads of plus and minus one, with zero-flux boundaries elsewhere. Note that the nine streamlines shown actually appear to the program as 18 streamlines. The starting points are nine data points in the middle of the model, located where the streamlines intersect the 0-head contour. Two streamlines start from each data point, one moving forward through the flux field to the right-hand boundary, and the other moving backward through the flux field to the left-hand boundary. The program works this way because, in the tomographic equations, head drops computed from flux integrals are compared to differences between head values measured at points within the model domain and head values at the boundaries. Thus, the

path-tracing algorithm will start at any arbitrary point in the domain, representing a measurement point, and trace both an upstream and a downstream path until each encounters a boundary.

Natural Log of Hydraulic Resistivity Field

Figure 3 shows the synthetic spatially-varying resistivity field used for the next example. The natural log of the resistivity field is shown. Low values of resistivity correspond to high values of conductivity, so that the lighter band above the middle of the model represents a more conductive flow path. Each constant-resistivity block shown here represents a 5X5 block of grid cells. The range of resistivities is from about 0.2 to about 12.

Variable Hydraulic Resistivity Solution

Figure 4 shows the head contours and streamlines computed using the variable-resistivity field and the same boundary conditions as for the constant-resistivity case. The same nine points in the middle of the model are used as the starting points for the streamlines. The general configuration of the flow field is, of course, determined by the boundary conditions, so the variable-resistivity case looks like a wrinkled version of the constant-resistivity case. This seemingly trivial observation is actually fairly important to the success of the tomographic inversion scheme. The flux integrals used in the inverse process are computed along the flow paths derived from the current estimate of the hydraulic resistivity distribution. If the flow path trajectories changed radically with variations in the resistivity values, the iteration process would wander hopelessly. As it is, computed trajectories are fairly similar from one iteration to the next.

Tomographic Equations

The tomographic equations result from applying an integral version of Darcy's law along each streamline leading from a data point to a boundary. Viewed along each streamline, Darcy's law reduces to the simple ordinary differential form

$$q_s(s) = -K(s)\frac{dh}{ds} \qquad \text{(II.D.7)}$$

where s represents displacement along the streamline, K(s) is the conductivity as a function of that displacement, and dh/ds is the head derivative along the streamline. Rearranging this and integrating along the length of the streamline, from 0 to L, shows

that the head drop along the streamline, H, can be derived directly from the hydraulic resistivity and flux values encountered along that streamline:

$$H = \int_0^L R(s) q_s(s) ds \qquad \text{(II.D.8)}$$

If the model is discretized into N cells, each of constant resistivity, R_i, then the head drop is given by the sum of the discrete resistivity values, each multiplied by the flux integral along the streamline of interest within the corresponding cell:

$$H = \int_0^L R(s) q_s(s) ds = \sum_{i=1}^{N} \left(R_i \int_{si} q_s(s) ds \right) \qquad \text{(II.D.9)}$$

The flux integrals along each streamline within each cell can be collected into a coefficient matrix, with rows corresponding to streamlines and columns corresponding to model cells. The cells can be collected into constant-resistivity zones to reduce the number of unknown resistivities and thus the number of columns of the coefficient matrix. This coefficient matrix will contain quite a few zeroes, since each streamline passes through a relatively small number of cells or zones. Multiplying this flux integral coefficient matrix times the vector of zonal resistivities produces a vector of computed head drops, with each element representing the head drop between a particular data point and a boundary. The differences between these computed head drops and observed head drops form a vector of head drop residuals. Linear least squares can then be used to produce a vector of resistivity correction values which will reduce the sum of squared head drop residuals. These correction values are added to the current resistivity estimates, flow path trajectories and flux integrals are recomputed based on the new resistivities, and the process continues until the resistivity estimates converge. This is very similar to the algorithms used in seismic tomography (Peterson et al., 1985).

Flux Integral Within Cell

The flux integral along a given streamline in a cell is simplified by converting it to an integral over time, using the relationship between the spatial increment, ds, and the time increment, dt, ds = q(s)dt. Applying this substitution leads to a convenient simplification, since the integral over time breaks down into two pieces, each involving the square of either q_x or q_y:

$$\int_{si} q_s(s)ds \quad = \quad \int_0^{tc} q_s^2(t)dt \quad = \quad \int_0^{tc} q_x^2(t)dt + \int_0^{tc} q_y^2(t)dt \qquad \text{(II.D.10)}$$

Since we already have simple analytical expressions for q_x and q_y as functions of time, it is straightforward to evaluate these integrals. The general result for q_x is:

$$\int_0^{tc} q_x^2(t)dt = \frac{q_{xp}^2}{2A_x}\left(\exp(2A_x t_c) - 1\right) \quad if \quad A_x \neq 0 \qquad \text{(II.D.11)}$$

A special case occurs when either q_x or q_y is constant over the cell. In this case the integral is given simply by the square of the flux component multiplied by the travel time in the cell:

$$\int_0^{tc} q_x^2(t)dt = q_{x0}^2 t_c \quad if \quad A_x = 0 \qquad \text{(II.D.12)}$$

Layered Aquifer

The numerical examples are based on simulated experiments using the simple layered aquifer shown in Figure 5. The values are shown directly in terms of hydraulic resistivity. First, a sequence of nine tests was simulated, with each test involving a pair of specified head intervals, one on each end of one of the constant-resistivity layers. For example, for the first test the five grid cells at the left end of the bottom layer were set at a head of +1 and the five grid cells at the right end of the bottom layer were set at a head of -1. The same nine points in the middle of the model were used as observation points, generating 18 streamlines per test (one forward, one backward for each point), for a total of 162 streamlines over all nine tests. Running the program in forward mode using the true resistivity distribution shown here generated the data used in the inverse run. The heads computed at the data points by the finite difference model were taken as the observed heads at those points. Also, the flux value at each specified head boundary cell was computed. The flux values for the right-hand intervals were averaged over the five nodes in the interval and these averaged flux values were used for the boundary conditions on the right side when the inverse run was performed. There has to be at least one specified flux boundary condition along each streamline in order to obtain a unique solution for the resistivities. In the inverse run, the differences between the head values computed at the interior data points and the known head values at the boundary intervals on the left and right served as the observed head drops.

Except for the fact that a linear, rather than radial, flow problem is being solved here, this experiment simulates the way we envision applying this method in the field. The data obtained from stressing different vertical intervals between a pumping well and an injecting well would be combined in order to estimate the conductivity distribution in the vertical plane between the two wells.

Nine-Test Results

Figure 6 shows the results of the nine-test inverse run. In this case the model was zoned into layers corresponding exactly with the layers in the true model. The true resistivity values are shown by the solid line and the estimates are shown by the dashed line. Starting from an initial resistivity value of 1.0 for every layer, the model converged to the solution shown here in 7 iterations, with the largest relative change in a resistivity value being about 6.5%. Overall the estimated resistivities are reasonable, with the estimates for each layer tending to be influenced somewhat by the resistivities of adjacent layers as well. After the seventh iteration the ratio changes in the resistivities continued to decrease slightly, but the sum squared head drop residual went up just slightly.

Five-Test Results

Figure 7 shows the results of a set of five simulated tests in the same layered aquifer. Each test involved stressing a nine-node interval, with specified head values at the left and right sides of the interval, as before. The aquifer in this case was zoned into five layers, corresponding with the stressed intervals. Thus, the assumed layering is coarser than the actual layering. As shown here, the overall pattern of estimated resistivities still preserves the general character of the actual resistivities.

Fifteen-Test Results

Figure 8 shows the results of stressing fifteen consecutive three-node intervals, with the aquifer being zoned into fifteen corresponding layers. Again, the estimates preserve the overall character of the actual resistivity variation. You may note that the resistivity of the upper portion of the top layer is significantly underestimated. This upper layer is a fairly high resistivity (or low conductivity) layer sandwiched between the no-flow boundary above and a higher conductivity layer below. These conditions cause the flow to avoid this upper layer as much as possible, leading to a relatively small amount of information on its properties and a poor estimate of its resistivity.

Concluding Remarks

Two advantages of this method have not been emphasized earlier. One advantage is that the model responses, the estimated head drops, are given by linear combinations of the model parameters, the hydraulic resistivities. Thus, in the hypothetical case that you knew the true model, the parameter covariance matrix would give an exact description of parameter confidence intervals, not just linear approximations of nonlinear confidence intervals, as in most inverse procedures. Although this hypothetical case is not achievable in real world applications, at least the effects of nonlinearity should be fairly small when the estimated parameters are near the optimal parameters for a given zonation.

In addition this method iteratively identifies the streamlines, or the characteristics of the flow system, as described by Neuman [1973]. Again, if the true model were known with certainty, the head drop along each streamline would be only a function of the resistivities along that streamline, completely independent of resistivity values elsewhere in the flow domain. Since, in reality, the estimated solution does depend on the resistivity estimates throughout the domain, this independence is not completely realized. However, this method should produce fairly low correlations among the parameter estimates as the resistivities approach the optimal values. Preliminary results show that this seems to be the case.

Ongoing work is addressing some problems encountered so far on this project. One problem has been the dependence of the results on the computed flux gradient terms, A_x and A_y. As mentioned before, these values are computed from differences of differences of computed head values and, in some cases, can be in error by large amounts. Frind and Matanga [1985] suggest that flux estimates derived from a stream function solution tend to be more accurate than those derived from a head solution. Work on recasting the program in terms of a stream function solution is underway.

Another problem encountered so far is that the head drops computed from flux integrals tend to underestimate the head drops computed from taking differences of the heads computed by the finite difference model. This inconsistency between the finite difference model and the flux integral results leads to convergence problems for the estimation algorithm. This could result from the use of harmonic averages of adjacent cell conductivities to represent the conductivity at each cell face. Desbarats [1993] pointed out that these harmonic averages underestimate the distribution of actual cell values. Thus the finite difference model sees a lower distribution of conductivities and predicts higher head drops than the flux integral formulation. Therefore, the program is being recast in terms of a point-centered finite difference formulation, with conductivities

being averaged arithmetically at cell faces (resistivities in the stream function formulation).

In addition, we still need to work out how to approach this problem in radial coordinates. A simple logarithmic coordinate transformation can be used to recast the single-well radial case in a form that is identical to the linear flow case presented here. However, modeling a well pair or dipole is not as straightforward. This is an important case, since we envision using a recharge-discharge pair in field applications of this method.

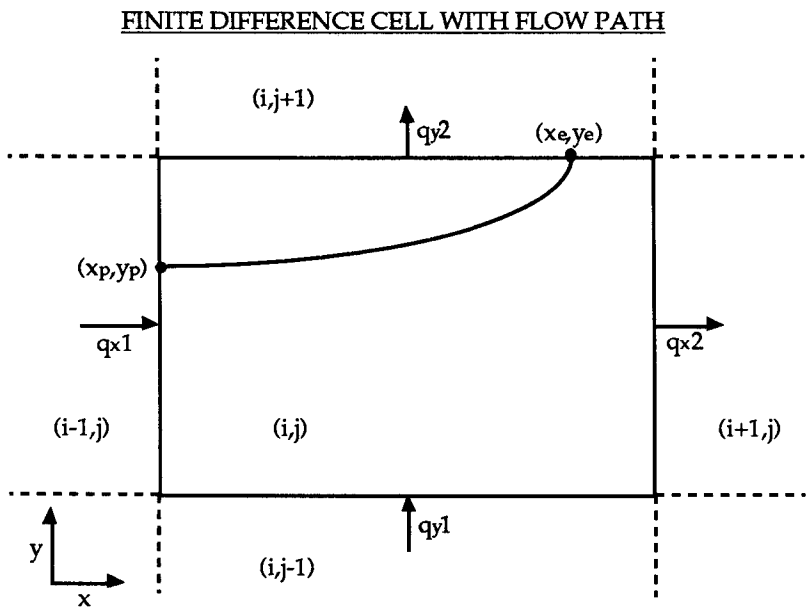
FINITE DIFFERENCE CELL WITH FLOW PATH
(i,j+1)
qy2
(xe,ye)
(xp,yp)
qx1
qx2
(i-1,j)
(i,j)
(i+1,j)
qy1
(i,j-1)
y
x

Figure 1.

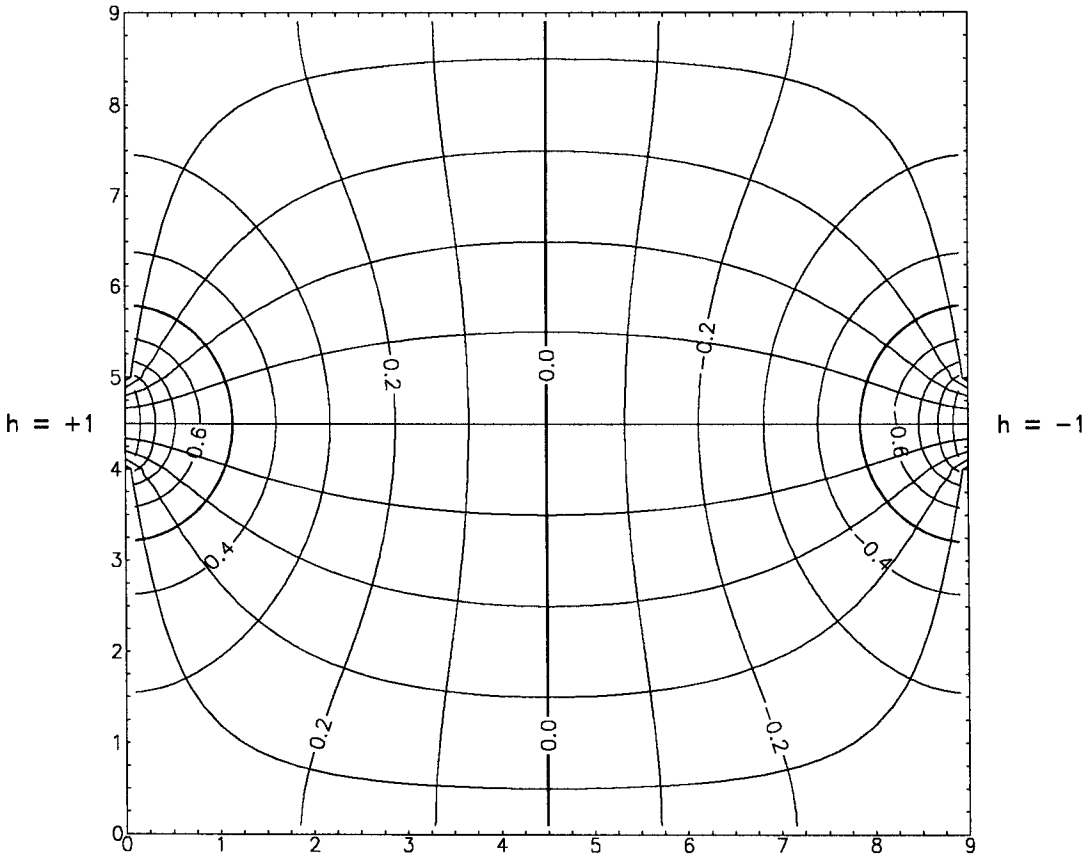

Figure 2. Constant hydraulic resistivity solution.

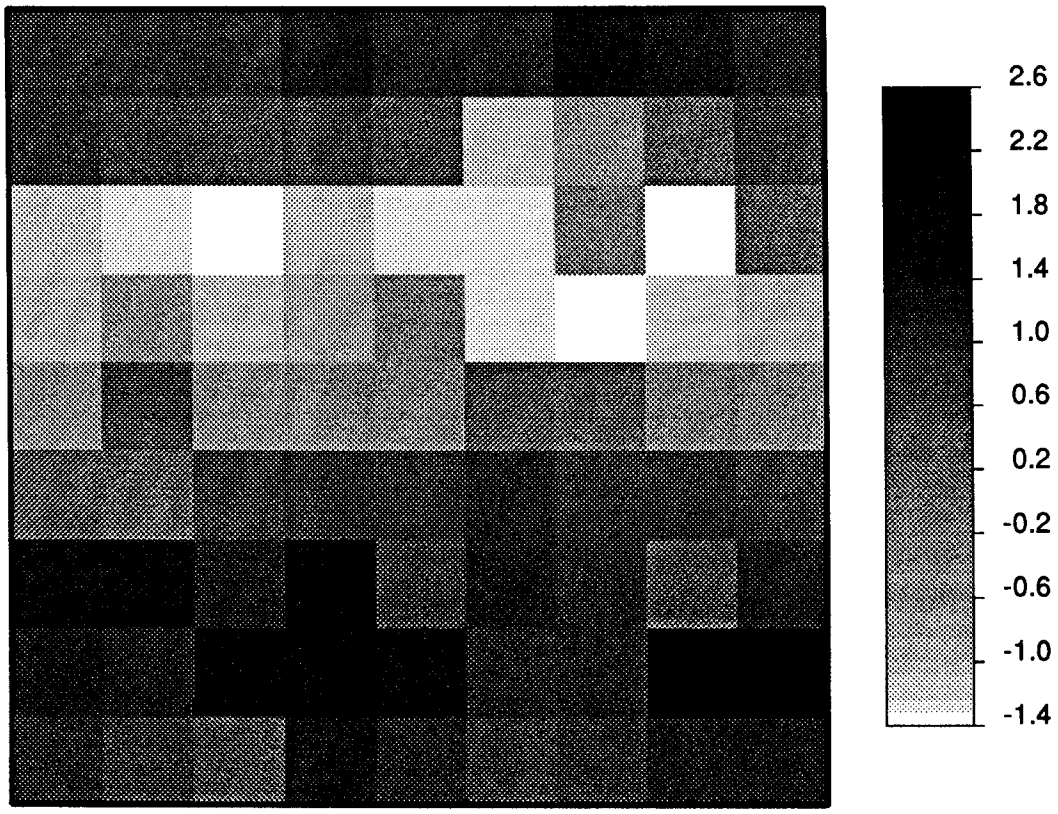

Figure 3. Natural log of hydraulic resistivity.

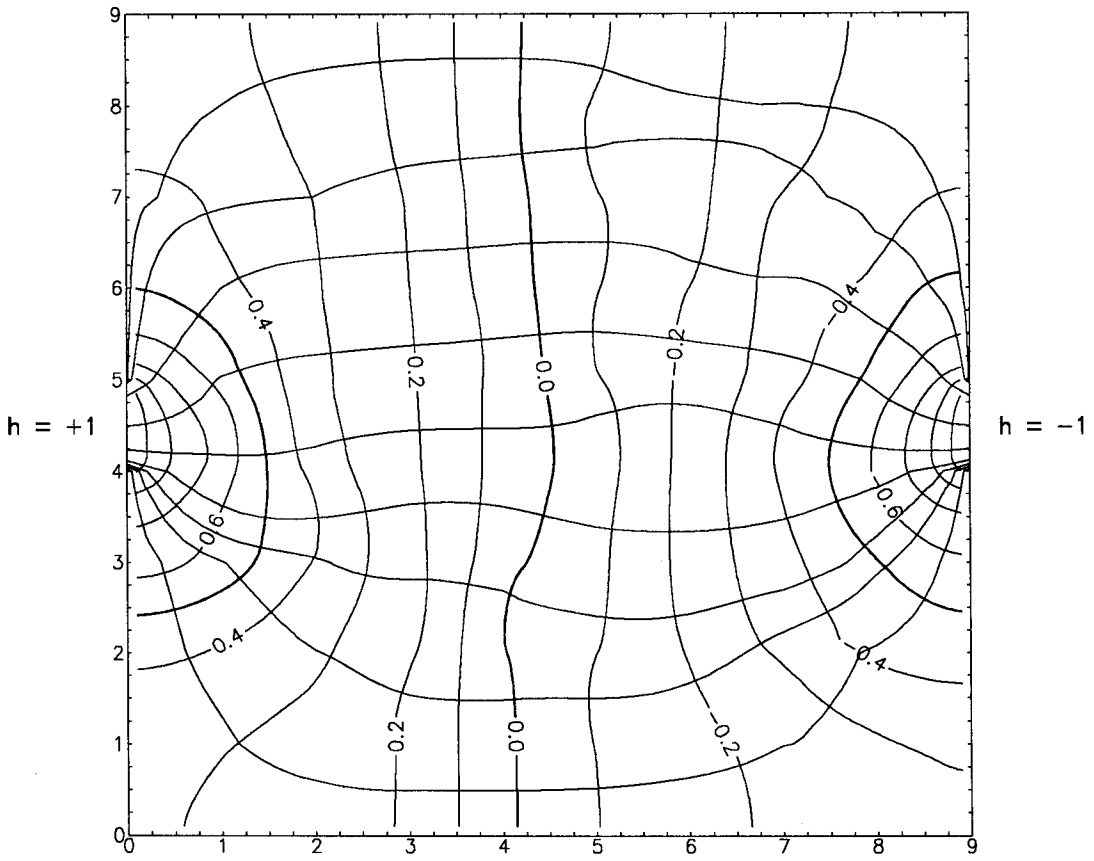

Figure 4. Variable hydraulic solution.

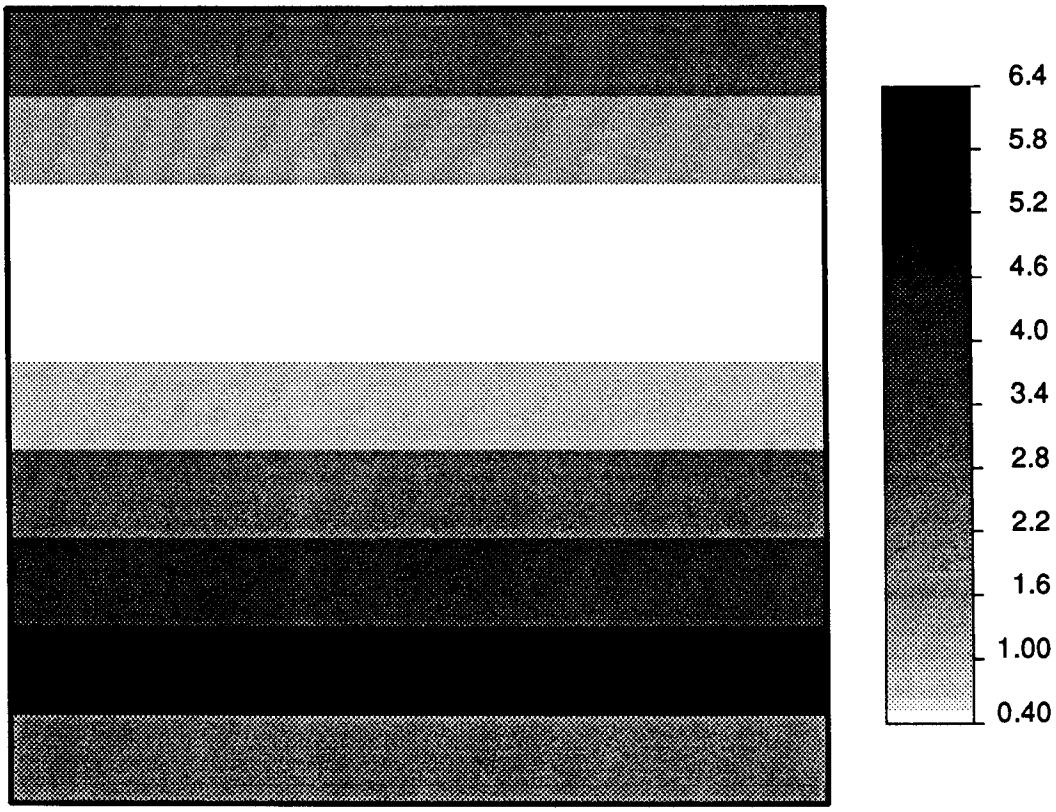

Figure 5. Hydraulic resistivity.

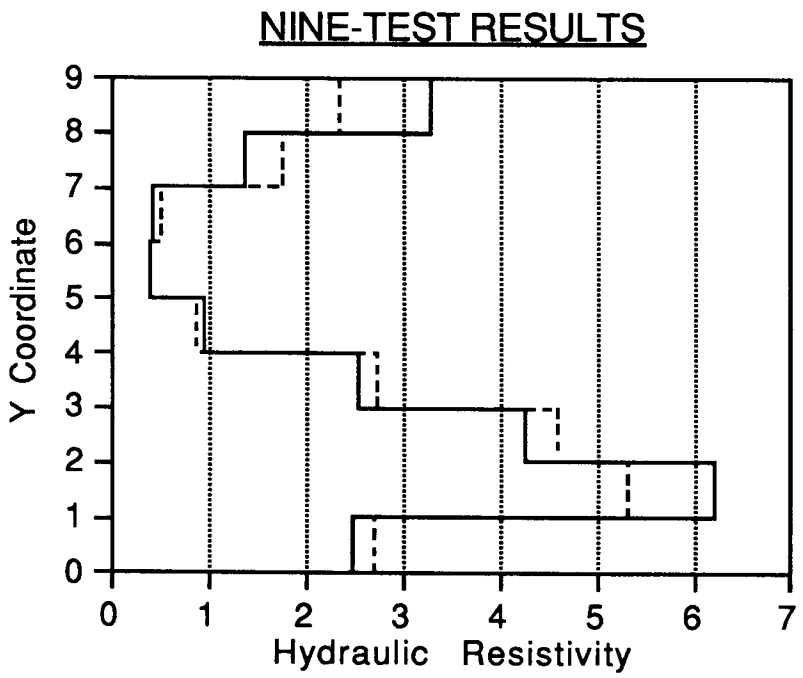

Figure 6. Nine-test results.

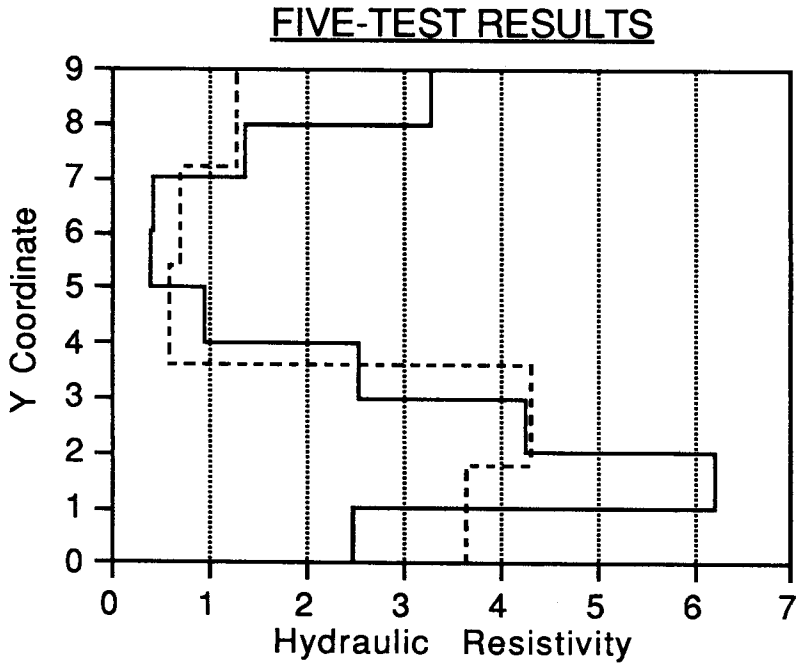

Figure 7. Five-test results.

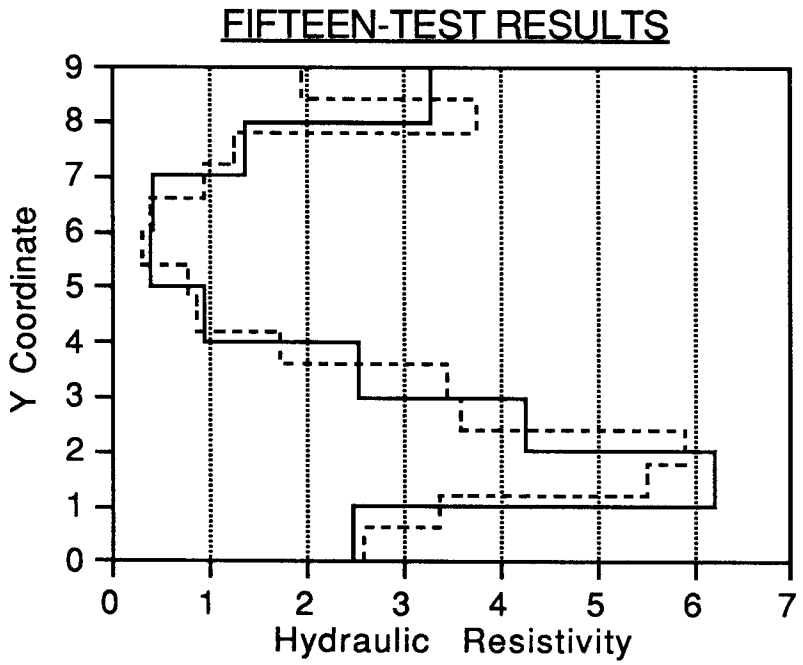

Figure 8. Fifteen-test results.

E. INVERSE PARAMETER ESTIMATION USING PULSE-TEST DATA

Introduction

Time-varying pumping signals have been reported to yield promising information about lateral inhomogeneities of the hydraulic parameters of an aquifer (Johnson et al. 1966, Vela & McKinley 1970, Butler & McElwee 1990). In order to assess if periodically time-varying perturbations of the hydraulic head can be used to identify lateral heterogeneities of the hydraulic conductivity field of an aquifer, an analytical one-dimensional solution for the hydraulic head in a two-zone aquifer subjected to sinusoidal time-varying Dirichlet boundary conditions was developed. The analytical structure of the solution was then compared to the head-solution for a homogenous aquifer to investigate whether or not effective parameters (that is, appropriately averaged hydraulic parameters leading to a system response identical to that of a homogeneous aquifer) can be derived for such a simple heterogeneous case like a two-zone aquifer.

Analytical Solution for Two-Zone Model

The flow processes in the two-zone model aquifer are governed by two mass balance equations of the form :

$$\frac{d^2h_1}{dx^2} = \frac{1}{\nu_1}\frac{dh_1}{dt} \qquad \nu_1 = \frac{T_1}{S_1}$$

$$\frac{d^2h_2}{dx^2} = \frac{1}{\nu_2}\frac{dh_2}{dt} \qquad \nu_2 = \frac{T_2}{S_2} \tag{II.E.1}$$

h_1 and h_2 are the head solutions in the first and the second zone of the aquifer, T_1, T_2, S_1, S_2 denote the transmissivities and storage coefficients of both zones. With $x_{B.}$ representing the boundary between both zones, the boundary conditions for the system are :

$$h_1(0,t) = h_0 \sin(\frac{2\pi t}{t_0}) = h_0 \sin(\omega t)$$

$$h_1(x_{B.},t) = h_2(x_{B.},t) \tag{II.E.2}$$

$$T_1 \left.\frac{dh_1}{dx}\right|_{x=x_{B.}} = T_2 \left.\frac{dh_2}{dx}\right|_{x=x_{B.}}$$

$$h_2(\infty,t) = 0$$

The solution of equations (II.E.1) subject to the boundary conditions (II.E.2) can be seen to be of the following complex form :

$$h_1(x,t) = [Ae^{\beta_1 x} + Be^{-\beta_1 x}]e^{i(\omega t - \pi/2)}$$
$$h_2(x,t) = Ce^{-\beta_2 x}e^{i(\omega t - \pi/2)} \qquad \text{(II.E.3)}$$

with :

$$\beta_1 = \left[\frac{1}{\sqrt{2}} + \frac{i}{\sqrt{2}}\right]\sqrt{\frac{\omega}{\nu_1}}$$

$$\beta_2 = \left[\frac{1}{\sqrt{2}} + \frac{i}{\sqrt{2}}\right]\sqrt{\frac{\omega}{\nu_2}}$$

The constants A, B, and C are to be determined from the first three boundary conditions in (II.E.2). The physically meaningful part of equations (II.E.3), that is, the respective real parts of the solutions (II.E.3), will then take the final form :

$$h_1(x,t) = \mathrm{Re}\{[h_0 e^{\beta_1 x} - \frac{gh_0}{f}e^{\beta_1(x_{B.}+x)} + \frac{gh_0}{f}e^{\beta_1(x_{B.}-x)}]e^{i(\omega t - \pi/2)}\}$$

$$h_2(x,t) = \mathrm{Re}\{[\frac{h_0 - gh_0 e^{\beta_1 x_{B.}}}{f}e^{(\beta_1+\beta_2)x_{B.}}e^{-\beta_2 x}$$

$$+\frac{gh_0}{f}e^{\beta_1(x_{B.}-x)}]e^{i(\omega t - \pi/2)}\}$$

with :

$$g = T_1\beta_1 + T_2\beta_2$$

$$f = 2[T_1\beta_1 \cos(\beta_1 x_{B.}) + iT_2\beta_2 \sin(\beta_1 x_{B.})]$$

A solution of system (II.E.1) subject to boundary condition (II.E.2) can also be obtained by using a fully real representation of h_1 and h_2 :

$$h_1(x,t) = h_0 e^{-Ax}[(1-F)\sin(\omega t - Ax) + G\cos(\omega t - Ax)]$$
$$+h_0 e^{Ax}[F\sin(\omega t + Ax) - G\cos(\omega t + Ax)] \qquad \text{(II.E.4)}$$
$$h_2(x,t) = h_0 e^{-Cx}[D\sin(\omega t - Cx) + E\cos(\omega t - Cx)]$$

Again, the constants A, F, G, C, D, and E have to be determined from the first three boundary conditions in (II.E.2). The resulting expressions for those constants are :

$$A = \sqrt{\omega S_1 / 2T_1}$$

$$C = \sqrt{\omega S_2 / 2T_2}$$

$$F = \frac{e^{-Ax_{B.}}}{U}(1 - \frac{AT_1}{CT_2})[SINEXP * \sin(Cx_{B.} - Ax_{B.}) - COSEXP * \cos(Cx_{B.} - Ax_{B.})]$$

$$U = COSEXP^2 + SINEXP^2$$

$$SINEXP = e^{-Ax_{B.}}(1 - \frac{AT_1}{CT_2})\sin(Cx_{B.} - Ax_{B.}) - e^{Ax_{B.}}(1 + \frac{AT_1}{CT_2})\sin(Cx_{B.} + Ax_{B.})$$

$$COSEXP = -e^{-Ax_{B.}}(1 - \frac{AT_1}{CT_2})\cos(Cx_{B.} - Ax_{B.}) + e^{Ax_{B.}}(1 + \frac{AT_1}{CT_2})\sin(Cx_{B.} + Ax_{B.})$$

$$G = \frac{(1-F)e^{-Ax_{B.}}(1 - \frac{AT_1}{CT_2})\sin(Cx_{B.} - Ax_{B.}) + Fe^{Ax_{B.}}(1 + \frac{AT_1}{CT_2})\sin(Cx_{B.} + Ax_{B.})}{-e^{-Ax_{B.}}(1 - \frac{AT_1}{CT_2})\cos(Cx_{B.} - Ax_{B.}) + e^{Ax_{B.}}(1 + \frac{AT_1}{CT_2})\cos(Cx_{B.} + Ax_{B.})}$$

$$D = \frac{AT_1}{CT_2} e^{Cx_{B.}} \{e^{-Ax_{B.}} [(1-F)\cos(Cx_{B.} - Ax_{B.}) - G\sin(Cx_{B.} - Ax_{B.})] - e^{Ax_{B.}} [F\cos(Cx_{B.} + Ax_{B.}) - G\cos(Cx_{B.} + Ax_{B.})]\}$$

$$E = \frac{AT_1}{CT_2} e^{Cx_{B.}} \{e^{-Ax_{B.}} [(1-F)\sin(Cx_{B.} - Ax_{B.}) + G\cos(Cx_{B.} - Ax_{B.})] - e^{Ax_{B.}} [F\sin(Cx_{B.} + Ax_{B.}) - G\cos(Cx_{B.} + Ax_{B.})]\}$$

Specifically, if $T_1 = T_2 = T$ and $S_1 = S_2 = S$: $F = G = E = 0$, $D = 1$, and $A = C = \sqrt{\omega S / 2T}$ so that (4) reduces to the one-zone solution (Ingersoll et al. 1948) :

$$h(x,t) = h_0 e^{-x\sqrt{\omega S/2T}} \sin(\omega t - x\sqrt{\omega S/2T}) \qquad \text{(II.E.5)}$$

In the case of only small variations in the transmissivities and storage coefficients, that is, for $T_1 \sim T_2$ and $S_1 \sim S_2$, a simplification of the constants A, C, D, E, F, and G leads to the following approximate expressions for the two-zone solutions :

$$h_1(x,t) = h_0 e^{-Ax} \sin(\omega t - Ax)$$
$$h_2(x,t) = h_0 \frac{AT_1}{CT_2} e^{-C(x-x_{B.})-Ax_{B.}} \sin(\omega t - Cx) \qquad \text{(II.E.6)}$$

This result shows that the amplitude decay is a function of the spatially weighted average of the parameters :

$$Amp \propto f(e^{-\sqrt{\omega S_2/2T_2}(x-x_{B.})-\sqrt{\omega S_1/2T_1}x_{B.}}) \qquad \text{(II.E.7)}$$

Effect of Initial Estimates on Parameter Estimation

Solutions (II.E.4) were investigated in conjunction with the Levenberg-Marquardt algorithm to inversely estimate the transmissivities and storage coefficients of both zones for predefined model situations. To uncover the influence of the particular set of initial parameter guesses on the estimated transmissivities and storage coefficients, eight Monte

Carlo simulations were performed, each simulation based on a slightly altered set of initial guesses. Every Monte Carlo simulation is based on 800 single simulations. For each single simulation the initial transmissivities and storage coefficients were taken from predefined parameter intervals in the form of a uniform deviate. The estimation was then performed by incorporating synthetic data which were generated by using the analytical two-zone solution in conjunction with a defined parameter set of the hydraulic aquifer parameters. As there are five parameters to be estimated for this model (two transmissivities, two storage coefficients, and the boundary separating both aquifer zones), five observation positions were chosen at which the synthetic data were generated. Two observation positions were located within the first zone and three observation positions were located within the second zone. The sequences of observation data were generated at lateral distances of 4.3, 7.2, 11.0, 14.8, and 19.3 meters from the origin at which sinusoidal head boundary conditions were specified. The boundary between both zones is located at $x_{B.}$ = 10.0 meters from the origin. The synthetic observation data were generated by (II.E.4) at times t=n*dt, n=0,1,2,3,... according to the following parameter setup :

T_{10} = 1.5535E-3 m**2/sec
S_{10} = 1.3300E-5
T_{20} = 9.9678E-3 m**2/sec
S_{20} = 4.7200E-4

t_0 = 1800 sec.	period of input signal
h_0 = 1.0 m	amplitude of input signal
dt = 90.0 sec	time step
Tmax = 27000 sec	max. simulation time

t = n*dt

$\omega = 2*\pi/t_0$

The eight Monte Carlo simulations are numbered from 3 to 10. For Monte Carlo simulation no. 3 the following set of initial parameters was chosen :

$T_1 = T_{10} + 0.5*u*T_{10}$	;	T10 = 1.5535E-3 m**2/sec
$S_1 = S10 + 0.5*u*S_{10}$	;	S_{10} = 1.3300E-5
$T_2 = T_{20} + 0.5*u*T_{20}$	;	T_{20} = 9.9678E-3 m**2/sec
$S_2 = S_{20} + 0.5*u*S_{20}$	;	S_{20} = 4.7200E-4
$x_{B.} = x_{B.0} + u*0.9999$	;	$x_{B.0}$ = 10.0 m

T_{10}, S_{10}, T_{20}, S_{20}, and $x_{B.0}$ are the initial values with which the synthetic data at the observation positions were generated. u is a uniform deviate with values between -1 and +1. The initial parameters for Monte Carlo simulation no. 4-10 were chosen to be the

same as for Monte Carlo simulation no. 3 with the exception of the T_2 parameters. Those parameters were chosen as follows :

Monte Carlo simulation #	T_2 (m**2/sec)
4	$T_2 = T_{20}/1.5 + 0.5*u*T_{20}$
5	$T_2 = T_{20}/2.0 + 0.5*u*T_{20}$
6	$T_2 = T_{20}/2.5 + 0.5*u*T_{20}$
7	$T_2 = T_{20}/3.0 + 0.5*u*T_{20}$
8	$T_2 = T_{20}/3.5 + 0.5*u*T_{20}$
9	$T_2 = T_{20}/4.0 + 0.5*u*T_{20}$
10	$T_2 = T_{20}/5.0 + 0.5*u*T_{20}$

Thus, the interval from which the uniform distributed T_2-parameters for the 800 single simulations of each Monte Carlo simulation were drawn, is shifted to smaller and smaller values. The averages of the 800 estimates of the parameters of each Monte Carlo simulation are summarized in table 1, the respective standard deviations are given in table 2.

Table 1 : Average estimated transmissivities, storage coefficients, and boundary between both aquifer zones of Monte Carlo simulation no. 3 - 10.

Simulation	Av. T_1	Av. S_1	Av. T_2	Av. S_2	Av. $X_{boundary}$
3	1.4128E-3	1.2096E-5	9.0656E-3	4.2928E-4	10.0000
4	1.3027E-3	1.1153E-5	8.3585E-3	3.9580E-4	10.0000
5	1.1848E-3	1.0143E-5	7.6021E-3	3.6000E-4	10.0000
6	1.1130E-3	1.0159E-5	6.9098E-3	1.5012E-3	10.0564
7	1.1341E-3	1.1336E-5	6.0792E-3	3.0164E-3	10.0738
8	1.0572E-3	1.2036E-5	5.9890E-3	3.4456E-3	10.1055
9	1.0727E-3	1.0899E-5	5.4940E-3	3.9800E-3	10.1536
10	1.1245E-3	1.1124E-5	5.2809E-3	3.3926E-3	10.1516

Table 2 : Standard deviations of estimated transmissivities, storage coefficients, and boundary between both aquifer zones of Monte Carlo simulation no. 3 - 10.

Simulation	St.d. T_1	St.d. S_1	St.d. T_2	St.d. S_2	St.d. $X_{boundary}$
3	1.3001E-7	9.5299E-12	5.3528E-6	1.2000E-8	0.0000E0
4	1.2540E-7	9.1915E-12	5.1628E-6	1.1576E-8	0.0000E0
5	1.5688E-7	1.1499E-11	6.4587E-6	1.4482E-8	0.0000E0
6	5.8629E-7	6.2613E-11	9.5502E-6	7.6498E-5	6.0784E-2
7	1.8181E-6	2.8913E-10	1.2730E-5	2.5131E-4	1.3800E-1
8	2.0577E-6	1.9830E-9	1.3282E-5	2.1593E-4	1.3473E-1
9	5.1606E-6	5.6008E-10	1.4629E-5	2.2780E-4	1.8718E-1
10	1.0355E-5	2.3900E-10	3.1645E-5	1.5293E-4	2.0820E-1

Figures 1, 2, 3, and 4 show selected histograms of the estimated transmissivities of the second zone of Monte Carlo simulation no. 3, 4, 8, and 9. Those histograms reveal that the relative errors of the arithmetic averages of the estimated T_2-value stays within 35% of the true one as long as the deviation of the centroid of the interval from which the transmissivities of the second zone were drawn does not exceed 50% of the true value used to generate the synthetic data (the histograms for the remaining parameters (not shown) exhibited exactly the same behavior). If the centroid deviates more than 50% from the original value, then the error of the average estimated S_2-value quickly rose to several 100% (Figure 8). The growth of the relative errors of the averages of estimated transmissivities and storage coefficients is shown in Figures 5, 6, 7, and 8. In a typical real application we would not be able to bracket expected real parameter values with the required precision as outlined above, therefore we can conclude that, although we might arrive at reasonable convergence properties of the employed inverse algorithm, it would be difficult to relate the calculated results reliably to true physical parameters, when all five parameters are estimated simultaneously. To evaluate if better estimations of the true parameters would be obtained when using more observation wells, for example, we would have to perform more extensive numerical investigations. Note that the present results required a CPU-time of approximately 15 days on a 486 personal computer with a mathematical coprocessor. Therefore, any attempts to use a numerical groundwater flow model to estimate the aquifer parameters when using pulse testing with many observation wells at GEMS would require appropriate computer resources.

Parameter Estimation with SUPRPUMP

The major difficulty in simultaneously estimating all five parameters stems from high correlations between them. It can be directly infered from equations (II.E.1) that high correlations between T_1 and S_1 and T_2 and S_2 are to be expected as those parameters are comprised within the two diffusivities v_1 and v_2 which might be viewed as the actual two parameters governing groundwater flow described by (II.E.1). To investigate the estimation properties when keeping fixed four of the five parameters, the two-zone solution was implemented into SUPRPUMP. In a first step 30 simulations were performed to test the convergence properties of each physical parameter. Within each of those 30 simulations only one parameter (either one transmissivity value or one storage coefficient) was estimated. The boundary between both zones was always kept fixed at a value of 10m. The initial guesses for the transmissivities covered the parameter range from $4.8m^2/sec$ to $5.22*10^{-7}m^2/sec$, the initial guesses for the storage coefficients

covered a parameter range of $3.3*10^{-2}$ to $3.9*10^{-8}$. Convergence of the estimation procedure was always achieved after at most 21 iterations. In all cases the respective estimated parameter excellently matched the true one. In a further study 47 simulations were performed in which two parameters were now simultaneously estimated again keeping the boundary between both zones fixed as well as the two remaining parameters. 25 simulations were designed to simultaneously estimate T_1 and T_2, 11 simulations were designed to simultaneously estimate S_1 and T_2, and 11 simulations were designed to simultaneously estimate T_2 and S_2. The initial guesses for the transmissivities lay within a range of $10^{-2}m^2$/sec to $10^{-6}m^2$/sec, those for the storage coefficients lay in the range of 10^{-3} to 10^{-6}. Again convergence was always achieved within at most 22 iterations with an excellent match of estimated and true parameters. Problems, however, arose when trying to simultaneously estimate two physical parameters and also the boundary location or when trying to simultaneously estimate all four physical parameters keeping the boundary location fixed. In the former case 16 of 24 performed simulations did not converge. In the later case the estimated storage coefficient of the second zone always became unrealistically small (10^{-20}) and convergence to the true parameters could never be achieved. In comparision to the estimations performed by employing a Monte Carlo simulation in conjunction with the Levenberg-Marquardt technique we see that the convergence behavior of the Newton-like estimation technique as implemented in SUPRPUMP might be due to worse convergence properties of the latter method. Similar observations were stated elsewhere (e.g. Sacher 1983, Schwarz 1986).

Parameter Estimation Using Approximate Solution

We note that the application of the approximate expressions (II.E.6), although of intuitive interest, must be applied cautiously to situations for which the assumptions inherent in the derivation of (II.E.6) do not hold, that is, to aquifers showing significant variabilities in the hydraulic parameters. 13 Monte Carlo simulations were performed to support this statement. The same initial parameter setup was chosen for those simulations as was for the Monte Carlo simulations 4-10. In the present case, however, the storage coefficients were kept fixed as was the boundary location $x_{B,0}$. Only the transmissivities were disturbed by a uniform deviate u according to the following scheme :

Monte Carlo simulation #	T_1 (m**2/sec)	T_2 (m**2/sec)
11	$T_1 = T_{10} + 0.5*u*T_{10}$	$T_2 = T_{20} + 0.5*u*T_{20}$
12	$T_1 = T_{10} + 0.5*u*T_{10}$	$T_2 = T_{20}/3.0 + 0.5*u*T_{20}/3.0$

13	$T_1 = T_{10} + 0.5*u*T10$	$T_2 = T_{20}/6.0 + 0.5*u*T20/6.0$
14	$T_1 = T_{10} + 0.5*u*T_{10}$	$T_2 = T_{20}/9.0 + 0.5*u*T_{20}/9.0$
15	$T_1 = T_{10} + 0.5*u*T_{10}$	$T_2 = T_{20}/12.0 + 0.5*u*T_{20}/12.0$
16	$T_1 = T_{10} + 0.5*u*T_{10}$	$T_2 = T_{20}/15.0 + 0.5*u*T_{20}/15.0$
17	$T_1 = T_{10} + 0.5*u*T_{10}$	$T_2 = T_{20}/30.0 + 0.5*u*T_{20}/30.0$
18	$T_1 = T_{10}/3.0 + 0.5*u*T_{10}/3.0$	$T_2 = T_{20} + 0.5*u*T_{20}$
19	$T_1 = T_{10}/6.0 + 0.5*u*T10/6.0$	$T_2 = T_{20} + 0.5*u*T20$
20	$T_1 = T_{10}/9.0 + 0.5*u*T_{10}/9.0$	$T_2 = T_{20} + 0.5*u*T_{20}$
21	$T_1 = T_{10}/12.0 + 0.5*u*T_{10}/12.0$	$T_2 = T_{20} + 0.5*u*T_{20}$
22	$T_1 = T_{10}/15.0 + 0.5*u*T_{10}/15.0$	$T_2 = T_{20} + 0.5*u*T_{20}$
23	$T_1 = T_{10}/30.0 + 0.5*u*T_{10}/30.0$	$T_2 = T_{20} + 0.5*u*T_{20}$

Again each Monte Carlo simulation consists of 800 single simulations. The chosen scheme once again realizes a systematic shift of the intervals from which the initial transmissivities were drawn. For simulation 11-17 the T_2-interval was systematically shifted to smaller transmissivity values, for simulation 18-23 the T_1-interval from which the initial transmissivities were drawn was continously shifted to smaller values. The averages of the 800 estimated parameters of each Monte Carlo simulation are listed in table 3. The values significantly deviate from the true parameters T_{10} and T_{20}.

Table 3 : Average estimated transmissivities of Monte Carlo simulation no. 11 - 23.

Simulation	Av. T_1	Av. T_2
11	1.6828E-2	1.3903E-3
12	1.7725E-2	1.2081E-3
13	1.7725E-2	1.2081E-3
14	1.7725E-2	1.2081E-3
15	1.7725E-2	1.2081E-3
16	1.7725E-2	1.2081E-3
17	1.7725E-2	1.2081E-3
18	2.3654E-3	2.5691E-3
19	3.0087E-4	1.4255E-3
20	3.2287E-4	8.8096E-4
21	3.7956E-4	6.1106E-4
22	1.0763E-3	4.5610E-4
23	2.4751E-3	1.9340E-3

Application of a Kalman Filter for Hydraulic Parameter Estimation

Today, the use of a Kalman filter (Kalman 1960, Kalman & Bucy 1961) is well known for yielding improved estimates not only of the respective state variables but also of the associated parameters. Lim & Lee (1992), for example, use a Kalman filter to

predict the growth of *Trichoderma viride* grown on glucose while simultaneously estimating the kinetic parameters of the underlying Monod model. Geer (1982, 1984) applied the Kalman filter algorithm to design monitoring networks in the Netherlands, and Sen (1984) based a Kalman filter on the Theis-equation to estimate the hydraulic parameters of an aquifer. For the present work the two-zone solution developed above was employed as a base-model for a Kalman filter. To derive a suitable state equation, the system describing equations for the two-zone aquifer must be compiled appropriately. Assuming that the transmissivities, storage coefficients, and the boundary between both aquifer zones shall not depend on the time, the governing system equations have the form :

$$\frac{dh_1}{dt} = f_1(T_1, S_1, T_2, S_2, x_{B.}) \qquad \frac{dh_6}{dt} = \frac{dT_1}{dt} = 0$$

$$\frac{dh_2}{dt} = f_2(T_1, S_1, T_2, S_2, x_{B.}) \qquad \frac{dh_7}{dt} = \frac{dS_1}{dt} = 0$$

$$\frac{dh_3}{dt} = f_3(T_1, S_1, T_2, S_2, x_{B.}) \qquad \frac{dh_8}{dt} = \frac{dT_2}{dt} = 0$$

$$\frac{dh_4}{dt} = f_4(T_1, S_1, T_2, S_2, x_{B.}) \qquad \frac{dh_9}{dt} = \frac{dS_2}{dt} = 0$$

$$\frac{dh_5}{dt} = f_5(T_1, S_1, T_2, S_2, x_{B.}) \qquad \frac{dh_{10}}{dt} = \frac{dx_{B.}}{dt} = 0$$

Here the f_i, which stem from the time-derivative of the two-zone aquifer solutions h_i, are functions in the free parameters T_1, S_1, T_2, S_2, and $x_{B.}$ as are the h_i :

$$h_i = h_i(T_1, S_1, T_2, S_2, x_{B.}, x_i, t) \qquad \text{i=1,...,5 ; } x_i \text{ - observation node}$$

h_i - two-zone solution

Using a local linear approximation to the derivative of these equations the system equations can be summarized by an augmented dynamic equation of the form :

$$\left.\frac{d\vec{h}}{dt}\right|_{t+\Delta t} = \left.\frac{d\vec{h}}{dt}\right|_{t} + \Delta t[\underline{\underline{A}}\frac{d\vec{h}}{dt}]\Big|_t \qquad \text{(II.E.8)}$$

where $\mathbf{h} = (h_1,...,h_{10})$ and $\underline{\underline{A}}$ is the Jacobian of the process which is given by :

$$A = \begin{bmatrix} \frac{d\dot{h}_1}{dh_1} & \frac{d\dot{h}_1}{dh_2} & \frac{d\dot{h}_1}{dh_3} & \frac{d\dot{h}_1}{dh_4} & \frac{d\dot{h}_1}{dh_5} & \frac{d\dot{h}_1}{dT_1} & \frac{d\dot{h}_1}{dS_1} & \frac{d\dot{h}_1}{dT_2} & \frac{d\dot{h}_1}{dS_2} & \frac{d\dot{h}_1}{dx_{B.}} \\ \frac{d\dot{h}_2}{dh_1} & \frac{d\dot{h}_2}{dh_2} & \cdots & \cdots & & & & & \cdots & \frac{d\dot{h}_2}{dx_{B.}} \\ \vdots & \vdots & & & & & & & & \vdots \\ \frac{d\dot{T}_1}{dh_1} & \frac{d\dot{T}_1}{dh_2} & \cdots & \cdots & & & & & \cdots & \frac{d\dot{T}_1}{dx_{B.}} \\ \vdots & \vdots & & & & & & & & \vdots \\ \frac{d\dot{x}_{B.}}{dh_1} & \frac{d\dot{x}_{B.}}{dh_2} & \frac{d\dot{x}_{B.}}{dh_3} & \frac{d\dot{x}_{B.}}{dh_4} & \frac{d\dot{x}_{B.}}{dh_5} & \frac{d\dot{x}_{B.}}{dT_1} & \frac{d\dot{x}_{B.}}{dS_1} & \frac{d\dot{x}_{B.}}{dT_2} & \frac{d\dot{x}_{B.}}{dS_2} & \frac{d\dot{x}_{B.}}{dx_{B.}} \end{bmatrix}$$

$\underline{\underline{A}} \in \mathbf{R}^{10x10}$. The vector $\vec{h} = (h_1,...,h_{10})$ represents not only the time dependent two-zone solutions of the hydraulic heads $h_1,...,h_5$ at the five observation wells but also a state representation $h_6,...,h_{10}$ of the five aquifer parameters T_1, S_1, T_2, S_2, and $x_{Boundary}$ which are simultaneously estimated during the filter process. The time derivative of vector $\vec{h}$ is given by :

$$\frac{d\vec{h}}{dt} = \left[\frac{dh_1}{dt}, \frac{dh_2}{dt}, \frac{dh_3}{dt}, \frac{dh_4}{dt}, \frac{dh_5}{dt}, \frac{dT_1}{dt}, \frac{dS_1}{dt}, \frac{dT_2}{dt}, \frac{dS_2}{dt}, \frac{dx_{B.}}{dt} \right]$$

Rearranging equation (II.E.8) yields :

$$\left.\frac{d\vec{h}}{dt}\right|_{t+\Delta t} = [\underline{\underline{I}} + \Delta t \underline{\underline{A}}]_t \left.\frac{d\vec{h}}{dt}\right|_t \qquad \underline{\underline{I}} \in \mathbf{R}^{10x10}$$

where $\underline{\underline{I}}$ is the identity matrix. Multiplying both sides of this equation formally by dt and replacing $d\vec{h}$ by $\Delta\vec{h}$ gives the final state equation which was used in a Kalman filter :

$$\Delta\vec{h}\Big|_{t+\Delta t} = (\underline{I} + \Delta t\,\underline{\underline{A}})\Big|_t \Delta\vec{h}\Big|_t \qquad \text{(II.E.9)}$$

Note that generally only the upper right 5x5-submatrix of $\underline{\underline{A}}$ is different from zero, the transition matrix $(\underline{I} + \Delta t\,\underline{\underline{A}})\Big|_t$ of the process, however, is never zero as the identity is added to the product $\Delta t\,\underline{\underline{A}}$. Assuming that the state vector $\Delta\vec{h} = 0$, that is assuming that all states and parameters are known at the beginning of the filter process, the parameters for times t>0 are modeled as time independent. For example, equation (II.E.8) results in the following expression for parameter T1 : $T_1\big|_{t+\Delta t} = T_1\big|_t + \Delta h_6\big|_t$. As $\Delta h_6\big|_{t=0} = 0$, the transmissivity of the first aquifer zone is modeled as independent of time. Analogous equations hold for the remaining system parameters.

Initial attempts to estimate parameters with the Kalman filter technique have not been successful. The reason is unknown at this time. Work will continue on this technique to locate the source of the difficulty. A reformulation of the proposed methodology and a reprogramming of the Kalman filter program will be pursued to include the ε-technique described by Gelb (1974).

Conclusion

An analytical solution for a simple heterogeneous aquifer configuration was developed and combined with statistical estimation techniques to investigate how reliable the respective aquifer parameters might be inversely estimated using pulse-test data. Although the Levenberg-Marquardt algorithm always led to good convergence properties of the estimation processes, the averaged parameter estimates deviated significantly from the true ones when the initial guesses of the parameters were chosen too far off the true parameters.

For the case of only small variations in the hydraulic parameters the analytical solution of the two-zone model can be simplified to yield significant insight into the averaged aquifer properties which determine the signal amplitude of pulse-test data. However, real situations are usually characterized by strong variations in the hydraulic conductivity field. The approximate solution for small variations in the parameters may have limited application to such situations. The analytical structure of the exact two-zone solution is complex. The expansion of this solution to more complicated heterogeneous systems would be very difficult. Consequently, numerical studies will be used in further work to investigate the potential of hydraulic tomography to delineate aquifer heterogeneity.

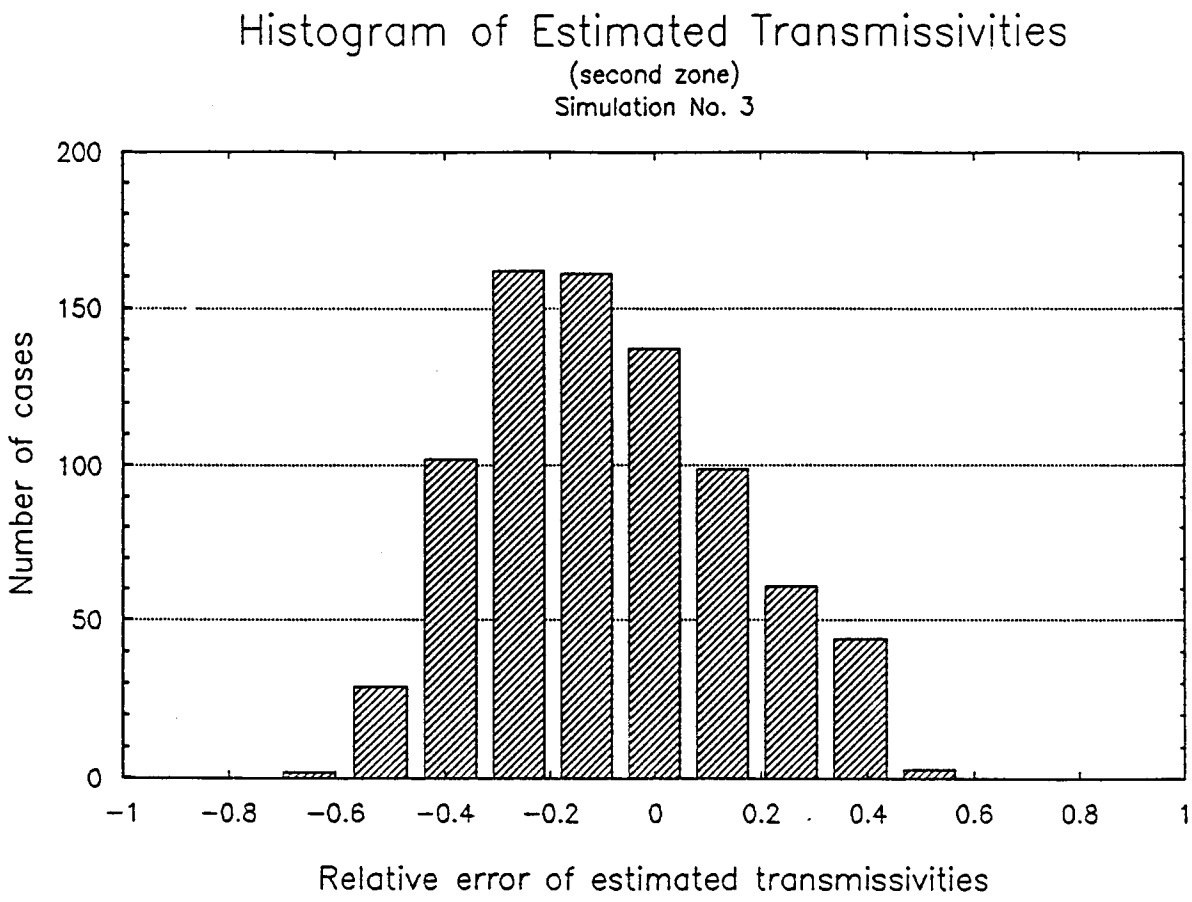

Figure 1. Histogram of the relative errors of the estimated transmissivities of the second zone (Monte Carlo simulation no. 3).

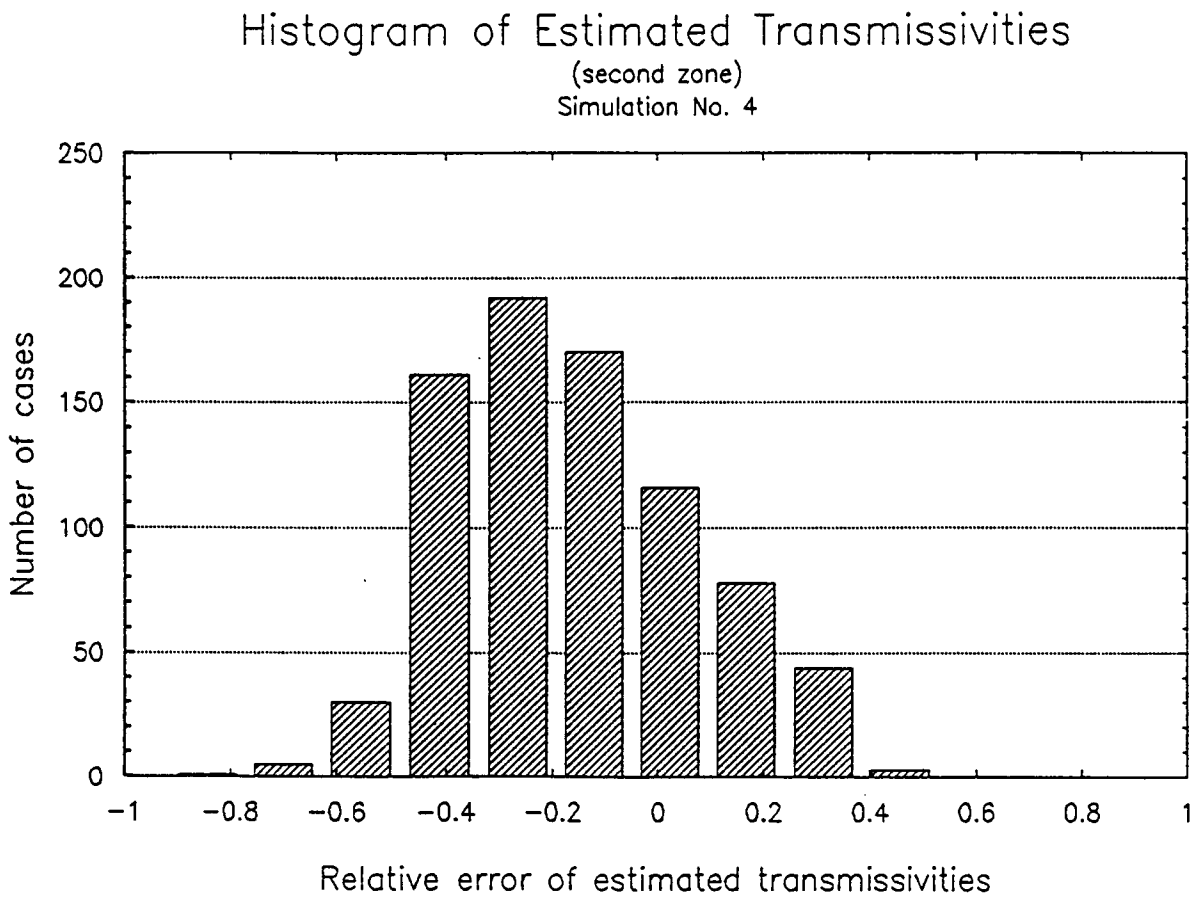

Figure 2. Histogram of the relative errors of the estimated transmissivities of the second zone (Monte Carlo simulation no. 4).

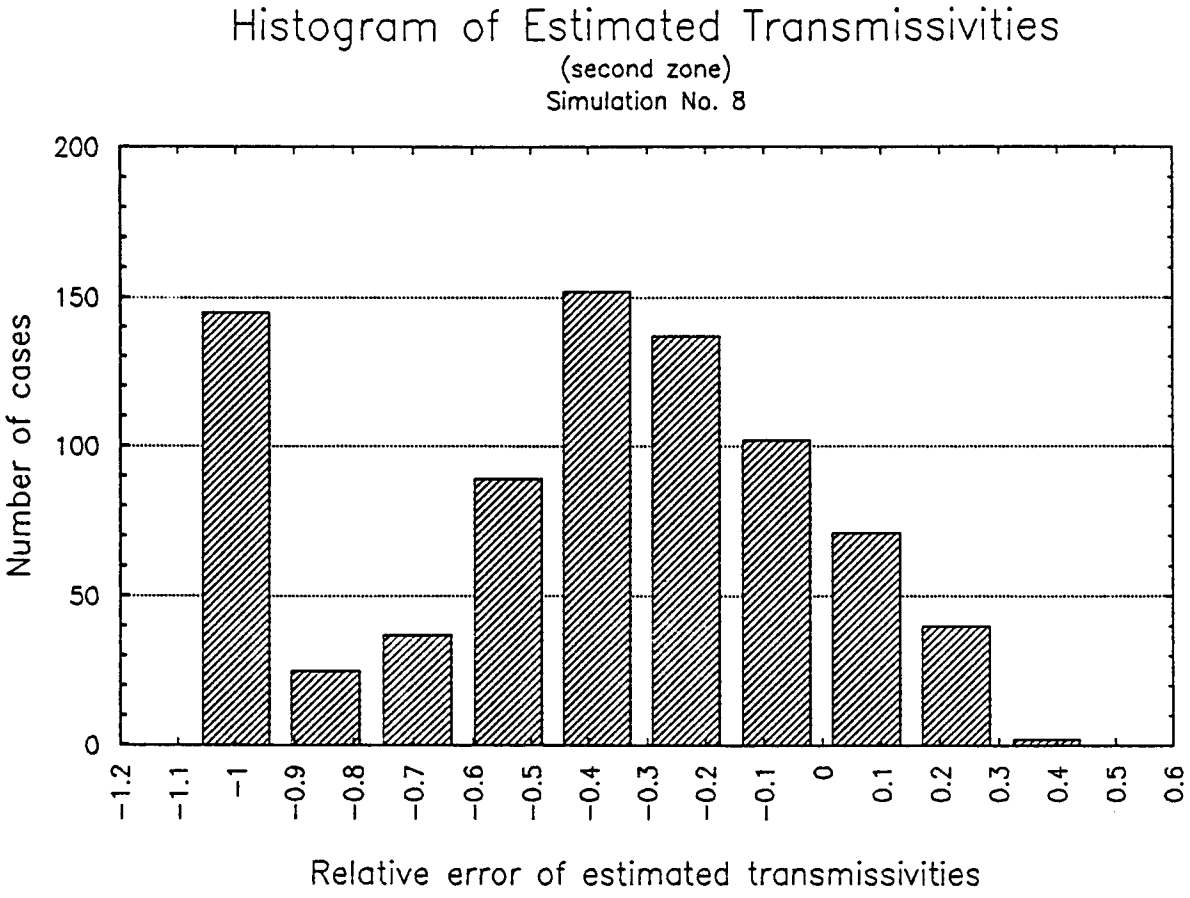

Figure 3. Histogram of the relative errors of the estimated transmissivities of the second zone (Monte Carlo simulation no. 8).

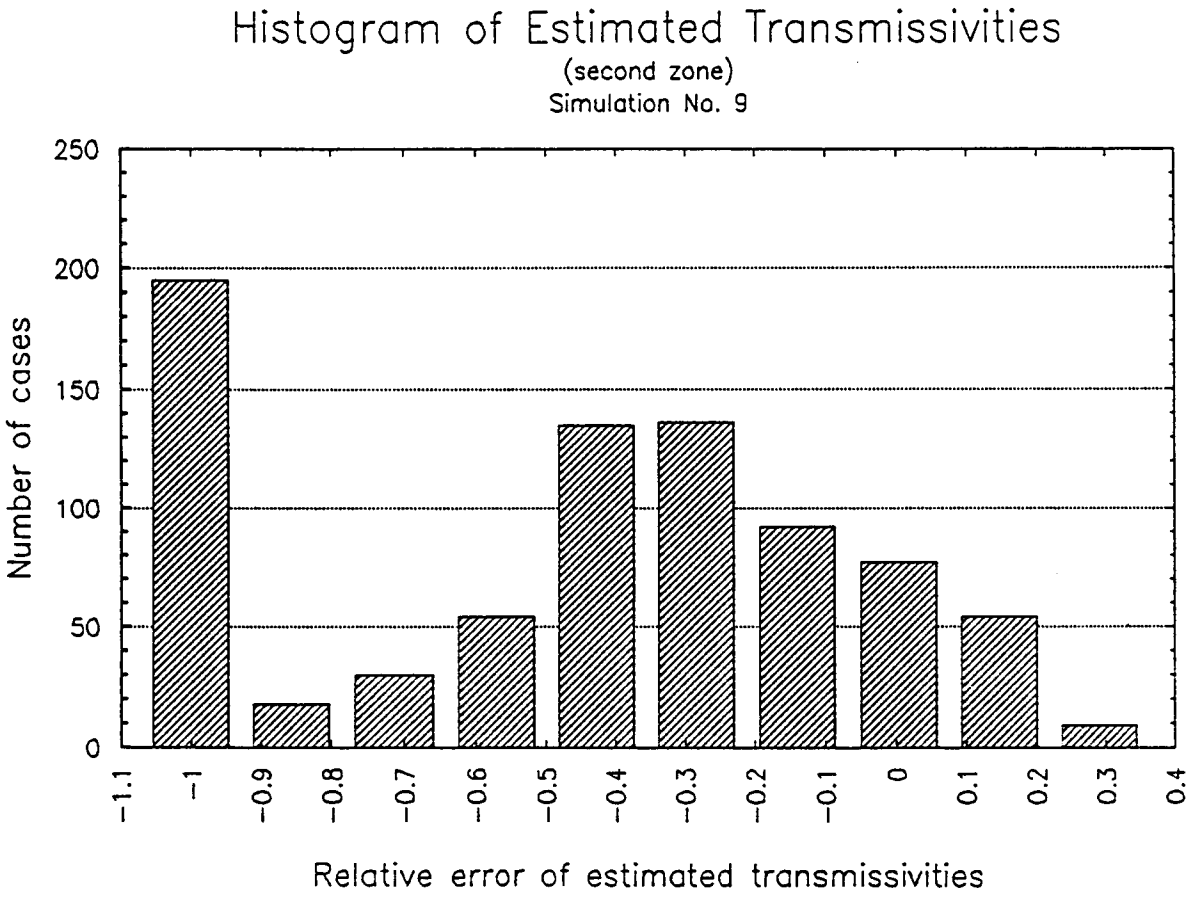

Figure 4. Histogram of the relative errors of the estimated transmissivities of the second zone (Monte Carlo simulation no. 9).

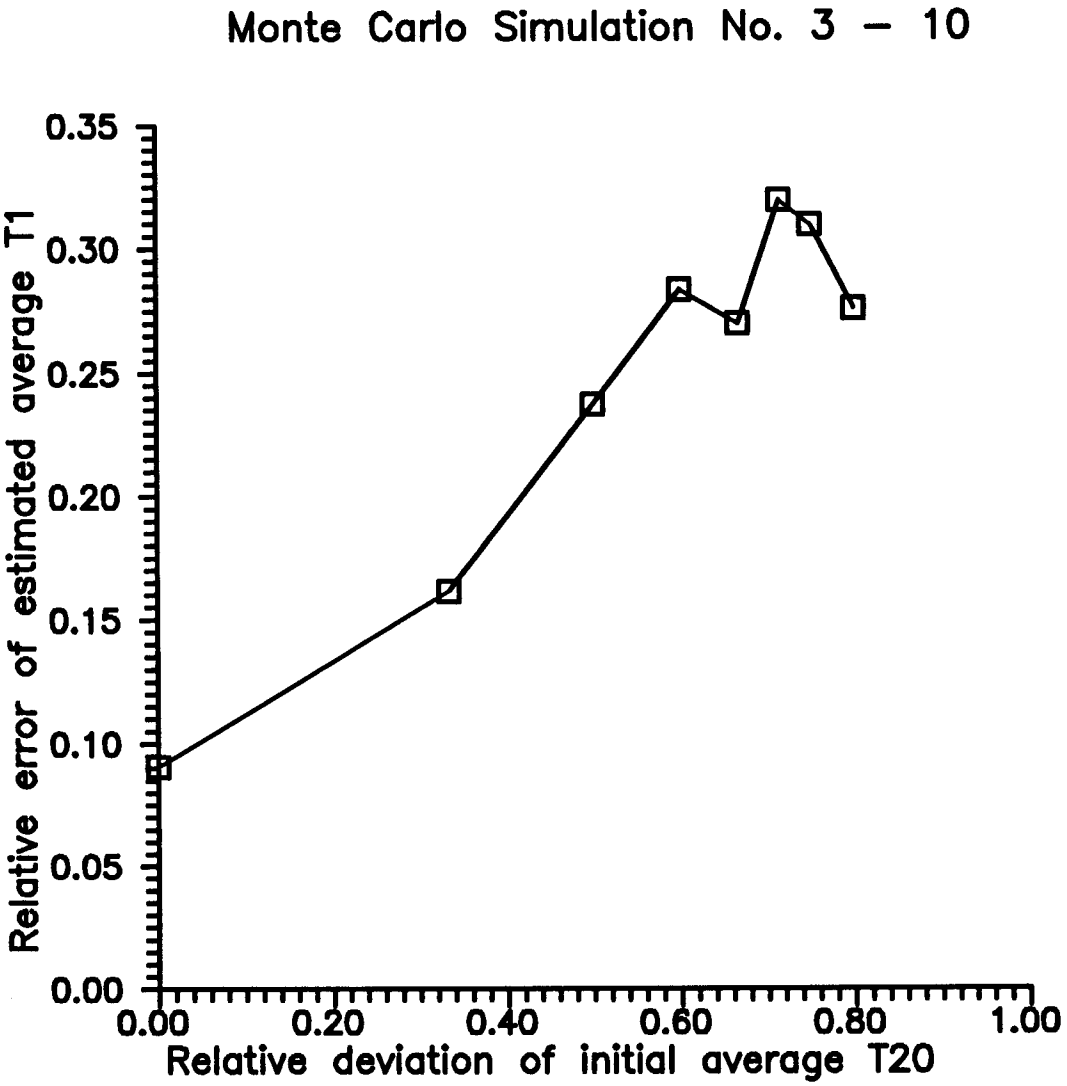

Figure 5. Relative errors of average estimated transmissivities of the first zone plotted versus the relative location of the centroid of the interval from which the initial guesses of the transmissivities of the second zone were drawn.

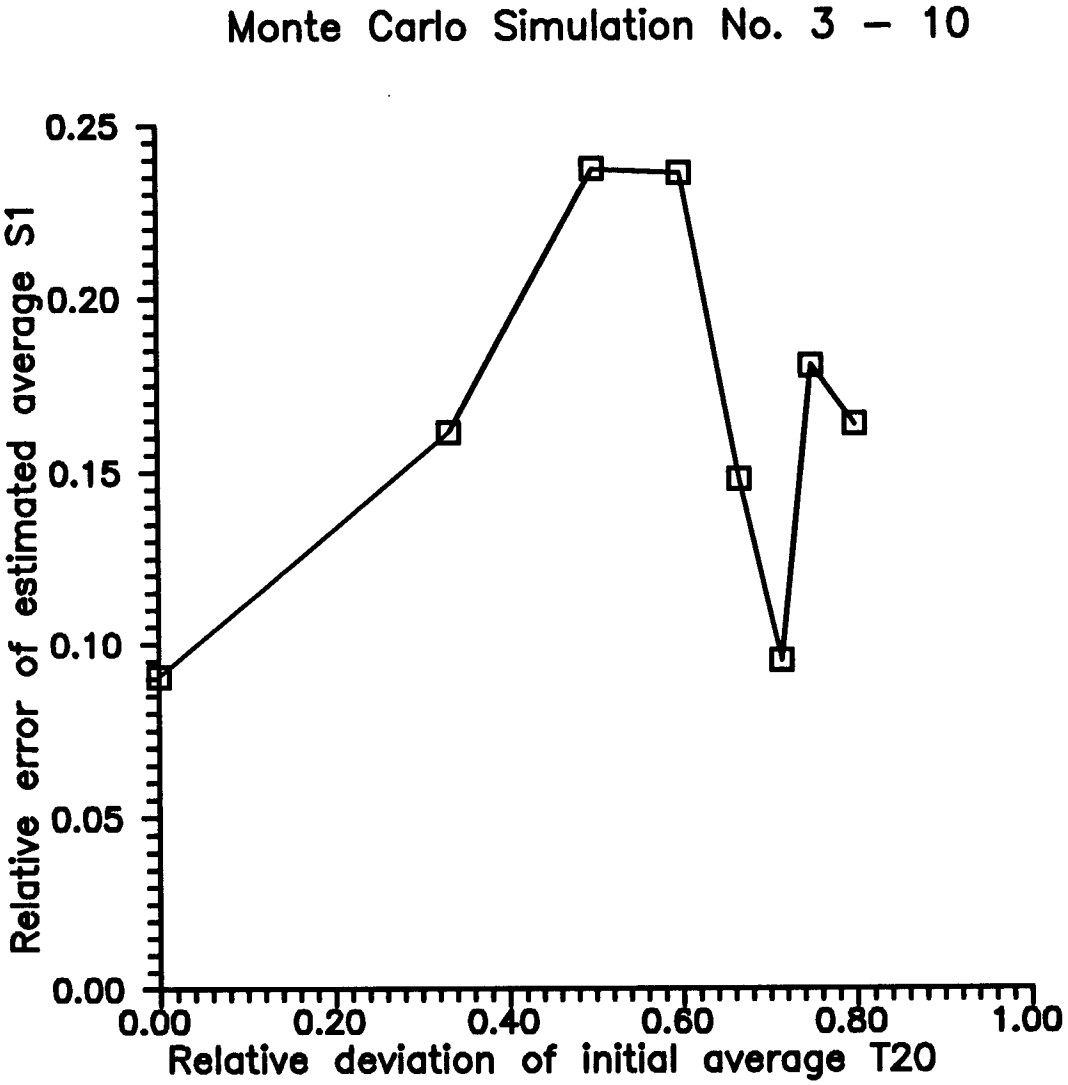

Figure 6. Relative errors of average estimated storage coefficients of the first zone plotted versus the relative location of the centroid of the interval from which the initial guesses of the transmissivities of the second zone were drawn.

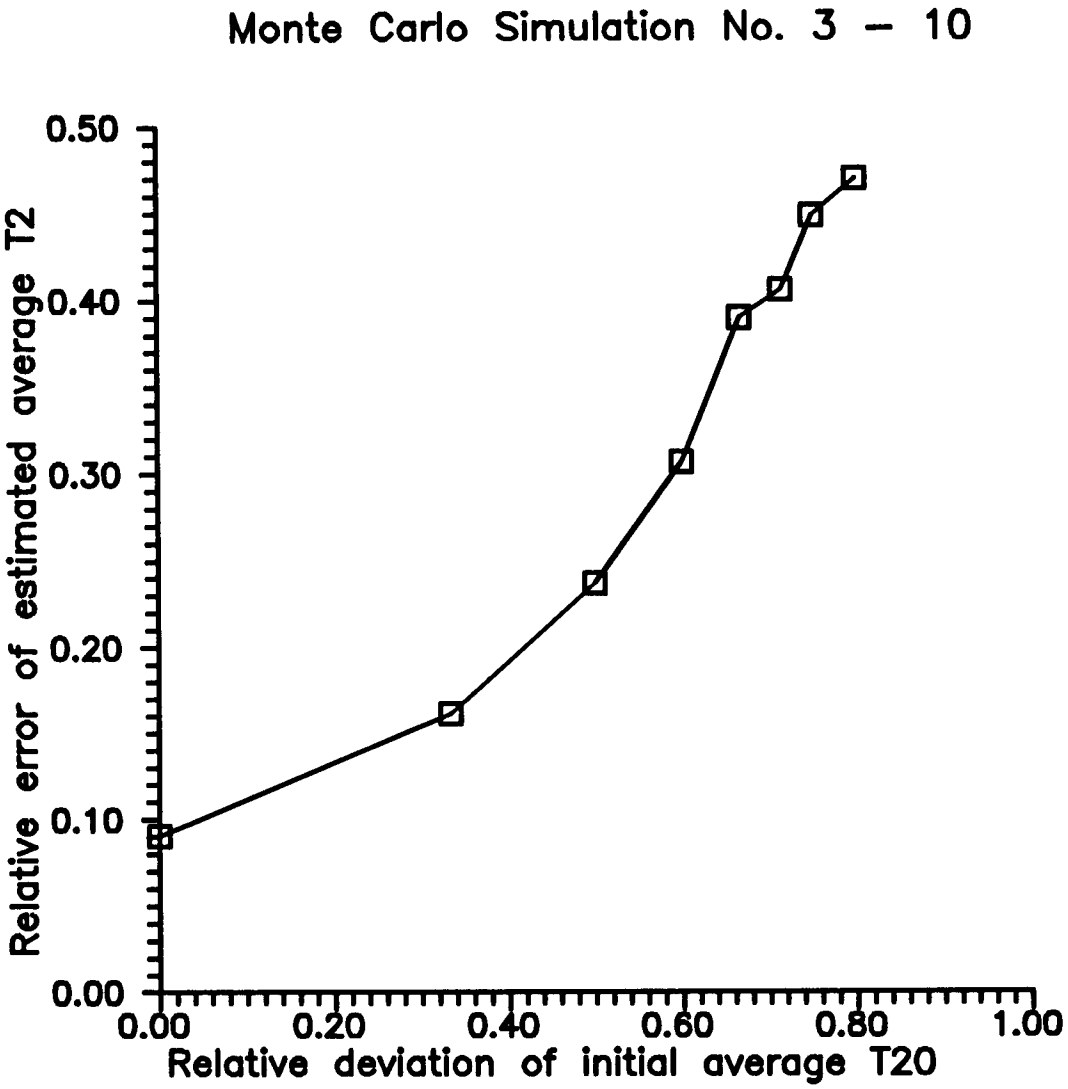

Figure 7. Relative errors of average estimated transmissivities of the second zone plotted versus the relative location of the centroid of the interval from which the initial guesses of the transmissivities of the second zone were drawn.

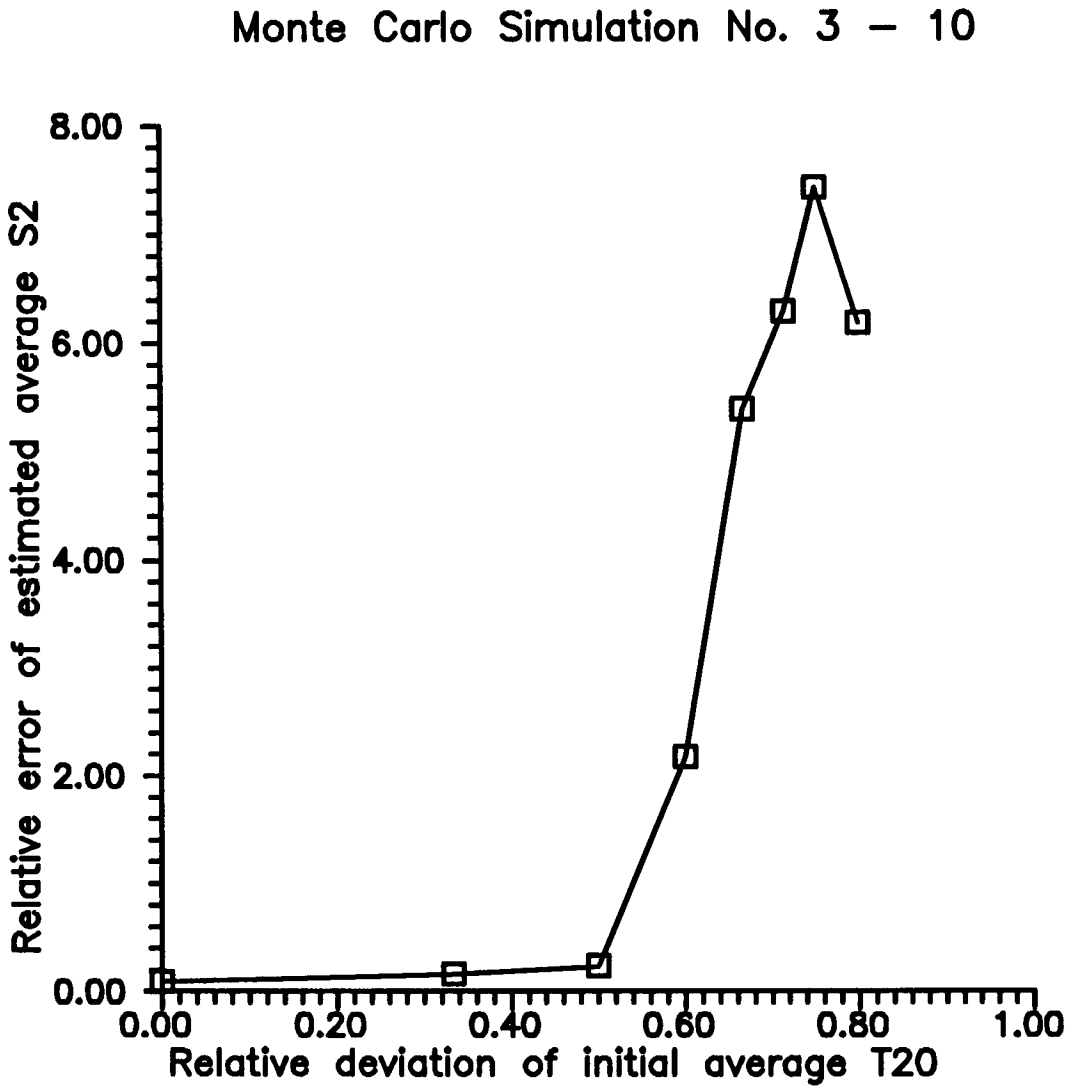

Figure 8. Relative errors of average estimated storage coefficients of the second zone plotted versus the relative location of the centroid of the interval from which the initial guesses of the transmissivities of the second zone were drawn.

F. SLUG TESTS IN THE PRESENCE OF A WELL SKIN

Introduction

Slug tests are frequently used to characterize the transmissivity of an aquifer. However, in the presence of heterogeneity it is uncertain how the slug test is averaging the aquifer properties. In the year one report we looked at the effect of a well skin in some detail. A well skin can be created by the process of establishing the well, and may have a transmissivity value (T1) greater or less than that of the aquifer transmissivity (T2). The effective transmissivity obtained from analysis of the data is a weighted average of T1 and T2 and can be predicted with a simple empirical formula. The effective transmissivity is highly weighted by the smallest transmissivity and is a weak function of the skin radius. We have done additional work on understanding how the two transmisisvities are averaged and on justifying the use of the empirical formula.

Fitting Well Skin Data to the C-B-P Model

When analyzing slug test data, the obvious question is: What is the effective transmissivity when a well skin is present? In general, the effective transmissivity resulting from the application of the C-B-P model (Cooper et al., 1967) to well skin data is an average of the skin and aquifer transmissivities. We have found that a good empirical equation for the effective transmissivity is

$$\frac{1}{T_{eff}} = \left[\frac{\ln(R_s / r_w)}{T_1} + \frac{\ln(r_{eff} / r_w) - \ln(R_s / r_w)}{T_2} \right] \left[\ln(r_{eff} / r_w) \right]^{-1} \qquad \text{(II.F.1)}$$

r_{eff} = effective radius influenced by the slug test. (Incidently, there was a typing omission in the first year report the correct formula is given above.) In the year one report we postulated that the effective radius was related to the storage coefficient in the following way,

$$r_{eff} / r_w = [C / S]^{1/2} \quad 1 \le C \le 2 \qquad \text{(II.F.2)}$$

where S is the storage coefficient.

The result given by this equation is highly weighted by T_1 and has a weak dependence on the skin radius when $T_1 << T_2$. In general, the lowest value of transmissivity (whether it

is the aquifer or the skin) will be the dominant factor in determining the effective transmissivity.

Steady-State Derivation

Consider an aquifer with two transmissivity zones. T_1 is the skin transmissivity and T_2 is the regional transmissivity. Radial flow considerations require the steady-state solution to be of the following form,

$$h_1 = -\frac{Q}{2\pi T_1}\ln\left(\frac{r}{r_w}\right) + h_w \qquad r_w \le r \le R_S$$
$$h_2 = -\frac{Q}{2\pi T_2}\ln\left(\frac{r}{R_S}\right) + h_{R_S} \qquad R_s \le r \le \infty \tag{II.F.3}$$

where Q is the flow rate. Boundary conditons must be applied to the solution. If we require that h_2 is approximatedly zero at r_{eff} and that the solutions match at the boundary R_S, then equation (II.F.3) becomes

$$h_1 = -\frac{Q}{2\pi T_1}\ln\left(\frac{r}{r_w}\right) - \frac{Q}{2\pi}\left[\frac{\ln\left(\frac{R_S}{r_{eff}}\right)}{T_2} + \frac{\ln\left(\frac{r_w}{R_S}\right)}{T_1}\right] \qquad r_w \le r \le R_S$$
$$h_2 = -\frac{Q}{2\pi T_2}\ln\left(\frac{r}{r_{eff}}\right) \qquad R_s \le r \le \infty \tag{II.F.4}$$

An effective transmissivity can be defined in the usual way requiring the same inner and outer boundary conditions.

$$h_{eff} = -\frac{Q}{2\pi T_{eff}}\ln\left(\frac{r}{r_w}\right) + h_w \qquad r_w \le r \le r_{eff} \tag{II.F.5}$$

At $r = r_{eff}$ the head is effectively zero by assumption, so equation (II.F.5) can be solved for the effective transmissivity.

$$\frac{1}{T_{eff}} = \frac{2\pi}{Q}\left[\ln\left(\frac{r_{eff}}{r_w}\right)\right]^{-1} h_w$$

$$\frac{1}{T_{eff}} = -\left[\frac{\ln\left(\frac{r_w}{R_S}\right)}{T_1} + \frac{\ln\left(\frac{R_S}{r_{eff}}\right)}{T_2}\right]\left[\ln\left(\frac{r_{eff}}{r_w}\right)\right]^{-1} \qquad \text{(II.F.6)}$$

The quantity h_W has been identified by simply comparing (II.F.3) and (II.F.4) and substituted into the first line of (II.F.6) to yield the final result. It is seen that this formula for the effective transmissivity is identical with (II.F.1), after some minor algebra manipulation.

Derivation Under Hvorslev Assumptions

The derivation in the preceding section assumes steady state conditions which are not correct during the performance of a slug test. We may relax this assumption by making a Hvorslev type of approximation for the time dependence. Assume that the equations of the preceding section hold at any instant but that the Q is varying as the slug test is carried out. This assumes a kind of instantaneous steady state with a varying Q, which in effect is ignoring the effect of storage. However, it is less restrictive than the steady state assumption and should be valid when a Hvorslev type of analysis is appropriate. Q can be written as

$$Q = vA = -\frac{dh_w}{dt} 2\pi r_w^2 \qquad \text{(II.F.7)}$$

v is the velocity of water in the well casing. Using equation (II.F.7) for Q and evaluating (II.F.4) at $r = r_W$ gives

$$h_w = \frac{dh_w}{dt} r_w^2 A$$

$$A = \left[\frac{\ln\left(\frac{r_w}{R_S}\right)}{T_1} + \frac{\ln\left(\frac{R_S}{r_{eff}}\right)}{T_2} \right] \qquad \text{(II.F.8)}$$

Integrating this equation gives the normal Hvorslev-type solution.

$$\ln(h_w) = \frac{t}{A r_w^2} + Constant \qquad \text{(II.F.9)}$$

In a similar way the effective radial equation (II.F.5) can be evaluated at r_{eff} and solved for the head at the well to yield

$$h_w = \frac{Q}{2\pi T_{eff}} \ln\left(\frac{r_{eff}}{r_w}\right). \qquad \text{(II.F.10)}$$

Using the expression for variable Q (II.F.7) gives the final form

$$h_w = \frac{dh_w}{dt} r_w^2 \frac{\ln\left(\frac{r_w}{r_{eff}}\right)}{T_{eff}} , \qquad \text{(II.F.11)}$$

which can be integrated to also give a Hvorslev-type solution.

$$\ln(h_w) = \frac{T_{eff}}{r_w^2 \ln\left(\frac{r_w}{r_{eff}}\right)} t + Constant \qquad \text{(II.F.12)}$$

Comparing (II.F.9) and (II.F.11) allows the same expression for effective transmissivity to be identified as in equations (II.F.1) and (II.F.6).

In fact we do not need to require that the head goes to zero at some effective radius, it is sufficient to simply require that the head there be a small fraction of the head at the well

$$h(r_{eff}) = \varepsilon h_w << h_w. \qquad \text{(II.F.13)}$$

In this case the preceding analyses go through as before, allowing the same expression for effective transmissivity to be defined. However, the decay in time is modified slightly. A factor of $1/(1-\varepsilon)$ must multiply the right hand side of equations (II.F.8) and (II.F.11). This results in the Hvorslev decay rate being modified slightly; however, as long as ε is small the effect is negligible.

Summary

We have shown that the formula (II.F.1) may be more general than would be supposed at first glance. In particular, it seems to hold well for situations adequately described by the Hvorslev type of model. Our experience is that it also works well for the C-B-P model. The effective radius is not a strong function of the aquifer parameters. It may be possible to define some empirical rules for selecting the effective radius in certain cases. In that case, the effective transmissivity obtained from analysis of slug test data might be more useful in estimating the regional transmissivity, especially in those situations where the radius of the skin may be estimated from independent data such as the diameter of the auger flights. Analysis of slug tests in the presence of a skin is a very difficult problem and will require ongoing research in order to gain additional insight.

III. FIELD INVESTIGATIONS OF SLUG TESTS

A. SLUG TESTS WITH OBSERVATION WELLS

Introduction

Traditionally, slug tests have been performed using the central test well as both the site of the stress and the site at which measurements are taken. In the first year of this project, theoretical and field results were reported that demonstrated the benefits of using observation wells other than the stressed well in slug tests. The most noteworthy of the reported results was the finding that the reliability of the parameter estimates can be improved through the use of observation wells. In the case of the storage parameter, the improvement is quite dramatic. The field experiment described in the first year's report involved wells approximately 6.5 meters apart. The transmission of the slug-induced pressure disturbance over that distance indicates that the estimated parameters from slug tests are reflective of conditions over a much larger volume of the formation than is normally considered to be influencing the results of a slug test. In cases where large volumetric averages of formation parameters are desired, slug tests may provide an alternative to pumping tests. Clearly, slug tests present several advantages to the conventional pumping tests. As discussed in Section II.A, these include the small amount of equipment and manpower required to perform a test, the relatively short duration of the test, and the need for only a small amount of water (if any) to be added/removed from the well during the course of the test. The advantage of being able to initiate a slug test without adding or removing water from the well is very important for testing at sites of known or suspected contamination. However, if information about the hydraulic boundaries of a flow system is desired, the slug test does not provide a viable alternative to pumping tests.

To date, there has been very little work on the use of observation wells with slug tests (henceforth designated as multiwell slug tests). One of the few contributions in this area outside of the research of this project has been the work of Novakowski (1989) in which he presents an analytical solution for the response in an observation well to a pressure disturbance introduced instantaneously at a central well. Both the observation well and the stressed well are assumed to be fully screened across the aquifer. Well-bore storage is accounted for at the stressed well and, in an approximate fashion, at the observation well. Recently, van Dyke et al. (1993) describe the use of multiwell slug tests at a monitoring site in New Jersey. Unfortunately, the method that they employ for the analysis of the response data ignores well-bore storage effects at the stressed and

observation wells, thereby introducing a large amount of error into the parameter estimates.

In this section, additional field and theoretical work concerning multiwell slug tests is reported. A program of multiwell slug tests at the Geohydrologic Experimental and Monitoring Site (GEMS) is described. The estimated parameters from these tests were considerably larger than expected. A theoretical examination of multiwell slug tests using the analytical solution discussed in Section II.A is then presented. The results of this theoretical examination provide one explanation for the larger than expected parameter estimates.

Field Testing at GEMS

Well 10-1 (depth 17.32 m, screen length 0.76 m) was selected as the test well for a program of multiwell slug tests because of its proximity to several groups of wells that could be used as observation wells (see Figure 1 of Section IV.B). The tests reported here involved using well 6-2 (depth = 21.55 m, screen length = 11.55 m, distance from 10-1 = 5.62 m) and well 00-1 (depth = 17.04 m, screen length = 0.76 m, distance from 10-1 = 6.61 m). In all cases, the slug test was initated at 10-1 using the slug-test packer system described in the report of the first year of this project (McElwee and Butler, 1992). Measurements at the observation wells were taken using a transducer attached to the bottom of a packer located beneath the static water level in the well. The packer enabled effects associated with wellbore storage at the observation well to be kept very small. The response data could thus be analyzed without considering the effects of wellbore storage at the observation well.

Figures III.A.1 and III.A.2 display the responses observed at wells 6-2 and 00-1, respectively, for a slug test performed at well 10-1. In all cases, the responses at the stressed well exhibited the nonlinear behavior discussed in Section III.B of this report. Note the very low normalized heads measured at the two observation wells. The head changes at the observation wells were so small that the effective resolution of the transducers produced a stepped pattern in the measured responses. Note that the responses at well 6-2 were approximately 33% smaller than those at 00-1, even though 6-2 is one meter closer to 10-1 than 00-1. Several explanations can be advanced for the difference between the responses at 6-2 and 00-1: 1) the well at 6-2 is screened for a considerable length, so head increases at the same vertical interval as the stressed well are dampened by vertical movement of water in the well; 2) the resolution of the transducer causes the measured difference in the responses to be greater than the actual difference; and 3) spatial variations (heterogeneities) in flow properties produce a lower

diffusivity (K/S_s) between wells 10-1 and 6-2 than that between wells 10-1 and 00-1. Additional testing with a higher resolution pressure transducer and use of additional wells is currently being carried out to evaluate which of these explanations is the most reasonable.

Figures III.A.3 and III.A.4 display the results of an analysis of the response data using the fully penetrating slug-test model of Cooper et al. (1967). Note that although the fits appear relatively good (especially considering the stepped nature of the measured responses), the parameter estimates are much larger than the results obtained from the single-well slug tests discussed in Section III.B of this report. In addition, the parameter values exceed the maximum values that would be plausible for the sand and gravel aquifer at GEMS. In an attempt to explain the anomalously high parameter values that were obtained in the field testing, a further theoretical investigation of multiwell slug tests was initiated at the end of the second year of this project. The results of the initial portion of this work are reported below.

Theoretical Investigation of Multiwell Slug Tests

The Cooper et al. model that was used in the analysis of the responses at wells 6-2 and 00-1 is based on the assumption that both the stressed well and the observation well are fully screened across the aquifer. Since well 10-1 is screened for only .76 meters of a 10.7 meter sequence of sands and gravels, the fully screened assumption of the the Cooper et al. model is clearly being violated. In order to assess the error that is introduced into parameter estimates through use of partially penetrating wells in multiwell slug tests, the partially penetrating slug test solution presented in section II.A of this report was extended to the case of observation points at other than the stressed well. The head at an observation point anywhere in the aquifer for the case of a slug test performed in a well with a finite-radius well skin in an anisotropic confined aquifer can be written in a non-dimensional form as

$$\phi_1(\xi,\eta,p)=\frac{\frac{\gamma}{\alpha}F_c^{-1}(F_c(\omega)f_2)}{[1+\frac{\gamma}{\alpha}pF_c^{-1}(F_c(\omega)f_1)]},\ \xi\le\xi_{sk} \qquad \text{(II1.A.1a)}$$

$$\phi_2(\xi,\eta,p)=\frac{\frac{\gamma}{\alpha}F_c^{-1}(F_c(\omega)f_3)}{[1+\frac{\gamma}{\alpha}pF_c^{-1}(F_c(\omega)f_1)]},\ \xi_{sk}\le\xi \qquad \text{(II1.A.1b)}$$

where the notation is as in Section II.A except for

$$f_2 = \frac{[\Delta_2 K_0(\nu_1\xi)-\Delta_1 I_0(\nu_1\xi)]}{\nu_1[\Delta_2 K_1(\nu_1)+\Delta_1 I_1(\nu_1)]};$$

$$f_3 = \frac{N[K_0(\nu_1\xi_{sk})I_1(\nu_1\xi_{sk})+K_1(\nu_1\xi_{sk})I_0(\nu_1\xi_{sk})]K_0(\nu_2\xi)}{\gamma\nu_1[\Delta_2 K_1(\nu_1)+\Delta_1 I_1(\nu_1)]}.$$

Note that the inverse Fourier transforms in the numerator of Equations (III.A.1a) and (III.A.1b) are performed for η in the screened interval of the observation well, while the inverse Fourier transforms in the denominator are performed for η in the screened interval of the well at which the test is initiated.

Equation (III.A.1b) was employed to simulate a series of slug tests in a hypothetical aquifer with a hydraulic conductivity of 1.0e-3 m/s and a specific storage of 1.0e-5 /m. For the initial analysis discussed here, the well skin was assumed to have the same properties as the aquifer and the formation was considered isotropic with respect to hydraulic conductivity. This series of tests was designed to examine the effect of the fully screened assumption of Cooper et al. A slug test was simulated in which the well was assumed to be fully screened across a one-meter thick aquifer. A second simulation was performed in which a slug test was done in a well, with a screen one meter in length, that is at the center of a very thick aquifer. Figure III.A.5 displays the simulated responses for an observation point located ten meters in the radial direction from the stressed well. In both cases, the observation point is at the center of the screen. Note that the responses in the partially penetrating case are close to an order of magnitude smaller than those in the fully penetrating case. An analysis of the partially penetrating responses using the Cooper et al. model produced the results displayed in Figure III.A.6. Note that the estimated hydraulic conductivity and specific storage are 7.8 and 33 times, respectively, larger than the actual parameters employed in the

simulations. Clearly, the misapplication of the Cooper et al. model to data from a partially penetrating well can produce parameter estimates that are much larger than the actual parameters for that site.

Given this result, it is clear that the data from the multiwell slug tests at GEMS must be reanalyzed using the partially penetrating slug test model. Figure III.A.7 displays the results of the reanalysis of the test at well 00-1. Note that the estimated hydraulic conductivity and specific storage values are 22 and 38 times, respectively, smaller than the parameters obtained in the fully penetrating case. Note also that the estimated conductivity of 3.4e-4 m/s (29.4 m/d) is in keeping with the results of the core analyses reported in Section IV.C. In the early part of the third year of this project, the remainder of the multiwell slug test data will be reanalyzed using the partially penetrating model.

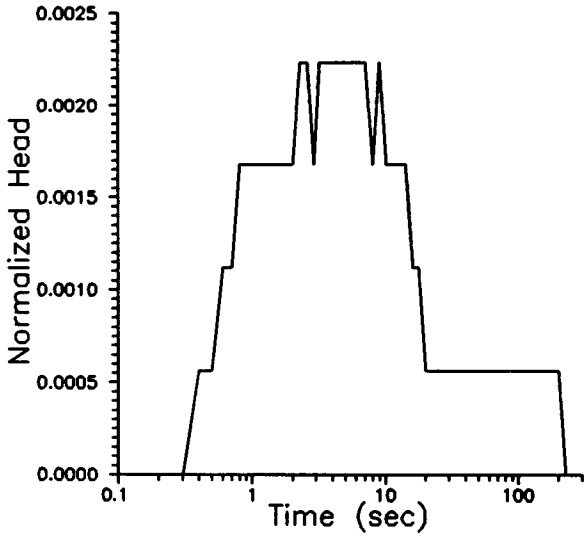

FIGURE III.A.1 - Normalized head ($h(t)/H_0$) versus time plot for well 6-2.

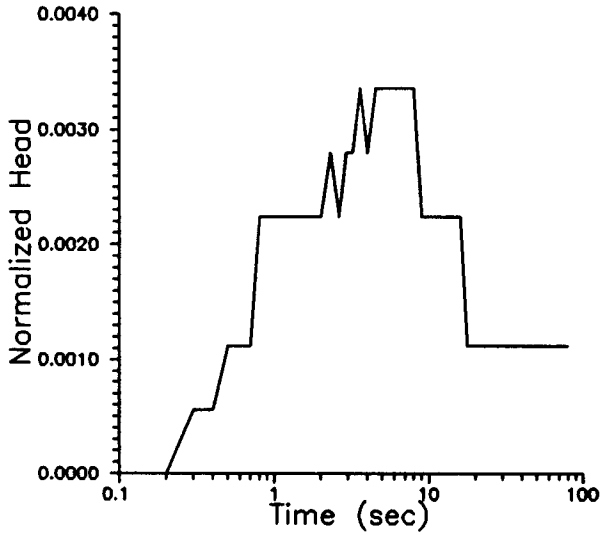

FIGURE III.A.2 - Normalized head ($h(t)/H_0$) versus time plot for well 00-1.

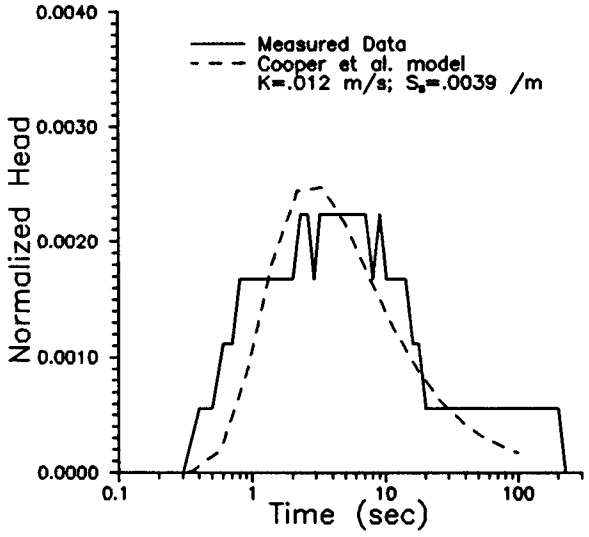

FIGURE III.A.3 - Normalized head versus time plot and the best-fit Cooper et al. model for well 6-2.

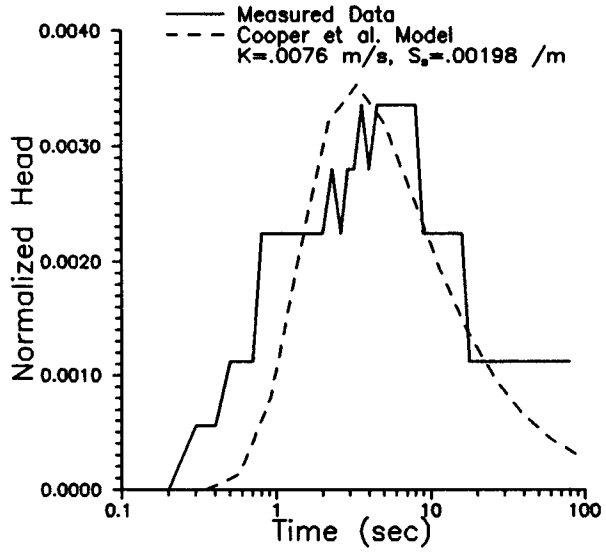

FIGURE III.A.4 - Normalized head versus time plot and the best-fit Cooper et al. model for well 00-1.

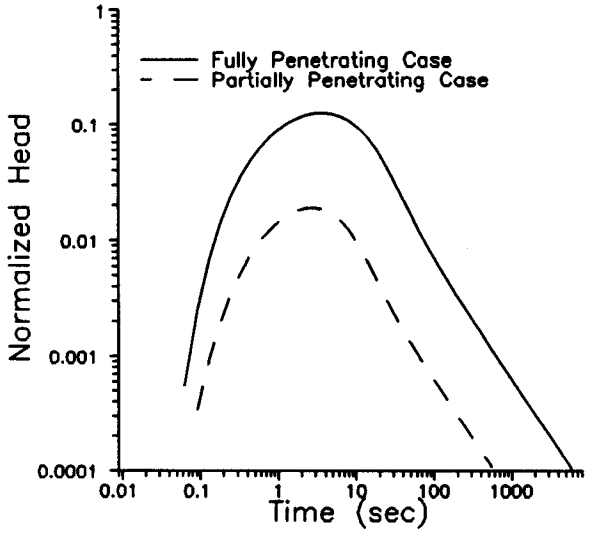

FIGURE III.A.5 - Normalized head versus time plot of simulated slug-test data (simulations employ the partially penetrating slug test model of Section II.A).

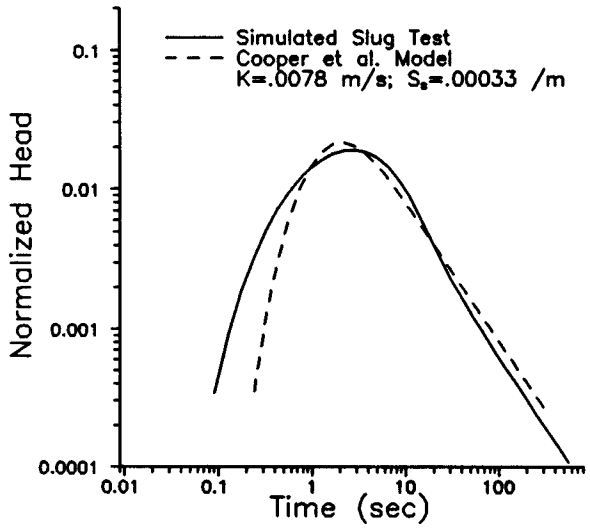

FIGURE III.A.6 - Normalized head versus time plot and the best-fit Cooper et al. model for the simulated partially penetrating well data of Figure III.A.5.

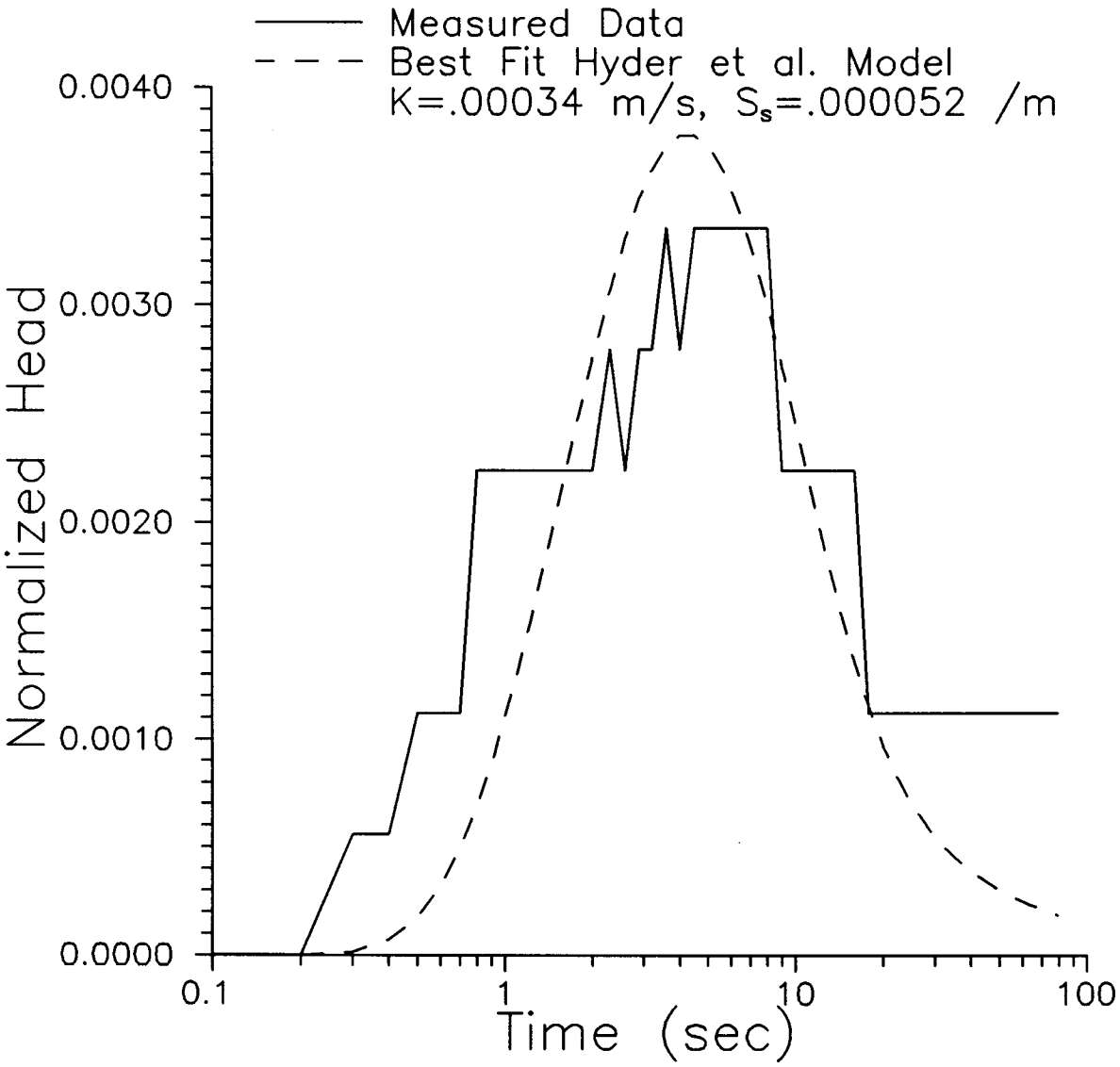

FIGURE III.A.7 - Normalized head versus time plot and the best-fit Hyder et al. model (partially penetrating slug test model of Section II.A) for well 00-1.

B. NONLINEAR MODELS FOR ANALYSIS OF SLUG-TEST DATA

Abstract

Slug tests are frequently used to characterize the transmissivity of an aquifer. However, in highly permeable aquifers problems arise when the conventional analytical techniques are applied. In an aquifer consisting of coarse sand and gravel overlain by silt and clay, we have consistently seen deviations from the expected response of linear theoretical models. For example, in the Hvorslev method the log of the slugged head in the well is plotted against time on a linear scale. Ideally this plot is a straight line, the slope of which is proportional to the hydraulic conductivity of the aquifer. Typically, we do not see a straight line on this plot, but rather a concave downward curve. Also, we see a dramatic dependence of the duration of the slug test on the initial height. If the slug-test data are normalized to the initial height, conventional models predict that all curves for different initial heights should be the same. We find that the curves are dramatically shifted to larger times for our field data. The sand and gravel at our field site is so coarse that the slug tests generally only last a few tens of seconds. This means that the water velocity is much faster than in finer sediments. We have investigated three non-linear variants of the Hvorslev model. One considers frictional effects caused by the flow of water in the casing and through the screen. We assume this frictional effect is proportional to a power of the velocity. Another model assumes non-Darcian flow, with the hydraulic gradient proportional to the first and second powers of velocity. A third model considers a modification of Darcy's law, adding in an inertial term proportional to the acceleration. All models can be shown to have the same mathematical form, even though they represent different physical processes. There are two parameters in the models: one is the hydraulic conductivity, and the other is related to the nonlinearity. We have developed a numerical solution for these models and have found that the solutions do exhibit downward curvature and do show the correct form of dependence on initial head. We have applied these models to field data and have found that the downward curvature and the dependence on head can be fit very well. Initial findings are that the hydraulic conductivity can be determined with some consistency, at a given well, for tests with different initial heads. However, a traditional Hvorslev analysis gives very different results for the hydraulic conductivity, with these same data for varying initial heads.

Introduction

Slug tests are frequently used to characterize the hydraulic conductivity of an aquifer. However, in highly permeable aquifers problems arise when the conventional analytical techniques are applied. At the GEMS (Geohydrologic Experimental and Monitoring Site) research and teaching site in the Kansas River alluvium, consisting of coarse sand and gravel overlain by silt and clay, we have consistently seen deviations from the expected response of linear theoretical models. For example (Figure 1), in the Hvorslev (1951) method the log of the slugged head in the well is plotted against time on a linear scale. Ideally this plot is a straight line, the slope of which is proportional to the hydraulic conductivity of the aquifer. Typically, we do not see a straight line on this kind of plot.

Field Data

When we plot field data (Figure 2) on a Hvorslev-type plot, concave downward curves are seen. Chirlin (1989) has shown that for the transient C-B-P model (Cooper et al, 1967) concave upward curves should result. Also, we see a dramatic dependence of the duration of the slug test on the initial height. If the slug-test data are normalized to the initial height, conventional models predict that all curves for different initial heights should be the same. We find that the curves are dramatically shifted to larger times for our field data.

Nonlinear Models

The sand and gravel at our field site is so coarse that the slug tests generally only last a few tens of seconds. This means that the water velocity is much faster than in finer sediments. We have investigated three nonlinear variants of the Hvorslev model. One considers frictional effects caused by the flow of water in the casing and through the screen. The Hvorslev approximation for the flow during a slug test is

$$Q(t) = \pi r_c^2 \frac{\partial H(t)}{\partial t} = -FK \cdot h(t) \qquad \text{(III.B.1)}$$

where

Q(t) = flow of water into aquifer

H(t) = height of water in well at any time,

h(t) = head of water just outside the screen in the aquifer,

K = hydraulic conductivity,

F = Hvorslev geometric factor, and

r_c = casing radius.

Equation (III.B.1) is the usual equation used to start the Hvorslev derivation, except that the right hand side contains h(t) which may be different from the head in the casing due to frictional effects. Assume a loss in head across the screen due to friction

$$Q(t) = \left(\frac{H(t) - h(t)}{R} \right) \tag{III.B.2}$$

R is the resistance factor. The flow through the screen [Q(t) in equation (III.B.2)] is assumed to be proportional to the head loss in the casing and screen and inversely proportional to a resistance factor (R). Replacing h(t) in equation (III.B.1) with equation (III.B.2) gives

$$\pi r_c^2 \frac{\partial H(t)}{\partial t} = -FK \cdot (Q(t)R + H(t)) \tag{III.B.3}$$

which involves only the head in the casing H(t). Q(t) can be replaced by using equation (III.B.1) again.

R is an empirical resistance factor that we have introduced. We assume this factor is proportional to a power of the velocity.

$$R = A \cdot |V| = A \left| \frac{dH(t)}{dt} \right| \tag{III.B.4}$$

where A is an assumed constant of proportionality. Equation (III.B.4) assumes that R is proportional to the first power of the velocity. A is a measure of the nonlinearity (nonlinear factor), if A = 0 then we have the usual Hvorslev solution. Replacing R in equation (III.B.3) yields

$$\frac{dH(t)}{dt} \left[1 + FKA \left| \frac{dH(t)}{dt} \right| \right] = -\frac{FK}{\pi r_c^2} H(t). \tag{III.B.5}$$

It is clear that equation (III.B.5) is a nonlinear equation which must be solved for the head in the casing, H(t).

There is other work in the literature that suggests the frictional effects may be proportional to higher powers of the velocity (Barker and Herbert, 1992; Singh and Shakya, 1989). The generalization for any power (N) of the velocity is:

$$R = A \cdot |V|^N = A\left|\frac{dH(t)}{dt}\right|^N . \qquad \text{(III.B.6)}$$

Similarly, the generalization of equation (III.B.5) is:

$$\frac{dH(t)}{dt}\left[1 + FKA\left|\frac{dH(t)}{dt}\right|^N\right] = -\frac{FK}{\pi r_c^2} H(t). \qquad \text{(III.B.7)}$$

Consequently, equations (III.B.6) and (III.B.7) give the generalization to the case when R is proportional to the Nth power of the velocity.

The second model we shall employ assumes non-Darcian flow, with the hydraulic gradient proportional to the first and second powers of velocity (Bear, 1972; Guppy et al., 1982).

$$\frac{\partial h}{\partial r} = -\frac{1}{K} V + bV^2 \qquad \text{(III.B.8)}$$

where b is a constant. After some algebra the result is the same as for the resistive loss case with N = 1, even though they represent different physical processes.

$$\frac{dH(t)}{dt}\left[1 + FKA\left|\frac{dH(t)}{dt}\right|\right] = -\frac{FK}{\pi r_c^2} H(t), \qquad \text{(III.B.9)}$$

where the relationship between A and b is

$$A = \frac{br_c^2}{4\pi L^2 r_w}. \qquad \text{(III.B.10)}$$

L is the length of the well screen and r_W is the screen radius. b is the nonlinear factor in equation (III.B.8), again if b = 0 we have the usual Hvorslev solution.

A third model to describe nonlinear slug test response has been investigated following Mohamed et al.(1992). They consider a generalization of Darcy's law keeping the acceleration term, which is usually assumed negligible. In this case we can write

$$\varepsilon \frac{dv_a}{dt} + v_a = -K\nabla h \qquad \text{(III.B.11)}$$

where v_a is the velocity in the aquifer and

$$\varepsilon = \frac{K}{g\theta} \quad . \qquad \text{(III.B.12)}$$

Here g is the acceleration of gravity and θ is the porosity of the aquifer. A continuity equation between the well casing and the aquifer requires that

$$Q = -\pi r_c^2 \frac{dH}{dt} = 2\pi r_s B v_a \qquad \text{(III.B.13)}$$

at the boundary between the casing and the aquifer, where r_c is the casing radius, r_s is the screen radius and B is the thickness of the aquifer. Solving equation (III.B.13) for v_a at the screen radius yields

$$v_a = -\left(\frac{r_c^2}{2r_s b}\right)\frac{dH}{dt} \qquad \text{(III.B.14)}$$

Differentiating (III.B.14) with respect to time gives the result

$$\frac{dv_a}{dt} = -\left(\frac{r_c^2}{2r_s b}\right)\frac{d^2H}{dt^2} \qquad \text{(III.B.15)}$$

at the screen radius. Substituting equations (III.B.14) and (III.B.15) into equation (III.B.11) results in the following

$$\varepsilon\left(\frac{r_c^2}{2r_s b}\right)\frac{d^2H}{dt^2}+\left(\frac{r_c^2}{2r_s b}\right)\frac{dH}{dt}=K\nabla h \qquad \text{at the screen radius} \qquad \text{(III.B.16)}$$

It should be emphasized that this equation only holds at the screen radius. It serves as a boundary condition for the general aquifer solution. In general, equation (III.B.11) and a continuity equation must be solved everywhere in the aquifer for the head subject to the boundary condition given by equation (III.B.16). However, if we make the usual Hvorslev assumptions the right-hand side of (III.B.16) can be assumed proportional to KH as

$$K\nabla h=-\frac{FKH}{2\pi r_s b} \quad , \qquad \text{(III.B.17)}$$

where F is the usual Hvorslev shape factor, then equation (III.B.16) can be written as

$$\varepsilon\frac{d^2H}{dt^2}+\frac{dH}{dt}=-\frac{FKH}{\pi r_c^2} \quad . \qquad \text{(III.B.18)}$$

By making the identification that

$$\varepsilon = FKA \quad , \qquad \text{(III.B.19)}$$

it can be seen that equation (III.B.18) is identical to equation (III.B.5).

From here on, we shall use only A for the nonlinear factor, realizing that three different physical models can be combined for N = 1. There are two parameters in the models that may be fitted: one is the hydraulic conductivity (K), and the other is the nonlinear factor (A). We have also done some analysis with the N =2 case but preliminary results indicates that the N = 1 model is more consistent with the data and it has the advantage of representing all three physical models discussed here.

Numerical Solution of Nonlinear Models

The three physical models can be represented by the same nonlinear equation III.B.5) in the variable $H(t)$. In general, it can not be solved in closed form. Using an iterative numerical solution technique, one obtains the following form:

$$H^{n+1(m+1)} = H^n - \frac{\frac{\Delta t}{2t_0}\left(H^{n+1(m)} + H^n\right)}{\left[1 + FKA\left|\frac{H^{n+1(m)} - H^n}{\Delta t}\right|^N\right]} \qquad \text{(III.B.20)}$$

where we have also used the usual definition of the Hvorslev time lag

$$t_0 = \frac{\pi r_c^2}{FK} \qquad \text{(III.B.21)}$$

and $H^{n(m)}$ is the m th iteration value at the nth time level. Equation (III.B.20) must be iterated for each time step until there is relatively little difference in the $H(t)$ for consecutive iterations. Equation (III.B.20) can be used for sequential time steps to generate the entire nonlinear type curve.

Figure 3 shows some of these type curves for typical parameters that might occur at the GEMS site. The solutions do exhibit downward curvature and do show the correct form of dependence on initial head. As the initial head increases the length of the test increases also. This implies that, when all data is given equal weight and a normal Hvorslev analysis is applied, one will estimate a lower hydraulic conductivity for tests with larger initial heads. However, looking carefully at the type curves in Figure 3, one can see that the long time behavior of all the curves for differing initial heads become parallel with a slope that is proportional to the hydraulic conductivity. Therefore, the late time data is more sensitive to the hydraulic conductivity, while the early time behavior may be heavily influenced by the nonlinear behavior.

Fitting and Editing Considerations

Figures 4 and 5 show some data from a 2 inch PVC well at GEMS with approximately 2.5 feet of screen. The initial slug height is about 23 feet. The field data are shown by asterisks and the solid curves are fitted by using an equal weight regression program (Bohling and McElwee, 1992). There are problems in fitting both the traditional Hvorslev model (Figure 4) and the nonlinear model (Figure 5) using an equal weight

regression program. First of all, the late-time data is small in magnitude so its effect on the least squares fit is minimized. This shows up as substantial deviation of the data from the curve at late time. Of course the deviation in Figures 4 and 5 is emphasized by taking the log of the head. The second problem in fitting the field data centers about the fact that field data will be dominated by noise at late time when the head has decayed to nearly the static level. Unfortunately, the late-time data is most sensitive to the hydraulic conductivity, so these two problems must be dealt with carefully in order to achieve the best estimate of hydraulic conductivity. First of all the late-time data can be emphasized by fitting the log of the slugged head; this tactic will give greater weight to the late-time data. Secondly, careful editing of the log of the slugged head must be done before fitting, since taking the log of the slugged head emphasizes the importance of the late-time data. We must be certain that the signal level of all late-time data used in the fit is substantially above the ambient noise level. The last data point in Figures 4 and 5 is an example of data that is not substantially above the ambient noise level and should be edited out.

Figure 6 shows field data from four slug tests with varying heights from well GEMS 02, which is a 2 inch PVC well that is approximately 45 feet deep with a screen length of approximately 2.5 feet. Clearly, the late-time data must be edited. The edit line we used is shown in the figure. It is uncertain what causes all the ambient noise (some sites will be noisier than others due to cultural effects), however, part of the late time noise level comes from elastic effects which are probably greater for larger initial heads.

Results

We have applied the nonlinear models to carefully edited field data and have found that the downward curvature and the dependence on head can be fit very well to the log of the slugged head. The data in Figure 7 are also from GEMS 02; the initial head is 8.62 feet. The fit is good; the early time curvature and late time behavior are well represented by the nonlinear models. Fits for other values of initial head are similar. However, the systematic deviations from the model fit seem more pronounced at early time for the smaller values of initial head (not actually shown here).

Analysis of eight separate slug tests at GEMS 02 are summarized in Table 1. The initial heads range from 2.75 feet to 23.1 feet. This table shows that the hydraulic conductivity can be determined with some consistency at this well, for tests with different initial heads. The fitted hydraulic conductivity (K) varies from .00485 ft./sec. to .00296 ft./sec., with an average value of .00388 ft./sec. The nonlinear factor (A) varies from 177

to 63.9, with an average of 108. We have revisited this well several months later with differing hydraulic conditions: the water table was several feet higher due to a very wet spring. Another set of eight slug tests with varying initial heads was performed and analyzed with the nonlinear model and the results were very consistent with the values given in Table 1. Ideally, K and A should be constant within the limitations of the data noise level, if the physical model is correctly describing the test. It is clear that there are some systematic trends in Table 1; K and A both decrease as the initial head is increased. This systematic trend indicates that our physical model is still not quite correct. In addition, in some recently conducted slug tests in other wells we have observed some oscillatory behavior at late time. These nonlinear models do not predict any such oscillatory behavior, so clearly there is additional work to be done to completely describe the results of slug tests at GEMS. However, these nonlinear models have certainly described the major features of the data: that of downward curvature and shifting to longer times for higher heads. A traditional Hvorslev analysis, giving equal weight to all data, would yield very different results for the hydraulic conductivity, for varying initial heads.

Inertial Effects in Slug-Test Analysis

An independent test of the influence of inertial effects on slug tests was obtained by running a series of tests with a numerical model (without the Hvorslev approximation) considering the "non-steady Darcy-law" as presented by Mohamed et al. (1992). Those authors show that, when accounting for the local acceleration of groundwater, the original form of the governing equation of groundwater flow in radial symmetry will be expanded by a term involving the second derivative of the hydraulic head with respect to time. The final governing equation then reads (Mohamed et al. 1992) :

$$\frac{K}{g\phi_0}\frac{d^2h}{dt^2}+\frac{dh}{dt}=\frac{K}{S_0}\Delta h \qquad \text{(III.B.22)}$$

where K is the hydraulic conductivity, S_0 is the specific storage coefficient, g is the gravitational acceleration, ϕ_0 is porosity of the aquifer, and Δ is the Laplacian operator. This additional acceleration term, that is the first term on the left hand side of (III.B.22), was implemented in a radial symmetric 2D-FD groundwater flow model (Zenner 1992). The numerical methodology of the underlying groundwater flow simulator is based on the publication of Rushton & Redshaw (1979). In order to assess if the representation of local water acceleration significantly affects the hydraulic head history within a slugged

well, we investigated the following four model scenarios. All four simulations consider radial flow only. Vertical flow components are always neglected. The first model scenario is characterized by the following parameter setup :

1) $k_r = 10^{-5}$m/sec
2) Aquifer thickness = 300m
3) Storage coefficient = 0.002
4) Initial head H_0 = 3m
5) Well radius = 0.1m

The second model includes a skin effect :

1) $k_r = 10^{-5}$m/sec
2) $k_{r,skin} = 10^{-4}$m/sec
3) r_{skin} = 1m
3) Aquifer thickness = 300m
4) Storage coefficient = 0.002
5) Initial head H_0 = 3m
6) Well radius = 0.1m

The third model employes a higher hydraulic conductivity throughout the aquifer (no skin) :

1) $k_r = 10^{-4}$m/sec
2) Aquifer thickness = 300m
3) Storage coefficient = 0.002
4) Initial head H_0 = 3m
5) Well radius = 0.1m

The fourth model incorporates a very high initial head H_0 :

1) $k_r = 10^{-5}$m/sec
2) Aquifer thickness = 300m
3) Storage coefficient = 0.002
4) Initial head H_0 = 19.8m
5) Well radius = 0.1m

And the fifth model, finally, represents a highly permeable aquifer :

1) $k_r = 10^{-2}$m/sec
2) Aquifer thickness = 300m
3) Storage coefficient = 0.002
4) Initial head H_0 = 3m
5) Well radius = 0.1m

For all simulations a time step of 0.01sec was chosen. The overall simulation time of 15min was therefore devided into 90000 time steps. The spatial discretization is realized by the employed numerical model through the usage of a logarithmic transformation applied to the radial coordinate r to yield the logarithmic radius a = log(r). Numerical experiments have shown that the model is sensitive to the chosen time step size and to the number of nodes per tenfold of radial distance. The results of these simulations indicate that the effect of local acceleration of the water on slug test can usually be neglected. Only in the case of high hydraulic conductivities of the aquifer can this effect be significant. The maximum head differences within the well, as determined by comparision to identical simulations not involving the inertial term, are summarized in table 2. Further tests are needed to quantify the inertial effect in high permeability wells such as at GEMS.

Table 2 : Maximum deviations H_{max} of simulated drawdown in the borehole with respect to simulations not involving inertial effects.

Model	Hmax (m)
1	$7.8*10^{-6}$
2	$4.99*10^{-3}$
3	$5.14*10^{-5}$
4	$3.02*10^{-3}$
5	$6.77*10^{-2}$

Summary

In summary, some slug tests in highly permeable aquifers seem to exhibit non-linear behavior. Field data show a downward curvature when plotted in the normal Hvorslev fashion. The duration of the slug test in field data is dependent on the value of the initial head. Models based on frictional loss, non-Darcian flow, or inertial effects seem to explain the gross features of this noted field behavior. Through careful editing and fitting the log of the slugged head, reasonable consistency in hydraulic conductivity values for various initial heads can be obtained. Further refinement of the non-linear models is needed because systematic trends in the fitted parameters with initial head are observed and recently some late time oscillatory behavior has been observed in some wells. One possible refinement of the model would be to fit the power of the velocity dependence, rather than assume N = 1. The treatment given here is based on a Hvorslev type analysis, and therefore essentially quasi steady state. A fully transient model incorporating nonlinear, inertial, and other effects would be an additional possible improvement.

Table 1. Summary of Eight Slug Tests at Well GEMS 02

INITIAL HEAD	HYDRAULIC COND.	NON-LINEAR FACTOR
2.88 ft.	.00450 ft./sec	177.
6.63	.00414	116.
8.81	.00349	103.
23.1	.00308	77.0
2.75	.00485	131.
7.14	.00430	108.
8.62	.00376	85.6
23.1	.00296	63.9
Average	**.00388**	**108.**

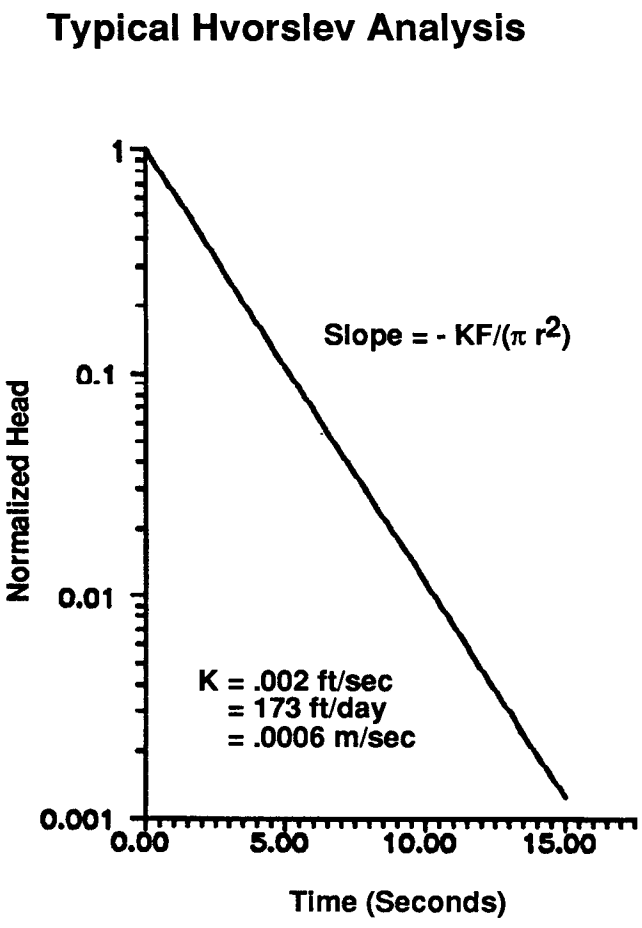
Typical Hvorslev Analysis
1
0.1
0.01
0.001
Normalized Head
Slope = - KF/(π r2)
K = .002 ft/sec
= 173 ft/day
= .0006 m/sec
0.00
5.00
10.00
15.00
Time (Seconds)

Figure 1.

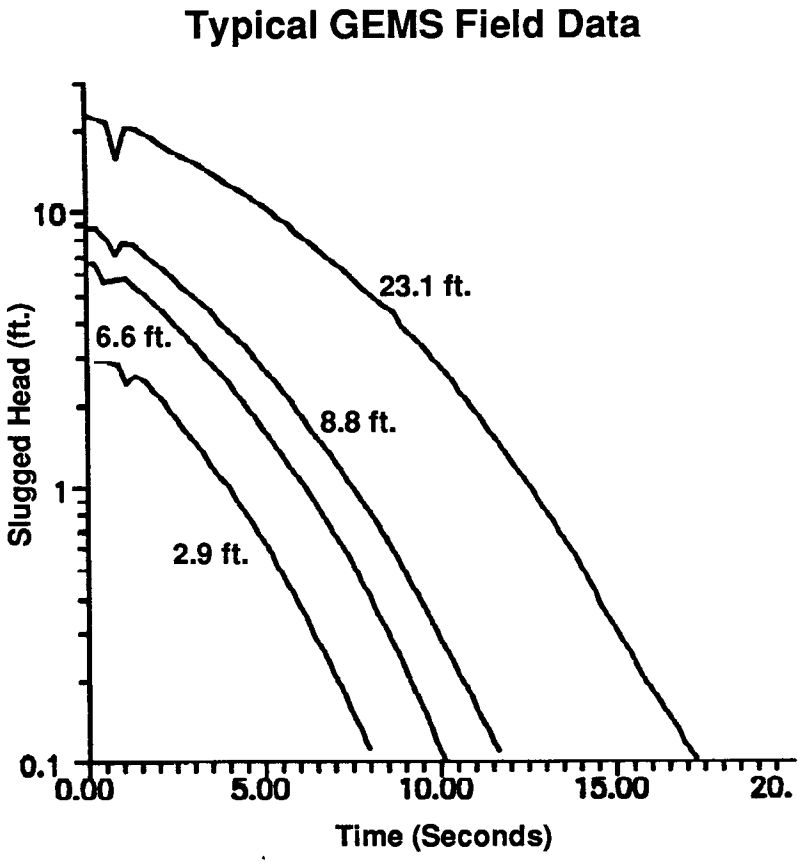

Figure 2.

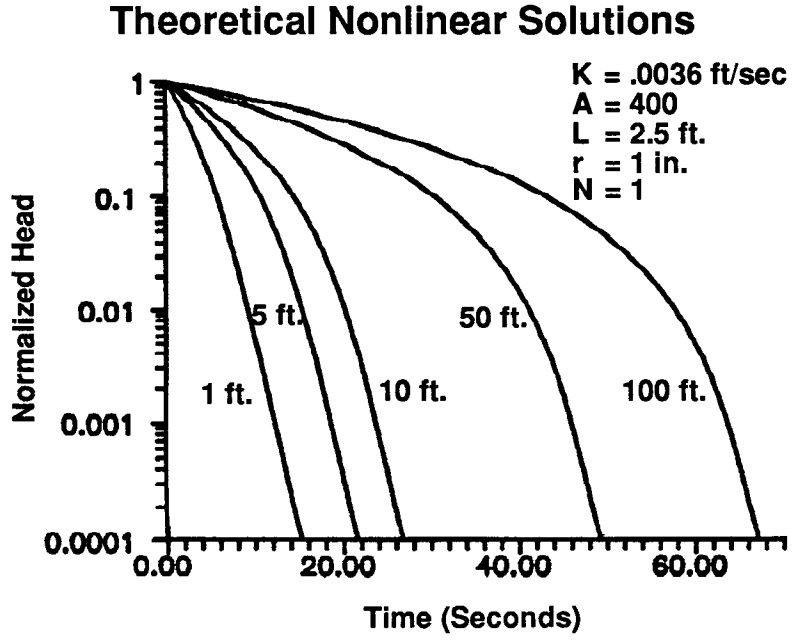

Figure 3.

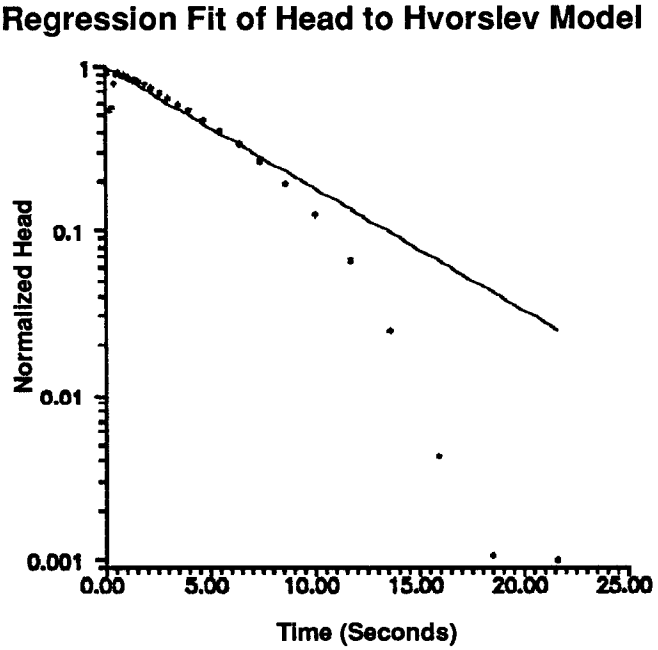

Figure 4.

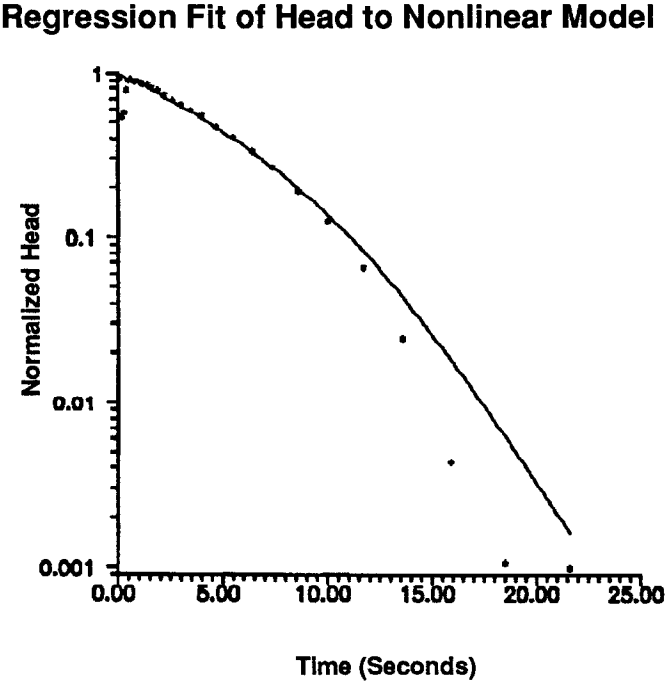

Figure 5.

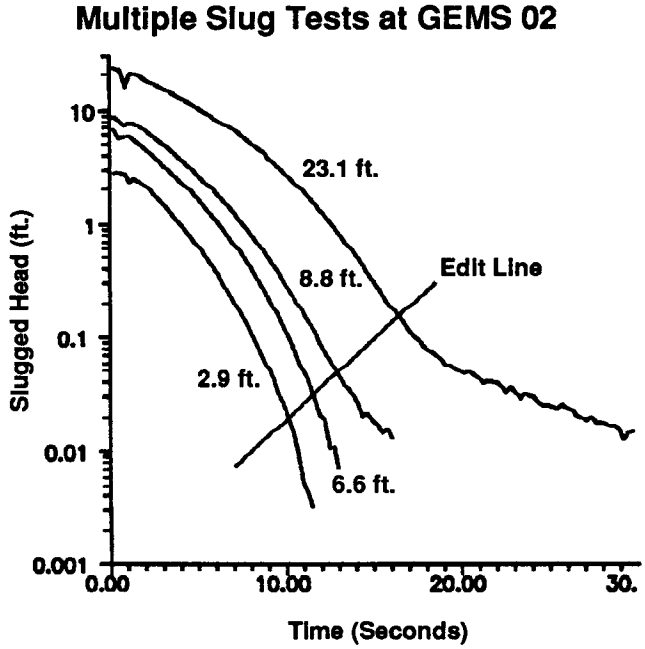

Figure 6.

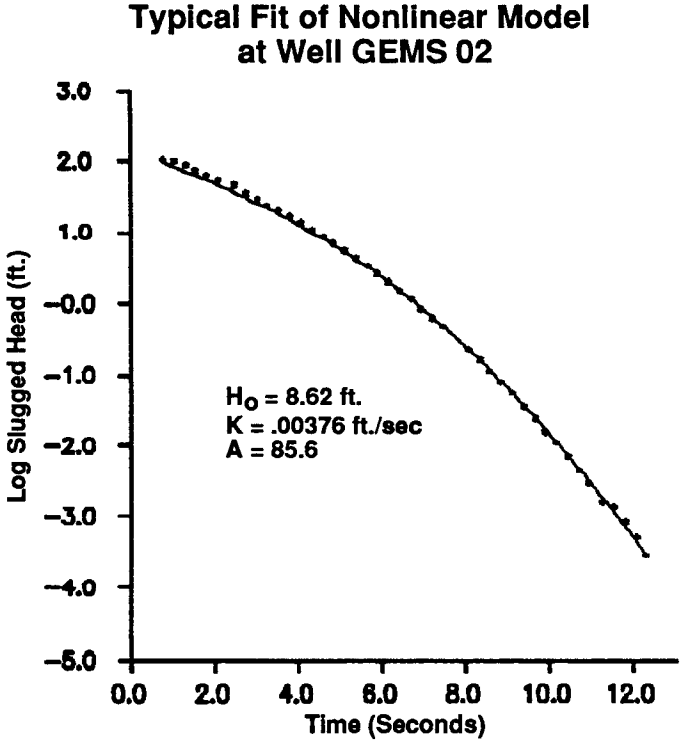

Figure 7.

IV. SITE CHARACTERIZATION ACTIVITIES

A. AQUEOUS GEOCHEMISTRY AT GEMS

Introduction

During the first year of the project, some of the wells at GEMS were sampled for chemical analysis, and samples were collected during a short (2-hour) pumping test on the single well completed in bedrock underlying Kansas River alluvium. Conclusions of that year's work were that the chemistry of ground water in the alluvium and the bedrock were sufficiently different to allow evaluation of leakage from the alluvium into the bedrock. The chemical parameter most useful as a tracer of leakage was nitrate (NO_3-N), because it is relatively easy to detect and because the bedrock aquifer does not contain quantifiable concentrations of it. Some of the future goals stated during last year's report were to:

1. Characterize vertical stratification of water chemistry by sampling wells completed at different levels within the sand and gravel alluvium.
2. Repeat bedrock pumping test, but extend the test for a longer period of time to try to assess the steady-state leakage time. Use this to attempt to calculate aquifer properties.

During this year's work, samples from 20 wells were analyzed for anion content, and cations were analyzed in seven well samples. A longer pumping test on the bedrock well (7 hours) was performed and samples taken to better evaluate leakage from the alluvium into the bedrock aquifer. A preliminary assessment of those results shows that a simple vertical flow model provides an inadequate description of the water chemistry during the entire pumping test, but that it may be useful in the early parts of the test.

Methodology--Chemical Analysis

Sample collection and processing followed procedures described in last year's report. Water samples were collected from 20 of the observation wells at the site during one sampling event (Table 1), and periodically during the 7-hour pumping test on another day (Table 2). All samples for anions were filtered immediately by gravity feed through 0.45μ membrane filters and stored in an ice chest until transport to the laboratory at the end of the pumping test or well-sampling event. In the laboratory, samples were stored in the refrigerator until the next day, when the samples were analyzed by ion chromatography (EPA, 1984) for NO_3-N, chloride (Cl), and sulfate (SO_4). Samples from the pumping test were reanalyzed two weeks after the first analysis as well, to check for stability of NO_3-N in the samples. There was no significant difference between these

two sets of analyses. Samples for analysis of cations were field filtered as described above, and acidified with 5 mL of HNO_3 per 250 mL of sample. These samples were stored at room temperature until analysis of major cations by atomic absorption spectrophotometry according to standard methods (Fishman and Friedman, 1989).

Results

Well Chemistry Survey

Profiles of anion chemistry with depth are shown for sampled wells in Figures 1-3. Wells from three nests were sampled, and each nest shows unique changes in NO_3-N, Cl, and SO_4 with depth, despite the fact that the nests are only between 20 and 40 meters apart. The NO_3-N profile (fig. 1) demonstrates that well nest #0 has the highest NO_3-N content, and that the NO_3-N concentration changes dramatically with depth, with two distinct spikes at about 8 meters and near the middle of the sand and gravel aquifer at about 17 meters depth. Well nests #1 and #2 also have a small NO_3-N spike at about 8 meters depth, but no corresponding spike at 17 meters. The bedrock well (shown as the deepest of Nest #0 wells, although technically not in well nest #0) has undetectable concentrations of NO_3-N. Well 0-1 (nest #0) is screened throughout the thickness of the sand and gravel aquifer, and its NO_3-N concentration is approximately the same as NO_3-N at the 17-meter depth. Chloride (fig. 2) profiles in the three well nests are not so regular as NO_3-N. Well nest #0 shows a Cl spike at about 20 meters depth, nest #1 shows a broad spike shallower than that at between 14 and 17 meters depth, and nest #2 shows sine-wave-type variation over the profile between concentrations of about 5 to 7.5 mg/L. The bedrock well, the deepest of the nest #0 points, has the lowest Cl concentration. Well 0-1 has approximately the same Cl concentration as the sample from 17 meters depth. Sulfate may show a slight increase in concentration with depth in nest #0, and a decrease in depth in nests #1 and #2. Sulfate in the bedrock well is close to the same concentration as that in the deepest wells in the well nests. Well nest 0-1 SO_4 may be somewhat lower than sulfate in the 17-meter well at nest #0, an observation which is not easily explained.

Pumping Test

During October, 1992, a seven-hour pumping test on the bedrock well was run to see if changes in geochemistry corresponded with last year's 2-hour test, and to see if the chemistry of the pumped water would stabilize indicating attainment of steady-state leakage from the alluvial aquifer into bedrock. The pumping rate during the test was approximately steady at about 6 gallons per minute. Samples were collected every 15

minutes for the first one-half hour, every 30 minutes for the next two and one-half hours, and every hour thereafter.

Time profiles of NO_3-N, Cl, and SO_4 (figs. 4-6) show the chemical change in the produced ground water during the pumping test. The NO_3-N profile (fig. 4) shows no detectable NO_3-N (less than 0.05 mg/L) until about 1.5 hours into the pumping test. Thereafter, the NO_3-N content increases almost steadily until the end of the test. Some curvature is apparent in the profile. The Cl profile (fig. 5) also shows an increase through time, although the concentration change is harder to resolve because of the difficulty in measuring small changes in Cl. There is some increase in SO_4 concentration with time, although the change is smaller than the Cl change, and is nearly within analytical error. In both the SO_4 and Cl profiles there is a distinct difference between the sample collected at the start of the test and one collected 15 minutes later. This may be attributable to stagnant water in the well casing, although the casing should have been evacuated after 8-10 minutes of pumping.

Discussion

The profiles of chemical differences in the aquifer with depth show that ground water in the sand and gravel aquifer is not uniformly mixed and that chemical processes such as denitrification may be affecting one of the parameters (NO_3-N) in the water. Furthermore, the chemistry of water in the mud and silt above the sand and gravel aquifer is different from the sand and gravel aquifer, and the bedrock-aquifer chemistry is different still. These facts make calculations of travel times and distances difficult, but a preliminary attempt is made below.

The bedrock pumping test demonstrated that steady-state leakage (as evidenced by achievement of constant chemical signature) was not attained after 7 hours of pumping. If leakage is not occurring as a point or line source, but is evenly distributed along the presumably horizontal interface between the bedrock and overlying sand and gravel, then is it possible to do some simple evaluations of aquifer parameters.

The well test performed is a simple case of a well penetrating bedrock which, when pumped, causes a cone of depression of the hydraulic head around the well. The maximum radius of this cone of depression is ideally a circle on the plane separating the two units. Flow lines are mostly horizontal, from the bedrock sandstone into the bedrock well. However, the cone of depression induces downward flow from the alluvium, and this flow moves vertically or obliquely toward the bedrock well.

Assuming the bedrock sandstone is homogeneous and isotropic, it is possible to represent this flow by a vertical plane including the well. The maximum horizontal

extent of the cone of depression caused by the pumping test is attained at steady-state, apparently not reached during the October, 1992 test. Flow lines to the well are probably curved, but for purposes of this exercise they are represented as being straight. The length of the path from the boundary between the alluvium and bedrock increases with increasing distance from the well, with the longest path being from the boundary between the two units starting at the maximum diameter of the cone of depression. The shortest path is that path which is vertical or nearly vertical, closest to the well bore. Water from the alluvium travelling along this path will reach the well screen first. Because this path is nearly vertical, it can be treated, as a first approximation, in the same way that column experiments of continuous sources of contaminants are treated. That is, the concentration distribution in the column is described by:

$$D_x \frac{\partial^2 C}{\partial x^2} - v_x \frac{\partial C}{\partial x} = \frac{\partial C}{\partial t}$$

where D_x is the dispersion coefficient in the x direction

C is concentration of a tracer species

x is distance

v_x is flow velocity in the x direction

t is time

Using the boundary and initial conditions that the tracer is a continuous source (or $C(0,t) = C_0$) and that the tracer is not present in the aquifer before the test begins, the above equation is integrated to produce the following solution:

$$C(x,t) = C_0 / 2 \quad \text{erfc} [(x - v t) / 2 (\alpha_x v t)^{0.5}]$$

where α_x is the longitudinal dispersivity

erfc is the complementary error function

v is the linear velocity of the water, assumed to be that of the tracer

Figure 7 shows the NO_3-N profile during the pumping test, and several curves showing ideal vertical profiles of NO_3-N with time (breakthrough curves) with varying longitudinal dispersivity and velocity. Table 3 shows the values of the variables used in these calculations. The distance (x) is taken as the distance between the midpoint of the screen in the bedrock aquifer well and the interface between the alluvium and bedrock. Initial NO_3-N concentration is taken as the concentration in the deepest partially screened (20-meter) well in Nest #0. It is not known whether this concentration is representative of water at the base of the alluvium, because there is no partially screened well at the base

of the alluvium in Well Nest #0. The concentration of NO_3-N used is probably too high, based on extrapolation from the known NO_3-N profile in the upper part of the alluvium.

The shapes of the calculated breakthrough curves differ from that of the observed chemical changes in that the observed curve is concave down, whereas the calculated curves are concave up or nearly linear after the first third of the pumping test. Because the cone of depression grows outward during the pumping test and progressively more ground water from the bedrock aquifer is produced, the observed curve is an integration of an infinite series of breakthrough curves, one for each flow line. Only during the very first part of the test does the simplified situation of vertical flow hold true, and, in fact, vertical flow almost certainly does not hold by the time NO_3-N is first detected in the pumped water, about 1.5 hours after pumping began. Figure 8 shows a close-up of NO_3-N versus time during the early part of the test with the calculated curves superimposed. Although there is no unique solution to the equation, because both dispersivity and velocity can be varied and because the shape of the curve during the later part of the test is obscured by dilution from other flow lines, it is apparent that the solutions with larger dispersivities (10 m to 100 m) are better fits than with small dispersivity (1 m). These values are high for the typical range of dispersivity in single well tests (0.03 to 0.3 m; Palmer and Johnson, 1989), and support the statement above that by the time NO_3-N arrived in detectable concentrations at the outflow point, the water produced was a mixture from vertical and inclined flow lines from the alluvium into the bedrock aquifer. This is analagous to the difference between breakthrough curves observed at specific points (depths) in a layered aquifer versus the breakthrough curve observed in a fully penetrating well (National Research Council, 1990, p. 119).

Conclusions

The survey of wells at GEMS shows that the chemistry of the water varies spatially, both vertically and horizontally. This makes it possible to evaluate leakage from the alluvial aquifer into the bedrock aquifer, but because the chemistry within the alluvial aquifer also varies considerably, these calculations will be complex. The bedrock pumping test showed that steady-state chemistry was not attained after seven hours of pumping. A preliminary assessment of dispersivity and ground-water velocity shows that an evaluation of these parameters is difficult because of the relatively late arrival time of the single measured parameter which is found in the alluvium ground water but not in the bedrock ground water (NO_3-N). Because of the late arrival time of NO_3-N, the water produced at the time of detectable concentrations of NO_3-N is a mixture of many flow lines coming from the alluvium through the bedrock, and is not simple vertical flow. For

this reason, the parameters fitted to the one-dimensional advection-dispersion equation are overestimates of dispersivity in this system. Future work should include a better mathematical formulation of the physical problem, possibly using two-dimensional advection-dispersion, as well as an attempt at "thief"-sampling the alluvial aquifer in order to get a better understanding of the chemical changes with depth within that aquifer.

Table 1: Chemistry of GEMS Wells

Well Name (Nest # -Well #)	Depth (meters)	NO3-N (mg/L)	Cl (mg/L)	SO4 (mg/L)	Ca (mg/L)	Mg (mg/L)	Na (mg/L)	K (mg/L)
0- 1	21.74	8.6	5.5	26.4	110	8.3	10.4	1.27
0- 2	14.08	0.05	7.5	38.8				
0- 3	11.00	0.36	7.3	26.6	58.4	7.7	11.3	1.12
0- 4	7.94	9.07	5.5	29.6	74.1	8.4	12.7	1.06
0- 5	19.84	4.11	9.7	39.9				
0- 6	24.66	0.07	2.0	36.5	103	17.4	23	1.17
0- 7	16.57	8.61	6.4	32.8				
1- 1	14.26	0.24	10.5	55.2				
1- 2	11.22	0.56	7.6	45.3	93.2	13.4	12.3	1.7
1- 3	8.55	1.61	8.4	49.2	85.5	11.8	49.7	1.5
1- 4	6.15	0.1	6.7	60.2	98.6	14.7	53.4	1.4
1- 5	20.33		6.1	39.0				
1- 6	17.06	0.09	11.0	37.8				
2- 1	11.92		7.4	40.8				
2- 2	14.72		6.9	38.7				
2- 3	8.53	1.09	5.5	50.3				
2- 4	6.04							
2- 5	21.42	0.11	6.3	35.5				
2- 6	20.24		5.7	40.3				
2- 7	17.17	0.36	4.6	31.1				

Table 2: Anion Chemistry of Pumping Test Samples, 10/92			
Time (minutes)	NO3-N (mg/L)	SO4 (mg/L)	Cl (mg/L)
2.5	0.000	37.6	2.35
17.5	0.000	37.6	2.64
32.5	0.000	37.8	2.63
62.5	0.000	37.5	2.59
92.5	0.070	37.5	2.64
122.5	0.124	37.5	2.71
152.5	0.176	37.5	2.86
182.5	0.234	37.9	3.09
242.5	0.326	38.0	3.24
302.5	0.404	38.0	3.31
362.5	0.454	38.0	3.43
416	0.490	38.0	3.47

Table 3: Values of Parameters Used in Solving the Advection-Dispersion Equation for Figures 7 and 8

All Simulations:	Plot Symbol	α (m)	v (m/min)
x: 2.16 m	Diamonds	1	0.002
C0 : 4.11 mg/L NO_3-N	Circles	10	0.0005
t : 0 to 422 minutes	Squares	100	0.00005

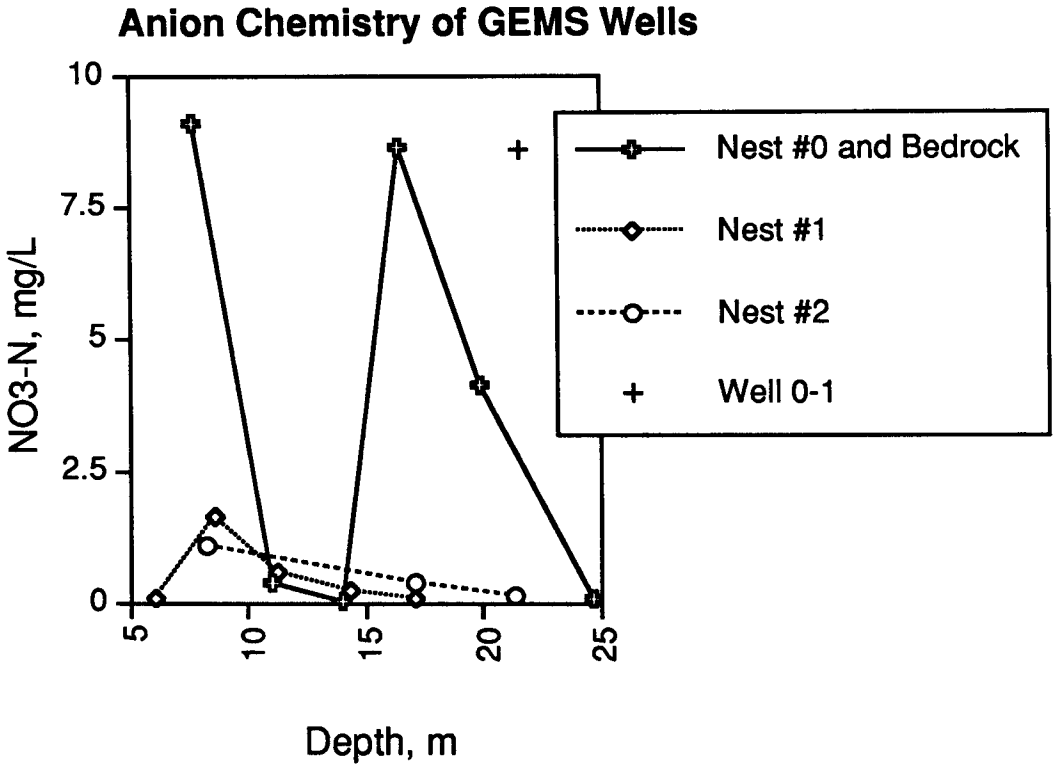

Figure 1: Nitrate concentration versus depth in three wells nests at GEMS. The single well completed in Paleozoic bedrock beneath the Kansas River Alluvium is shown as the deepest point on the profile for Nest #0, although it is not physically located within that nest. Well #0-1 is shown as a separate point because it is screened over the entire sand and gravel interval, but it is plotted at the depth corresponding to the total depth of the well.

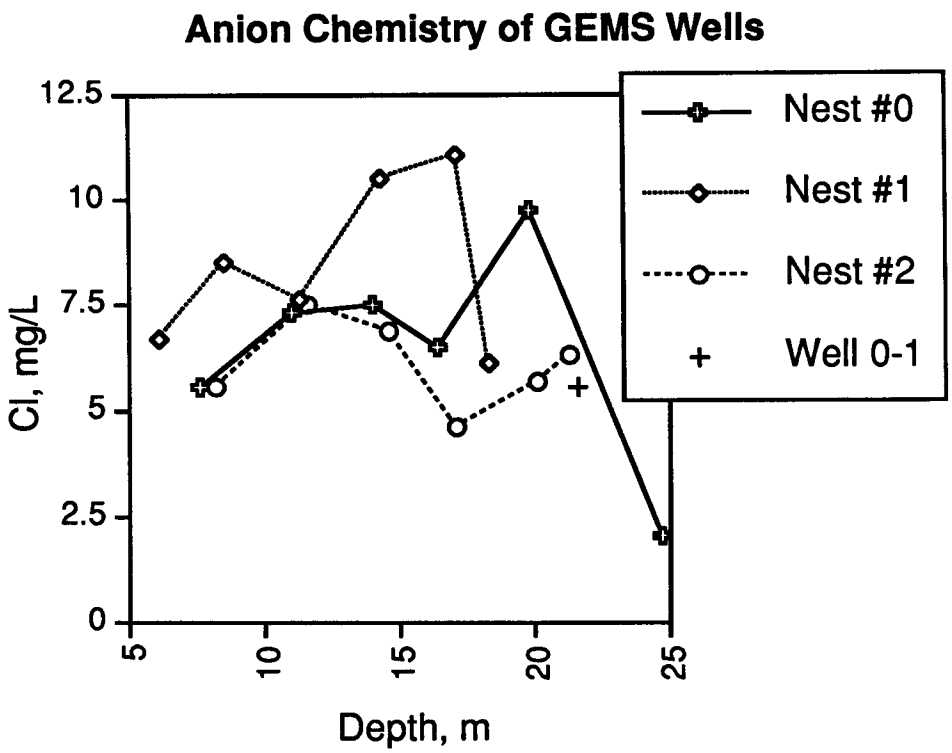

Figure 2: Chloride concentration versus depth in three well nests at GEMS. Bedrock well and Well #0-1 are as described in Figure 1.

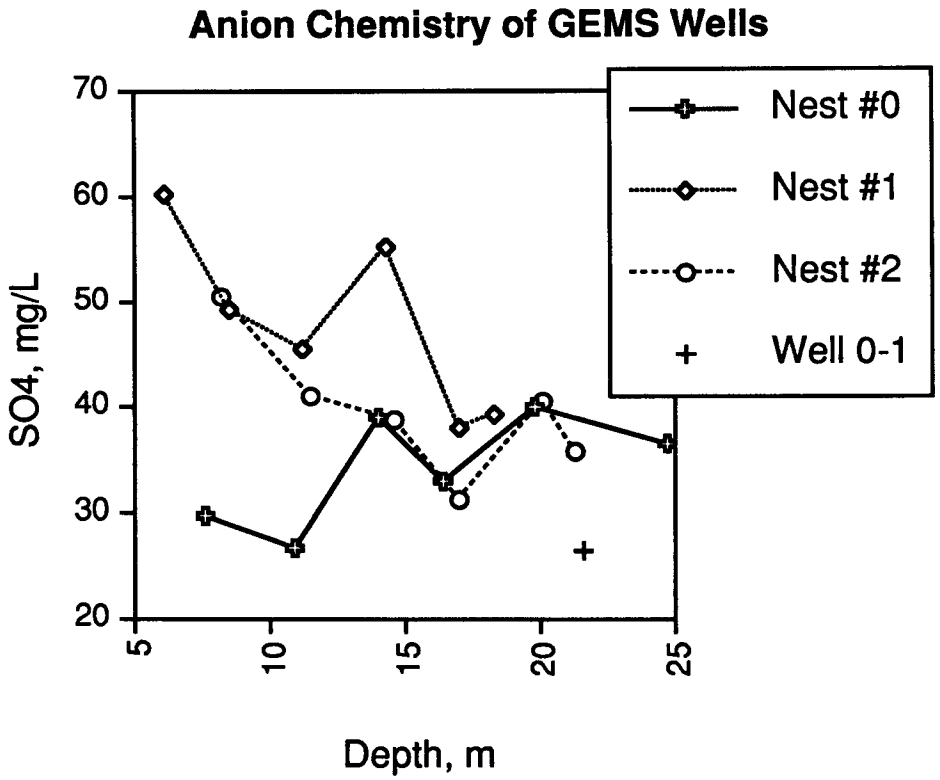

Figure 3: Sulfate concentration versus depth in three well nests at GEMS. Bedrock well and Well #0-1 are as described in Figure 1.

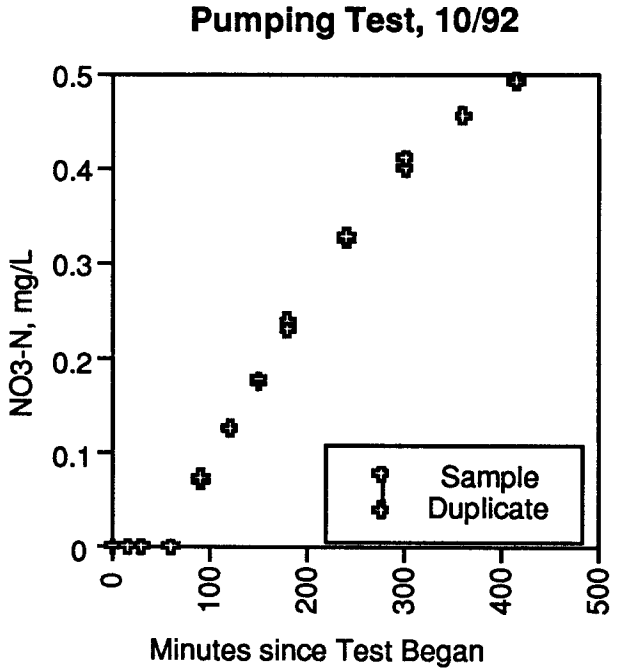

Figure 4: Nitrate concentration versus time during the bedrock pumping test of October, 1992. Each sample was analyzed twice, so duplicate concentrations for each sampling time are plotted.

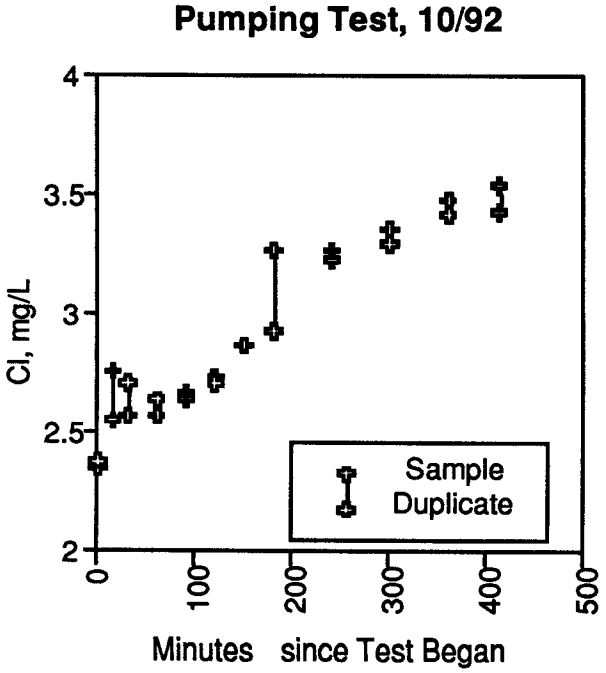

Figure 5: Chloride concentration versus time during the bedrock pumping test of October, 1992. Each sample was analyzed twice, so duplicate concentrations for each sampling time are plotted. The differences between the duplicates illustrate the difficulty in analyzing Cl by ion chromatography without optimizing for Cl.

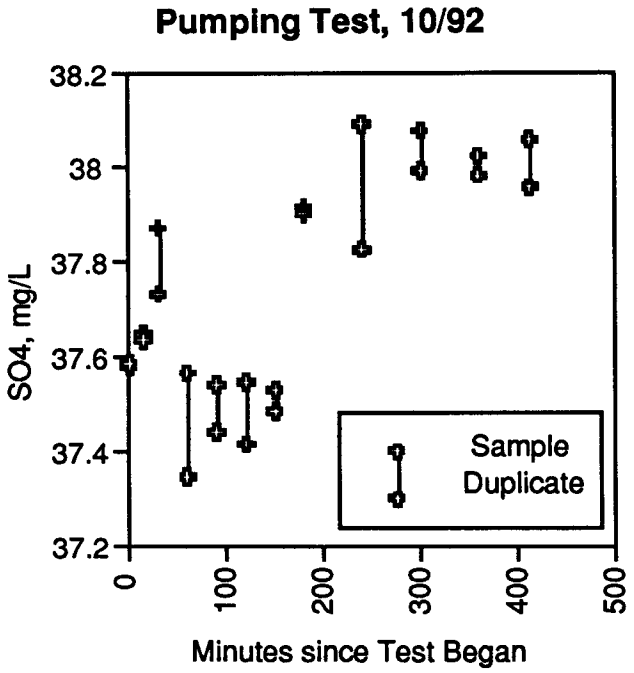

Figure 6: Sulfate concentration versus time during the bedrock pumping test of October, 1992. Each sample was analyzed twice, so duplicate concentrations for each sampling time are plotted. The differences between the duplicates illustrate the precision of sulfate determination, which is less than 2 %; maximum difference in sulfate concentration shown on this graph (all data) is about 2.1%.

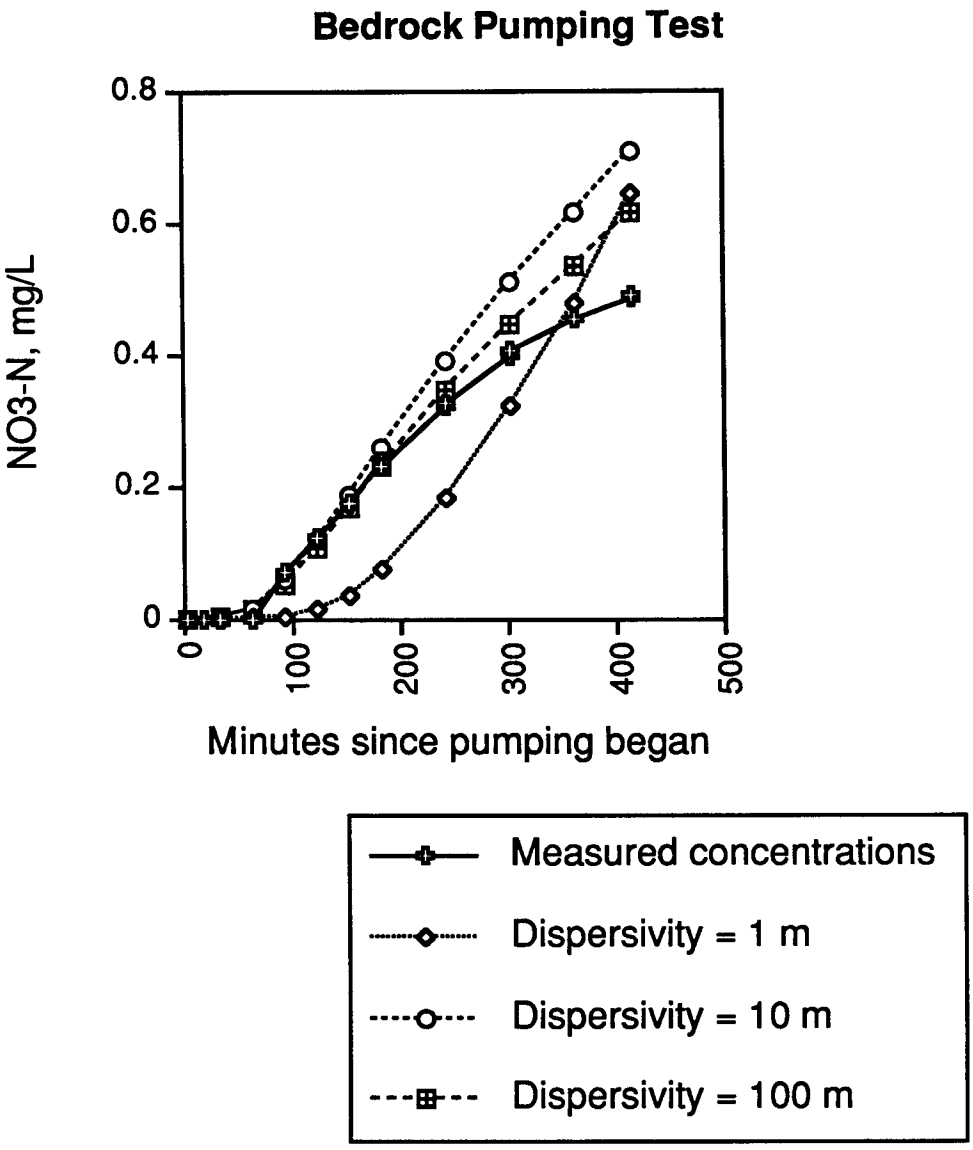

Figure 7: NO_3-N concentration as measured and several breakthrough curves calculated using the advection-dispersion equation.

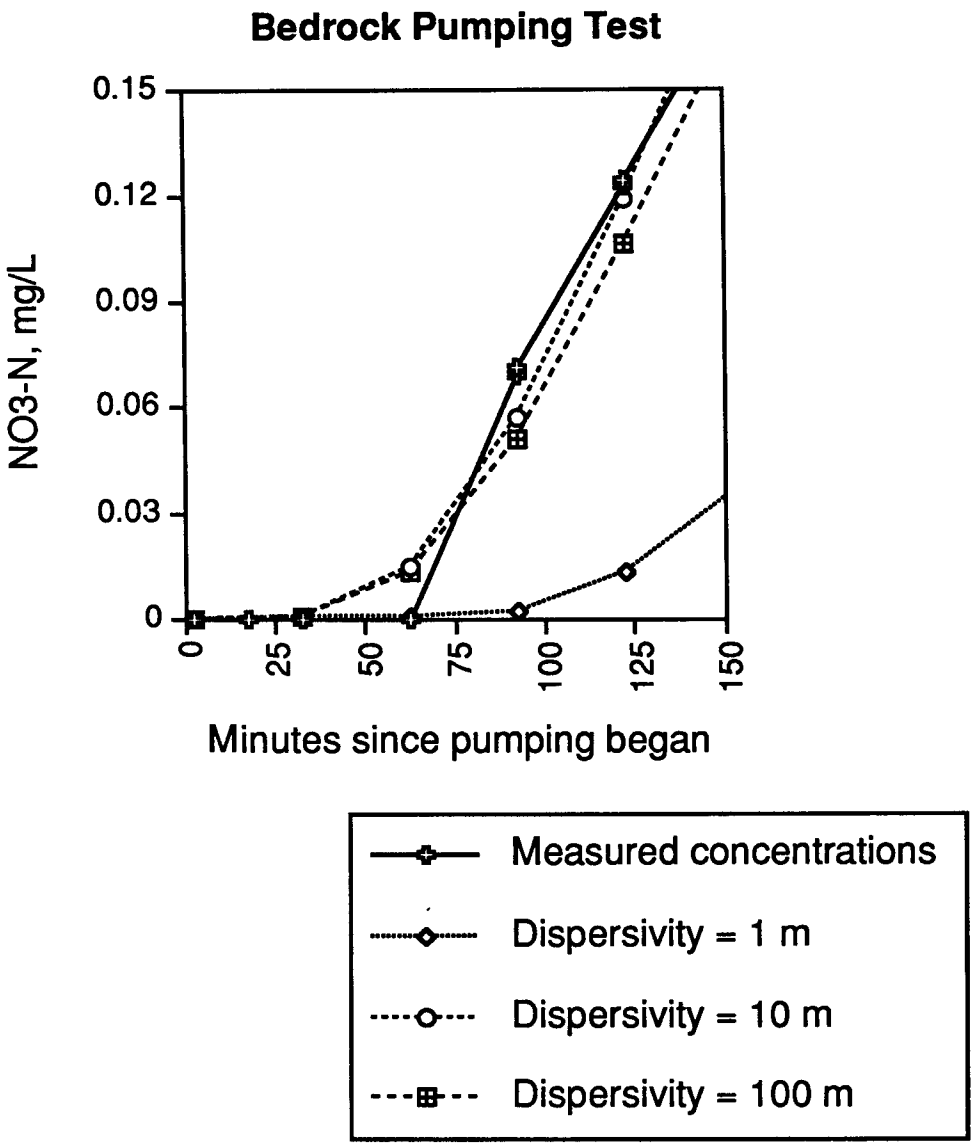

Figure 8: NO_3-N concentration as measured and calculated for several values of dispersivity and ground-water velocity at the beginning of the well test.

B. DRILLING AND SAMPLING ACTIVITIES

Introduction

Prior to 1992, twenty nine wells had been installed at GEMS in the Kansas River alluvium. Ten of these wells were cored through 30-35 feet of coarse sand and gravel at depths of 35-70 feet using various techniques (four of these core holes were reported on in detail in the year one report). In 1992 eleven new holes were drilled at GEMS bringing the total to 40 observation wells. Four holes (5-1, 7-1, 9-1, and 11-1) were cored from the surface to the bedrock. Core samples of the first approximately 35 feet of silt and clay were obtained using a split-spoon sampler two feet in length. Cores in the sand and gravel section were taken using the new sampler design (McElwee et al., 1991) which incorporates an inflatable bladder, located in the drive shoe, which closes off the end of the sampler during recovery. Six new wells were drilled at the 00 nest (00-2 through 00-7) site to complete the usual complement of wells at a nest. One new 4 inch well (0-8) was drilled with the new large diameter auger flights that were obtained as part of this research effort in year two.

Drilling Procedure

All except a few of the monitoring wells at GEMS have been installed with hollow-stem auger techniques. A review of hollow-stem auger techniques and equipment is given by Hackett (1987). Auger flights with 3 1/4 inch inside diameter and 6 5/8 inch outside diameter were used for most holes (2 inch wells). New larger diameter auger flights were purchased as part of the year research effort. These auger flight have an inside diameter of 6 1/2 inches and an outside diameter of 10 inches. The deepest alluvial wells at the site are about 70 feet. One bedrock well, which was installed with mud rotary techniques, is about 80 feet deep and extends into bedrock about 10 feet. A typical nonsampling installation (with either set of auger flights) would proceed by drilling to the desired depth with a knock-out plate installed in the auger head in place of a pilot bit (Perry and Hart, 1985; Hackett, 1987). At that point, the well casing would be installed through the hollow flights and the plate would be knocked out .

Heaving sands or sandblows (Minning, 1982; Perry and Hart, 1985; Keely and Boateng, 1987; and Hackett, 1987) are a severe problem at this site in the zone of sand and gravel (35-70 ft.). It is absolutely essential to maintain greater hydrostatic pressure inside the auger flights than in the formation when drilling or coring in heaving sands. The water level inside the auger flights is maintained higher than the ambient water table by adding water at critical times (mainly, when tools are moved within the flights or the

flights are moved). If a greater hydrostatic head within the auger flights is not maintained at critical times, several feet of sediment may quickly enter the flights, with the result that the possibility of obtaining an undisturbed sample at that depth is lost. Adding water to maintain a higher head in the flights may affect the chemistry and biota of an aquifer, so an investigator must balance this concern with the need to control heaving sands.

Typically, when sampling the sand and gravel portion the new bladder sampler design is used (McElwee et al., 1991). The sampler is driven 5 feet and then a flexible bladder is inflated on the end to hold the sediments in place during recovery. Water is added during recovery to prevent heaving sands. After each 5 foot sample collection, the hole is advanced 5 feet by continued augering. Typically, we take 7 of these 5 foot sections in each cored well. Usually the last sample is less than 5 feet due to reaching consolidated bedrock. Due to the physical construction of the sampler (length and position of the bladder), six inches is always lost on the end of each sample. This means that 90% is the maximum recovery under ideal conditions. We usually lose another several percent due to compaction, premature piston movement, and wall friction or large cobbles preventing material from moving into the sampler. This usually shows up as head space above the sample in the sampler tube.

Drilling and Sampling - 1992

During the 1992 field season four additional wells were drilled, cored and completed (three of which were required by the terms of this project), six wells were added at the 00 nest to give the usual complement, and one 4 inch well was completed with the new larger diameter flights. Additional 4 inch wells are planned for year three. This brings the total to forty monitoring wells at GEMS. Table 1 is a summary of pertinent information about all these wells. Figure 1 is a map of the GEMS area showing the location of all the wells. Figue 1 was able to be produced this year due to the purchase of some new surveying equipment for this research. This equipment allowed us to measure relative elevations and distances quickly and accurately. The absolute elevations relative to sea level were obtained through a cooperative surveying exercise with the 1st Battalion of the 127th Field Artillery of the Kansas Army National Guard in 1991.

All the wells cored during the summer of 1992 were cored from the surface to the bedrock, using the techniques outlined above. The split-spoon sampler was used for approximately the first thirty-five feet and then the bladder sampler was used until we hit bedrock at approximately seventy feet. These four wells (5-1, 7-1, 9-1, and 11-1) were

cored in a line approximately perpendicular to the line containing most of the previously cored holes (see Figure 1). With this X pattern of cores across the site we should get fairly good two dimensional coverage of the area. The samples of silt and clay from the first thirty-five feet were examined visually and detailed written logs of the visible physical features were prepared. At that point the silt and clay samples were discarded, except for a few representative samples from each hole about 5-6 inches long. The silt and clay samples were preserved in containers with formation water until hydraulic conductivity measurements can be run on them later. We have bought appropriate equipment to measure hydraulic conductivity on these samples as part of the year two equipment purchase. We currently have it set up and plumbed with the needed supply of air. The samples that have been collected will be run as soon as we are able to schedule the time and personnel. Starting at approximately thirty-five feet, the bladder sampler was used to collect samples of the sand and gravel. After recovery, the sand and gravel cores are x-rayed for structure determination and then taken to the laboratory to be cut up and processed for storage until measurement of hydraulic conductivity, porosity, density and particle-size fraction can be done. Table 2 summarizes the sample recovery for all holes cored in this time period (5-1, 7-1, 9-1, and 11-1). Other data about these wells can be found in Table 1. The overall recovery was about 72% which is about 13% lower than the 85% we were expecting and hoping for. The additional loss this season was due to a number of factors. In a several holes we had problems with cobbles blocking the sampler throat. Mechanical problems also plagued us this year. Several times the retraction mechanism failed so that the bladder could not be inflated. In one instance this resulted in the complete loss of the sample (#1 of hole 7-1). The sampler takes a great deal of punishment in being driven by a jack hammer, so one must expect some mechanical failures. The net result is that the recovery rate was not as high as we had hoped and planned for.

Six holes (00-2 through 00-7) were drilled to complete nest 00. Typically wells are completed at each nest at 25, 35, 45, 55, 65 feet with approximately 2.5 foot screens. We installed a few more wells at this 00 location to better define the silt and clay interface with the underlying sand and gravel. Information about each of these wells is contained in Table 1 and their location is shown on Figure 1. Some hydraulic testing has been done in these wells and more is planned.

The last hole (0-8) was a large diameter (4 inch casing) well to be used for hydarulic testing later. With the new larger diameter auger flights we can easily install 4 inch casing. The larger casing means that larger pumps can be used and the aquifer can be stressed more than from a 2 inch well. This should make it invaluable in some pulse

testing work, allowing a larger volumes per unit time to be pumped. In addition, we plan to use this well with a number of slug tests, since the larger diameter will allow much more instrumentation to be placed in the well.

Table 1

Well Data

Well Number	Elevation (m)	Depth (m / ft)	Screen Length (m)
00-1	252.724	17.04 / 55.90	0.76
00-2	252.780	14.41 / 47.28	0.76
00-3	252.670	21.37 / 70.11	NA
00-4	252.667	11.18 / 36.68	NA
00-5	252.021	9.74 / 31.96	NA
00-6	252.746	12.91 / 42.36	NA
00-7	252.734	20.34 / 66.73	NA
0-1	252.796	21.74 / 71.32	9.14
0-2	252.756	14.08 / 46.19	0.70
0-3	252.787	11.00 / 36.09	0.74
0-4	252.707	7.94 / 26.05	0.76
0-5	252.793	19.84 / 65.09	0.70
*0-6	252.945	24.66 / 80.90	1.52
0-7	252.743	16.57 / 54.63	0.70
0-8	252.827	15.33 / 50.30	0.76
1-1	252.799	14.26 / 46.78	0.76
1-2	252.714	11.22 / 36.81	0.61
1-3	252.814	8.55 / 28.05	0.65
1-4	252.796	6.15 / 20.18	1.45
1-5	252.791	20.33 / 66.70	9.14
1-6	252.899	17.06 / 55.97	0.73
1-7	252.735	21.42 / 70.28	9.14
2-1	252.791	11.92 / 39.11	0.57

2-2	252.785	14.72 / 48.29	0.56
2-3	252.784	8.53 / 27.98	0.63
2-4	252.779	6.04 / 19.82	1.41
2-5	252.791	21.42 / 70.28	9.14
2-6	252.735	20.24 / 66.40	9.14
2-7	252.728	17.17 / 56.33	0.79
4-1	252.724	21.58 / 70.80	9.14
5-1	252.949	21.54 / 70.67	9.14
6-1	252.753	20.34 / 66.73	0.77
6-2	252.754	21.55 / 70.70	11.55
7-1	253.452	17.74 / 58.20	9.14
8-1	252.703	17.44 / 57.22	NA
9-1	252.639	20.93 / 68.67	13.26
10-1	252.566	17.32 / 56.82	NA
11-1	253.412	19.63 / 64.40	13.72
A1	252.511	9.91 / 32.51	0.76
A2	252.931	7.86 / 25.79	0.61
+PW	NA	21.84 / 71.65	6.10

KGS Reference Mark: Latitude-North 39°00' 55.628" Longitude-West 95°12' 21.272" Elevation 252.242 m

* Well diameter is .127 m; all other wells except PW are .051 m diameter.
\+ High capacity pumping well, screen and casing is .254 m in diameter, drop pipe is .102 m in diameter.
NA - information not currently available.

Table 2

Sample Recovery Analysis

Well Number	Segment Number	Segment Length (ft)	Head Space (ft)	% of Segment Length
5-1	1	5.00	.29	5.8
5-1	2	5.00	.45	9.0
5-1	3	5.00	.25	5.0
5-1	4	5.00	.35	7.0
5-1	5	5.00	.56	11.2
5-1	6	5.00	1.55	31.0
5-1	7	4.54	.54	12.0
5-1 Totals		34.54	3.99	11.6
		Theoretical Recovery		88.4
		Bladder Loss		10.0
		Actual Recovery		78.4
7-1	1*	5.00	4.5	90.0
7-1	2	5.00	.53	10.6
7-1	3	5.00	.78	15.6
7-1	4	5.00	1.02	20.4
7-1	5	5.00	.75	15.0
7-1	6	5.00	1.00	20.0
7-1	7	3.00	.54	18.0
7-1 Totals		33.00	9.10	27.6
		Theoretical Recovery		72.4
		Bladder Loss		10.0
		Actual Recovery		62.4
9-1	1	5.00	.35	7.0
9-1	2	5.00	.27	5.4

9-1	3	4.75*	1.67	35.2
9-1	4	5.00	.29	5.8
9-1	5	4.83*	.49	10.1
9-1	6	5.00	.76	15.2
9-1	7	4.29	1.34	31.2
9-1 Totals		33.87	5.17	15.3
		Theoretical Recovery		84.7
		Bladder Loss		10.0
		Actual Recovery		74.7
11-1	1	5.00	1.90	38.0
11-1	2	5.00	.44	8.8
11-1	3	5.00	.41	8.2
11-1	4	5.00	.77	15.4
11-1	5	5.00	.69	13.8
11-1	6	5.00	1.81	36.2
11-1	7	3.35	.62	18.5
11-1 Totals		33.35	6.64	19.9
		Theoretical Recovery		80.1
		Bladder Loss		10.0
		Actual Recovery		70.1
Well Totals		134.76	24.90	18.5
		Theoretical Recovery		81.5
		Bladder Loss		10.0
		Actual Recovery		71.5

The procedure used in obtaining all segments was a pneumatic jackhammer technique.

* Mechanical failure produced some anomalous results.

Bladder Loss - 10% of the total segment length, 13.48 ft, is lost due to the bladder mounting dimensions.

Figure 1

Map of GEMS Site

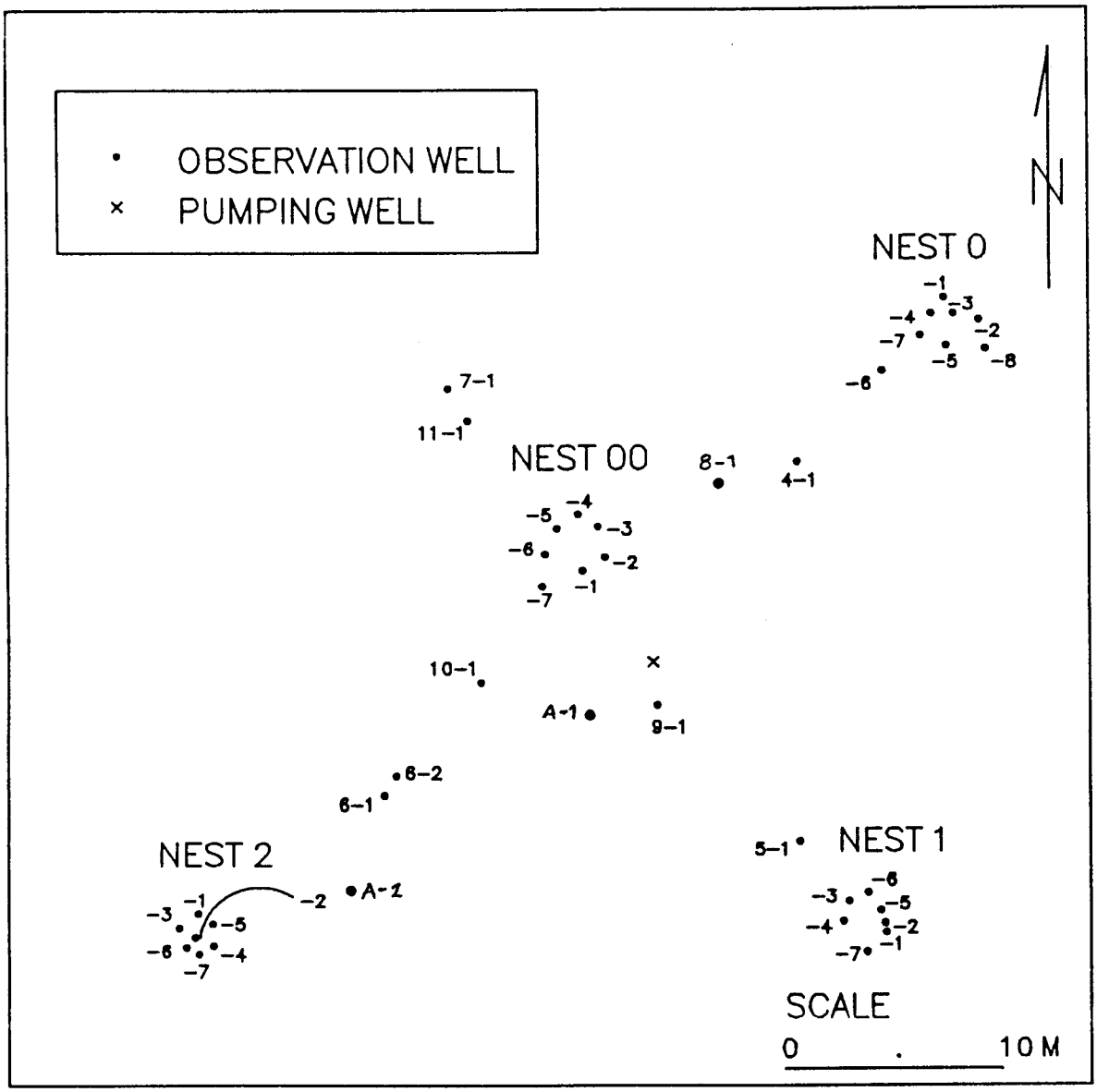

C. LABORATORY ACTIVITIES

Laboratory Procedures and Methods

The cores recovered from the drilling and sampling summarized in the previous section of this report were taken to the laboratory for measurement of core properties. The procedures and methods used in analyzing the core samples are essentially the same as those described in the report of the first year of this project (McElwee and Butler, 1992) with the exception of the changes noted below.

The constant head permeameter used in this work for the measurement of hydraulic conductivity was originally designed to process four cores at one time. The permeameter has now been enlarged to increase the number of cores that can be processed at one time to eight. Most parts of the permeameter that had been composed of opaque PVC have been replaced with clear PVC in order to more easily assess flow of water, transport of fine sediment, and entrapment of air bubbles within the system. The single filter that had been used in the permeameter setup has been replaced by a double filter system. Water first flows through a 5 micron filter to remove most sediment particles and other debris in the water; it then passes through a .5 micron filter that should remove bacteria and virtually all sediment particles.

The hydraulic conductivity of some of the cores is too low to be determined using the constant-head permeameter in any reasonable time frame. In order to determine the hydraulic conductivity of these cores, a permeameter designed for the measurement of low-conductivity cores, the Brainard-Kilman S-480 Permeability Cell, has been purchased. This system has only recently been installed and has not yet been used for the measurment of cores from GEMS.

As noted in the report of the first year of this project, the decrease in hydraulic conductivity with time that was observed for many of the cores may be due to deposition of calcite in pore throats. Another possible explanation would be the expansion and/or dispersion of clays, which would also produce a clogging of pore throats. In an attempt to identify the primary mechanism responsible for the observed decreases in conductivity with time, a series of experiments was conducted using a single core in the permeameter. The chemistry of the water prior to passage through the core and after passage through the core was carefully monitored with the assistance of the Analytical Services Section of the Kansas Geological Survey.

As described in the report of year one, the water circulated in the permeameter is obtained from wells at GEMS that are screened close to or over the same interval from

which the core was taken. At the time water was collected for use in the permeameter experiments, samples were taken in the field for analysis by the Analytical Services Section. The collected water was then taken to the laboratory where it was allowed to sit for two weeks in order to equilibrate with laboratory temperatures and pressures. Additional water samples were taken during this period in order to assess changes occurring with equilibration to laboratory conditions. Once the water was placed in the permeameter, samples were taken several times a day from the water that had passed through the core and once a day from the permeameter water that had not passed through the core. A subset of these samples was chosen for major cation analysis by the Analytical Services Section using the observed changes in the hydraulic conductivity as the selection criterion. Note that the permeameter setup used here involves recirculating water that has passed through the cores. For these experiments, however, no recirculation was allowed so that any chemistry changes occurring in the water passing through a core could be readily identified.

In addition to the major cation analyses performed by the Analytical Services Section, the pH and dissolved oxygen of the water prior to passage through the core (henceforth designated as permeameter water) and after passage through the core (henceforth designated as outflow-tube water) were monitored in the laboratory. The pH was determined using a CARDY Twin pH meter (Horiba Instruments). Measurement of the pH of the ouflow-tube water was done several times a day, while measurement of the pH of the permeameter water was done at least once a day. Dissolved oxygen (DO) was measured using a K-7512 CHEMets colorimetric kit (CHEMetrics). DO was determined for outflow-tube water once a day and once every 3 to 4 days for the permeameter water.

Sediment samples from the cores used in these experiments were collected for x-ray analysis of clay mineralogy both before and after being processed in the permeameter.

Results and Discussion

Core Analyses

Graphs of the original and repacked porosities, the percent fines (<53 microns), and the mean grain size for core segments from GEMS wells 00-1, 1-7 and 5-1 are presented in Figures IV.C.1 - IV.C.12. Hydraulic conductivities for original and repacked core segments from wells 1-7 and 5-1 are presented in Figures IV.C.13 - IV.C.16 (note that plots of the hydraulic conductivity for well 00-1 were presented in the report of year one). Both wells 1-7 and 5-1 show some overlap between the top two

samples where an interval was resampled during core recovery. Note that processing of sample #5 (16.8-18 m) from well 5-1 has not been completed. Grain size and porosity data for segment #4, sample #1 (11.51-11.69 m) from well 5-1 are not available because some of the sediment was lost during sieving. Information for several other segments is missing because those segments were suspected of having very low permeabilities and thus will not be further processed until the Brainard-Kilman permeability cell is operational.

Porosity values were calculated for both the original and repacked cores from the particle density, bulk density and core volume. The original cores from well 00-1 have porosities ranging from 23.2% to 37.4% with an arithmetic mean of 28.4% and a standard deviation of 3.1% (Figure IV.C.1). The porosity of the repacked cores ranges from 23.8% to 35.8% with an arithmetic mean of 28.8% and a standard deviation of 2.7% (Figure IV.C.2).

The differences between the original and repacked porosities from well 00-1 range from 0.03% to 3.22% with an arithmetic mean of 1.23%. For 35 of the 49 cores, the repacked porosity is greater than the original porosity; 14 of the repacked cores have lower porosities than the original cores. The primary reasons for differences between the original and repacked porosities are 1) inability to repack the cores to exactly the same volume as the original cores, and 2) loss of sediment during the repacking process.

The original cores from well 1-7 have porosities ranging from 23.1% to 33.1% with an arithmetic mean of 28.2% and a standard deviation of 2.0% (Figure IV.C.3). The porosity of the repacked cores ranges from 23.2% to 32.5% with an arithmetic mean of 28.6% and a standard deviation of 2.1% (Figure IV.C.4).

The differences between the original and repacked porosities from well 1-7 range from 0.00% to 5.07% with an arithmetic mean of 0.98%. For 36 of the 54 processed cores, the repacked porosity is greater than the original porosity; 17 of the repacked cores have lower porosities than the original cores and one core has identical original and repacked porosities.

The original cores from well 5-1 have porosities ranging from 20.6% to 32.3% with an arithmetic mean of 27.2% and a standard deviation of 2.4% (Figure IV.C.5). The porosity of the repacked cores ranges from 22.2% to 36.2% with an arithmetic mean of 27.7% and a standard deviation of 2.6% (Figure IV.C.6).

The differences between the original and repacked porosities from well 5-1 ranged from 0.01% to 5.36% with an arithmetic mean of 1.19%. For 30 of the 47 processed cores, the repacked porosity is greater than the original porosity; 17 of the repacked cores have lower porosities than the original cores.

The mean phi grain size was calculated for each core using the method of moments. The phi sizes for well 00-1 range from -1.02 to 2.55 with an arithmetic mean of -0.02 and a standard deviation of .65 (Figure IV.C.7). The phi sizes for well 1-7 range from -1.19 to 2.24 with an arithmetic mean of -0.05 and a standard deviation of .69 (Figure IV.C.8). The phi sizes for well 5-1 range from -1.05 to 2.44 with an arithmetic mean of 0.26 and a standard deviation of .78 (Figure IV.C.9). All profiles show a general fining upward sequence.

The percent fines (< 53 microns) was also calculated for each core. The percent fines for the segments from well 00-1 exhibit a range from .2% to 40.6% with an arithmetic mean of 2.9% and a standard deviation of 6.1% (Figure IV.C.10). The percent fines for the segments from well 1-7 ranges from .01% to 20.3% with an arithmetic mean of 2.1% and a standard deviation of 3.7% (Figure IV.C.11). The percent fines for the segments from well 5-1 ranges from .1% to 8.6% with an arithmetic mean of 1.8% and a standard deviation of 1.9% (Figure IV.C.12).

Hydraulic conductivity values from GEMS well 00-1 were presented in the report of the first year of this project.

The undisturbed cores of well 1-7 have an arithmetic mean conductivity of 16.43 m/day, with a sample standard deviation of 20.47 m/day (Figure IV.C.13). Values range from a minimum of 0.83 m/day to a maximum of 129.03 m/day. There is a general increase in hydraulic conductivity with depth.

The repacked cores exhibit a higher mean conductivity and greater variability than the undisturbed cores (Figure IV.C.14). Values range from 0.39 m/day to 171.28 m/day with a mean of 58.26 m/day and a standard deviation of 38.11 m/day. For 52 of the 54 processed segments, the repacked hydraulic conductivity is greater than the original measurement. Possible explanations for this were discussed in the first year report.

The undisturbed cores of well 5-1 have an arithmetic mean conductivity of 14.05 m/day, with a sample standard deviation of 13.40 m/day (Figure IV.C.15). Values range from a minimum of .12 m/day to a maximum of 65.32 m/day. There is no apparent trend in hydraulic conductivity with depth.

As was observed for well 1-7, the repacked cores of well 5-1 have a higher mean conductivity and greater variability than the undisturbed cores (Figure IV.C.16). Values range from 4.97 m/day to 159.61 m/day with a mean of 38.11 m/day and a standard deviation of 34.05 m/day. For 44 of the 47 processed segments, the repacked hydraulic conductivity is greater than the original measurement.

Chemistry Analyses

Monitoring of the pH of permeameter water did not reveal any trend with time while equilibrating to laboratory conditions or while circulating through the permeameter, and no significant change after the water has passed through the cores.

Dissolved oxygen measurements indicate that the oxygen content of the water increases after the water is placed in the permeameter. Before the water is placed in the permeameter, it has a DO content of 1 to 2 ppm. After the water has been placed in the permeameter, the DO content increases to 5 to 8 ppm. There is no significant change in DO content after the water has passed through a sediment core

Major cation analyses of the water in the permeameter and outflow tube for the three cores employed in these experiments indicate that the calcium content of the water generally decreases with time, further demonstrating that precipitation of calcite is occuring within the permeameter apparatus. One core shows a consistently lower calcium content in the outflow-tube water as compared to that in the permeameter. This indicates that calcite is being precipitated in the core and perhaps contributing to a decrease in conductivity.

Results of the x-ray analysis of clay mineralogy are not yet available, but, while preparing the samples for x-raying, it was noted that the clays are easily flocculated and dispersed. This tendency to readily flocculate and disperse could result in the clogging of pore throats and decreases in hydraulic conductivity.

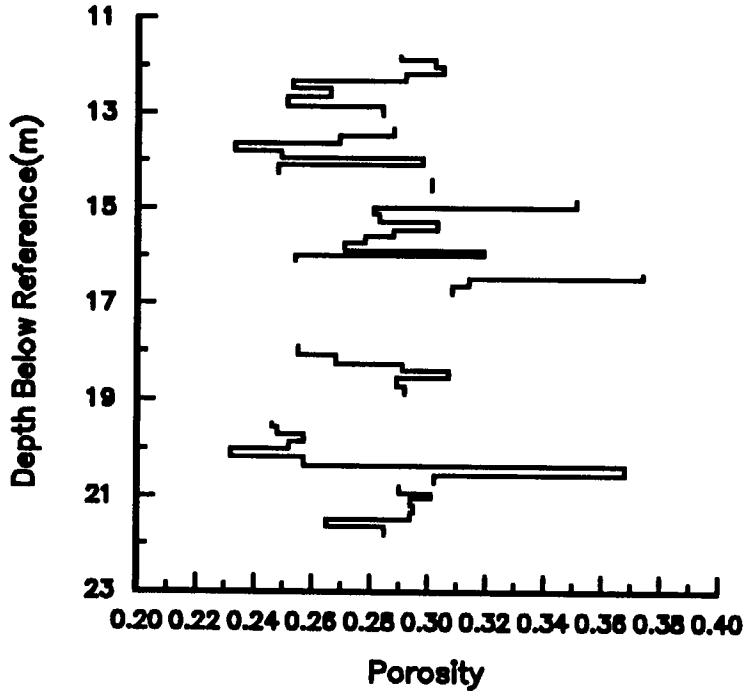

Figure IV.C.1. Original porosity versus depth for GEMS well 00-1.

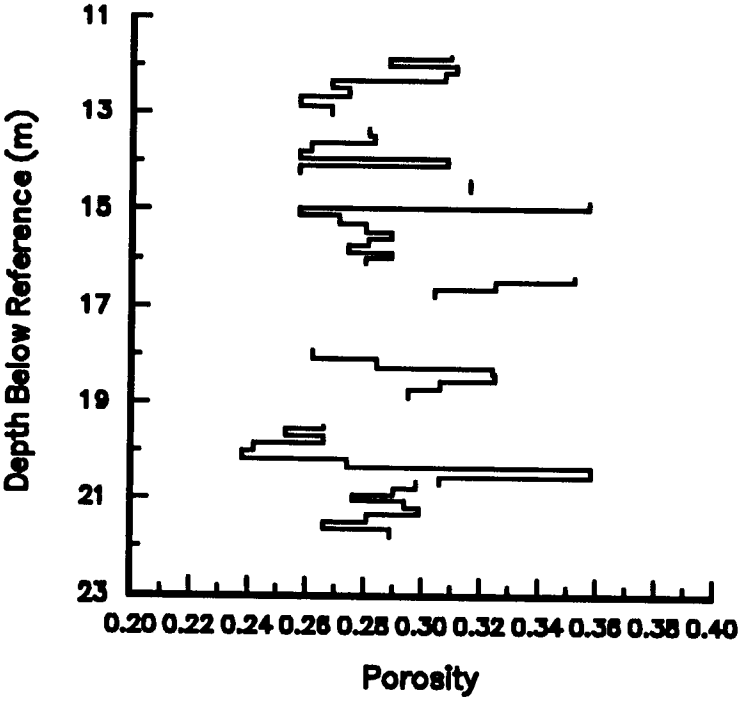

Figure IV.C.2. Repacked porosity versus depth for GEMS well 00-1.

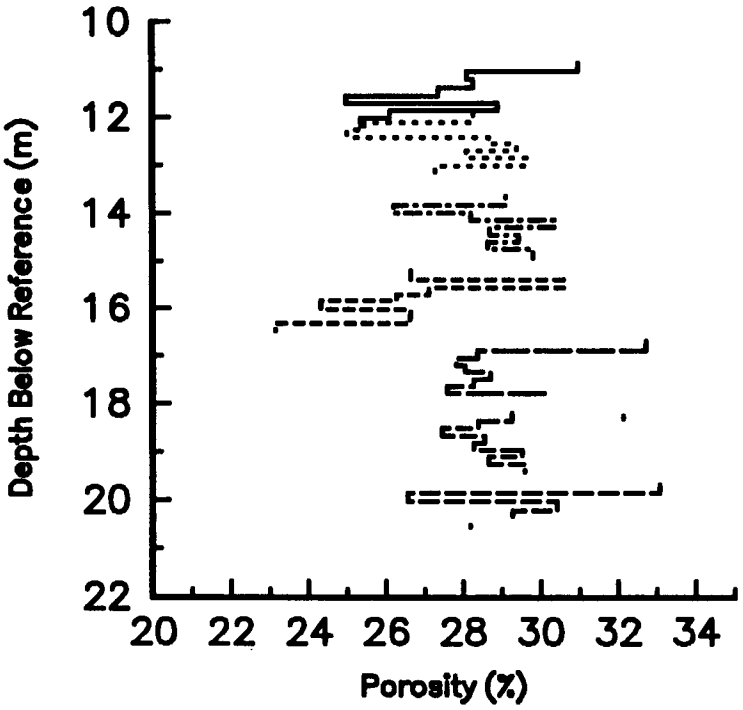

Figure IV.C.3. Original porosity versus depth for GEMS well 1-7.

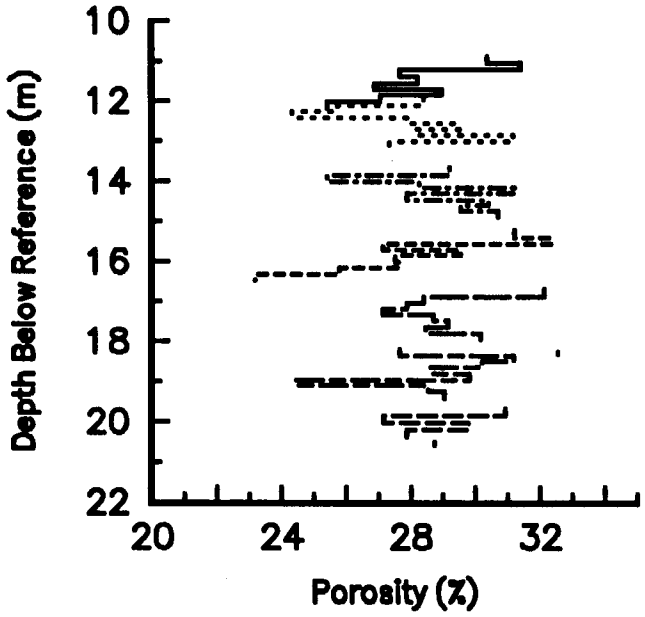

Figure IV.C.4. Repacked porosity versus depth for GEMS well 1-7.

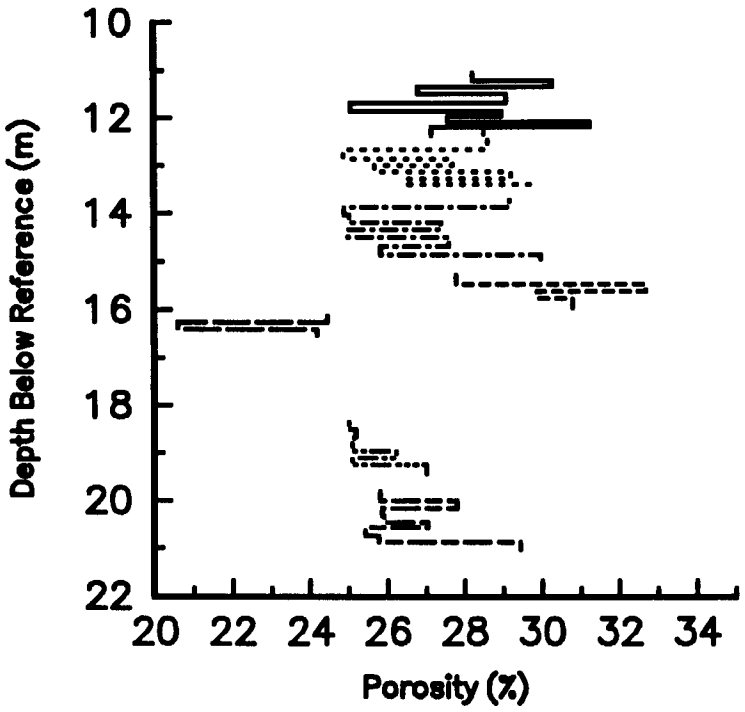

Figure IV.C.5. Original porosity versus depth for GEMS well 5-1.

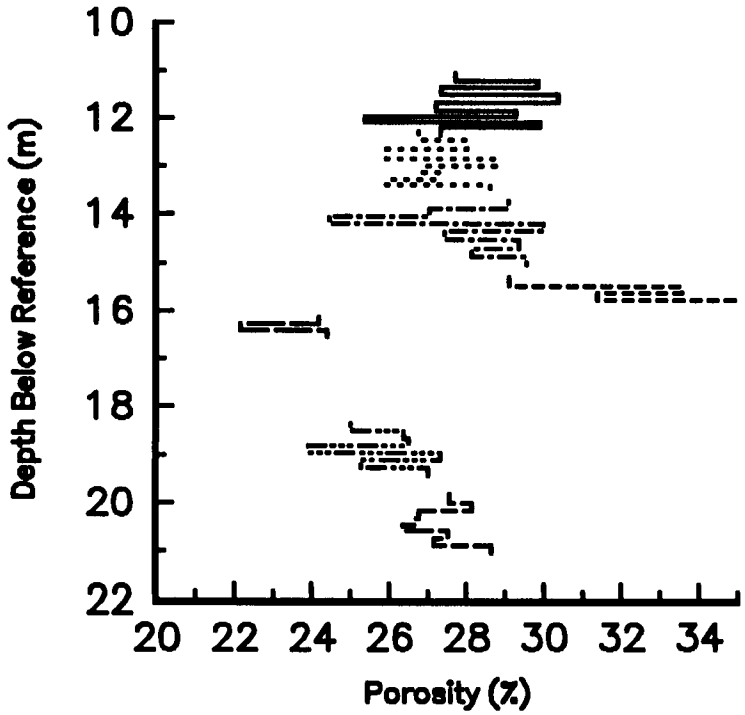

Figure IV.C.6. Repacked porosity versus depth for GEMS well 5-1.

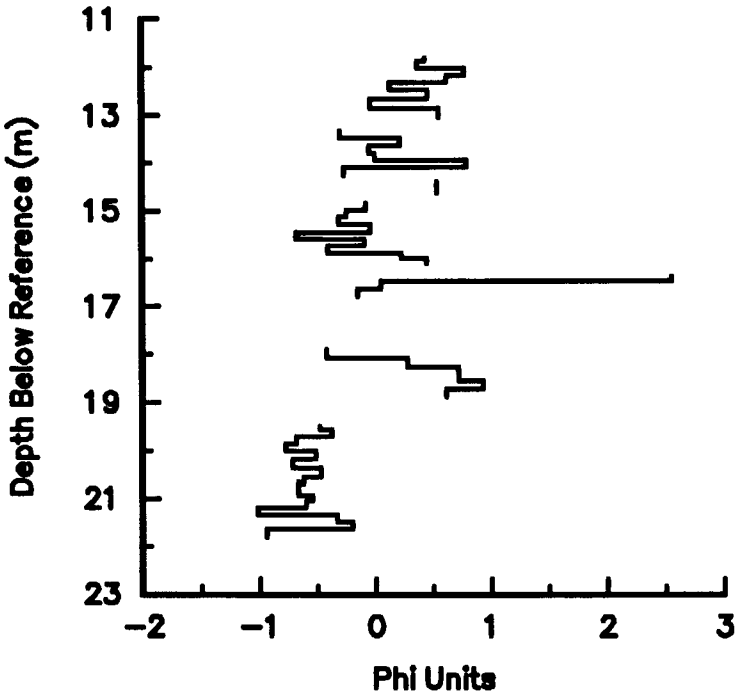

Figure IV.C.7. Mean grain size (in phi units) versus depth for GEMS well 00-1.

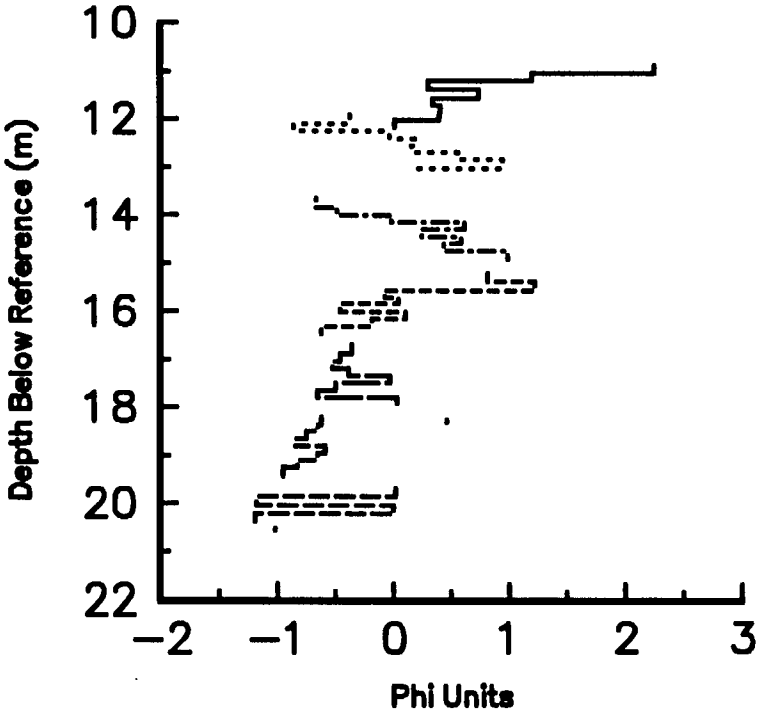

Figure IV.C.8. Mean grain size (in phi units) versus depth for GEMS well 1-7.

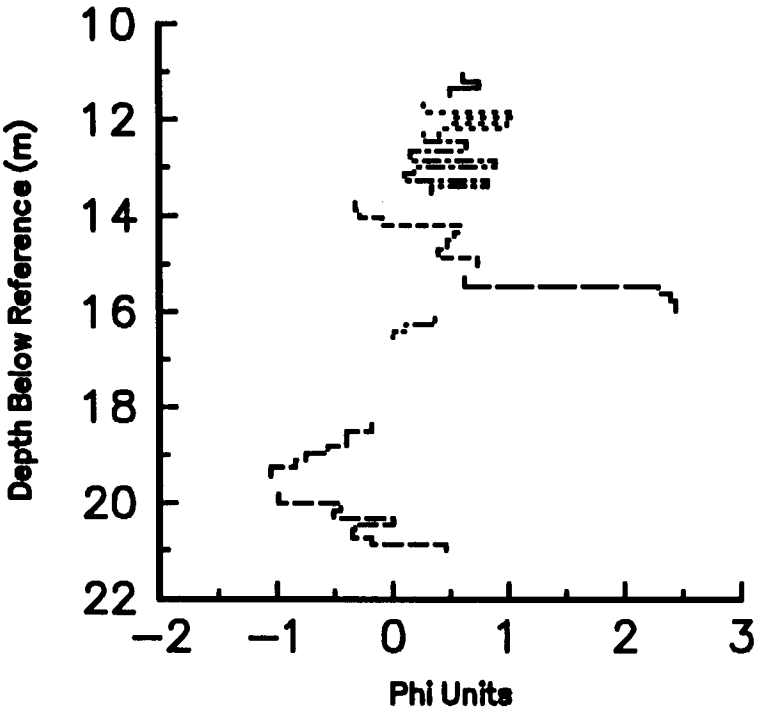

Figure IV.C.9. Mean grain size (in phi units) versus depth for GEMS well 5-1.

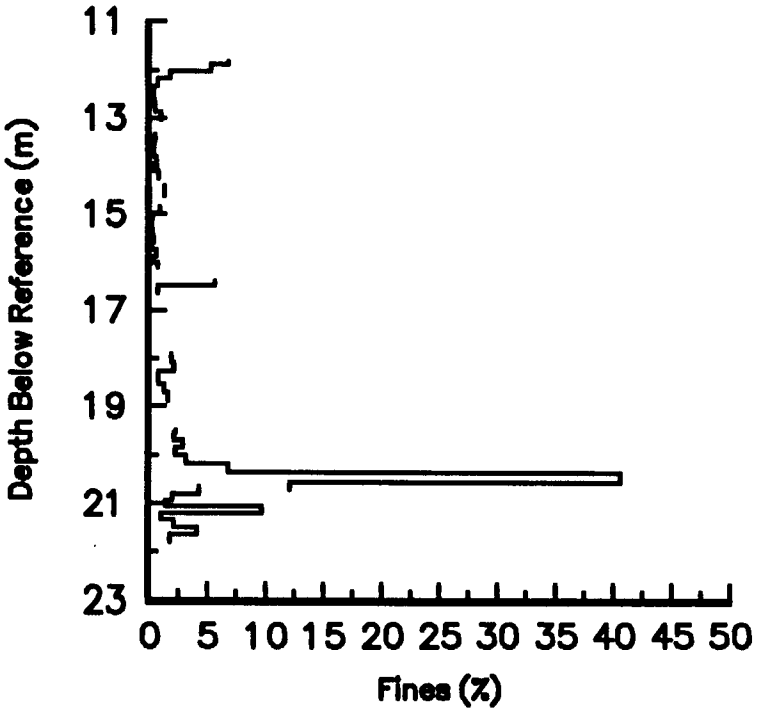

Figure IV.C.10. Percent fines (<.053 mm) versus depth for GEMS well 00-1.

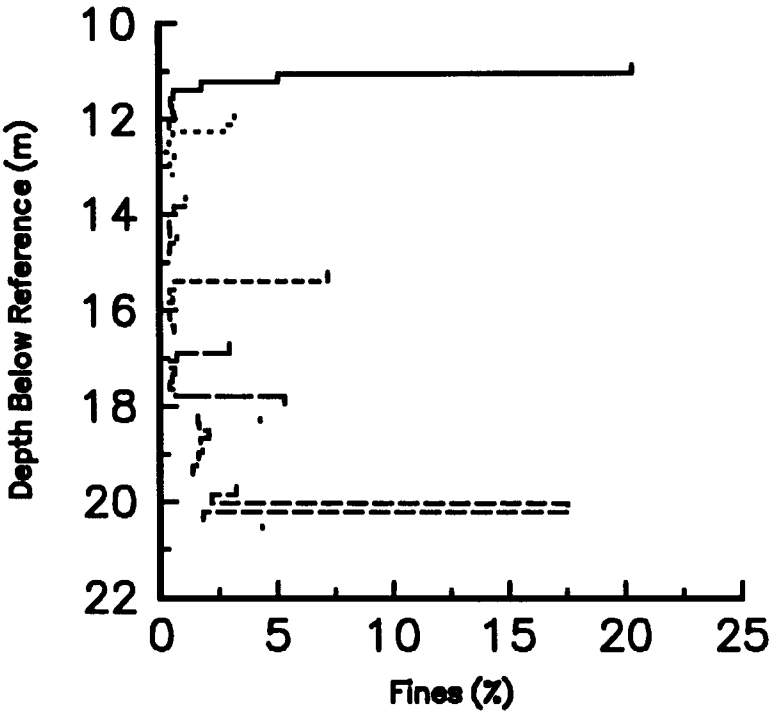

Figure IV.C.11. Percent fines (< .053 mm) versus depth for GEMS well 1-7.

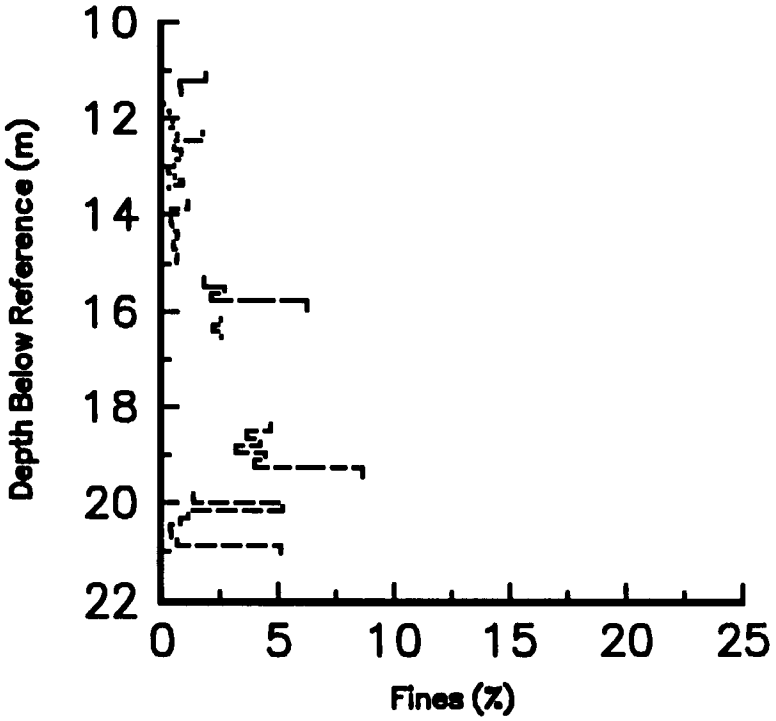

Figure IV.C.12. Percent fines (< .053 mm) versus depth for GEMS well 5-1.

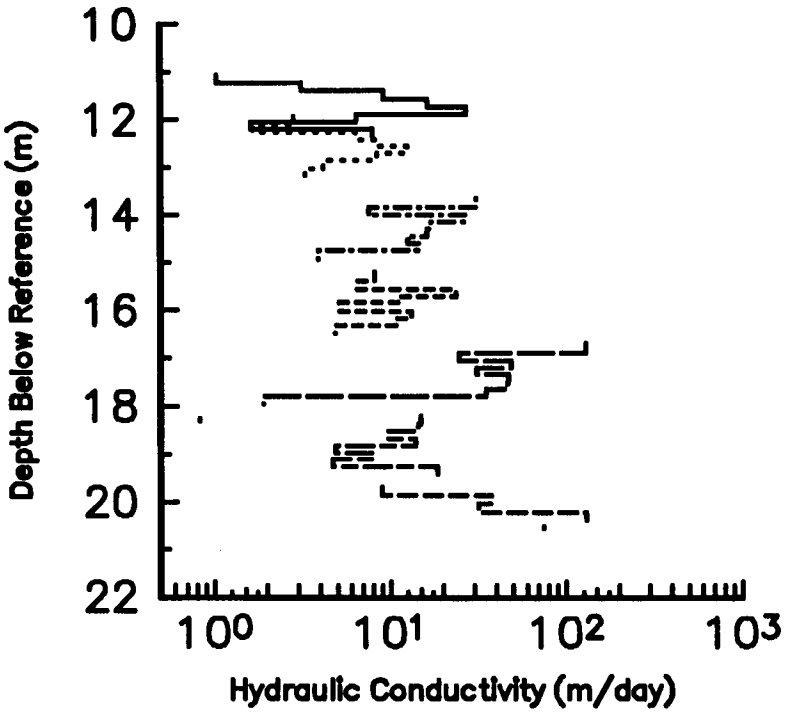

Figure IV.C.13. Original conductivity versus depth for GEMS well 1-7.

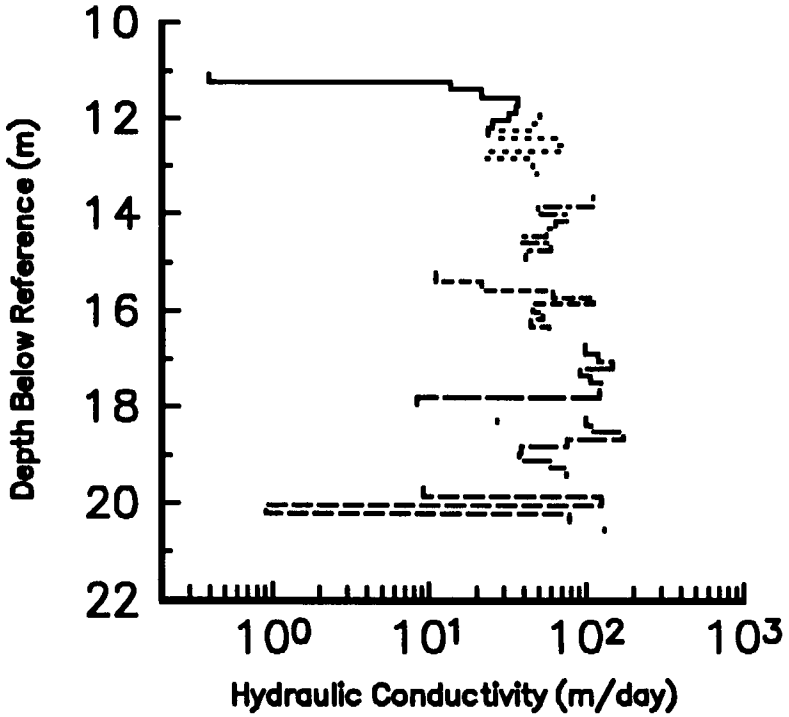

Figure IV.C.14. Repacked conductivity versus depth for GEMS well 1-7.

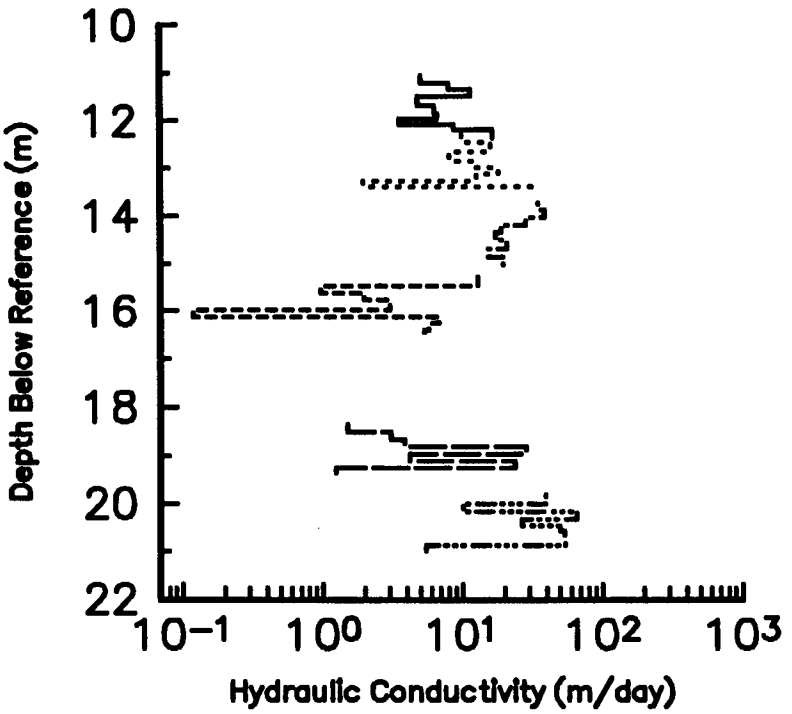

Figure IV.C.15. Original conductivity versus depth for GEMS well 5-1.

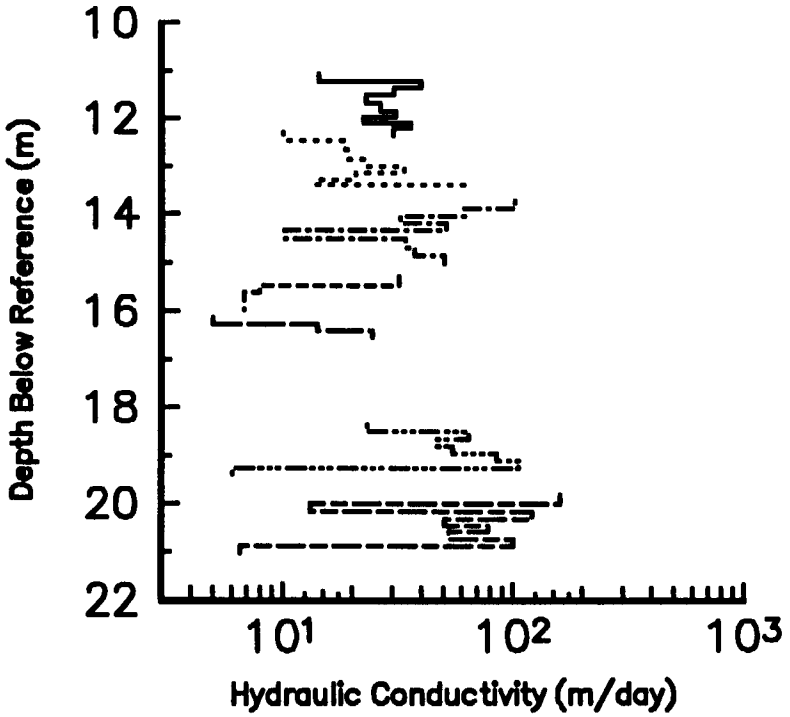

Figure IV.C.16. Repacked conductivity versus depth for GEMS well 5-1.

D. WIRELINE LOGGING ACTIVITIES - GEMS NATURAL GAMMA AND INDUCTION LOG SURVEY

Introduction

As part of the effort to describe the spatial variations in lithologic properties in the subsurface at GEMS, natural gamma and induction log surveys were performed in strategically located wells penetrating the sand and gravel section and the overlying silt and clay section. The surveys were run using logging equipment recently purchased by the Kansas Geological Survey. The goals of the surveys are (1) to determine the lateral extent of distinct lithologies with the greatest resolution possible (2) to establish a data base that will aid in the planning of future logging and groundwater investigations, and (3) to familiarize the research group with logging theory and the field equipment in preparation for future research and experimentation. A typical set of logs from GEMS well 1-7 are shown in Figure 1.

Formation Induction

Induction borehole tools contain a transmitter and a receiver coil, positioned vertically with a specified separation distance. A medium frequency alternating current is passed through the transmitter coil, producing a magnetic field about the coil. The vertical component of the magnetic field induces a current in a ring of formation material between the transmitter and receiver coils, but outside the borehole. The magnitude of the electric current is proportional to the electrical conductivity (or resistivity) of the formation. This current will also produce a magnetic field that will induce a current in the receiver coil. The voltage measured at the receiver coil is also proportional to the electrical properties of the formation and is converted to conductivity (right column in Figure 1) and resistivity (reciprocal of conductivity, middle column of Figure 1) by an automated calibration curve. These properties are measured periodically as the horehole tool is raised in the well and is plotted versus depth. The resulting curve is called an induction log.

The electrical conductivity and resistivity of a formation are a measure of the materials ability to carry or resist an electric current. Different lithologies have different electrical properties. Shale, for example, generally has a high electrical conductivity and a correspondingly low resistivity. On the other hand, clean sandstone generally has a low conductivity and a high resistivity. Identifying these relative differences on an induction log, allows a geologist to identify changes in lithology in the subsurface.

In most geologic material, the porosity and pore fluid chemistry are more important controls of the electrical properties of the material than the mineral grains (Dobrin and Savit, 1988). This inherent property will allow the determination of aquifer hydraulic properties by observing the movement of a conductive groundwater tracer with a borehole induction tool. This research will be conducted at GEMS and is slated for the summer of 1993.

The initial induction logs from GEMS are as expected. Repeat logs (from the same borehole) display no deviation due to changes in logging rate or lag time between repeat runs. The contact between the sand and gravel aquifer and the overlying silt and clay aquitard is blatantly obvious in all of the logs. The water table and smaller subunits (1 to 3 m thick) are also identifiable. The observed lithologic contacts were correlated between wells by hand and with an interactive computer program. The results of the correlation will be discussed below.

Natural Gamma Radiation

A natural gamma ray log is a plot of the amount of gamma radiation emitted from a segment of geologic material surrounding a borehole versus depth (left column in Figure 1). The source of the gamma rays is the instantaneous decay of radioactive elements naturally occurring in the rock. Trace levels or radioactive isotopes of potassium, thorium, and uranium are concentrated in fine-grained sedimentary deposits. Chemical weathering of rocks containing feldspar minerals produces clay minerals that may contain up to 1% potassium and are the largest source of formation radioactivity (Ellis, 1987). Thorium is quite rare, but is associated with heavy minerals that are often resistive to chemical and physical erosion. As a result, they remain as erosional remnants of their parent rock and become concentrated during transportation due to their high relative density. Uranium-bearing minerals are also quite rare, but when present, they are commonly from the precipitation of uranium salts and are frequently found in organ-rich shales (Ellis, 1987).

The gamma rays produced from these sources are detected by a scintillator. This devise contains a NaI crystal that is sensitive to radiation and emits a pulse of light when struck by a gamma ray. A photomultiplier detects the minute flashes of light and transforms them into an electrical pulse that is monitored and counted. Our natural gamma-ray counter is encased in the same tool that houses the induction devise. The two sensors act independently and record data simultaneously.

Natural gamma ray logs have been used by geologists for correlation of lithologies between wells, identification of subsurface lithologies, and for the estimation

of the volume of clay in an observed stratigraphic unit. Traditionally, correlation of natural gamma logs is attained with resolution measured in feet. Typical objectives are: the elevation of the base of a reservoir cap composed of shale overlying a porous limestone, or the thickness of an aquifer at a certain location. The magnitude of variation in natural gamma emissions across these boundaries of distinctly different lithologies is quite great and is easily identified on a log. However, if one is interested in identifying small (10 to 20 %) variations of clay content in thin beds within a sand aquifer, much greater resolution is needed. Procedures for collecting data to be analyzed at this scale (resolution of one foot or greater) are poorly outlined. As a result, a detailed investigation of the nature of radioactive decay and the methods used to measure it is necessary to collect the data correctly and accurately interpret the results.

The instantaneous rate of decay of radioactive elements in the earth is not constant. If the rate of decay is measured over a short time interval, the value attained may over- or underestimate the true rate. However if measured over a long period of time, random variations in the instatnaneous rate of decay will cancel each other out and a reliable value for the rate can be attained.

As the gamma ray counter is raised in a well, it continuously measures the rate of decay over a specified time interval (0.1 seconds for our counter). All of the rates measured as the tool (devise containing the gamma ray counter) is raised in the well are averaged over a specified sample length. Therefore, each value on a log is the result of several samples of the rate of disintegration. To increase the accuracy of the resulting averaged value, more 0.1 second samples of the rate must be averaged. This can be accomplished by increasing the length of the segment of the borehole that the rate is averaged over, or by increasing the time the radiation sensor measures rates for each sample interval (decreasing the rate the sensor is raised in the borehole).

The initial natural gamma ray logs collected display poor well-to-well correlation at the desired resolution. It is known from cores from GEMS that bedding exists in the sand and gravel aquifer at the scale of 0.02 to 0.3 m, yet natural gamma logs from wells separated by only 2.1 m, allow only the correlation of beds at the scale of 1 to 3 m. Considering that this material was deposited by point bar accretion, beds 0.1 m thick and greater should be laterally continuous over a distance of 2.1 m.

The lack of correlation at this scale with gamma ray logs suggests that variation in gamma radiation produced by changes in lithology are drowned by variability in the decay rates. It is possible that the contribution of gamma rays from the feldspar content in the sand is much grater than that of the clay. If the feldspar content in the sand is relatively consistent with depth, and the variations comprising the bedding are produced

only by differences in grain-size and/or clay content, then it is possible that the contribution of the lithologic variation is negligible compared to the statistical variability in the contribution of the feldspar.

An experiment was conducted, "simulating" the tool rising in the well as it sampled. The tool actually remained in the same position for approximately 2 to 10 minutes. Different speeds and depths were simulated in order to observe the effect of increased sampling time and magnitude of rate on the variation in decay rate observed at a single point. The variability observed during that period accounted for essentially all of the variation observed on the original logs from the sand and gravel aquifer. Clearly, most of the variation in gamma radiation due to the changes in lithology seen in the cores is completely obliterated by the variability in the decay rates.

At this time, it was also learned from the manufacturer of the logging equipment that the radius of influence of the tool is 1 m. Because such a large segment of geologic material is sampled for each measurement interval, the contribution of gamma radiation from a thin bed in this sphere will be averaged with the radiation from the entire sphere and will be decreased if not entirely masked by the variability in the rate of gamma ray emission for the entire sphere.

These developments are discouraging, but there is hope to attain better vertical resolution. In order to decrease the uncertainty in the natural gamma values attained, even slower logging rates can be used to allow more 0.1 second rates to be averaged. Repeat logs can also be run. The values from each log are added at every interval and averaged. This will also decrease the variability by essentially doubling the averaging time for each repeat log added. A statistical review of the data already collected is currently underway to determine what logging rate and number of logs can be used to minimize the uncertainty in the log values and the time spent in the field. An investigation of the expected contributions of gamma radiation from the feldspar grains and the changes in clay content seen in cores is also being conducted to determine the origin of the observed gamma ray signal.

Despite the high level of statistical noise in the natural gamma logs from the initial survey, some lithological correlations can be made between the eight wells logged. The boundary between the sand and gravel section and the overlying silt and clay section are definitively identifiable in each well. Subsections, ranging in thickness from 1 to 3 m, are identified in both sections and can be correlated across the site. Other subsections however, are distinctly apparent in one well and seemingly absent in adjacent wells. The signals from these units may be present on the logs, but are masked by the variability in

the gamma emissions, or have been erased due to the averaging effect of the large radius of influence.

Computer Correlation

In addition to the hand correlation of the logs, a computer program, CORRELATOR (Olea, 1988), was also used to aid in the well-to-well correlation. The program uses two logs from each well. One log must be sensitive to the clay content in the lithologic sequence, and the second must measure a lithologic property that is laterally consistent on a regional scale. Natural gamma and aquifer resistivity logs were chosen for the correlation. The resulting correlation is statistically high across the site and appears reasonable considering the environment of deposition of the deposits. Although the correlation is statistically high, the resolution of laterally continuous lithologies is still less than what was anticipated.

Conclusion

An understanding of lateral continuity is vitally important for any investigation of the physical controls of groundwater flow. Clearly, the vertical resolution that was hoped for of a few tenths of a meter is not possible. However, better resolution can be attained and will give us the best data to date on the extent lateral continuity of lithologic variations at GEMS. Natural gamma ray logging will continue at GEMS through the summer of 1993 in accordance with the procedures outlined above.

Typical Natural Gamma and Induction Log from GEMS Well 1-7

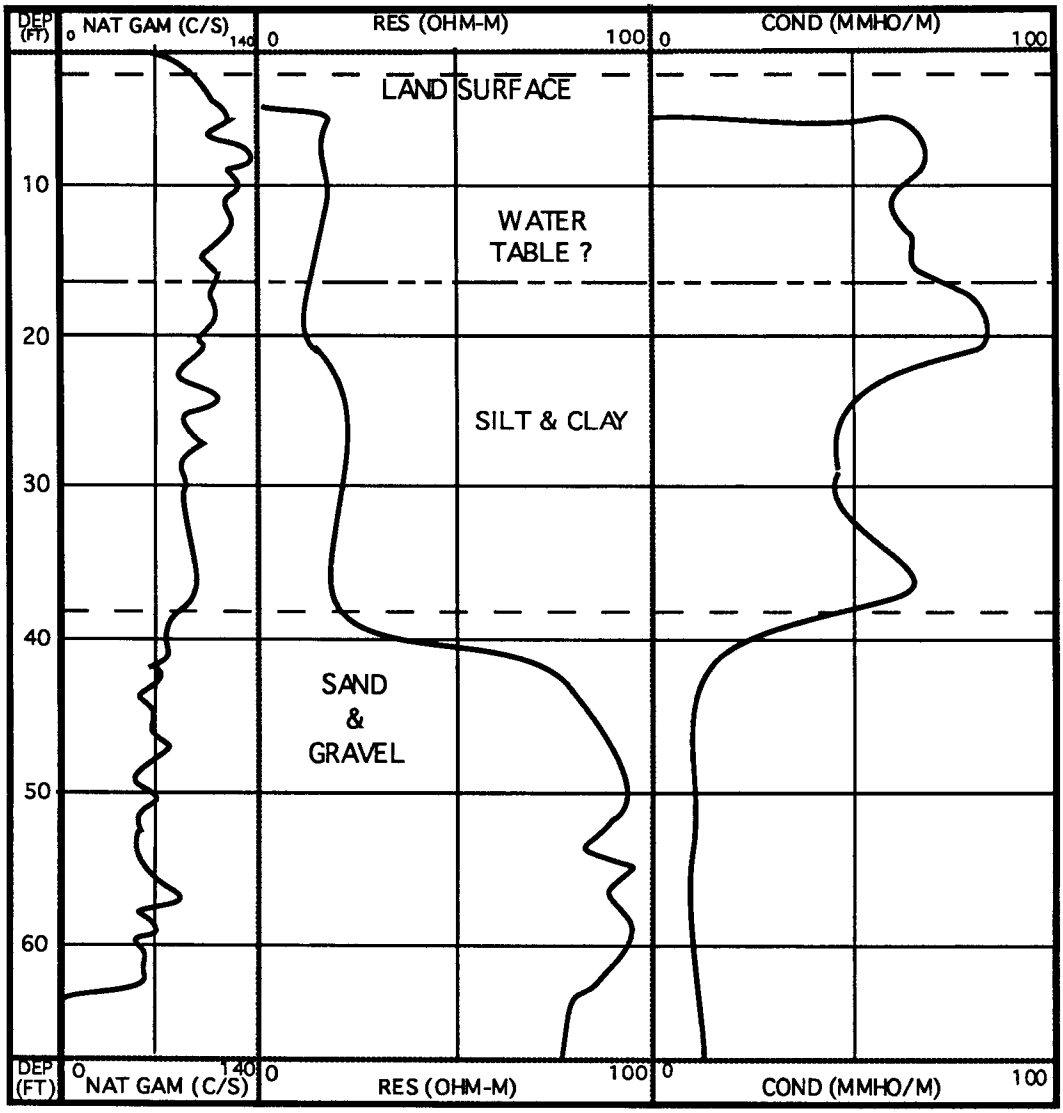

Figure 1.

E. HIGH-RESOLUTION SEISMIC REFLECTION STUDY

Introduction

Seismic-reflection surveys have been extensively used for more than 60 years to image the subsurface for petroleum exploration. The successful use of the technique in shallow engineering applications, however, depends on several key conditions. First and foremost is the existence of acoustic velocity and/or density contrasts between geologic units in the subsurface. The second relates to the ability of the near-surface to propagate high-frequency seismic signal. Finally, the acquisition parameters and recording equipment must be compatible with the proposed target, resolution requirements, and environmental constrains of the survey. The application of shallow, high-resolution seismic reflection methods to specific geologic situations or problems requires a thorough understanding of the basic principles (See Appendix B from the first year report).

Shallow high-resolution seismic-reflection profiles can be useful in characterizing shallow structures significant to a variety of hydrogeologic settings. High-resolution seismic reflection has only recently developed as a practical and effective method for identifying zones of low permeability (Birkelo et al., 1987; Merey et al., in press), unconsolidated layers above bedrock (Steeples and Miller, 1990, Grantham, 1990), and mapping shallow (<30 m) bedrock surfaces (Hunter et al., 1984; Miller et al., 1989; Miller et al., 1990). The shallow seismic-reflection technique is inexpensive (relative to drilling) and can often decrease the need for drilling by an order of magnitude. While the seismic-reflection method can identify variations in the bedrock surface and stratigraphic relationships, it can give only estimates of depth and explicit identification of lithologies requires confirmation drilling.

This report displays and interprets seismic-reflection data acquired and processed between June 1992 and June1993 from the GEMS site (Figure 1). The purpose of surveys displayed in this report was to determine the feasibility of delineating stratigraphic or structural features of potential hydrogeological significance between the 30-35 ft deep clay/sand interface and the top of a 70 ft deep bedrock surface. Two CDP seismic reflection lines (totalling 250 shotpoints over 277 ft) were acquired and processed along with a third data set (acquired during the year prior) into CDP format. The 250 shotpoint CDP surveys had 1 ft station spacing and was conducted using the downhole 30.06 rifle, 100 Hz geophones, 400 Hz analog low cut filters, and a Geometrics 2401x 48 channel seismograph. The near-surface conditions where drastically different for data collected during 1992 versus data collected during 1993 (moisture conditions), resulting in significant differences in overall data quality. Data acquired during 1993 focused

primarily on discontinuous intra-alluvial features that lay between the clay/sand interface and bedrock.

Data Acquisition

All data for this study were acquired with an EG&G Geometric's 2401x seismograph. The Geometric's seismograph amplifies, filters (analog), digitizes the analog signal into a 15-bit word, and stores the digital information in a demultiplexed format. The 400 Hz low cut filters have an 18 dB/octave rolloff from indicated -3 dB points. The 1/5 ms sampling interval resulted in a 5000 Hz sampling frequency, recording 1024 samples for a record length of 204 ms. The 2401x is a 48 channel floating point seismograph.

A variety of field parameters and equipment were tested to insure optimization of recorded data. The source for the study of these lines was a downhole 30.06 (Steeples et al., 1987). The receivers for the entire study were single Mark Products L-40A 100 Hz geophones. Final filter settings, receiver spacing, and source offset were determined from analysis of preliminary test shots.

Data Processing

Data processing was done on an Intel 80486-based microcomputer using *Eavesdropper*. The processing flow was similar to those used in petroleum exploration (See Table 1 from the first year report). The main distinctions relate to the conservative use and application of correlation statics, the precision required during velocity and spectral analysis, the extra care during muting operations, and the lack of deconvolution. Processes such as deconvolution have basic assumptions that are violated by most shallow data sets. Migration is another operation that many times due to non-conventional scaling (vertical and/or horizontal) may appear to be necessary, when in actuality geometric distortion may be simple scale exaggeration. Processing/ processes used on data for this report have been carefully executed with no assumptions and with care not to create artifacts.

Seismic data from the first year were processed to enhance the bedrock reflection. The processing flow deviated from normal shallow reflection processing during the muting and filtering aspects. The filtering was much narrower band and the muting was much more severe. The muting was necessary to reduce the contamination of the pre-bedrock reflection arrivals with noise that adversely effected many of the correlation statics routines and resulted in coherent events that were not the direct result of near-vertically incident reflections.

The air-coupled wave and the cyclic nature of the direct wave energy proved to be unremovable with spectral filtering, f-k filtering, and the 24-fold CDP stacking process.

The optimum offset window was chosen to be later than the arrival of the air-coupled wave to allow reflections shallower than bedrock to become apparent. The nearby trees, pumping well head, and monitor well clusters proved to provide a source of reflected air coupled wave that affected the entire data set. All attempts to remove the air-coupled wave proved futile. The reflections present on field files possessed statics problems and trace-to-trace amplitude irregularities which combined with the air-coupled wave problems to inhibit the effectiveness of established shallow reflection processing techniques.

Results

Unequivocal identification of reflection energy on field files is essential for accurate interpretation of CDP stacked sections. Many of the field files acquired for the production portion of the 1992 survey (line 2) have confidently identifiable reflection events at approximately 65 ms (Figure 2). The 65 ms reflection has a dominant frequency of approximately 140 Hz and an apparent NMO velocity of around 3000 ft/sec. This represents an approximate depth to the reflector of 70 ft and a vertical resolution potential of about 5 ft. The signal-to-noise ratio on the field file is sufficient to confidently identify bedrock reflections on many files at offsets longer than about 50 ft. The air coupled wave and direct wave are the highest amplitude events on most files and increases the background noise of near-vertically incident reflection energy arriving later in time.

The reflection event identifiable at approximately 65 ms is less evident and possess almost a 40% drop in dominant frequency on field files recorded during the production portion of the first year's study (Figure 2) in comparison to either the walkaway files from the first year or the reflections on field files from the second year's research (Figure 5). Frequency content of the second year's data is consistent with that achieved during the walkaway portion of the first year's research. The higher frequency information obtained the second year is a result of both the increased low cut filters and saturated ground conditions. The overall inconsistency in signal characteristics between the four CDP data sets predicates care and a conservative approach to interpretations and line-to-line correlation of coherent energy on stacked data. Both the first and second year's data possess unique characteristics of potential significance to the detection and mapping of alluvial features.

Reflections are easily interpretable from interfaces beneath the bedrock surface on line 2 (Figure 4). Line 2 intersects line 1 (Figure 3) at approximately CDP 700. The near-surface along this line was very disturbed due to the high level of truck activity associated with the drilling of dense clusters of monitor wells. The static anomalies introduced by

this activity are significant, resulting in velocity anomalies that made reflection from the shallow portion of the section difficult to identify. The apparent dip on the bedrock surface is probably related to velocity variations across the line. Undulations similar to those interpreted on line 1 can be inferred on line 2. If the interpretation of the bedrock surface is accurate, when the static problem that produced the apparent dip on reflections from beneath the bedrock surface is corrected for, the bedrock surface dips slightly to the southeast. It is also possible that the interpreted bedrock surface is actually intra-alluvial features that are discontinuous across the line and when interpreted in a continuous manner appear to possess dip.

The events that appear to be coherent between 40 and 60 msec could represent acoustic boundaries within the alluvium. Some indication of the gravel/clay interface is suggested at about 35 to 40 msec. The interpreted reflection from the gravel interface possesses a narrow frequency bandwidth and is much more discontinuous than on the line 1 section. The dominant frequency of reflection on this line is approximately 200 Hz, which is about 30 % better than that observed on line 1. This would suggest a 30% increase in vertical resolution. The data has only limited potential for mapping the clay/ gravel interface, but does allow for more speculation than line 1 about intra-alluvial material between the basal contact of the clay and the bedrock surface.

Reflection on field files from lines 3 and 4 can be interpreted during all stages of pre-stack processing (Figure 5). The reflection from bedrock has classic hyperbolic curvature with an origin time of approximately 55 msec. Problems with the air coupled wave and the ringing direct/refracted wave are evident on raw files. The dead traces on shot gather 79 is a result of the large pumping well and associated well curb or platform. The inconsistency in reflection arrivals is evident on processed shot gathers. The dominant frequency on filtered field files is in excess of 300 Hz. Processing clearly enhances the coherency and resolution of the data and appears to generate a sufficient increase in signal-to-noise ratio to allow for a good CDP stacked section.

Line 3 (Figure 6) acquired in the second year of research did not seem to have as good a signal to noise ratio as line 4 (Figure 7). This was probably a result of the near-surface that had been significantly altered during the installation of three different well clusters and a large pumping well, which was avoided during the acquisition of line 4. The apparent diffraction centered on about CDP 180 is the result of the of the large pumping well and the associated well pad (8 ft square cement pad) and power pole. This apparent diffraction is air-wave echo that could not be removed during processing. Subtle indications of a coherent reflection can be interpreted on the extreme southwest end of the line. The diffraction looking event with air wave velocity on the extreme southwest end

of line 3 is suspected to be from the road bank or trees that were at the edge of the study area. The data do possess some reflection energy. Only hints of reflections can be interpreted across most of line 3. Various processing techniques were tested to determine if the coherent reflections observed on field files from line 3 could be enhanced to form uniform reflections on CDP stacked records. All attempts to generate a stack section of the data with coherent reflections across the entire section were met with only limited success. Reflections are present in the data as evident on processed field files and in places on the CDP stacked section.

The shorter line acquired during the second year's research (line 4) does possess interpretable reflection information (Figure 7). A strong event at approximately 52 to 55 msec is interpreted to be the bedrock alluvial interface. The dominant frequency of this event is nearly double the reflection interpreted as bedrock on line 1. Subtle undulations on the bedrock surface could be indicative of either velocity variations between the surface and bedrock or structure on the bedrock surface. Both possible interpretations have been suggested at this site on previous data sets. The event interpreted at approximately 35 msec is most likely the basal contact of the clay. Slight changes in arrival time of this event could represent variations in thickness of the clay unit. The extreme variability obviously present in this area is bore out by the close proximity of line 3 and 4. Line 4 was placed only 8 ft southeast of line 3. At approximately CDP 370 to 390 drill hole information suggests an anomaly within the otherwise consistent clay unit. This anomaly could be interpreted as a pull up on the bedrock surface or a slightly deeper basal reflection arrival (2 msec) from the clay in that area. The time window between the base of the clay and top of the bedrock surface appear to be relatively quite with only a rare coherency over distances of more than a couple of traces. The increased frequency content and decreased receiver spacing improved the resolution of the data set and verified the lack of any interfaces with significant acoustic variability between the base of the clay and top of bedrock.

Conclusions

Shallow seismic reflection can be used to delineate structural features present between the clay/gravel interface at about 30 ft and the bedrock surface at slightly more than 70 ft. The close proximity and total number of boreholes on this site would suggest that any feature which could potentially alter the hydrologic characteristics at this site between the ground and bedrock surface should have been detected by direct contact. The subtle events interpreted just below the clay/gravel interface at several places on both lines 1 and 4 could represent localized stratigraphic changes that could alter the local

hydrologic properties. The presence of the deeper reflection events allows confidence in the interpretations of relative topographic change on the bedrock surface on lines 1, 2, and 4 as actual elevation changes and not as caused by near-surface irregularities.

The data quality of the data set as a whole (lines 1, 2, 3, and 4) is extremely variable. This is due in part to the time between the acquisition of the various lines, changes in saturation, and inconsistencies in the near-surface as a result of vehicle and/or drilling activities. Due to the extremely close spacing of boreholes and borehole activities much of the ground surface has been non-uniformly altered. The high resolution seismic method is very sensitive to near-surface conditions. Improvement in signal-to-noise and dominant frequency would be possible in this area if data were acquired in relatively undisturbed locations.

Data collected during the second year suggest that the variable saturation present in the very near-surface (as evidenced by the standing water surface) causes sufficient static problems to be extremely detrimental to the stacking of reflections with dominant frequencies in excess of 350 Hz. Improvements in the processing of data with this much variability will be critical to allow vertical resolution on the order of one-half foot at this site. The processed, unstacked data possess the potential to resolve beds as thin as 0.5 ft.

Recommendations

Continuous core holes will be necessary to completely analyze the effectiveness of shallow seismic reflection at this site to delineate inter-alluvial features. Borings will not be sufficient to definitely determine the cause of some of the reflections between the basal contact of the clay and the bedrock surface as interpreted on lines 1, 2, and 4. The reflection technique should be correlated with existing hydrologic data to extract any hidden significance associated with anomalies not interpreted as coherent reflection events on the CDP stacked sections.

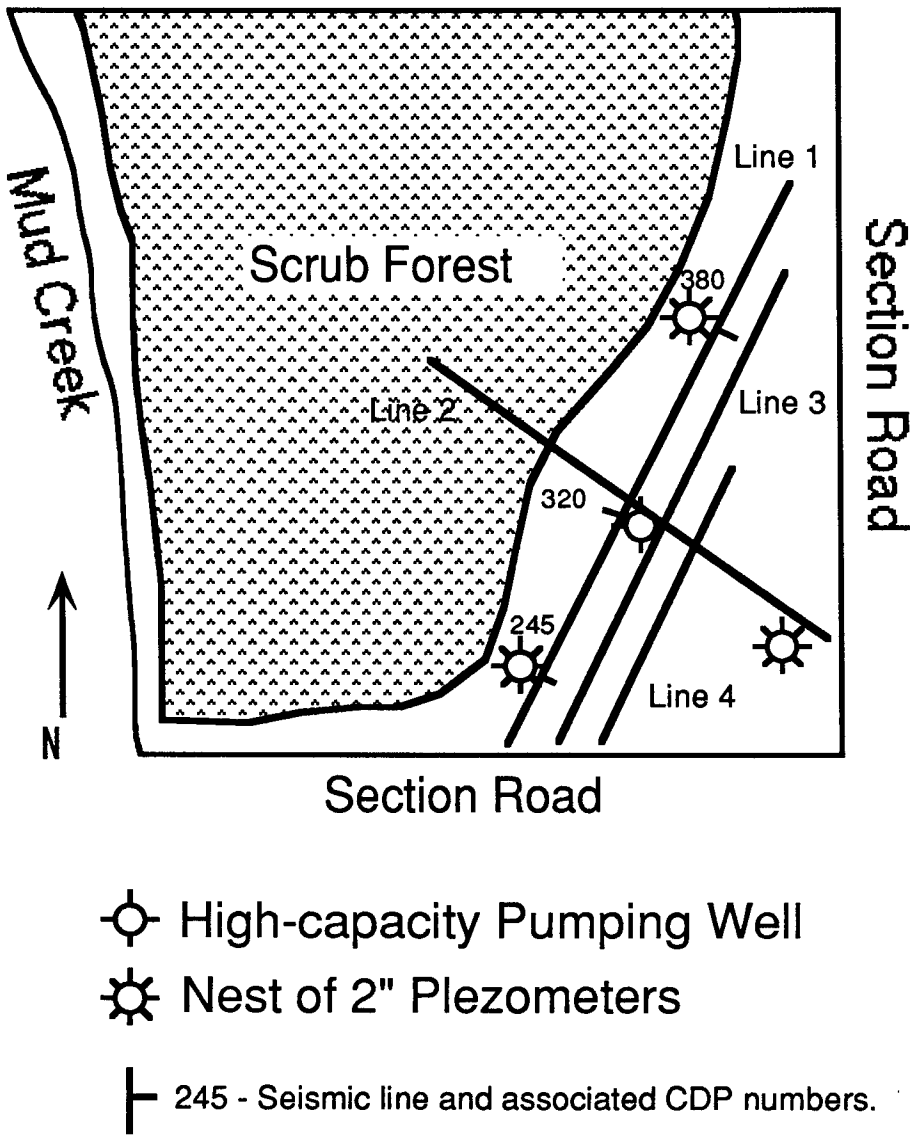

Figure 1. Map of the GEMS site showing locations of seismic lines.

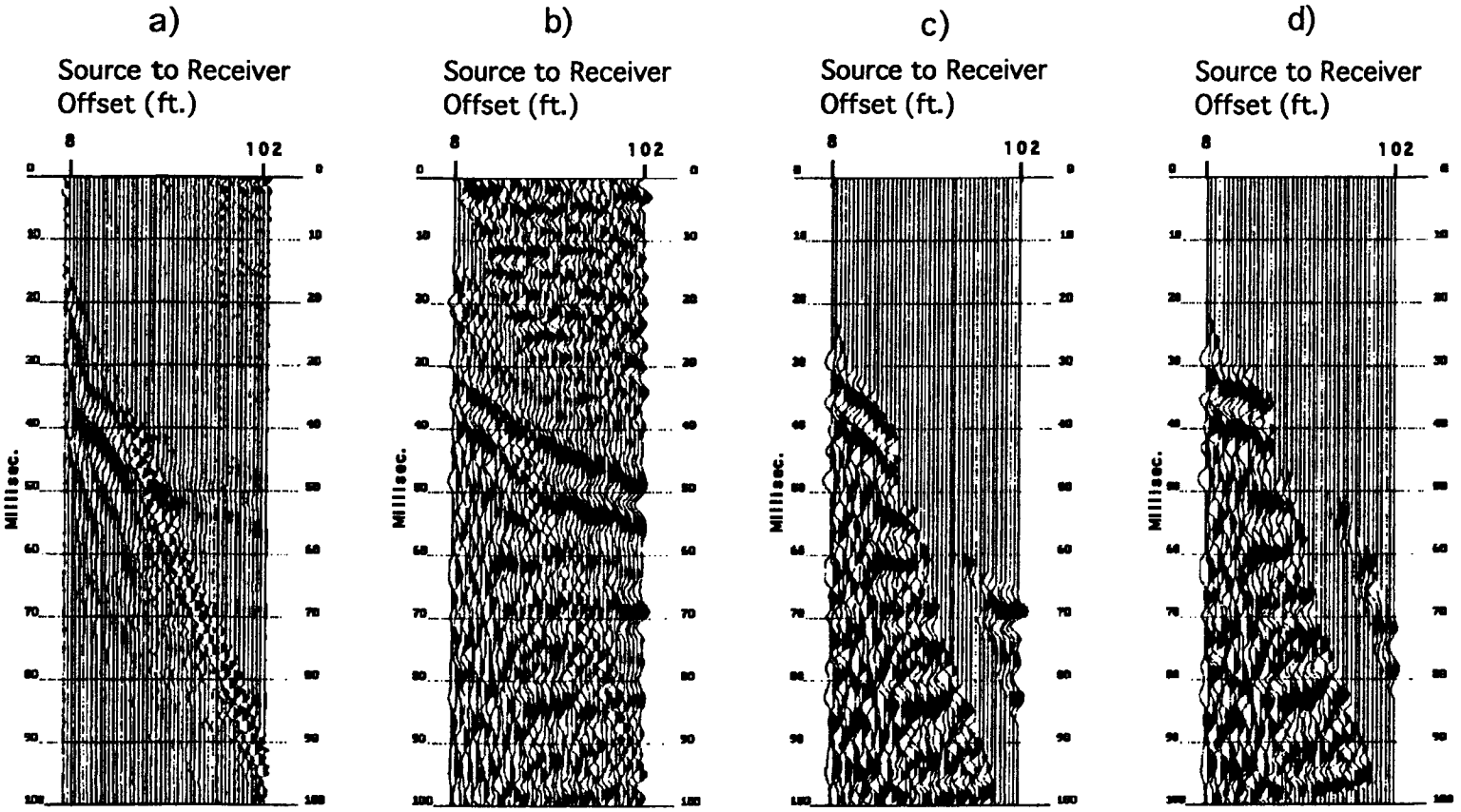

Figure 2. Selected field file displaying the processing sequence. a) raw field file normalized, b) f-k filtered, AGC scaled to 25 ms, and digital filtering 125 to 250 Hz, c) appropriate muting and trace balancing, d) moved out to adjust for non-vertical incidence.

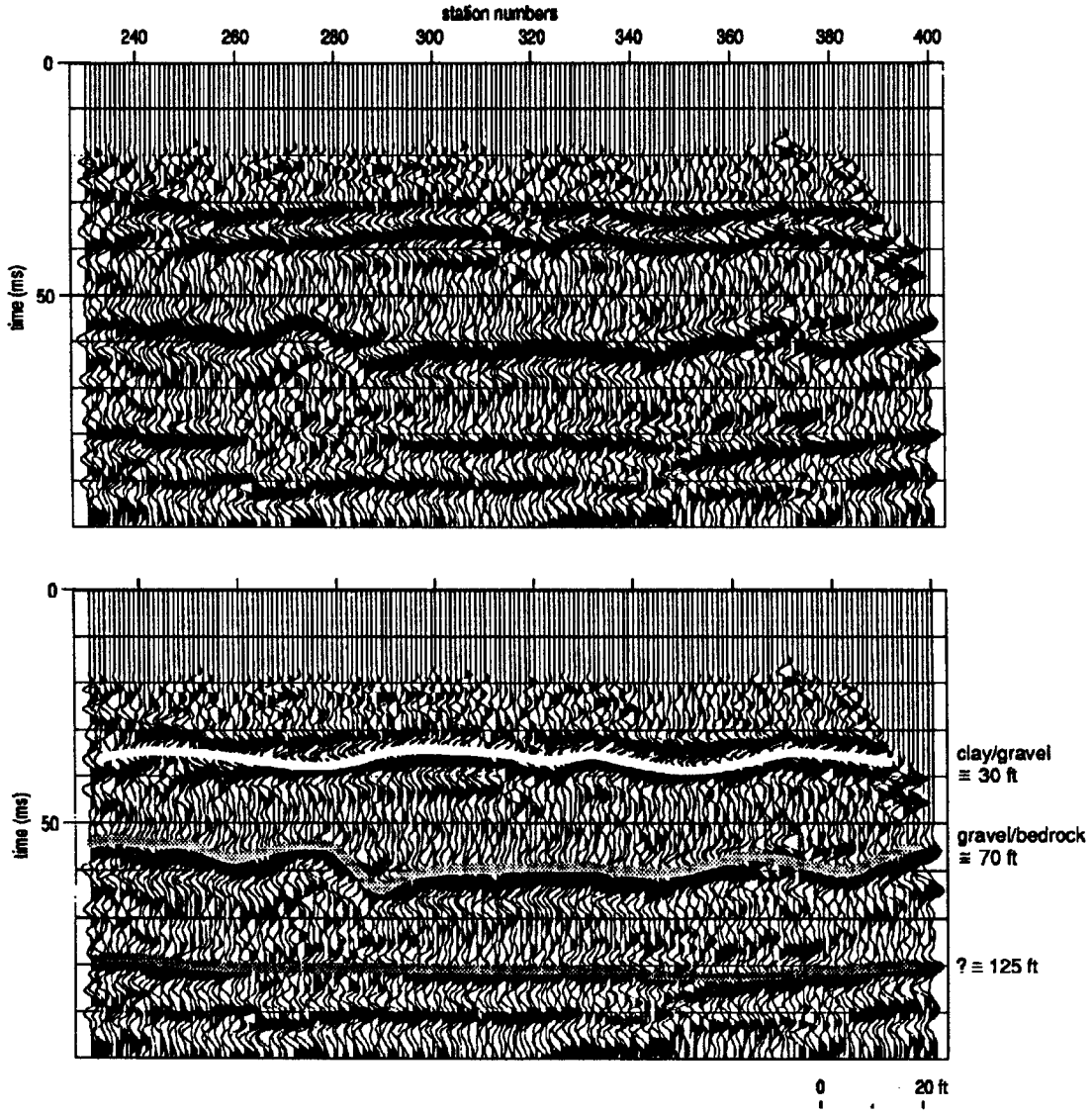

Figure 3 CDP stacked, 24 fold seismic reflection section from GEMS line 1. At least three reflection events are easily interpretable on the stacked section. The interpretation suggest several feature of acoustic significance that could influence the hydrologic setting.

LINE #2

SE CDP NUMBERS NW

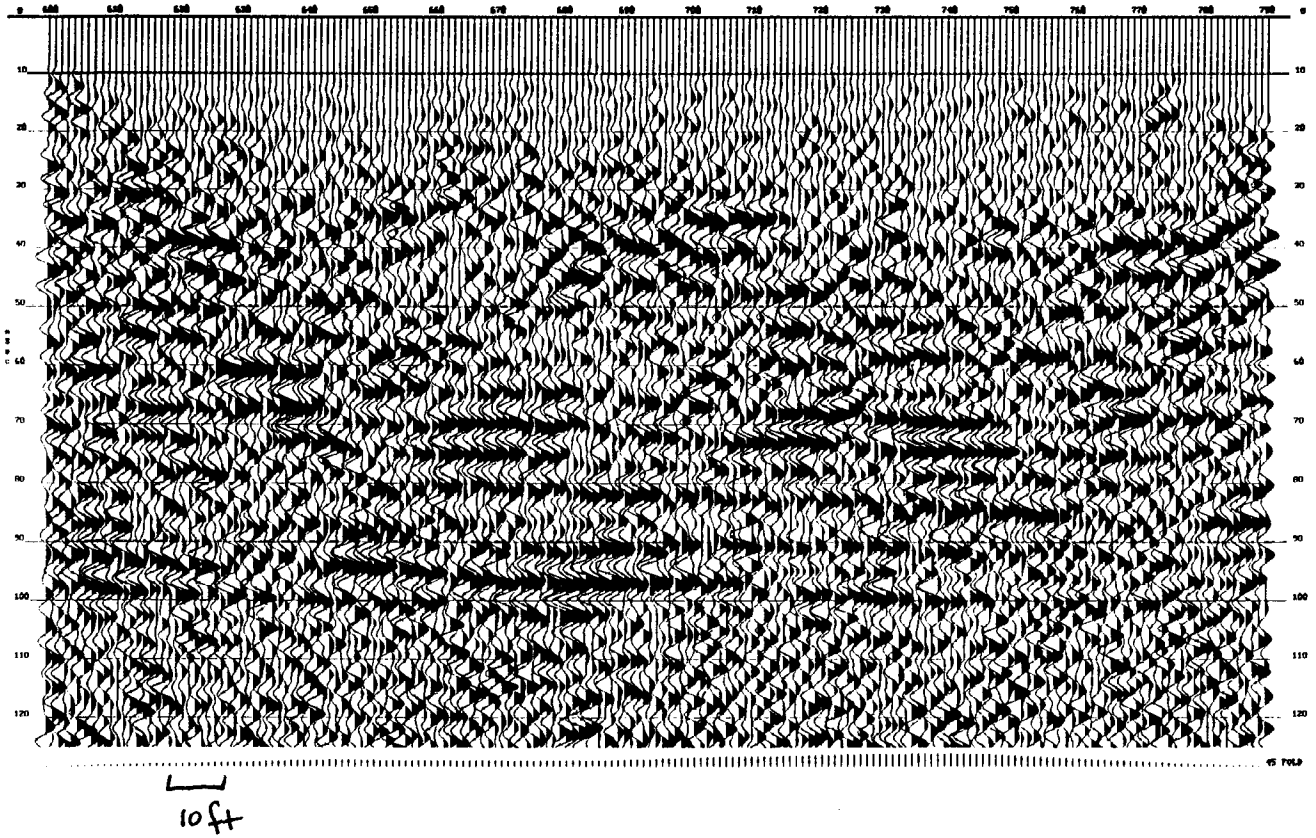

Figure 4a.

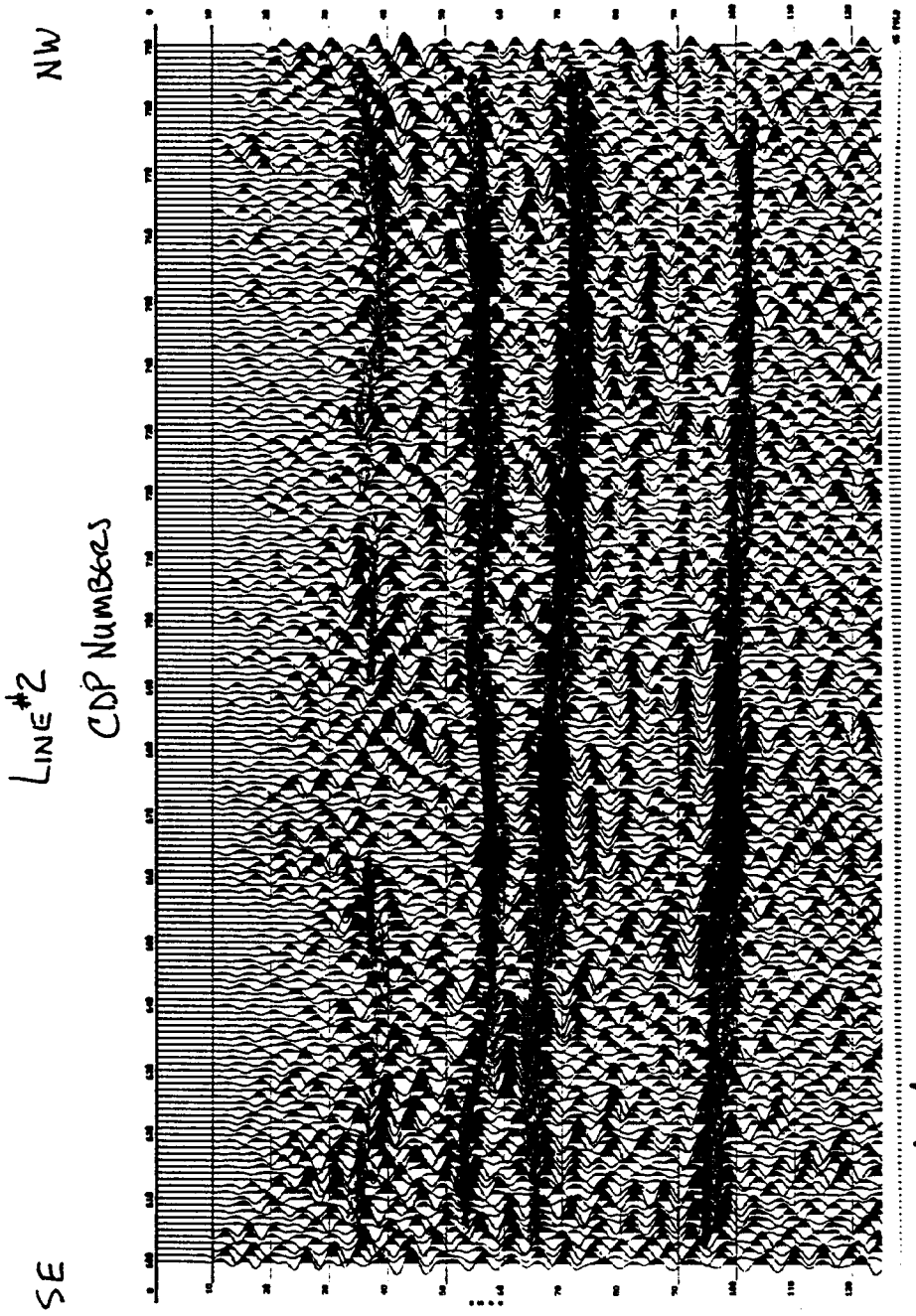

Figure 4b.

Figure 4. CDP stacked, 24-fold seismic reflection from line 2. Good coherency can be observed on the uninterpreted data (a) across most of the line. The bedrock surface as well as two reflection events within the consolidated sedimentary section and the proposed clay/gravel interface are interpreted on the stacked section (b). The stacked data possess good coherency on arrivals beneath the bedrock surface and hints of potential reflections from the base of the clay unit.

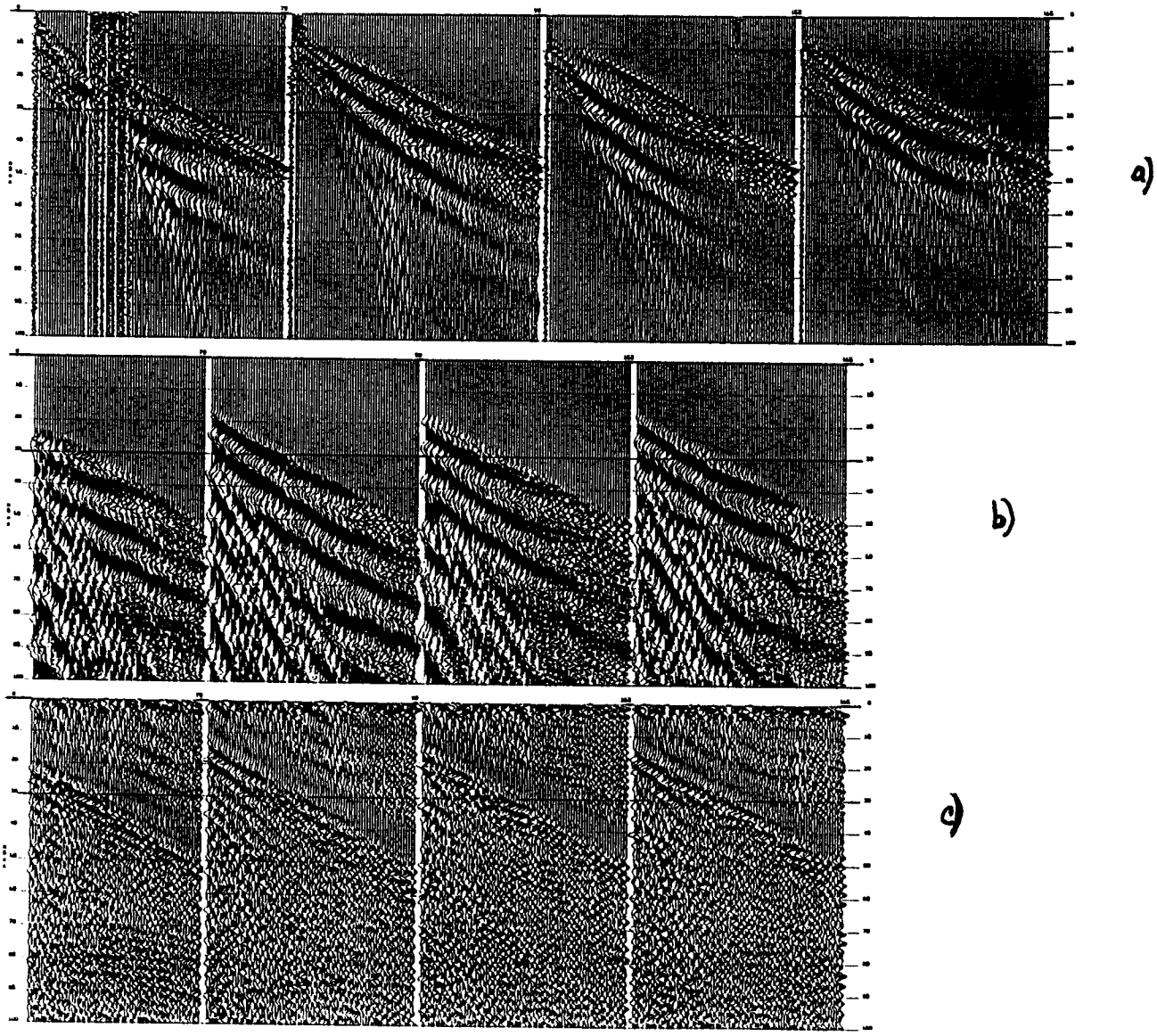

Figure 5. Shot gathers from various location on lines 3 and 4. (a) Unprocessed files, (b) first arrival muted files, and (c) filtered files.

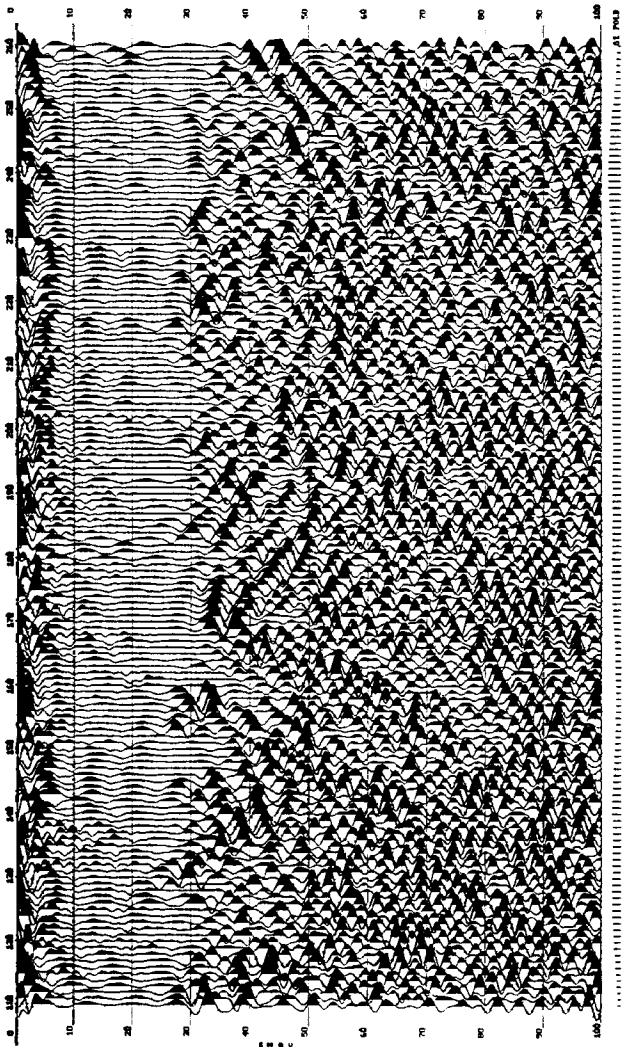

Figure 6. CDP stacked section from line 3. Some indication of reflection from 50 msec exist across the line. The effects of the large pumping well and road bank/trees are evident at CDP 170 and 260.

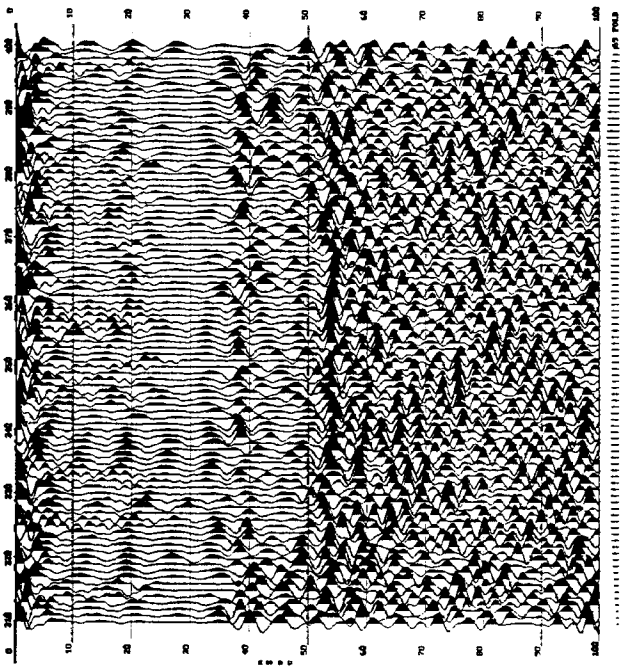

Figure 7. CDP stack of line 4. The effects of the road bank/trees evident on line 3 can be observed here at CDP 310. The signal-to-noise is much better on this line. The 50 msec bedrock reflection is easily interpretable with the base of the clay also visible across most of the line.

V. CONSTRUCTION PROJECTS AND EQUIPMENT PURCHASES

Laboratory Equipment

The laboratory apparatus for measuring hydraulic conductivity on sand and gravel cores has been upgraded for greater efficiency and the number of stations doubled to eight. We have a backlog of sand and gravel samples to be run in the laboratory. During this grant period it was decided that the number of sample stations should be doubled from four to eight. In the process of doing this several changes were made to allow greater efficiency. Several valves were added to make each sample station relatively independent of the others. That way each sample can be mounted or dismounted as needed. Ten new laboratory pressure transducers were acquired to replace some older ones that have or will fail and to expand the system by four stations.

Equipment to measure the hydraulic conductivity of low permeability samples, such as silt and claly, has been acquired. This equipment will allow us to measure the hydraulic conductivity of silt and clay samples that were acquired this year from the upper portions of the four cored wells. The flexible wall permeability cell will handle sample sizes up to 4 inches. It is currently set up for 2.5 inch samples. The system also includes a triaxial permeability panel for accurate measurement of volume changes and flow rates with regulators and burettes. In addition, the system has digital transducer readout with an RS-232 serial port for computer interface. We have gotten it set up and the appropriate supply lines such as air and water run, but have not yet begun measurements on the collected samples.

An electronic function or signal generator and combination frequency counter has been obtained to calibrate our flow meter. The flow meter is capable of being used in several different pipe sizes. However, it has to be calibrated for each one. For any of the hydraulic tests where accurate flow rate measurement is essential, the flow meter is an important piece of equipment. This purchase will allow us to quickly and accurately calibrate the flow meter. Previously, we had borrowed calibration equipment from another group at KGS.

Near the end of the 92-93 grant year, a portable water quality monitoring system for use in the field (surface and .05 m and greater ID boreholes) and laboratory was purchased from SOLOMAT Neotronics with funds from this grant. This system consists of a data logger and five sensors for measuring various water quality parameters. The sensors that were purchased were a combination bromide ion selective electrode, a temperature-compensated galvanic dissolved oxygen probe, a pH/temperature combination epoxy electrode, and two 1.0 K dip conductivity probes. Note that each

sensor and attached cable can be placed down a well and completely submerged to water depths of up to 15 meters. This system will be extensively utilized in the field and laboratory during the third year of this project.

Field Equipment

New larger diameter auger flights were purchased. Our previously owned auger equipment would only allow the installation of 2 inch wells. This is a great restriction in terms of the usefullness of the well. The smaller wells are generally fine for observation only situations. However, if the well needs to be pumped the small diameter puts severe restrictions on the capacity. We have purchased 75 feet of 6 1/2 inch ID and 10 inch OD auger flights. This will allow augering to bedrock at the GEMS site. Wells drilled with these new auger flights will accept 4 inch well casings. Larger pumps and more instrumention can be put down these wells.

New survey equipment, including a transit, tripod, measuring tape, and tape and strecher has been acquired. Older KGS survey equipment, which we had been using, failed this year and needed to be replaced. The new equipment allows two axis angles to be measured in addition to elevations. With this equipment we were able to produce a map to scale of the GEMS site showing the locations of wells. This map can be found in section IV.B.

Two field pressure transducers failed this year and had to be replaced. Repair would have been near the replacement price, so new improved versions were obtained at a good price by trading in the old ones. The new transducers have desiccant chambers to remove moisture which may enter through the surface vent tube.

A portable digital borehole logging system for small-diameter boreholes (.05 m ID or larger) was purchased from Century Geophysics by the Kansas Geological Survey during grant year 92-93. Money from this grant was used as part of the payment for the logging system. The system consists of a surface unit, which is essentially a weatherized 386 IBM-compatible laptop computer; an electrical winch, steel cable, and tripod; and two downhole probes. The two probes are a focussed induction probe (four coil focussed conductivity) for electrical conductivity measurements and a probe for measuring the temperature and conductivity of the borehole fluid. Note that both probes also have a natural gamma detector (employing a Na(Tl) scintillation crystal) for measuring the natural radiation in the subsurface and each probe performs all digitizing downhole prior to signal transmission to surface unit. Also note that the induction probe is designed so that measurements are essentially unaffected by fluid or plastic casing in the well. Use of this unit at GEMS is discussed in Section IV.D of this report.

Computer Laboratory

A computationally intensive project like this one needs the benefit of state-of-the-art computers. A computer laboratory has been set up to give access to the computers for both research and teaching. The laboratory currently contains five computers: one 486 machine, three 386 machines, and one 286 machine. A network for printer sharing has been set up so that every computer has access to a high quality laser printer. Two laser printers are available in the computer laboratory. In addition, a 486 machine is available in each office of the PI and CoPI. Each computer is connected to our mainframe computer (Data General machine) either by direct cable or through an Ethernet card. In this way each computer can act as a terminal into the mainframe and information can be shared between the two systems. Several Ethernet cards have been purchased, which allows the computers to be attached to the University Ethernet Backbone network. This connection allows direct access to internet and many other computing networks across the US. Miscellaneous software has been obtained to allow the computers to function efficiently for our specific tasks.

Additions to the computer equipment this year include an Apple IIci and a Hewlett Packard Scanjet IIC. The Apple IIci allows better interaction with other groups at the Kansas Geological Survey, since much of the word processing here is done in the Apple environment. The new Apple computer has a super drive which will read MS-DOS disks and that allows greater conversion of material between the PC and Apple environments. An additional item purchased during the 92-93 grant year was a Hewlett Packard Scanjet IIC flat-bed scanner for use with IBM-compatible PCs. This scanner is able to operate using a single pass in black-and-white scanning mode, gray-scale scanning mode, and color scanning mode with optical resolution of 400 dpi (a resolution of 1600 dpi can be achieved through pixel averaging and pixel replication). In addition, miscellaneous software has been purchased to allow the computers to function efficiently or perform specialized tasks.

The computer laboratory is used by our research group and other geohydrology graduate students. The computer laboratory allows hands on computer training to geohydrology graduate students through formal class work. We have taught two classes: Geology 752, Field Hydrogeology, fall semester 1992 (7 students), and Physics 727/Geology 771, Finite Difference Methods, fall semester 1992 (3 students). In addition, we have made the laboratory available for other computer oriented classes taught by other hydrogeology faculty members. We expect this computer laboratory to continue to be a valuable asset to our research and graduate education in geohydrology.

VI. PERSONNEL AND PRODUCTIVITY ISSUES

A. PUBLISHED AND PLANNED PAPERS

Published Papers

The following paper was published in this grant period, however, it was not directly supported by this grant due to the long lead time for publication. However, the material covered is very closely related to the present work.

Butler, J.J., Jr., and Liu, W.Z., 1993, Pumping tests in nonuniform aquifers: The radially asymmetric case: *Water Resour. Res.*, v. 29, no. 2, pp. 259-269.

The following two abstracts dealing with our DoD sponsored work were published this grant year. The material also exists as KGS open file reports.

McElwee, C.D., Butler, J.J., and Bohling, G.C., 1992, Nonlinear analysis of slug tests in highly permeable aquifers using a Hvorslev-type approach: *Eos, Trans. Amer. Geophys. Union*, v. 73, no. 43, p. 164. also KGS Open-File Report no. 92-39, 22 pp.

Bohling, G.C., 1993, Hydraulic tomography in two-dimensional, steady-state groundwater flow: *Eos, Trans. Amer. Geophys. Union*, v. 74, no. 16, p. 141. also KGS Open-File Report no. 93-17, 24 pp.

Papers Submitted for Publication

The following papers have been or very soon will be submitted for publication in professional journals.

McElwee, C.D., Bohling, G.C., and Butler, J.J., Jr., Sensitivity analysis of slug tests: *Journal of Hydrology*.

Hyder, Z., Butler, J.J., Jr., McElwee, C.D., and Liu, W.Z., Slug tests in partially penetrating wells, *Water Resources Research*.

Butler, J.J., Jr., G.C. Bohling, Z. Hyder, and C.D. McElwee, The use of slug tests to describe vertical variations in hydraulic conductivity:*Journal of Hydrology*.

McElwee, C.D., Butler, J.J., Jr., Bohling, G.C., and Liu, W.Z., The use of observation wells with slug tests: *Journal of Hydrology*.

The following is scheduled for publication as a KGS refereed publication.

Bohling, G.C., McElwee, C.D., Butler, J.J., Jr., and W.Z. Liu, User's guide to well test design and analysis with SUPRPUMP version 1.1, KGS Technical Series No. 2, in press, 1993.

Papers Planned or in Preparation

The following papers are planned for future publication in professional journals. Currently they exist as informal Kansas Geological Survey Open File Reports.

Liu and Butler, A time-continuous numerical model for well tests in heterogeneous aquifers, *Journal of Hydrology*.

McElwee, C.D. and Butler, J.J., 1992, Effective Transmissivities from slug tests in wells with a skin: KGS Open-File Report no. 92-12, 31 pp.

McElwee, C.D., Butler, J.J., and Bohling, G.C., 1992, Nonlinear analysis of slug tests in highly permeable aquifers using a Hvorslev-type approach:KGS Open-File Report no. 92-39, 22 pp.

Bohling, G.C., Hydraulic tomography in two-dimensional, steady-state groundwater flow: KGS Open-File Report no. 93-17, 24 pp.

B. LIST OF PARTICIPATING PERSONNEL

McElwee, C.D.- PI, is a Senior Scientist at the Kansas Geological Survey (KGS) in the Mathematical Geology Section and is also an Adjunct Professor in the Geology and Physics Departments of the University of Kansas (KU).

Butler, J.J. Jr. - Co-PI, is an Associate Scientist at the KGS in the Geohydrology Section and is also an Adjunct Assistant Professor in the KU Geology Department.

Bohling, G.C. - Investigator, is a Research Assistant in the Mathematical Geology Section at KGS.

Macpherson, G.L. - Investigator, is an Assistant Professor in the KU Geology Department.

Miller, R.D. - Investigator, is an Assistant Scientist at the KGS and is the Chief of the Exploration Services Section of the KGS.

The following two students have been fully supported by this grant.

Mennicke, C.M. - is a student Research Assistant in the Mathematical Geology Section at KGS and is working on a Ph.D. degree in the KU Geology Department.

Huettl, T. - is a student Research Assistant in the Mathematical Geology Section at KGS and is working on a Master's degree in the KU Geology Department.

The following students have contributed to this work in substantial ways, however they have not been primarily supported by this grant.

Liu, W. - is a student Research Assistant in the Geohydrology Section at KGS and is working on a Ph.D. degree in the KU Civil Engineering Department.

Hyder, Z. - is a student Research Assistant in the Mathematical Geology Section at KGS and is working on a Ph.D. degree in the KU Civil Engineering Department.

Zenner, M. - is a student Research Assistant in the Geohydrology Section at KGS and is working on a Ph.D. degree in theKU Geology Department.

Orcutt, M. - is a student Research Assistant in the Geohydrology Section at KGS and is working on a Master's degree in the Architectural Engineering Department at KU.

C. INTERACTIONS WITH OTHER RESEARCH GROUPS

Professional Meetings Attended and Papers Presented

Carl McElwee attended the Fall AGU (American Geophysical Union) meeting in San Francisco in December 92 and gave a paper on the nonlinear analysis of slug test data.

McElwee, C.D., Butler, J.J., and Bohling, G.C., 1992, Nonlinear analysis of slug tests in highly permeable aquifers using a Hvorslev-type approach: *Eos, Trans. Amer. Geophys. Union*, v. 73, no. 43, p. 164. also KGS Open-File Report no. 92-39, 22 pp.

Geoff Bohling attended the Spring AGU meeting in Baltimore in May 93 and gave a paper on hydraulic tomography.

Bohling, G.C., 1993, Hydraulic tomography in two-dimensional, steady-state groundwater flow: *Eos, Trans. Amer. Geophys. Union*, v. 74, no. 16, p. 141. also KGS Open-File Report no. 93-17, 24 pp.

James Butler attended the NGWA (National Ground Water Association) sponsored Outdoor Action Conference in Las Vegas in May 93.

Sabbatical at the University of Birmingham, England

Carl McElwee worked at the University of Birmingham with Dr. K. R. Rushton and his Groundwater Research Group for four months, while keeping in close contact with the group and research here at the Kansas Geological Survery by e-mail. Dr. Rushton's book *Seepage and Groundwater Flow* published by John Wiley and Sons, Inc. in 1979 is a well respected treatment of groundwater modeling. He is known for his wide ranging applications of models to real world problems. Currently, there are eleven professionals in the Groundwater Research Group at the University of Birmingham. Dr. Rushton and this group continue to have an active research program that incorporates projects throughout the United Kingdom and the world. Dr. Rushton has done much work involving hydraulic testing for aquifer parameters and did some of the early work in looking at heterogeneities through hydraulic testing. It was a valuable experience allowing interaction with a number of groundwater professionals and graduate students having a variety of experience and interests on the issue of heterogeneity.

University of Nebraska Research Group

Dr. Vitaly Zlotnik is the leader of a research group working on well testing at the University of Nebraska at Lincoln. Jim Butler had numerous discussions throughout the year with Dr. Zlotnik and his graduate students on various issues related to slug tests in alluvial aquifers.

VII. SUMMARY OF YEAR TWO RESEARCH AND OUTLOOK FOR YEAR THREE

A. SUMMARY OF RESEARCH IN YEAR TWO

The major focus of the second year of this project was on the use of well tests to describe spatial variations in hydraulic conductivity. This research on well tests in heterogeneous formations had both theoretical and field components. Note that a major emphasis of our work again this year was on slug tests. As described in Section I, the analysis of response data from slug tests at GEMS has turned out to be considerably more challenging than expected. Thus, the majority of our research in year two was again concerned with slug tests.

The theoretical work was directed at developing a better understanding of the type of information that can be obtained from well tests in heterogeneous media. In order to assess the error that is introduced into parameter estimates by employing conventional methods for the analysis of data from slug tests performed in configurations not strictly addressed in the derivation of those methods, a semianalytical solution to a general mathematical model describing the flow of groundwater in response to a slug test was developed. This model incorporates the effects of partial penetration, anisotropy, finite-radius well skins, and upper and lower boundaries of either a constant-head or an impermeable form. This model was then employed to develop recommendations for approaches to the analysis of slug-test data than can be utilized by field practitioners. In the first year of this research, a study of slug tests in layered media was initiated. This study was concluded in the second year of this work. The results of this study help delineate the conditions under which multilevel slug tests can be used to provide accurate information concerning the vertical variations in hydraulic conductivity along the well bore. Two theoretical investigations of pulse-test methods were carried out during this year. The first involved the application of the principles of tomography, which has proven to be a valuable technique for imaging heterogeneous material using various forms of wave energy, to the characterization of spatial variations in flow properties. Pressure pulses in a groundwater system are diffusive in nature and are generally exponentially attenuated with distance, so the range of investigation will be smaller than for systems in which the pressure pulse travels as a propagating wave. Initial results of our work appear promising for some simple models. The basic configuration of the hydraulic conductivity distribution can be successfully estimated for linear models with no noise. However, this work needs to be extended to radial symmetry and evaluated in the presence of realistic

noise. The second theoretical investigation of pulse tests employed a sinusoidally varying signal to investigate a simple two-zone aquifer separated by a linear boundary. Five parameters are required to completely describe this system. Due to correlations between parameters, it is difficult to determine all five parameters simultaneously. However, one to three parameters can usually be determined when given appropriate response data at selected observation locations. Extending this work to several zones and radial symmetry appears to be difficult to do analytically. A numerical modeling approach will undoubtedly be needed to investigate the issue further. Although at this point the capabilities of hydraulic tomography and pulse testing are unknown, they clearly deserve further investigation. The final portion of the theoretical work of the second year of this project focussed on slug tests in the presence of well skins. We have developed an empirical formula for the effective transmissivity obtained from a slug test in the presence of a skin that appears to be quite general. In particular, the formula seems to provide very good estimates of the parameters obtained from analyses employing the Hvorslev (1951) or Cooper et al. (1967) models. The effective radius does not appear to be a strong function of the aquifer parameters. Thus, it may be possible to use the effective transmissivity estimate obtained from an analysis of response data from slug tests in the presence of well skins to estimate transmissivity of the formation. We are particularly optimistic in those situations where the radius of the skin may be estimated from independent data such as the diameter of the hole created by a particular drilling method. Clearly, however, analysis of slug tests in the presence of a skin is a very difficult problem and will require additional research in order to gain further insight.

The field components of this study of well tests in heterogeneous formations concentrated on slug tests in the second year of this research. A program of multiwell slug tests (slug tests with observation wells) was initiated at GEMS. The results of this program of field testing and a complementary theoretical analysis demonstrated that the assumption of a fully screened well can introduce a very large amount of error into parameter estimates determined from response data at observation wells. A new analytical model, which allows partial penetration at both the stressed and observation wells, was developed. Application of this model to data from GEMS yielded parameters that were in keeping with the values obtained from the laboratory analysis of cores. As was clearly shown in the report of the first year of this project, slug tests at most of the wells in the alluvial aquifer at GEMS appear to exhibit non-linear behavior. Response data from these tests show a downward curvature when plotted in a log-head linear-time format (Hvorslev format). The duration of the test is also dependent on the value of the initial head. Models based on frictional losses, non-Darcian flow, or inertial effects all

seem to explain the gross features of the observed field behavior. Careful application of these models to the field data produces reasonable consistency in hydraulic conductivity values for various initial heads. Further refinement of these non-linear models is needed, however, because systematic trends in the fitted parameters with initial head are still observed. In addition, late-time oscillatory behavior is seen at certain wells.

As in the first year of this research, a significant amount of the work in year two was directed at increasing our knowledge of the subsurface at GEMS. This work included a detailed study of the aqueous geochemistry of the alluvium and underlying bedrock at GEMS; continued drilling and sampling activities; continued laboratory analysis of the cores obtained with the bladder sampler; the beginning of a detailed wireline log survey; and a second seismic survey. These characterization efforts, which will continue throughout this project, are directed towards the development of a detailed picture of the subsurface at GEMS, so that we can better assess the results of the hydraulic and tracer tests that are being performed as part of this research.

A considerable amount of acquisition, construction, and modification of equipment took place during the second year of this project in support of the research effort. The purchased equipment included new pressure transducers for field and laboratory use, a permeameter for the measurement of the hydraulic conductivity of low permeability samples, a portable water quality monitoring system for use in the field and laboratory, new large diameter auger flights for drilling larger diameter monitoring wells, new surveying equipment, a portable digital borehole logging system for small-diameter boreholes, and additional computer equipment. A considerable amount of equipment for field and laboratory use was also constructed at the Kansas Geological Survey during the second year of this project.

B. OUTLOOK FOR RESEARCH IN YEAR THREE

The third year of this project will build upon the progress made in the first two years. One task of year three will be to bring to a close our study of slug tests in heterogeneous media. Although there is actually quite a bit more work that could be done with slug tests, we will bring this research to a reasonable conclusion early in the third year. The work on pulse tests, which was delayed in year two as a result of our increased emphasis on slug tests, will be expanded in the third year of this project. However, given the limited time that is available, we will not make this the major focus of our efforts in year three. Clearly, our work on slug and pulse tests, which has significant practical utility, could be expanded in an extension of this grant. The primary emphasis of the work of year three will be on the performance of tracer tests at GEMS

using low concentrations of conservative tracers such as chloride or bromide. The results of these tracer tests should provide us with a means to evaluate how well we have characterized the subsurface at GEMS. Using the information that we have obtained from our characterization efforts, we will be able to evaluate the utility of such information for the prediction of the tracer movement at GEMS. Although there will undoubtedly be some unexpected complexities, the results of the tracer tests should give us some information about the type of information needed for the prediction of contaminant movement in alluvial aquifers and the nature of flow property variations at different scales in alluvial systems. The ultimate goal of all this work is to improve our present capabilities for the prediction of contaminant movement in shallow alluvial aquifers.

As with year two of this project, a significant component of the work in year three will be continued efforts directed at characterization of the subsurface at GEMS. The detailed information collected in this characterization effort will be of vital importance in understanding the tracer tests to be performed at GEMS.

VIII. REFERENCES

Amoozegar, A., and Warrick, A. W., 1986, Hydraulic conductivity of saturated soils: Field methods: *in Methods of Soil Analysis, Part 1, Physical and Mineralogical Methods*, Agronomy Monograph Series 9, edited by A. Klute, pp. 735-770, American Soc. of Agronomy, Madison, Wi.

Barbier, M.G., Bondon, P., Mellinger, R., and Vialix, J.R., 1976, MiniSOSIE for shallow land seismology: *Geophys. Prosp.*, v. 24, pp. 518-527.

Barker, J.A. and Herbert, R., 1992, A simple theory for estimating well losses: With application to test wells in Bangladesh: *Applied Hydrology*, pp. 20-31.

Bear, J., 1972, *Dynamics of Fluids in Porous Media*: American Elsevier Publishing Co., Inc., New York, pp. 182-184.

Birkelo, B.A., Steeples, D.W., Miller, R.D., and Sophocleous, M.A., 1987, Seismic reflection study of shallow aquifer during a pumping test: *Ground Water*, v. 25, pp. 703-709, Nov.-Dec.

Bliss, J.C., and Rushton, K.R., 1984, The reliability of packer tests for estimating the hydraulic conductivity of aquifers: *Quart. Jour. of Eng. Geol.*, v. 17, pp. 81-91.

Bohling, G.C. and McElwee, C.D., 1992, SUPRPUMP: An interactive program for well test analysis and design: *Ground Water* , v. 30, no. 2, pp. 262-268.

Bouwer, H., 1989, The Bouwer and Rice slug test - an update: *Ground Water*, v. 27, no. 3, pp. 304-309.

Bouwer, H., and Rice, R.C., 1976, A slug test for determining hydraulic conductivity of unconfined aquifers with completely or partially penetrating wells: *Water Resour. Res.*, v. 12, no. 3, pp. 423-428.

Braester, C., and Thunvik, R., 1984, Determination of formation permeability by double-packer tests: *J. of Hydrology*, v. 72, pp. 375-389.

Brigham, E. O., 1974, *The Fast Fourier Transform* : Prentice-Hall, Inc, Englewood Cliffs, New Jersey, 252 pp.

Butler, J.J., and McElwee, C.D., 1990, Variable-rate pumping tests for nonuniform aquifers: *Water Resources Research,* v. 26, no. 2, pp. 291-306.

Butler, J.J., Jr., 1986, Pumping Tests in Nonuniform Aquifers: A deterministic and stochastic analysis (Ph.D. dissertation): Stanford Univ., Stanford, CA. 220 pp.

Butler, J.J., Jr., and Liu, W.Z., 1993, Pumping tests in nonuniform aquifers: The radially asymmetric case: *Water Resour. Res.*, v. 29, no. 2, pp. 259-269.

Butler, J.J., Jr., and McElwee, C.D., 1990, Hydrogeologic characterization of hazardous waste sites: Kansas Water Resources Research Inst. Contribution No. 283, 114 pp.

Butler, J.J., Jr., and McElwee, C.D., 1992, Well-testing methodologies for characterizing heterogeneities in alluvial-aquifer systems: First year report: Kansas Geol. Survey Open-File Rept. 92-53: 152 pp.

Butler, J.J., Jr., Bohling, G.C., Hyder, Z., and McElwee, C.D., The use of slug tests to describe vertical variations in hydraulic conductivity: *Jour. of Hydrology*, in review.

Butler, J.J., Jr., McElwee, C.D., and Hyder, Z., 1993, Slug tests in unconfined aquifers: Kansas Water Resources Research Inst. Contribution No. 303.

Butler, J.J., Jr., McElwee, C.D., Bohling, G.C., and Healey, J.M., 1990, Hydrogeologic characterization of hazardous waste sites: Kansas Water Resources Research Inst. Contribution No. 283: 114 pp.

Chirlin, G.R., 1989, A critique of the Hvorslev method for slug test analysis: the fully penetrating well: *Ground Water Monitoring Review,* v. 9, no. 2, pp. 130-138.

Chirlin, G.R., 1990, The slug test: the first four decades, *Ground Water Management* : v. 1, pp. 365-381.

Churchill, R.V., 1972, *Operational Mathematics*: McGraw Hill, New York, 481 pp.

Cooley, J. W., and Tukey, J. W., 1965, An algorithm for machine calculations of complex Fourier series: *Math. Computation*, v. 19, pp. 297-301.

Cooper, H.H., Bredehoeft, J. D., and Papadopulos, I.S., 1967, Response of a finite-diameter well to an instantaneous charge of water: *Water Resour. Res.*, v. 3, no. 1, pp. 263-269.

Dagan, G., 1978, A note on packer, slug, and recovery tests in unconfined aquifers: *Water Resour. Res.* , v. 14, no. 5, pp. 929-934.

Dagan, G., 1986, Statistical theory of groundwater flow and transport: pore to laboratory, laboratory to formation, and formation to regional scale: *Water Resour. Res.*, v. 22, no. 9, pp. 120S-134S.

Desbarats, A. J., 1993, Geostatistical analysis of interwell transmissivity in heterogeneous aquifers: *Water Resour. Res,* v. 29, no. 4, pp. 1239-1246.

Desbarats, A.J., 1992, Spatial averaging of transmissivity in heterogeneous fields with flow toward a well: *Water Resour. Res.* v. 28, no. 3, pp. 757-767.

Dobrin, M.B. and Savit, C.H., 1988, *Introduction to Geophysical Prospecting*: McGraw-Hill, New York, N.Y., 867 pp.

Dougherty, D.E., and Babu, D.K., 1984, Flow to a partially penetrating well in a double-porosity reservoir: *Water Resour. Res.*, v. 20, no. 8, pp. 1116-1122.

Ehlig-Economides, C.A., and Joseph, J.A., 1987, A new test for determination of individual layer properties in a multilayered reservoir: *SPE Formation Eval.*, v. 2, no. 3, pp. 261-283.

Ellis, V.D., 1987, *Well Logging for Earth Scientists* : Elsevier Science Publishing Co., Inc., New York, N.Y., 531 pp.

Environmental Protection Agency, 1984, Test Method--The determination of inorganic anions in water by ion chromatography--Method 300.0: U.S. Environmental Protection Agency, EPA-600/4-84-017, 5 pp.

Faust, C.R., and Mercer, J.W., 1984, Evaluation of slug tests in wells containing a finite-thickness skin: *Water Resour. Res.*, v. 20, no. 4, pp. 504-506.

Fishman, M.J. and Friedman, L. C., eds., 1989, Methods for determination of inorganic substances in water and fluvial sediments: U. S. Geological Survey, *Techniques of Water-Resources Investigations*, Book 5, Chapter A1, 545 pp.

Freeze, R.A., and Cherry, J.A., 1979, *Groundwater*, Prentice-Hall, Inc., Englewood Cliffs, N.J., 604 pp.

Freyberg, D.L., 1986, A natural gradient experiment on solute transport in a sand aquifer, 2, Spatial moments and the advection and dispersion of nonreactive tracers: *Water Resour. Res.*, v. 22, no. 13, pp. 2031-2046.

Frind, E. O, and Matanga, G. B., 1985, The dual formulation of flow for contaminant transport modeling, 1, Review of theory and accuracy aspects: *Water Resour. Res.*, v. 21, no. 2, pp. 159-169.

Geer, F.C. van, 1982, An equation based theoretical approach to network design for groundwater levels using Kalman filters: IAHS Publ., no. 136, pp. 241-250, pp. 25-36.

Geer, F.C. van, 1984, Kalman filter calibration of error covariance matrix of a groundwater model: In *Symposium proceedings on Stochastic Hydraulics,* IAHA, Urbana, Illinois, U.S.A., pp. 26-36.

Gelb, A., 1974, *Applied optimal estimation*, The M.I.T. Press.

Gelhar, L.W., 1986, Stochastic subsurface hydrology from theory to applications: *Water Resour. Res.*, v. 22, no. 9, pp. 135S-145S.

Grantham, R.L., 1990, Feasibility of using seismic reflection to detect gas trapped in alluvial materials: Masters thesis, University of Kansas Department of Geology.

Guppy, K.H., Cinco-Ley, H., Ramey, H.J., Jr., and Samaniego-V., F., 1982, Non-Darcy flow in wells with finite-conductivity vertical fractures: *Soc. of Pet. Eng. Jour.*, Oct., pp. 681-698.

Haberman, R., 1987, *Elementary Applied Partial Differential Equations*, Prentice-Hall, Inc., Englewood Cliffs, N.J., 547 pp.

Hackett, G., 1987, Drilling and constructing monitoring wells with hollow-stem augers Part 1: Drilling considerations: *Ground Water Monitoring Review,* v. VII, no. 4, pp. 51-62.

Harvey, C.F., 1992, Interpreting Parameter Estimates Obtained From Slug Tests in Heterogeneous Aquifers: M.S. thesis, Stanford Univ., Stanford, Ca., 99 pp.

Hayashi, K., Ito, T., and Abe, H., 1987, A new method for the determination of in situ hydraulic properties by pressure pulse tests and application to the Higashi Hachimantai geothermal field: *J. Geophys. Res.*, v. 92, no. B9, pp. 9168-9174.

Healey, J., Anderson, J., Miller, R.D., Keiswetter, D., Steeples, D.W., and Bennett, B., 1991, Improved shallow seismic-reflection source: building a better Buffalo : *Soc. Explor. Geophys. Exp. Abs.*, v. 1, p. 588-591.

Hess, K.M., Wolf, S.H., and Celia, M.A., 1992, Large-scale natural gradient tracer test in sand and gravel, Cape Cod, Massachusetts, 3: Hydraulic conductivity variability and calculated macrodispersivities: *Water Resour. Res.*, v. 28, no. 8, pp. 2011-2027.

Hinsby, K., Bjerg, P.L., Andersen, L.J., Skov, B., and Clausen, E.V., 1992, A mini slug test method for determination of a local hydraulic conductivity of an unconfined sandy aquifer: *J. of Hydrology,* v. 136, pp. 87-106.

Hufschmied, P., 1986, Estimation of three-dimensional anisotropic hydraulic conductivity field by means of single well pumping tests combined with flowmeter measurements: *Hydrogeologie*, pp. 163-174.

Hunter, J.A., Pullan, S.E., Burns, R.A., Gagne, R.M., and Good, R.L., 1984, Shallow seismic-reflection mapping of the overburden-bedrock interface with the engineering seismograph–Some simple techniques: *Geophysics*, v. 49, p. 1381-1385.

Hvorslev, M.J., 1951, Time lag and soil permeability in ground-water observations: Bull. no. 36, Waterways Exp. Sta., Corps of Engrs., U.S. Army. 50 pp.

Hyder, Z., and Butler, J.J. Jr., Slug tests in unconfined aquifers: *Ground Water*, in review.

Hyder, Z., Liu, W.Z., and Butler, J.J. Jr., 1993, Software for the evaluation of semianalytical solutions for slug tests in partially penetrating wells: *KGS Comput. Program Ser.*, no. 93-1, Kansas Geol. Survey.

Ingersoll, L.R., Zobel, O.J., and Ingersoll, A.C., 1948, Heat conduction with engineering and geological conditions, McGraw-Hill.

Jiang, X., 1991, A field and laboratory study of scale dependence of hydraulic conductivity: M.S. thesis, Univ. of Kansas, Lawrence, Ks., 149 pp.

Johnson, C.R., Greenkorn, R.A., and Woods, E.G., 1966, Pulse-testing: A new method for describing reservoir flow properties between wells: *J. of Pet. Tech.*, pp. 1599-1604.

Kalman, R.E. and Bucy, R.S., 1961, New Results in Linear Filtering and Prediction Theory: *Journal of Basic Engineering*, pp. 95-108.

Kalman, R.E., 1960, A New Approach to Linear Filtering and Prediction Problems: *Journal of Basic Engineering,* pp. 35-45.

Karasaki, K., 1986, Well Test Analysis in Fractured Media: Ph.D. dissertation, Univ. of Ca., Berkeley, 239 pp.

Karasaki, K., 1990, A systematized drillstem test: *Water Resour. Res.*, v. 26, no. 12, pp. 2913-2919.

Keely, J.F., and Boateng K., 1987, Monitoring well installation, purging and sampling techniques, Part 1: Conceptualizations: *Ground Water,* v. 25, no. 3, pp. 300-313.

Kruseman, G.P., and de Ridder, N.A., 1989, Analysis and Evaluation of Pumping Test Data : ILRI publication no.47, The Netherlands, 377 pp.

Lim, H.C. and Lee, K.S., 1992, Process Control and Optimization: in *Ponds, M.-N., Bioprocess Monitoring and Control,* Hanser Publisher.

McElwee, C.D., and Butler, J.J. Jr., 1992, Effective transmissivities from slug tests in wells with a skin: Kansas Geological Survey Open-File Rept. 92-12, 31 pp.

McElwee, C.D., Butler, J.J., Jr., and Healey, J.M., 1991, A new sampling system for obtaining relatively undisturbed samples of unconsolidated coarse sand and gravel: *Ground Water Monitoring Review,* v. 11, no. 3, pp. 182-191.

McElwee, C.D., Butler, J.J., Jr., Liu, W.Z., and Bohling, G.C., 1990, Effects of partial penetration, anisotropy, boundaries and well skin on slug tests: *Eos, Trans. Amer. Geophys. Union*, v. 71, no. 17, p. 505.

McLane, G.A., Harrity, D.A., and Thomsen, K.O., 1990, A pneumatic method for conducting rising and falling head tests in highly permeable aquifers: *Proc. of 1990 NWWA Outdoor Action Conf.*

Melville, J.G., Molz, F.J., Guven, O., and Widdowson, M.A., 1991, Multilevel slug tests with comparisons to tracer data: *Ground Water,* v. 29, no. 6, pp. 897-907.

Merey, C, Miller, R.D., Ticken, E.J., and Lewis, J.S., in press, Hydrogeological characterization using a shallow seismic reflection survey at Fort Ord, California: *Soc. Expl. Geophys. Exp. Abs.*

Miller, R.D., Steeples, D.W., and Brannan, M., 1989, Mapping a bedrock surface under dry alluvium with shallow seismic reflections: *Geophysics*, v. 54, pp. 1528-1534.

Miller, R.D., 1992, Normal moveout stretch mute on shallow-reflection data: *Geophysics*, v. 57, pp. 1502-1507.

Miller, R.D., and Steeples, D.W., 1986, Shallow structure from a seismic reflection profile across the Borah Peak, Idaho, fault scarp: *Geophysical Research Letters,* v. 13, p. 953-956.

Miller, R.D., Steeples, D.W., Hill, R., and Gaddis, B., 1990, Identifying intra-alluvial and bedrock structures shallower than 30 meters using seismic-reflection techniques: Soc. Explor. Geophys. volumes on Geotechnical and Environmental Geophysics, Stan Ward, ed., *Volume 3: Geotechnical,* pp. 89-97.

Minning, R.C. , 1982, Monitoring well design and installation: Proceedings of the Second National Symposium on Aquifer Restoration and Ground Water Monitoring, Columbus, Ohio, pp. 194-197.

Moench, A., and Ogata, A., 1984, Analysis of constant discharge wells by numerical inversion of Laplace transform solutions, in: Rosenshein, J., and Bennett, G.D., ed., *Groundwater Hydraulics,* AGU Water Resour. Monogr. 9, AGU, Washington, DC., pp. 146-170.

Moench, A.F., and Hsieh, P.A., 1985, Analysis of slug test data in a well with finite-thickness skin: in *Memoirs of the 17th Intern. Cong. on the Hydrogeology of Rocks of Low Permeability,* v. 17, pp. 17-29.

Mohamed, F.A., Guenther, R.B., Hudspeth, R.T., and McDougal, W.G., 1992, A damped wave equation for groundwater flow: *Advances in Water Resources,* v. 15, pp. 117-123.

Moltyaner, G.L., and Killey, R.W.D., 1988, Twin Lake tracer tests: Longitudinal dispersion: *Water Resour. Res.*, v. 24 , no. 10, pp. 1613-1627.

Molz, F.J., Guven, O., and Melville, J.G., 1989, Characterization of the hydrogeologic properties of aquifers: The next step: in: Proc. of the Conf. on New Field Techniques for Quantifying the Physical and Chemical Properties of Heterogeneous Aquifers, National Water Well Association, pp. 407-418.

Molz, F.J., Morin, R.H., Hess, A.E., Melville, J.G., and Guven, O., 1989, The impeller meter for measuring aquifer permeability variations: Evaluation and comparison with other tests: *Water Resour. Res.*, v. 25, no. 7, pp. 1677-1686.

Morin, R.H., Hess, A.E., and Paillet, F.L., 1988, Determining the distribution of hydraulic conductivity in a fractured limestone aquifer by simultaneous injection and geophysical logging: *Ground Water,* v. 26, no. 5, pp. 587-595.

Myers P.B., Miller, R.D., and Steeples, D.W., 1987, Shallow seismic reflection profile of the Meers fault, Comanche County, Oklahoma: *Geophysical Research Letters*, v. 14, p. 749-752.

National Research Council, 1990, *Ground Water Models--Scientific and Regulatory Applications*: National Academy Press, 303 pp.

Neitzel, E.B., 1958, Seismic reflection records obtained by dropping a weight: *Geophysics*, v. 34, p. 58-80.

Nelson, R. W., 1960, In-place measurement of permeability in heterogeneous media, 1, Theory of a proposed method: *J. Geophys. Res.*, v. 65, no. 6, pp. 1753-1758.

Nelson, R. W., 1961, In-place measurement of permeability in heterogeneous media, 2, Experimental and computational considerations: *J. Geophys. Res.*, v. 66, no. 8, pp. 2469-2478.

Nelson, R. W., 1968, In-place determination of permeability distribution for heterogeneous porous media through analysis of energy dissipation: *Soc. Pet. Eng. J.*, v. 8, no. 1, pp. 33-42.

Neuman, S. P., 1973, Calibration of distributed parameter groundwater flow models viewed as a multiple-objective decision process under uncertainty: *Water Resour. Res.*, v. 9, no. 4, pp. 1006-1021.

Novakowski, K.S., 1989, Analysis of pulse interference tests: *Water Resources Research*, v. 25, no. 11, pp. 2377-2387.

Olea, R.A., 1988, Correlator--an interactive computer system for lithostratigraphic correlation of wireline logs: *Petrophysical Series*, no. 4, Kansas Geological Survey, Lawrence, KS, 85 pp.

Orient, J.P., Nazar, A., and Rice, R.C., 1987, Vacuum and pressure test methods for estimating hydraulic conductivity: *Ground Water Monitoring Review*, v. 7, no. 1, pp. 49-50.

Palmer and Johnson, 1989, Chapter 2, Physical processes controlling the transport of contaminants in the aqueous phase: *in Environmental Protection Agency, Transport and Fate of Contaminants in the Subsurface*, EPA/625/4-89/019, pp. 5-22.

Papadopulos, I.S., and Cooper, H.H., Jr., 1967, Drawdown in a well of large diameter: *Water Resour. Res.* , v. 3, no. 1, pp. 241-244.

Perry, C.A. and Hart, R.J., 1985, Installation of observation wells on hazardous waste sites in Kansas using a hollow-stem auger: *Ground Water Monitoring Review*, v. V, no. 4, pp. 70-73.

Peterson, J. E., Paulsson, B. N. P. , and McEvilly, T. V., 1985, Application of algebraic reconstruction techniques to crosshole seismic data: *Geophysics*, v. 50, no. 10, pp. 1566-1580.

Pollock, D. W., 1988, Semianalytical computation of path lines for finite-difference models: *Ground Water*, v. 26, no. 6, pp. 743-750.

Press, W.H., Teukolsky, S.A., Vetterling, W.T., and Flannery, B.P., *Numerical Recipes in FORTRAN*, Cambridge Univ. Press, Cambridge, UK, 963 pp.

Ramey, H.J., Jr., Agarwal, R.G., and Martin, I., Analysis of "slug test" or DST flow period data, *J. Canadian Pet. Tech.*, v. 14, no. 3, pp.37-47.

Rehfeldt, K.R., Hufschmied, P., Gelhar, L.W., and Schaefer, M.E., 1989, Measuring hydraulic conductivity with the borehole flowmeter: Rept. EN-6511, Electric Power Res. Inst., Palo Alto, Ca.

Rushton, K.R. and Redshaw, S.C., 1979, *Seepage and Groundwater Flow*: John Wiley & Sons.

Rushton, K.R., and Chan, Y.K., 1977, Numerical pumping test analysis in unconfined aquifers: *J. Irrigation and Drainage Div.*, v. 103(IR1), pp. 1-12.

Sacher, H., 1983, Beruecksichtigung von Unsicherheiten bei der Parameterschaetzung fuer mathematisch-numerische Grundwasser-modelle: Dissertation, RWTH Aachen.

Schwarz, H.R., 1986, Numerische Mathematik: Teubner Stuttgart.

Scott, D. M., 1992, Evaluation of flow net analysis for aquifer identification: *Ground Water,* v. 30, no. 5, pp. 755-764.

Sen, Z., 1984, Adaptive Pumping Test Analysis: *J. of Hydrology,* v. 74, pp. 259-270.

Settari, A., and Aziz, K., 1974, A conputer model for two-phase coning simulation: *Society of Petroleum Eng.*, v. 14, no. 3, pp. 221-236.

Singh, S.R. and Shakya, S.K., 1989, A nonlinear equation for groundwater entry into well screens: *Jour. of Hydrology*, v. 109, pp. 95-114.

Steeples, D.W., and Miller, R.D., 1990, Seismic-reflection methods applied to engineering, environmental, and ground-water problems: Soc. Explor. Geophys. volumes on Geotechnical and Environmental Geophysics, Stan Ward, ed., *Volume 1: Review and Tutorial*, pp. 1-30.

Steeples, D.W., Miller, R.D., and Knapp, R.W., 1987, Downhole .50-caliber rifle—an advance in high-resolution seismic sources: *Soc. Explor. Geophys., Exp. Abs.*, 57th Ann. Mtg., pp. 76-78.

Stehfest, H., 1970, Numerical inversion of Laplace transforms: *Commun. ACM.*, v. 13, no. 1, pp. 47-49.

Taylor, K., and Molz, F., 1990, Determination of hydraulic conductivity and porosity logs in wells with a disturbed annulus: *J. of Contaminant Hydrology*, v. 5, pp. 317-332.

Taylor, K., Hess, J., Mazzella, A., and Hayworth, J., 1990, Comparisons of three methods to determine the vertical stratification of pore fluids: *Ground Water Monitoring Review*, v. 10, no. 1, pp. 91-95.

Treadway, J.A., Steeples, D.W., and Miller, R.D., 1988, Shallow seismic study of a fault scarp near Borah Peak, Idaho: *Journal of Geophysical Research*, v. 93, no. B6, p. 6325-6337.

U.S. Dept. of Navy, 1961, Bureau of Yards and Docks, Design Manual, Soil Mechanics, Foundations, and Earth Structures, DM-7, Chap. 4.

van Dyke, N.V.R., Rhodes, J.R., Richardson, D.W., and McTigue,W.H., 1993,Evaluating confined aquifer properties using thepneumatic displacement method and the repeated pressure pulse technique: in *Proc. of the Seventh National Outdoor Action Conf.*, Ground Water Management Series, v. 15, pp. 405-419.

Vela, S. and McKinley, R.M., 1970, How real heterogeneities affect pulse-test results: *Soc. Pet. Eng. J.,* v. 10, pp. 181-191.

Vennard, J.K., and Street, R.L., 1975, *Elementary Fluid Mechanics*: Wiley and Sons, New York, 740pp.

Widdowson, M.A., Molz, F.J., and Melville, J.G., 1990, An analysis technique for multilevel and partially penetrating slug test data: *Ground Water*, v. 28, no. 6, pp. 937-945.

Yu, Y.H., and Lloyd, J.W., 1992, A multi-layered radial flow model interpretation of drill stem test data: *J. of Hydrology*, v. 136, pp. 73-86.

Zapico, M.M., Vales, S. and Cherry, J.A., 1987, A wireline piston core barrel for sampling cohesionless sand and gravel below the water table: *Ground Water Monitoring Review*, v. VII, no. 3, pp. 74-82.

Zenner, M.A., 1992, Numerical Pumping Test Analysis : Program Implementation an Validation: Project report to Prof. C. McElwee, Advanced Geophysics : Finite Difference Methods, Geology 771 / Physics 727, Kansas Geological Survey, The University of Kansas.

IX. APPENDICES

APPENDIX A

Derivation of Partially Penetrating Slug Test Solution

In this section, the mathematical derivations of the solutions discussed in Section II.A are presented. For the sake of generality, the solutions are obtained in a dimensionless form. The solutions presented here will be in the form of transform-space expressions. Information concerning the scheme used to numerically invert these expression to real space is given in Appendix B. Note that the expressions given here are only for the head within the stressed well. Solutions for heads outside the stressed well are given in Section III.A.

Confined Aquifer Solution

Equations (II.A.1)-(II.A.9) describe the flow conditions of interest here. To work with the most general form of the solution, this derivation is performed using dimensionless forms of (II.A.1)-(II.A.9). The dimensionless analogues of (II.A.1)-(II.A.9) are as follows:

$$\frac{\partial^2 \phi_i}{\partial \xi^2} + \frac{1}{\xi}\frac{\partial \phi_i}{\partial \xi} + \frac{A_i}{a^2}\frac{\partial \phi_i}{\partial \eta^2} = R_i \frac{\partial \phi_i}{\partial \tau} \qquad \text{(A1)}$$

$$\phi_i(\xi,\eta,0) = 0,\ \xi > 1,\ 0 < \eta < \beta \qquad \text{(A2)}$$

$$\Phi(0) = 1 \qquad \text{(A3)}$$

$$\phi_2(\infty,\eta,\tau) = 0,\ \tau>0,\ 0<\eta<\beta \tag{A4}$$

$$\frac{\partial\phi_i(\xi,0,\tau)}{\partial\eta} = \frac{\partial\phi_i(\xi,\beta,\tau)}{\partial\eta} = 0,\ \xi>1,\ \tau>0 \tag{A5}$$

$$\phi_1(1,\eta,\tau) = \Phi(\tau),\ \tau>0,\ d/b\leq\eta\leq(d/b+1) \tag{A6}$$

$$\frac{\partial\phi_1(1,\eta,\tau)}{\partial\xi} = \frac{\gamma}{\alpha}\frac{d\Phi(\tau)}{d\tau}\square(\eta),\ \tau>0 \tag{A7}$$

$$\phi_1(\xi_{sk},\eta,\tau) = \phi_2(\xi_{sk},\eta,\tau),\ 0<\eta<\beta,\ \tau>0 \tag{A8}$$

$$\frac{\partial\phi_1(\xi_{sk},\eta,\tau)}{\partial\xi} = \gamma\frac{\partial\phi_2(\xi_{sk},\eta,\tau)}{\partial\xi},\ 0<\eta<\beta,\ \tau>0 \tag{A9}$$

where

$\phi_i = h_i/H_0$;

$\xi = r/r_w$;

$\eta = z/b$;

$\tau = (tK_{r2})/(S_{s2}r_w^2)$;

$A_i = K_{zi}/K_{ri}$;

$a = b/r_w$;

$R_i = (K_{r2}/S_{s2})/(K_{ri}/S_{si})$;

$\beta = B/b$;

Φ = head in the stressed well = H/H_0;

$\gamma = K_{r2}/K_{r1}$;

$\alpha = (2r_w^2bS_{s2})/r_c^2$;

$\square(\eta)$ = boxcar function = 0, $\eta < d/b$, $\eta > d/b + 1$,

= 1, elsewhere.

$\xi_{sk} = r_{sk}/r_w$.

A solution can be obtained for (A1)-(A9) through the use of integral transforms (Churchill, 1972). A Laplace transform in time followed by a finite Fourier cosine transform in the η direction produce a Fourier-Laplace space analogue to (A1) of the following form:

$$\frac{\partial^2\overline{\phi_i}}{\partial\xi^2} + \frac{1}{\xi}\frac{\partial\overline{\phi_i}}{\partial\xi} - \left(\frac{A_i}{a^2}\omega^2 + R_i p\right)\overline{\phi_i} = 0 \qquad \text{(A10)}$$

where

$\overline{\phi_i}$ = the Fourier-Laplace transform of ϕ_i, $f(\xi,\omega,p)$;

ω = the Fourier-transform variable = $(n\pi)/\beta$, n=0,1,2,..;

p = the Laplace-transform variable.

The Fourier-Laplace space solution to (A10) is quite straightforward, as (A10) is simply a form of the modified Bessel equation (Haberman, 1987). A solution can therefore be proposed in the form:

$$\overline{\phi_i} = C_i K_0(\nu_i\xi) + D_i I_0(\nu_i\xi) \qquad \text{(A11)}$$

where

$\nu_i = ((A_i/a^2)\omega^2 + R_i p)^{.5}$;

C_i, D_i = constants;

K_i = modified Bessel function of the second kind of order i;

I_i = modified Bessel function of the first kind of order i.

Using the transform-space analogues of auxiliary conditions (A4) and (A6)-(A9), the constants in (A11) can be evaluated. Since the focus of interest in most slug-test applications is responses in the stressed well, only the transform-space expression for

head at a radial distance of $\xi = 1$ is given here:

$$\overline{\phi_1}(1,\omega,p) = \frac{\gamma}{\alpha}[1 - p\Phi(p)]F_c(\omega)f_1 \qquad \text{(A12)}$$

where

$\Phi(p)$ = Laplace transform of $\Phi(t)$, the nondimensional form of H(t);

$F_c(\omega)$ = finite Fourier cosine transform of $\square(z)$

$$= \frac{2}{\omega}\sin(\frac{\omega}{2})\cos(\frac{\omega(1+2d/b}{2});$$

$$f_1 = \frac{[\Delta_2 K_0(\nu_1) - \Delta_1 I_0(\nu_1)]}{\nu_1[\Delta_2 K_1(\nu_1) + \Delta_1 I_1(\nu_1)]};$$

$$\Delta_1 = K_0(\nu_1\xi_{sk})K_1(\nu_2\xi_{sk}) - [\frac{N}{\gamma}]K_0(\nu_2\xi_{sk})K_1(\nu_1\xi_{sk});$$

$$\Delta_2 = I_0(\nu_1\xi_{sk})K_1(\nu_2\xi_{sk}) + [\frac{N}{\gamma}]K_0(\nu_2\xi_{sk})I_1(\nu_1\xi_{sk});$$

$$N = \nu_1/\nu_2.$$

The application of an inverse finite Fourier cosine transform to (A12) for η within the screen and utilization of the Laplace-space analogue of (A6) produces the following expression for head in the stressed well:

$$\Phi(p) = \frac{\gamma}{\alpha}[1 - p\Phi(p)]F_c^{-1}(F_c(\omega)f_1) \qquad \text{(A13)}$$

Solving for $\Phi(p)$ yields

$$\Phi(p)=\frac{\frac{\gamma}{\alpha}F_c^{-1}(F_c(\omega)f_1)}{[1+\frac{\gamma}{\alpha}pF_c^{-1}(F_c(\omega)f_1)]} \qquad \text{(A14)}$$

Appendix B provides details of the Fast Fourier Transform scheme used to invert the expression in parenthesis in (A14). The algorithm of Stehfest (1970) was used to perform the numerical Laplace inversion of (A14).

Unconfined Aquifer Solution

For the unconfined case, (A5) is replaced by the dimensionless analogues of (II.A.11) and (II.A.12):

$$\phi_i(\xi,0,\tau) = 0,\ \xi>1,\ \tau>0 \qquad \text{(A15)}$$

$$\frac{\partial\phi_i(\xi,\beta,\tau)}{\partial\eta} = 0,\ \xi>1,\ \tau>0 \qquad \text{(A16)}$$

A solution for (A1)-(A4), (A6)-(A9), and (A15)-(A16) is obtained using the same approach as in the confined case. The Fourier-Laplace expression for head at a radial distance of $\xi=1$ in the unconfined case can be written as:

$$\overline{\phi_{1_w}}(1,\omega^*,p) = \frac{\gamma}{\alpha}[1-p\Phi_{uc}(p)]F_s(\omega^*)f_1 \qquad \text{(A17)}$$

where

$\overline{\phi_{1_w}}$ = the Fourier-Laplace transform of ϕ_{1_w}, the nondimensional form of

h_1 for the unconfined case;

$\Phi_{uc}(p)$ = the Laplace transform of the nondimensional form of H(t) for the unconfined case;

$F_s(\omega^*)$ = modified finite Fourier sine transform of $\square(z)$

$$= \frac{2}{\omega^*}\sin\left(\frac{\omega^*(2d/b+1)}{2}\right)\sin\left(\frac{\omega^*}{2}\right);$$

ω^* =Fourier transform variable for the modified sine transform = $(n\pi)/2\beta$, n=1,3,5,...

The application of an inverse modified finite Fourier sine transform to (A17) for η within the screen and rewriting in terms of $\Phi_{uc}(p)$ produces the following expression:

$$\Phi_{uc}(p)=\frac{\frac{\gamma}{\alpha}F_s^{-1}(F_s(\omega^*)f_1)}{[1 + \frac{\gamma}{\alpha}pF_s^{-1}(F_s(\omega^*)f_1)]} \qquad \text{(A18)}$$

The modified finite Fourier sine transform employed in the unconfined case requires a bit of discussion. The standard finite Fourier sine transform is quite useful when a constant head is maintained at both boundaries. In the unconfined case, the upper boundary (η=0) is defined as a constant-head condition while the lower boundary ($\eta=\beta$) is defined as a no-flow condition. Churchill (1972) presents the modified finite Fourier sine transform

$$F_s(n) = \int_0^{\beta} f(\eta)\sin\left(\frac{n\pi\eta}{2\beta}\right)d\eta, \quad n=1,3,5,... \qquad \text{(A19)}$$

as an example of a Sturm-Liouville transformation. When this modified sine transform is applied to the second-order derivative with respect to η, integration by parts yields

$$\int_0^{\beta} \frac{\partial^2 \phi_i}{\partial \eta^2} \sin\left(\frac{n\pi\eta}{2\beta}\right) d\eta = -\omega^{*2}\overline{\phi_i} + \omega^* \phi_i(0) - \frac{\partial \phi_i(\beta)}{\partial \eta} \qquad \text{(A20)}$$

where

$$\omega^* = (n\pi)/2\beta, \; n=1,3,5,\ldots$$

For the boundary conditions employed here, (A20) reduces to

$$-\omega^{*2}\overline{\phi_i} \qquad \text{(A21)}$$

APPENDIX B

Numerical Inversion Procedures

In this section, details of the procedures employed to numerically invert the transform-space expressions derived in Appendix A are presented. As discussed in Section II.A, the Fast Fourier Transform (FFT) procedure was employed to perform the required Fourier transforms/inversions in this work. In order to demonstrate that the Discrete Fourier Transforms introduced negligible error into the numerically inverted solution, a comparison between the discrete solution and the continuous form is discussed.

For the confined case (cf. (A14)), a finite Fourier cosine transform was employed. The continuous form of this transform can be written as

$$F_c(n) = \int_0^{\beta} f(\eta)\cos\left(\frac{n\pi\eta}{\beta}\right)d\eta \qquad \text{(B1)}$$

where

F_c = finite Fourier cosine transform;

$f(\eta) = F_c(\omega)f_1$.

In order to utilize the FFT procedure, (B1) is approximated using a Discrete Fourier Transform:

$$F_c(n) \approx \Delta\sum_{k=0}^{N-1} f(\Delta k)\cos\left(\frac{n\pi k}{N}\right),\ n=0,1,2,..,N-1 \qquad \text{(B2)}$$

where

N = number of equally spaced points between 0 and β, must be an integer power of 2;

$\Delta = \beta/N$ = interval between equally spaced points.

For the unconfined case (cf. (A18)), a modified finite Fourier sine transform was

employed. The continuous form of this transform can be written as

$$F_s(n) = \int_0^{\beta} f_{uc}(\eta)\sin(\frac{n\pi\eta}{2\beta})d\eta, \quad n=1,3,5,\ldots \tag{B3}$$

where

F_s = modified finite Fourier sine transform;

$f_{uc}(\eta) = F_s(\omega^*)f_1$.

Equation (B3) is only defined for odd numbered n's. For ready implementation with standard FFT algorithms, (B3) is rewritten in terms of a continuous sequence of n's:

$$F_s(n) = [1+(-1)^{n+1}]\int_0^{\beta} f_{uc}(\eta)\sin(\frac{n\pi\eta}{2\beta})d\eta, \quad n=1,2,3,\ldots \tag{B4}$$

Equation (B4) is now approximated using a Discrete Fourier Transform :

$$F_s(n) \approx [1+(-1)^{n+1}]\Delta\sum_{k=1}^{N-1} f_{uc}(\Delta k)\sin(\frac{n\pi k}{2N}), \quad n=1,2,..,N-1 \tag{B5}$$

Equations (B2) and (B5) can be directly implemented in standard FFT algorithms. In this work, an FFT algorithm given in Press et al. (1992) was employed. The total number of sampling points (N) in η was constrained such that there would always be at least two points within the screened interval and Δ would never exceed .5 m. An additional series of simulations have shown that N equal to 256 should be sufficient for practical applications.

In order to check on the approach outlined above, an additional series of simulations were performed in which the continuous forms of the finite Fourier transforms were employed for the required transforms/inversions. The inverse finite Fourier transform that is employed in (A14) can be written in the continuous form for η at the center of the screen as:

$$F_c^{-1}(f(\eta)) = \frac{f_1}{\beta} + \frac{4}{\pi}\sum_{n=1}^{\infty}\frac{f_1}{n}\sin\frac{n\pi}{2\beta}\cos^2(\frac{n\pi(1+2d/b)}{2\beta}) \tag{B6}$$

The inverse finite Fourier transform that is employed in (A18) can be written in the continuous form for η at the center of the screen as:

$$F_s^{-1}(f_{uc}(\eta)) = \frac{4}{\pi}\sum_{n=1}^{\infty}[1+(-1)^{n+1}]\frac{f_1}{n}\sin\frac{n\pi}{4\beta}\sin^2\left(\frac{n\pi(1+2d/b)}{4\beta}\right) \qquad (B7)$$

In all cases, the inversion of (B6) and (B7) produced results that were indistinguishable from those found using a FFT algorithm with (B2) and (B5). The computational time, however, was significantly greater.

The inverse Laplace transform, the final step of the numerical inversion procedure, was performed here using the algorithm of Stehfest (1970). Sixteen terms were used in the summation of the Stehfest algorithm for all the cases examined in this work. Note that the procedures discussed here are implemented in a series of Fortran programs found in Hyder et al. (1993).